A thermodynamic investigation of an electricity storage system based on reversible solid oxide cells with methanol as fuel and steam electrolysis

M.Sc. in Energy and Process Technology

Sotiris Giannoulidis

TU Delft

BALANCE

A thermodynamic investigation of an electricity storage system based on Reversible Solid Oxide Cells with Methanol as fuel and steam electrolysis

Master of Science Thesis

Sotiris Giannoulidis

in partial fulfillment of the requirements for the degree of

Master of Science

in Mechanical Engineering: Track Energy and Process Technology

at the Delft University of Technology,

to be defended publicly on Monday, November 12, 2018, at 10:30 AM.

Supervisors:	Dr. A. Purushothaman Vellayani
	Dr. Vikrant Venkataraman
Thesis Committee:	Prof. Dr. D.J.E.M Roekaerts
	Dr. A. Purushothaman Vellayani
	Dr. RangaRao Venkatesha Prasad
	Dr. Vikrant Venkataraman
	Theo Woudstra

Acknowledgments

Before the start of this amazing journey of MSc studies at TU Delft, a process simulation thesis topic had been always my dream project. I am remembering myself telling to everyone that I wanted to become familiar with MATLAB but also with process design simulators such as Aspen Plus. To further show my inclination towards process design, Aspen Plus simulator had also been included within my cover letter when applying to TU Delft. I had no idea how to use it back then, but I had an innate feeling that I should strive for process simulation. This innate feeling was created during my Diploma Thesis in Laboratory of Steam Boilers and Thermal Plants in National Technical University of Athens (NTUA).

First and foremost, I would like to thank Prof. P.V. Aravind for giving me the chance to get my hands on a process simulation topic which confronts today's environmental problems. Personally, I think it is good to see that the EU funds projects such as the "Balance" Project which promotes the use of renewable energy technologies. The experience acquired from this project will be useful for my career either as a researcher or as a professional process engineer. I deeply desire that a project like this can light the spark so that more projects based on renewable energy adoption will further be conducted. Moreover, I would like to thank Dr. Theo Woudstra for his invaluable advice and the time devoted to the completion of this project.

I would like to give my special thanks to the Post-Doctoral researcher Vikrant Venkataraman for the impeccable cooperation. We both learned from our in-depth discussions. I hope, at some point in the future, that Vikrant will forgive me for talking too much. I was so deeply engaged in this project that my enthusiasm could not just disappear.

Moving to the Netherlands was not an easy task for me. Therefore finally, I would like to give my sincerest and deepest thanks to my family and friends who assisted me during my dark times in the Netherlands. More specifically I would like to give special thanks to George-Marios Papadimtropoulos, Miltiadis Gialousis, Georgios Marinos, Pratik Basarkar, Nitish Gadgil and Cesare Ressa for teaching me that "Everything will be perfect at the end. If it's not, then it's not the end!". In the end, those dark times, have made me stronger and mature and I consider those times as one of the most meaningful experiences in my life. Filled with optimism, I can work now towards the next steps of life.

"Everything is hard before it is easy!" – Goethe

Abstract

A lot of scientific research has been focusing on energy storage systems recently and there are numerous reasons for that. First of all, they can nullify the intermittent nature of renewable energy technologies, by storing excess energy in times of heightened solar irradiance and wind levels and utilizing it when electricity demand is surging. A combination of energy storage systems along with renewable energy technologies can eliminate CO_2 emissions in the future. It can also lead to state development, by liberating countries from the dependency on costly fossil fuel imports. Finally, population growth will result in increased energy peaks and energy storage systems can be seen as the means for achieving those enhanced power requirements.

In the current thesis, an extensive thermodynamic investigation of an efficient energy storage system based on steam electrolysis is presented. The core of the system is a reversible solid oxide cell stack. It can operate either as electrolysis (charging mode) or as a fuel cell (discharging mode). Apart from the core, around the stack, various balance of plant components can be placed for the synthesis of a plethora of fuels. In this case study, methanol is synthesized.

At first, process design of a model capable of converting electrical energy to methanol and vice versa is formulated in process simulation software Aspen Plus®. Extensive energy and exergy analysis have been conducted on the system for the identification of process conditions which maximize energy and exergy efficiency of each mode of operation. Furthermore, extensive exergy flow diagrams have been drawn in order to pinpoint the components which mostly contribute to the total exergy losses. Finally, roundtrip efficiency optimization has also been performed and the respective process conditions have been reported. For the calculation of the hot and cold utility of the system, the pinch technology has been employed.

Results indicate that during electrolysis mode energy and exergy efficiencies of 68.74% and 77.67% respectively, can be achieved when thermoneutral operation is applied. The same results for fuel cell mode operation are 60.22% and 56.78% respectively. Exergy and energy efficiency during fuel cell mode are still limited due to the intense refrigeration system employed for CO_2 condensation. For maximization of roundtrip efficiency, a thermal energy storage system was additionally employed in the process design which stores heat energy from fuel cell mode in order to satisfy the thermal requirements during the endothermic electrolytic operation. The maximum reported value of roundtrip efficiency is 56.72% while in scientific literature a maximum value of 54.3% has been cited, showing a clear improvement.

List of Symbols

A_{tot}	Total electrode area
$D_{eff,i}$	Effective diffusion coefficient of species i
D_{i-j}	Binary diffusion coefficient
$D_{kn,i}$	Knudsen diffusion coefficient of species i
E_{heat}	Exergy of heat
E_{BOP}	Energy requirement by BOP
$E_{act,i}$	Activation energy for exchange current density calculation
$E_{act,el}$	Activation energy for electrolyte conductivity calculation
$E_{TM\&CH}$	Thermomechanical and chemical exergy of flow of matter
M_i	Molecular weight of substance i
P_{CO_2}	Carbon Dioxide storage pressure
P_{H_2}	Hydrogen storage pressure
P_0	Reference Pressure
$P_{heating}$	Heating Power
P_{METH}	Methanol Synthesis pressure
P_{stack}	Stack Power
P_{total}	Total power requirement
Q_C	Cold Utility
Q_H	Hot Utility
Q_{diss}	Heat dissipated
T_{METH}	Methanol Synthesis Temperature
$U_{f,steam}$	Steam Utilization
U_f	Fuel Utilization
V_N	Nernst or Reversible voltage at current conditions
V_N^0	Nernst or Reversible voltage at reference conditions
V_{act}	Activation voltage losses
V_{cell}	Cell Voltage
V_{con}	Concentration voltage losses
V_{ohm}	Ohmic voltage losses
V_{tn}	Thermoneutral voltage
$W_{Cooling,Pump}$	Electricity consumed by the cooling pump
$W_{refrigeration}$	Electricity consumed by the refrigeration compressors
i_{tn}	Current density which corresponds at thermoneutral voltage
$j_{0,i}$	Exchange Current density
$\dot{m}_i$	Mass flow rate of substance i
$\dot{n}_i$	Molar flow rate of substance i
n_{RT}	Roundtrip Efficiency
n_{en}	Energy efficiency

n_{ex}	Exergy efficiency
$n_{is,C}$	Isentropic efficiency for compressors
$n_{is,T}$	Isentropic efficiency for turbines
$p_{i,bulk}$	Partial Pressure of i component at bulk (i.e. away from the electrode)
$p_{i,tpb}$	Partial Pressure of i component at the triple phase boundary
p_{p0}	Dead state pressure for reference substance
$r_{ohmic,const}$	Specific Ohmic resistance for interconnects and wires
$r_{ohmic,el}$	Specific Ohmic resistance for electrolyte
x_i	Mole fraction of substance i
Δh_R^0	Heat of reaction at reference conditions
ΔV_{OP}	Total overpotential voltage losses
Ex	Total Exergy
F	Faraday's Constant
HR	Fractional Recovery of heavy component
I	Total Current
LR	Fractional Recovery of light component
M	Stoichiometric ratio for Methanol Synthesis
P_s	Stack Pressure
R	Universal Gas Constant
i	Current Density
q	Charge Transferred
t	Time of operation
z	Number of electrons transferred per fuel molecule
ΔG	Change in Gibbs free energy
ΔH	Chang in enthalpy
ΔS	Change in entropy

Greek Symbols

β	Symmetry factor
γ_i	Activity Coefficient of substance i or pre-exponential factor for exchange current density calculation
δ_{el}	Electrolyte Thickness
δf_{el}	Fuel Electrode Thickness
δ_{ox}	Oxidant/Sweep gas Electrode Thickness
ε	Electrode Porosity
ε_{fuel}	Molar chemical exergy of fuel
ε_i	Molar chemical exergy of substance i
ε_{mix}	Molar chemical exergy of mixture
$\varepsilon_{physical}$	Molar Physical or Thermomechanical exergy
$\sigma_{0,el}$	Pre-exponential factor for conductivity calculation
σ_{el}	Electrolyte Conductivity
τ	Electrode Tortuosity

Subscripts

fc	Fuel Cell stack or Fuel Cell mode
el	Electrolysis Stack or electrolysis mode
sys	Refers to the system
$loss$	Refers to losses
in	Inlet
out	Outlet

List of Abbreviations

AC	Alternating Current
ASR	Area Specific Resistance
CAES	Compressed Air Energy Storage
CAPEX	Capital Expenses
COP	Coefficient of Performance
DC	Direct Current
DME	Dimethyl-Ether
ECN	Energy research Centre of the Netherlands
FE	Fuel Electrode
FT	Fischer-Tropsch
HEX	Heat Exchanger
HHV	Higher Heating Value
HRSG	Heat Recovery Steam Generator
LHV	Lower Heating Value
LiF	Lithium Fluoride
LSCM	Lanthanum Strontium Cobalt Manganese
MEA	Monoethanolamine
NRTL	Non-Random Two Liquid
OCV	Open Circuit Voltage
OPEX	Operating Expenses
PCM	Phase Change Material
PEM	Proton Exchange Membrane
PFR	Plug Flow Reactor
PHS	Pump-Hydro Storage
PSI	Paul Scherrer Institute
PSRK	Predictive Soave-Redlich-Kwong
PTSC	Parabolic Trough Solar Collectors
PV	Photovoltaic System
RFC	Reversible Fuel Cell
rSOC	Reversible Solid Oxide Fuel Cell
RT	Roundtrip
RWGS	Reverse Water-Gas Shift Reaction
S/C	Steam to Carbon Ratio
ScSZ	Scandia- Stabilized Zirconia
SGE	Sweep Gas Electrode
SNG	Synthetic Natural Gas
SOEC	Solid Oxide Electrolysis Cell
SOFC	Solid Oxide Fuel Cell
TPB	Triple Phase Boundary
WGS	Water-Gas Shift Reaction
YSZ	Yttrium-Stabilized Zirconia

Table of Contents

List of Tables

List of Figures

CHAPTER 1

INTRODUCTION

1.1 The need for seasonal electricity storage and the role of Reversible Solid Oxide Fuel Cell

Europe has initiated the transition to a low carbon economy by harnessing the potential of renewable energy technologies through Europe 2020 agenda [1]. In addition, the European Commission aims for 80-95% reduction in CO_2 generation by 2050 compared to CO_2 produced during 1990. This reduction encompasses also the electricity production sector for reductions up to 96-99% in CO_2 emissions [2].

The increase in CO_2 emissions has skyrocketed 70% during the period 1970-2004. Approximately up to 32 billion tonnes of CO_2 were emitted in 2014. Moreover, predictions show the rapid increase in emissions to 50 billion tonnes of CO_2 in 2050 [3]. The rapid expansion of renewable energy technologies along with the combination of fuel cell systems is an attractive option to provide electricity as well as fuels and energy carriers in order to sustain the world's growing energy demands. CO_2 capture from power plants offers recycle capabilities in synthesizing chemicals which can be directly consumed by further processing or utilized by means of chemical energy storage [3]. The main disadvantage of renewable energy technologies, such as solar and wind energy is their intermittent nature [4]–[7]. If solar energy is taken as an example, it is possible to store excess electricity generated as fuel by the use of an electrolyzer, which converts water (H_2O) and carbon dioxide (CO_2) into useful building blocks, such as hydrogen (H_2) and carbon monoxide (CO), for the synthesis of complex molecules. On the contrary, during winter where low solar irradiation levels are observed, the stored gases can be utilized in a fuel cell which produces electricity on demand. By coupling the electrolyzer and the fuel cell mode into a single device, the reversible fuel cell (RFC) is created. Research interest is developed in RFCs operated as large electrical energy storage systems [8]. It is stated that electricty storage is the key to electricity generation and consumption *via* two independent processes. This type of large-scale electricity storage system can also bring an extra boost to renewable energy technologies because it helps towards minimization of their intermittency through storage [9]. Electricity storage is also a key technology so that the grid can handle demand fluctuations in a stable and reliable manner [4], [10].

Estimates show that in the future, an energy amount equivalent to 15-20% of the annual energy demand has to be stored [5]. This energy amount will be stored by using long-term energy storage systems such as pump-hydro storage (PHS), compressed air energy storage (CAES) and RFCs. In contrast, it is also claimed that storage duration should vary between one and eight hours by using 1 kW-10 MW electricity storage systems that could reach roundtrip efficiencies of 80% [6]. These solutions can be offered by employing short-term energy storage systems such as batteries, flywheels or molten salts. Therefore a mix of long-term and short-term energy storage will be necessary in the future.

When it comes to storage, plenty of technologies come into play. Most of the large-scale storage systems are based on hydro-pump storage (see Figure 1-1), but on the other hand, a height difference is essential in order to build such systems. Even though much attention has been given to all those systems, there is no system which globally provides a solution to electricity storage [9]. Batteries have spectacular storage efficiencies (75-94%) but low storage densities (<2 GJ/m^3). Molten salts used in solar power plants have also low storage density (<3 GJ/m^3) and their efficiency is limited due to the incorporation of a Rankine Cycle. Finally for CAES, even though high storage densities have been reported, special geological sites are required for their

construction [11]. Another option is the use of a proton exchange membrane (PEM) or alkaline electrolyzer which are widely used for production and storage of hydrogen [10].

Combination of renewable energy technologies with electrolyzers are expected to play an important role in the future [12]. However, concerns are raised for their low roundtrip efficiency [10]. In contrast, due to recent cell developments in terms of lower degradation and repeatability of the cycle, reversible solid oxide cells (rSOC) is a very promising technology which addresses the problem of long-term electricity storage. Their ability to work with carbon-containing fuels, their low resistance due to high operating temperature and the possibility to catalyze desirable side reactions combined with high roundtrip efficiency makes them a potential candidate in long-term energy storage [10]. Another advantage of rSOC systems is that they can store power for several months by producing hydrogen *via* the electrolysis route or convert it to synthetic natural gas (SNG) and store it by using the existing infrastructure [10]. However, those systems have not been commercially available due to degradation and reduced cell lifetime. Other reasons include their high cost and reduced storage efficiency compared to batteries [13]. Reversible solid oxide cells have not been widely explored for their capabilities and therefore it is an active field of research. On the other hand, there has been quite an extensive research on using solid oxide cells either as an electrolyzer for fuel production or as a fuel cell for power generation [4], [10]. The scope of this thesis project focuses on rSOCs and their employment to large-scale electricity storage systems by producing synthetic fuels.

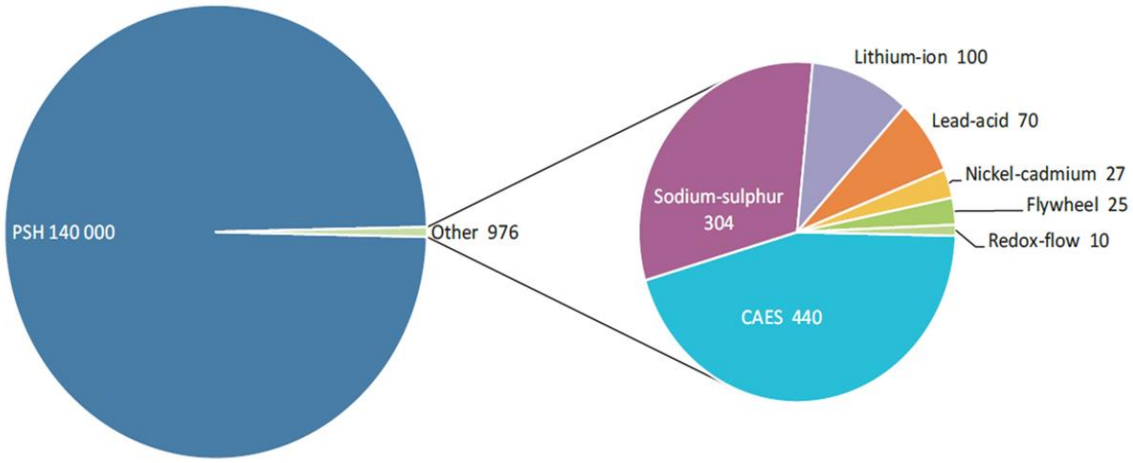

Figure 1-1: Electricity storage technology distribution across the world (Numbers in MW) [14]

In summary, electricity storage solutions are needed because of [15]:

- The surge of renewable energy technology which is necessary for a reduction in global CO_2 emissions. Excess stored energy will ensure adequate electricity during peak periods while low demand periods will offer opportunities for storage. This strategy can flatten out the inherently intermittent nature of renewable energy technology
- Energy storage systems in combination with renewable energy technologies can decrease fossil fuel dependency, lowering the imports from other countries and leading to self-sufficient countries in terms of energy needs
- There are still sectors that depend on fossil fuels. However, the surge of renewable energy technology with energy storage systems can produce many different energy carriers, either liquid or gaseous, in a renewable way. Combining various Power-to-X projects along with the existing infrastructure, gradual independency from fossil fuels can be achieved

1.2 Introduction to Solid Oxide Reversible Cell

Figure 1-2 depicts a simplified schematic of a rSOC [8], [9]. The main components of the structure, are 2 electrodes, an oxygen ionic electrolyte conductor as well as the interconnects. State-of-the-art electrolytes are manufactured with doped zirconia, yttria-stabilized zirconia (YSZ) or Scandia-stabilized zirconia (ScSZ) [8]. A state-of-the-art anode is constructed from Ni/YSZ cermet while the cathode is manufactured by strontium-doped lanthanum manganite [16]. For the vast variety of different materials for the anode, electrolyte or cathode as well as sealants and interconnects the reader is advised to study the thorough review by Mahato et al. [17]. During fuel cell mode, oxygen contained in atmospheric air is consumed and reactants (i.e. CH_4, CO, H_2 for carbonaceous fuels) are electrochemically oxidized and therefore, producing electricity [6]. Oxidant flow is also used as a heat removal medium during the exothermic fuel cell operation [5]. When operating in the electrolysis mode, oxygen is a product on the oxygen electrode and in order for its concentration to be reduced, a sweep gas stream is provided [18]. The sweep gas is necessary in order to reduce the partial pressure of the produced oxygen, enhancing the electrolysis process and demanding less amount of electrical power input. Of course, additional electrical power will be necessitated to drive the sweep gas into the stack. When co-electrolyzing rich CO_2/H_2O streams, syngas is produced which can be either stored or used for fuel synthesis and further processes [6]. Although it is desirable to have those compounds (i.e. CH_4, CO, H_2) when operating in fuel cell mode and CO_2, H_2O when operating in electrolysis mode, theoretically, any composition is possible for the fuel electrode which can contain H_2, H_2O, CO, CO_2, CH_4 and inert gases such as N_2 [6]. For example, during electrolysis mode, it is beneficial to have only CO_2 and H_2O since only these species can be reduced. If the inlet stream contains species such as CO, CH_4 or H_2, the initiation of the electrochemical reactions will be more difficult, leading to excessive power input.

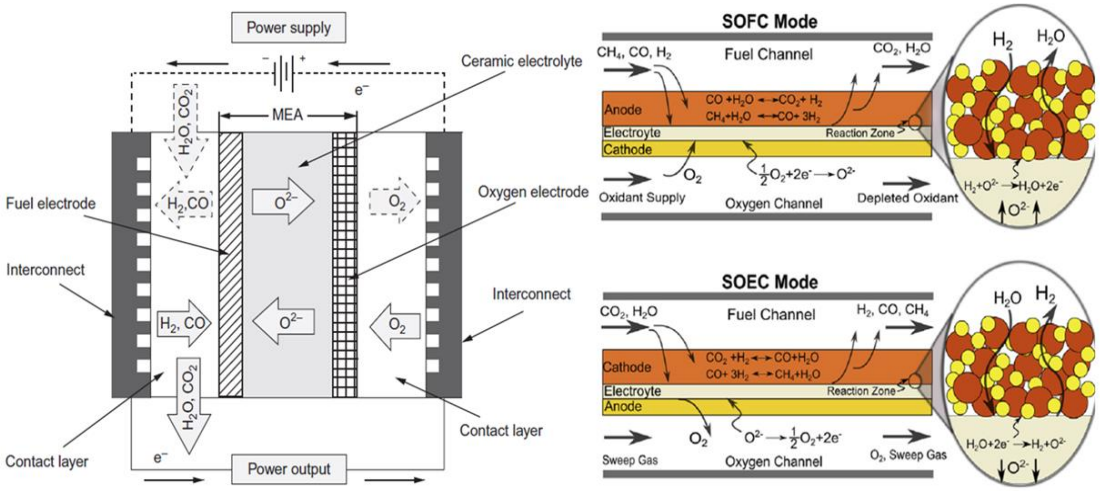

Figure 1-2: (Left) Schematic of a rSOC and basic operation. (Right) Representation of species transport during handling of carbonaceous feed inlets in a rSOC [8], [9]

The major advantages of high temperature reversible solid oxide fuel cells are that during electrolysis mode, fuel production can be done cheaply since more energy can be provided by heat instead of electricity, in contrast with low-temperature operation of polymer-electrolyte fuel cells (PEFC) or alkaline fuel cells (AFC) where the energy demand must be covered mainly by electricity, and secondly, activation losses are lessened, leading to fast reaction rates. Those systems have the capability of fuel production when coupled with renewable energy sources where electricity can be produced cheaply [8]. Another advantage is that high-temperature rSOC cells can handle carbonaceous inlet streams more comfortably than low-temperature reversible cells [9]. Typically, a reformer is necessary to convert any carbonaceous fuel into a mixture of H_2,

H_2O, CO, and CO_2, prior to the stack. Carbonaceous fuels can also provide efficient thermal management through methanation (during electrolysis mode) and methane reforming (during fuel cell mode) [19]. A more elaborate schematic providing some of the ongoing chemistry in the cell is provided in Figure 1-2.

For a better understanding of the operation of a rSOC stack or fuel cell stack, pure steam electrolysis (in electrolysis mode) and pure hydrogen oxidation (in fuel cell mode) will be considered. According to Figure 1-2, if the carbon-containing species are neglected the following major events are taking place.

Electrolysis Mode

- Steam is split at the fuel electrode according to the reaction $H_2O + 2e^- \leftrightarrow O^{2-} + H_2$. For the splitting process, three components are needed. Steam, electrolyte and electrode material. The fuel electrode is responsible for bringing the electrons since it is an electronically conducting material. The electrolyte is needed for the oxygen ion removal, since it is an ionic conductor. The region where the three components meet is called the *triple phase boundary*
- Oxide ions travel through the electrolyte, from fuel electrode to the oxygen electrode
- At the oxygen electrode, the following reaction occurs: $O^{2-} \leftrightarrow \frac{1}{2}O_2 + 2e^-$. Oxide ions place their excess electrons back while escaping as oxygen molecules. A sweep gas stream, usually atmospheric air, is provided to balance the heating/cooling of the electrolysis stack as well as to facilitate the removal of pure oxygen
- At the fuel electrode, electrons are required from an external circuit, therefore, electricity is consumed
- Although electrolysis is an endothermic process by its nature, the stack can operate either in endothermic or in exothermic mode as it will be explained in 0

Fuel Cel Mode

- At the fuel electrode, H_2 is oxidized to water. Again the triple phase boundary is necessary. Oxide ions are separated from their excess electrons while producing steam. The electrons move across the externally connected circuit, providing electrical power. The following reaction takes place: $O^{2-} + H_2 \leftrightarrow H_2O + 2e^-$
- Oxide ions travel across the opposite direction compared to electrolysis mode
- At the oxidant electrode, the oxidant consumes the excess electrons provided by the external circuit and refilling the electrolyte with anions. The ongoing reaction which takes place is: $O_2 + 2e^- \leftrightarrow O^{2-}$
- At the fuel electrode, electrons are produced and circulated through an externally connected circuit. Consequently, power is produced during this operation
- During this mode, in all cases, heat needs to be removed as it will be explained in 0

1.3 The concept of electricity storage via the use of Reversible Solid Oxide Fuel Cell

The concept of electricity storage through a reversible solid oxide fuel cell is shown in Figure 1-3. At the left side, a simplistic conversion of steam to hydrogen *via* electricity input is shown. When electricity demand is rising, the reverse process is happening. Hydrogen is converted back to its oxidized form with a simultaneous power production in fuel cell mode. Of course, the process is not only limited to hydrogen. Hydrogen is a feedstock stream for the synthesis of various carbonaceous fuels such as methanol, ethanol, DME, synthetic natural gas and higher order hydrocarbons. Therefore, the process can be extended as seen on the right of Figure 1-3 where X fuel is synthesized. The reverse process necessitates a reformer where X fuel is converted back to hydrogen and carbon monoxide (or carbon dioxide) and the final step of power production occurs in the

rSOC stack. Of course, electrolysis and fuel cell mode occur in the same piece of equipment but for ease of understanding, it is shown as separate pieces of equipment.

This feature of long-term storage is not a characteristic of batteries or supercapacitors. In addition, the need for specific geographical sites which require height difference is diminished for this system, in contrast with pump-hydro storage. On the other hand, more research has to be done on the efficiency of these systems as well as their long-term operation.

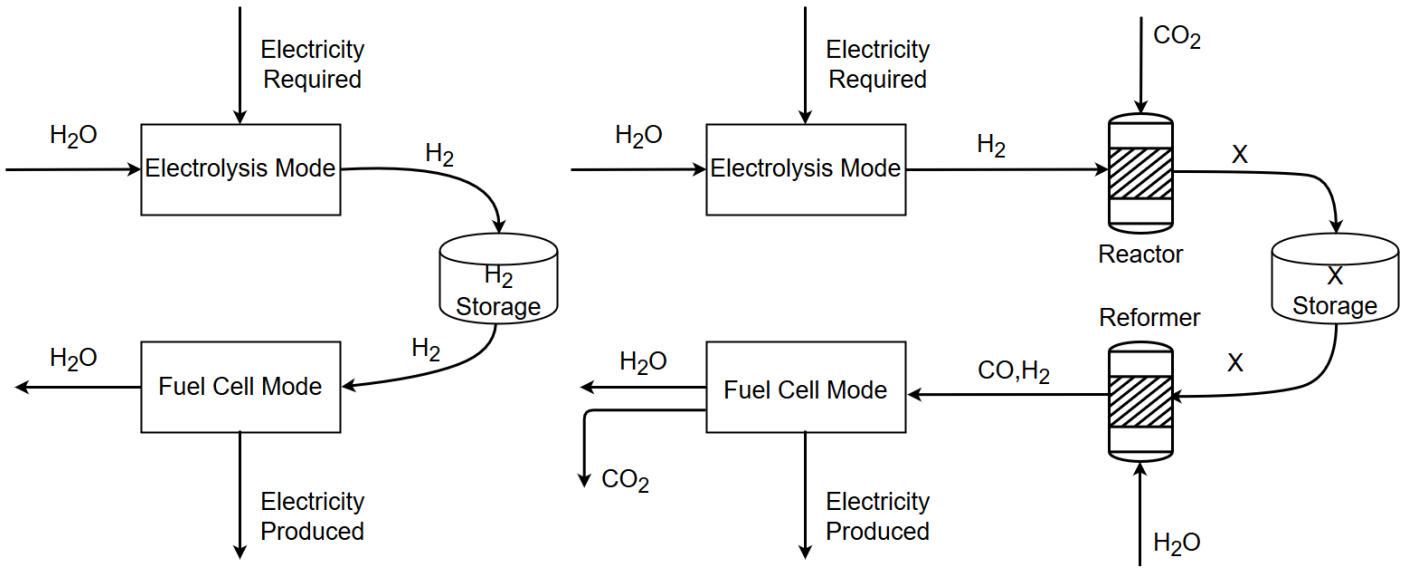

Figure 1-3: (Left) Simplified schematic for electricity storage *via* hydrogen production and storage, (Right) Simplified schematic of electricity storage *via* Synthetic Fuels

1.4 Thesis Objective

The current thesis' objective is the formulation of an efficient process design chain which employs steam electrolysis and excess renewable electricity for the production of methanol. The produced fuel can directly be used for consumption, however since the main objective is the electricity storage and generation, it will be assumed that all methanol stored will be electrochemically oxidized during fuel cell operation and hence, generating electricity. After the formulation of the model, system energy and exergy analysis will be conducted in order to define the optimum configuration for the minimization of system exergy losses, thus defining the most thermodynamically favorable conditions of operation.

A plethora of process design parameters can be varied in order to determine the optimum energy and exergy efficiencies. More specifically,

- *Stack Characteristics: Number of cells, Area of each cell*
- *Stack operating conditions: Stack Pressure, Stack Temperature, Fuel Utilization*
- *Flow rates: Water, Carbon Dioxide, Hydrogen*
- *Methanol synthesis dimensions: Length, Diameter, Number of tubes*
- *Methanol Synthesis Operation: Temperature, Pressure*
- *Pressure/Temperature of flash separators*
- *Isentropic and mechanical efficiencies of compressors/expanders/pumps*
- *Methanol reforming conditions: Temperature, Pressure*
- *Feed gas composition/liquid streams and presence of impurities (i.e. other species)*
- *Heat exchanger network (including working temperatures/pressures)*

- *Storage conditions (Temperature, Pressure) etc.*

First of all system efficiency will be optimized (i.e. assuming the perfect heat integration, a scheme which minimizes heating and cooling utility). Afterwards, the real efficiency will be defined with a manually imported heat exchanger network. Component level exergy analysis will be conducted afterwards while exergy flow diagrams will complete the results.

After energy and exergy analysis, optimization for roundtrip efficiency will follow and new proposed process conditions will be presented. In summary, the following research questions will be answered:

- Which process conditions maximize energy and exergy efficiencies for each mode when employing the pinch technology for heat integration?
  - What is the maximum value of energy and exergy efficiencies achieved at the aforementioned process conditions (for each mode)?
  - What is the maximum value of energy and exergy efficiencies achieved at the aforementioned process conditions when manually inserting a heat exchanger network and what is the effect of manual heat integration on system efficiency (for each mode)?
  - Which components contribute the most to the total exergy losses?
- Which process conditions maximize roundtrip efficiency for this energy storage system when employing the pinch technology for heat integration?
  - What process design changes have to be made in order to achieve the maximum roundtrip efficiency and why?
  - What is the maximum value of roundtrip efficiency at the optimized process conditions?

1.5 Topics not addressed in the present thesis

The thesis is about the development of a steady-state thermodynamic system for electricity storage. Therefore, dynamic phenomena are not taken into account. Start-up, shutdown or switching between modes and all the necessary control schemes to accomplish the aforementioned procedures are not part of the current study. It is assumed that those dynamic phenomena take place in short periods of time and most of the time the system will operate under steady-state conditions. Understanding the steady-state conditions in the first phase of the study is far more important in order to calculate system efficiency and actually prove that the system can be competitive for energy storage among other energy storage technologies.

Another major assumption of the current thesis is that CO_2 already exists in the system. This means that CO_2 has already been captured or injected into the system (i.e. with a CO_2 cylinder). Therefore, a certain amount of CO_2 exists in the system and it is not being continuously captured from industry stacks. CO_2 is stored into methanol while in fuel cell mode, the resulting CO_2 is stored separately without any further need for additional carbon capture. Industry chimneys induce further complication to the model as gas cleaning technologies should also be simulated. Since industry exhaust gases have typically ~15% CO_2 in volume, physical absorption could be harnessed in order to ensure the necessary quantities of CO_2 [20].

Moreover, since a steady-state model is formulated, gas leaks and losses are not included in the present study. It is assumed that the whole system is leak-tight and no make-up gas or liquid streams are necessary.

Finally, the outlet stream of one mode should be the inlet stream in the other mode. For example, during system evaluation, impure methanol is produced. However, in the model analysis, pure methanol is fed to the fuel cell operation. The assumption concerning the impurities relieves the process modeler from a lot of manual changes in composition between the two modes, which is an error-prone process while maintaining a high level of accuracy.

1.6 Thesis Outline

The thesis outline is summarized in Figure 1-4.

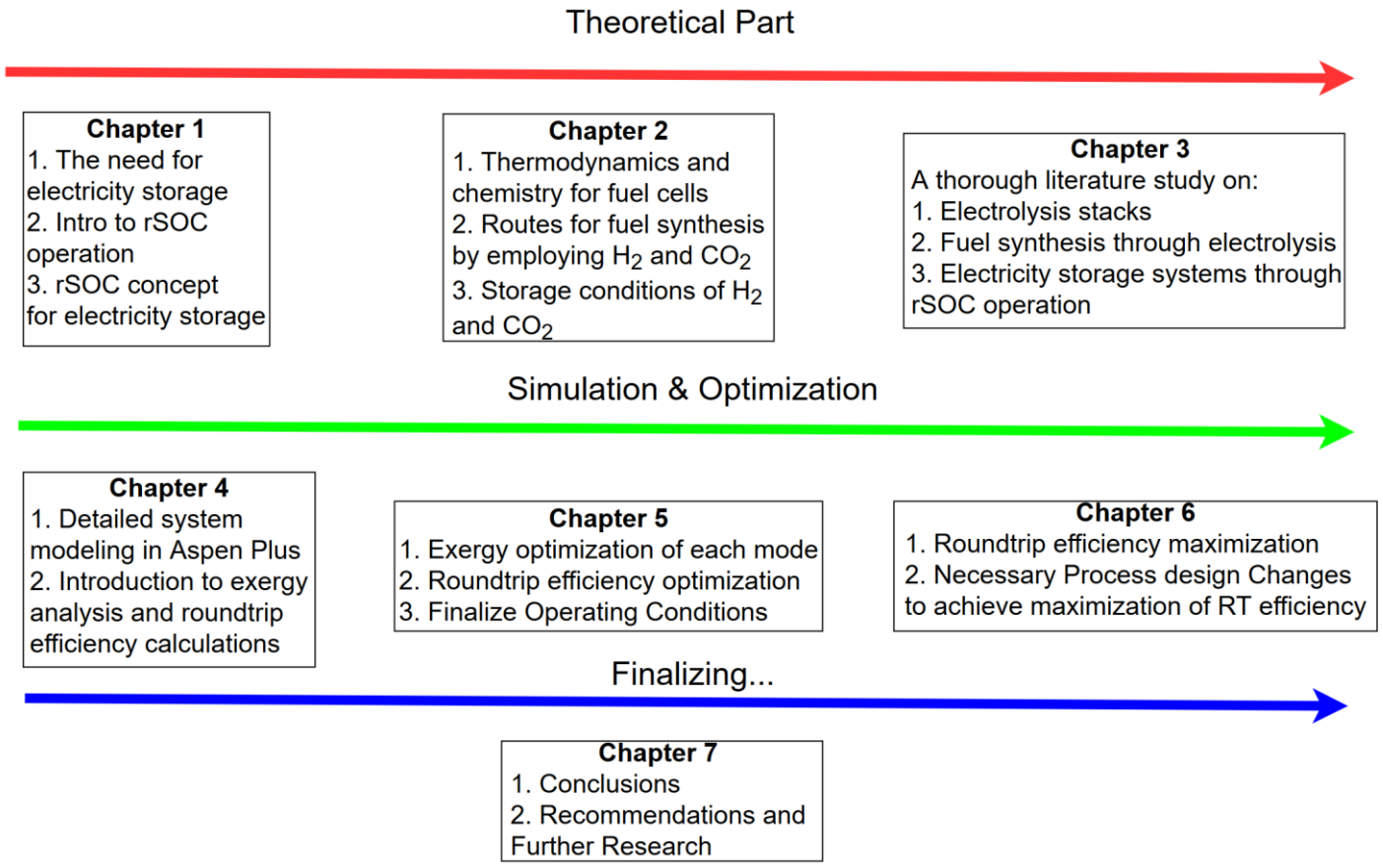

Figure 1-4: Thesis Outline

CHAPTER 2

THERMODYNAMICS OF SOLID OXIDE REVERSIBLE CELL

In this chapter, the necessary theoretical background regarding rSOC operation will be analyzed. Before moving on, the reader should be familiar with the fact that either in electrolysis or in fuel cell mode, every cell operates at a specific cell voltage, V_{cell}, while each cell, as well as the whole stack, is run through current I. This happens because it will be assumed that the cells are connected in series which is the most prevalent scenario. Dividing this current with the total electrode area, the current density is defined:

$$i = \frac{I}{A_{tot}} \quad \text{Eq. (2-1)}$$

The total power produced (or power expended), P_{stack}, in either fuel cell or electrolysis mode is given as:

$$P_{stack} = N_{cell} V_{cell} I = N_{cell} V_{cell} i A_{cell} \quad \text{Eq. (2-2)}$$

where N_{cell} is the number of cells and A_{cell} is the cell active electrode area

2.1 Electrochemical Oxidation of Hydrogen

Starting with the basic thermodynamics for fuel cells, a solid oxide fuel cell (SOFC) fed with pure hydrogen (H_2) will be considered. During this process, hydrogen is electrochemically oxidized to steam with simultaneous production of electricity and heat. The final reaction can be summarized as follows:

$$\frac{1}{2}O_2 + H_2 \rightarrow H_2O^{+\,electricity}_{+\,heat} \quad \Delta h = -248\ \text{KJmol}^{-1}\text{[9]}$$

Ideally, the process should convert the chemical energy of hydrogen into electricity. Due to thermodynamic limitations, if the reaction enthalpy (ΔH) of the above reaction represents the converted chemical energy, then the maximum amount of electricity produced is equal to the change in Gibbs free energy (ΔG), while their difference represents the reversible heat generation, denoted as $T \cdot \Delta S$. To sum it up:

$$\Delta G = \Delta H - T \cdot \Delta S \quad \text{Eq. (2-3)}$$

During this process, one mole and a half of reactants are converted to one mole of products, thus reducing the total number of moles. To compensate for this reduction in the number of species, a reversible heat generation term $T \cdot \Delta S$ appears [21]. Figure 2-1 depicts the abovementioned magnitudes as a function of temperature. It can be observed that at higher temperatures, reversible electricity production is lessened, while larger amounts of energy are liberated in the form of high-temperature heat. On the other hand, this high-temperature can be utilized for further heat integration and increase of exergy efficiency. In contrast, even if low-temperature heat can be integrated in the system, the exergy efficiency will not increase substantially.

When the fuel cell operates reversibly, the cell voltage is equal to the reversible voltage. The reversible voltage is defined as [8]:

$$V_N^0 = \frac{|\Delta G|}{zF} \quad \text{Eq. (2-4)}$$

where z refers to the number of electrons transferred per fuel molecule, and F is the Faraday constant (96485 C/mol). The Faraday constant contains the electric charge of 1 mol of electrons.

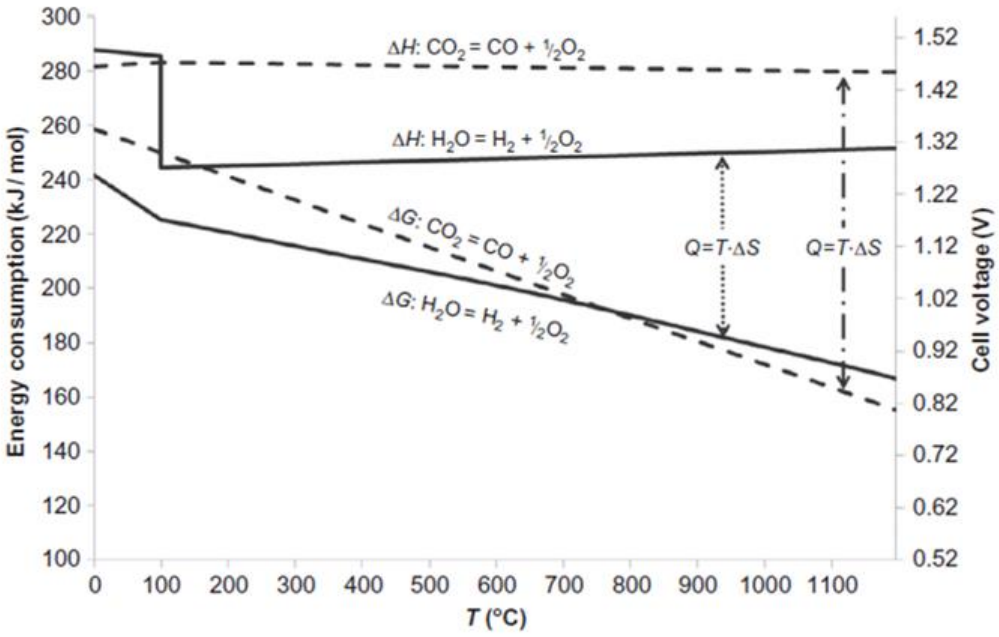

Figure 2-1: Electricity and Heat demand for idealized CO_2 and H_2O electrolysis reactions. At high-temperature electrochemical oxidation, more heat must be removed resulting in more opportunities for heat integration. At higher temperature electrolysis more energy can be provided as heat.

In the case of a rSOC, it can be seen from the chemical reactions provided in Chapter 1 that two electrons are transferred for each fuel molecule. Reversible voltage is also dependent on stream composition at both electrodes. Increasing the pressure also has a distinct effect on the reversible voltage as shown below [8], [9]:

$$V_N = V_N^0 + \frac{RT}{zF}\ln\left[\left(\frac{x_{H_2}x_{O_2}^{\frac{1}{2}}}{x_{H_2O}}\right)\left(\frac{p}{p_0}\right)^{1/2}\right] \quad \text{Eq. (2-5)}$$

where x_i is the mole fraction of component i, V_N^0 is the reversible voltage given by Eq. (2-4), p is the stack pressure while p_0 is the reference pressure and R is the ideal gas constant (R=8.31451 J/mol·K). In this study, the reference conditions are set to be at a temperature of 298.15 K and a pressure of 1 atm.

By observing Eq. (2-5) one can infer the following:

- Reversible voltage decreases with an increase of stack temperature in either mode. This observation derives mainly from the thermodynamics of hydrogen oxidation/steam electrolysis (see Figure 2-1)
- Increase of hydrogen content results in an increase of the reversible voltage, while the opposite happens with steam content. In electrolysis mode where steam content is higher than hydrogen content, a lower reversible voltage occurs. The situation is reversed in fuel cell mode
- An increase in oxygen content in either mode results in an increase of reversible voltage. This increase is less due to the 0.5 exponent associated with oxygen mole fraction

- An increase of system pressure is also associated with an increase in reversible voltage

In reality, when operating in fuel cell mode, the cell voltage is lower than reversible voltage. This overpotential accounts for thermodynamic irreversibilities (losses) of the system [8]. Therefore, fuel cell operation is no longer reversible [3]. In short, three categories of losses have been identified as they are all summarized in the following equation.

$$V_{cell} = V_N - V_{act} - V_{ohm} - V_{con} \quad \text{Eq. (2-6)}$$

In the above equation, V_{act} is further supplied to facilitate the charge transfer between the compounds and the electrodes [16]. V_{ohm} includes the ohmic-type of losses due to electrodes, electrolyte, interconnects etc. Lastly, V_{con} accounts for the appearance of diffusion limitations. The diffusion limitation intensifies when reactant concentration at the porous electrode surface is very low [8], [16]. For better understanding, consult Figure 2-2 which depicts a representation of each type of losses. In fuel cell mode, there is a voltage drop in order to initiate the electrochemical reactions. Initiation of reaction is accompanied by an increase of current density. Afterwards, in the ohmic region, voltage reduction is a linear function of current density as suggested by Ohm's law. Finally, at higher current densities where a large portion of reactants has been depleted, concentration losses are increasing rapidly, accompanied with higher voltage drop [16]. For more information on all types of losses, the reader is encouraged to study more from the suggested sources [16], [22], [23]. Finally, the depicted curves (see Figure 2-2) are called *polarization curves* or simply *I-V curves.*

It is observed that at higher temperatures, overpotential losses (i.e. irreversibilities) are lowered as well and more electrical power is produced. From Figure 2-3, it can be observed that by increasing the temperature, all types of losses are lessened. This leads to an overall increase in cell voltage during fuel cell operation. As far as the fuel cell operation is concerned, at high temperatures, reaction rates are increased and therefore, the "slowness" of reaction is reduced. In general, operation at high temperatures leads to faster reaction rates. In addition, at higher temperatures, the electrical resistance of the involved materials is also reduced. Finally, concentration losses also depend on temperature. For example, species diffusion into the active electrode area is facilitated through temperature enhancement because the *diffusion coefficient* increases. In total, even if thermodynamics restrict the reversible voltage at high temperatures, the reduction in all types of irreversibilities can eventually lead to operation at higher cell voltages, compared to low-temperature electrochemical oxidation.

It has been seen that operation at a very low current density (i.e. voltages close to the reversible voltage) is associated with high stack efficiency. Indeed, during fuel cell operation and at low current densities, the overpotential losses are reduced, but on the other hand, power is sacrificed. In fuel cell mode, power produced is given by Eq. (2-2). While it is beneficial to operate efficiently, a compromise between power and efficiency must be made as shown in Figure 2-4.

The difference between reversible voltage and operating cell voltage may be condensed in an equivalent resistance known as *Area Specific Resistance* (ASR).

$$ASR = \frac{V_{cell} - V_N}{i} = \frac{V_{cell} - V_N}{I/A_{tot}} \quad \text{Eq. (2-7)}$$

where i is the current density, I is the total current produced/extracted and A_{tot} is the total active electrode area. ASR is a very important measure in modeling studies. For example, Giglio et al. [24] modeled ASR as:

$$ASR(p,T) = De^{(-BT)}e^{(-Cp)} \quad \text{Eq. (2-8)}$$

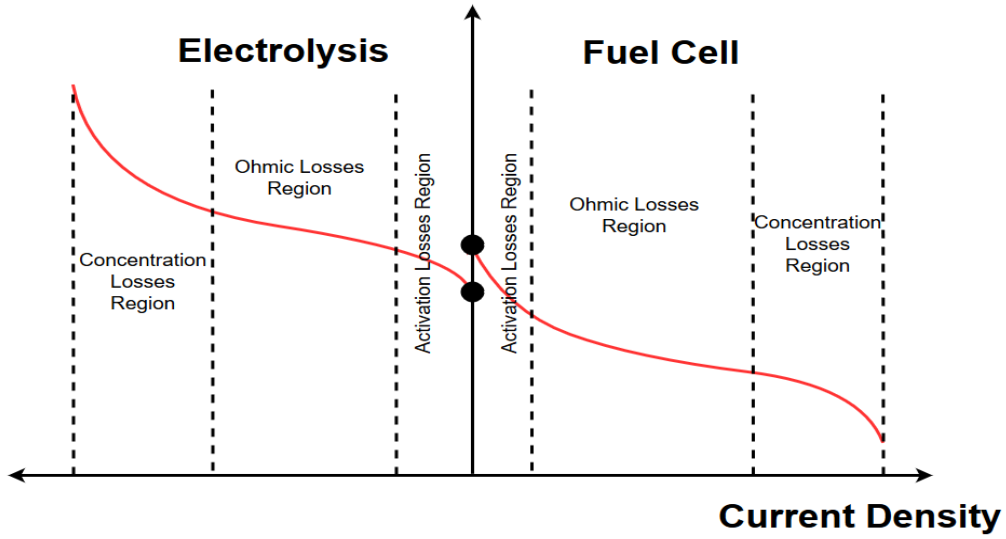

Figure 2-2: Differentiation between electrolysis mode and fuel cell mode - Polarization Curves

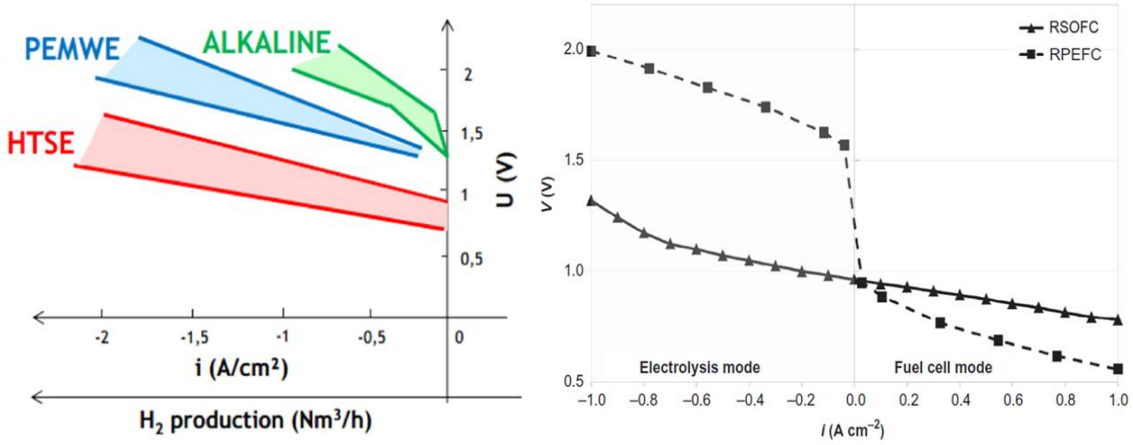

Figure 2-3: (Left) Representation of I-V curves of low temperature and high-temperature electrolyzer, (Right) Representation of I-V curves of low temperature and high-temperature RFCs [3], [8]. Lower temperature is associated with higher overpotential losses

where parameters B, C and D can be found in his work [24]. These models are just approximate while they model an operating *I-V curve* as a flat line. While this does not encapsulate the different operating regions where the individual type of losses occur (i.e. activation losses at low current densities), it gives a very good approximation of the reversible stack operation. In reality, ASR can be accurately found experimentally, but a general approximation like the one proposed by Giglio et al. can be very useful for system modeling. The proposed model of ASR (see Eq. (2-8)) will not be utilized in this study. The model proposed by Hauck et al. [13] will be used instead. This model includes equations for the modeling of each type of irreversibilities.

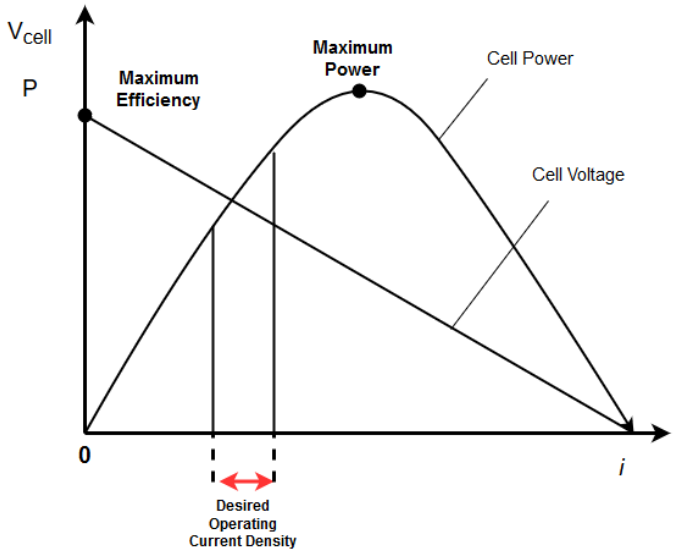

Figure 2-4: Compromise between stack efficiency and stack power

2.2 Oxidation of Hydrogen and Carbon Monoxide Mixtures

In this case, additional reactions take place in-situ as they are shown below:

Steam reforming /Methanation:	$CH_4 + H_2O \leftrightarrow CO + 3H_2$	Δh=226 kJmol^{-1}[9]
RWGS /Water-Gas Shift:	$H_2 + CO_2 \leftrightarrow CO + H_2O$	Δh=41.2 kJmol^{-1}[9]
Dry reforming [6], [8]:	$CH_4 + CO_2 \leftrightarrow 2CO + 2H_2$	
	$CH_4 + 2H_2O \leftrightarrow CO_2 + 4H_2$	

So far, dry reforming has been neglected. It is explained that during fuel cell mode the production of steam mainly promotes steam reforming of methane and if dry reforming occurs, it will be in a small region close to the inlet of the fuel electrode where CH_4 and CO_2 present [6]. In addition studies like [6] do not assume any presence of methane at the stack inlet, eliminating the possibility for dry reforming to take place during fuel cell operation.

A certain amount of H_2 and steam should always be present due to the following technical reasons [6]:

- Avoid nickel degradation
- Avoid large temperature gradients (i.e. by internal steam reforming)
- Inhibit carbon deposition by increasing the steam to carbon ratio. To provide a measure of steam to carbon ratio, a value of 2 is usually sufficient when operating the stack on light hydrocarbons

2.3 Steam Electrolysis

DC electrical current is utilized to split water into hydrogen (H_2) and oxygen (O_2). The overall reaction is [8], [10]:

$$H_2O \xrightarrow[+heat]{+electricity} \frac{1}{2}O_2 + H_2 \qquad \Delta h=248 \text{ KJmol}^{-1}[9]$$

When performing steam electrolysis, pure steam has to be provided in order to avoid degradation and corrosion of the stack. Further concerns encompass reduced lifetime and increased costs. However, due to further research of materials and cell geometries, an increased lifetime, as well as reduced costs, are expected in the forthcoming years [3]. The most prevalent poisonous species for Ni-YSZ is sulfur and it has to be removed thoroughly in any case [16], [25]. Thermodynamically, the steam electrolysis process is determined by using again the reaction enthalpy (ΔH), the change in Gibbs free energy (ΔG) as well as the entropy production term ($T \cdot \Delta S$) for the abovementioned reaction, as explained in Eq. (2-3). The electrical energy provided must be equal to the change of Gibbs free energy while adding the thermal losses of the system, but this is not necessary. The reversible heat addition term appears again due to a non-mole preserving process as it was explained in section 2.1.1. During electrolysis, this portion of energy (i.e. $T \cdot \Delta S$)) can also be compensated by either means of heat or electricity [26]. Figure 2-1 shows that for the water/steam electrolysis, ΔG is decreasing while ΔH remains almost constant when the temperature is varied. As a consequence, the required electricity decreases but the irreversible heat requirement is enhanced as the temperature is increased.

The term ΔG must be necessarily covered through electricity and in this case the cell voltage will be equal to the *Nernst Voltage* (V_N) or *reversible voltage* as shown in Eq. (2-4) [8]. Again, reversible cell voltage corresponds to reversible cell operation but no hydrogen is created yet. In reality, the cell voltage (V_{cell}) will be higher than the idealized reversible voltage when operating in electrolysis mode, leading to increased power consumption and hydrogen generation. In short, three categories of losses have been identified as they are all summarized in the following equation. The physical explanation of each term is the same as it has been explained during fuel cell operation. Examples of polarization curves can be seen at Figure 2-2 & Figure 2-3. Especially in Figure 2-3, the reader can observe reduced power consumption for high-temperature electrolysis, compared to low-temperature electrolysis.

$$V_{cell} = V_N + V_{act} + V_{ohm} + V_{con} \qquad \text{Eq. (2-9)}$$

For steam electrolysis, working temperatures vary in the range of 800-1000°C and pressures from 1-30 bar. The lower power consumption can further be visualized by observing the I-V curves of various types of electrolyzers (see Figure 2-3) [3].

In the case where the thermal losses are also provided by means of electricity, the *thermoneutral voltage* (V_{tn}) is defined as [8]:

$$V_{tn} = \frac{|\Delta H|}{zF} \qquad \text{Eq. (2-10)}$$

where z refers to the number of electrons transferred per fuel molecule, and F is the Faraday constant (96485 C/mol).

2.4 Operating regions for a Reversible Solid Oxide Cell

During fuel cell operation, net heat is generated not only due to reversible electricity generation but also due to the aforementioned thermodynamic irreversibilities and hence not all chemical energy can be converted fully to electricity. This means that the voltage generated during fuel cell operation of a rSOC stack is always less than the thermoneutral voltage (V_{tn}). Due to exothermic reactions when operating in fuel cell mode, the rSOC stack requires cooling in order to ensure its mechanical integrity and durability. This is usually done *via* excess oxidant flow (i.e. air flow) through the oxidant electrode or through internal reforming (i.e. steam methane reforming) [19].

In contrast with the exothermic nature of operation during fuel cell mode, one can distinguish three distinct modes during electrolysis [3], [8]:

- Thermoneutral ($V_{cell} = V_{tn}$): The rSOC stack operates adiabatically. No external heat source is required due to the fact that electricity balances the heat of reaction. Thermal ohmic losses also assist in thermal balance and streams are isothermal along the channels
- Endothermic ($V_{cell} < V_{tn}$): In this mode, heat should be provided to the rSOC stack in order to balance the heat of reaction. An external heat source is necessitated in this case to aid the provision of the $T \cdot \Delta S$ term
- Exothermic ($V_{cell} > V_{tn}$): In this mode, more electricity is provided to the rSOC stack and extra heat generated has to be extracted from the system by providing sufficient flow rates of sweep gas or feedstock flow. This heat is used to preheat sweep gas or feedstock streams

To sum up, heat generation requires: $V_{soec} > V_{tn} > V_N > V_{sofc}$ as it is depicted in Figure 2-5 [19], [27]:

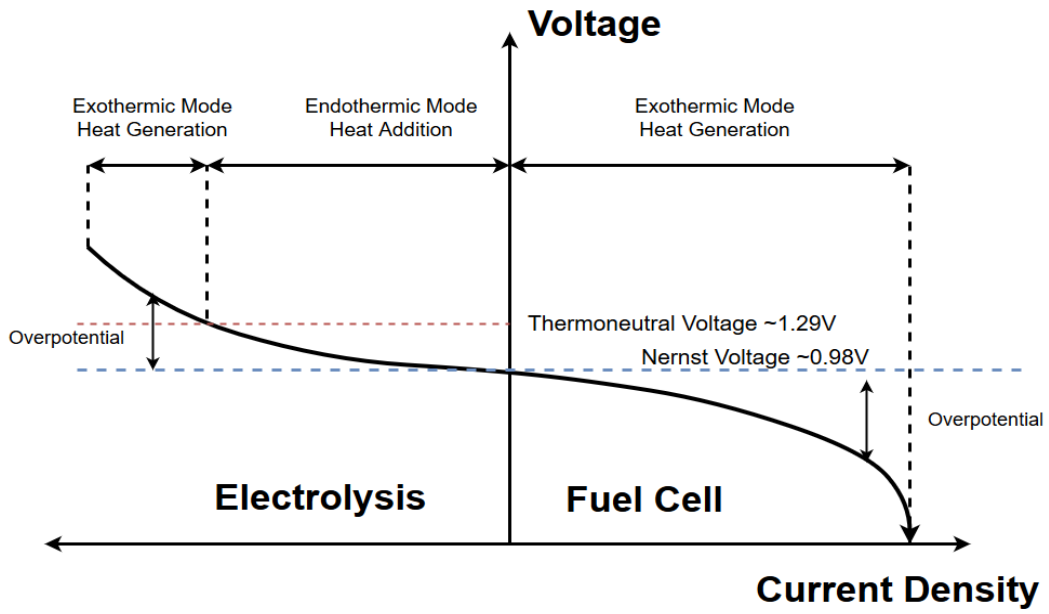

Figure 2-5: Representation of different operating modes in a rSOC

2.5 Useful definitions for thermodynamic evaluation

Another important parameter is the area-specific resistance (ASR) as defined in Eq. (2-7). It can provide information for all types of losses occurring in the cell.

Finally, other useful definitions are [9], [19]:

Stack roundtrip efficiency:
$$n_{RT,stack} = \frac{V_{fc} q_{fc}}{V_{el} q_{el}} = \frac{V_{fc}}{V_{el}} \quad \text{Eq. (2-11)}$$

System roundtrip efficiency:
$$n_{RT,sys} = \frac{V_{fc} q_{fc} - E_{BOP,fc}}{V_{el} q_{el} + E_{BOP,el}} \quad \text{Eq. (2-12)}$$

where q_i is the charge transfer and $E_{BOP,i}$ is the energy generated/provided due to the balance of plant (BOP) components for mode i. The BOP components include all the auxiliary components around the stack which are necessary for the successful plant design. These components include compressors, expanders, heaters, coolers, reactors etc.

Stack roundtrip efficiency is restricted for use only to the rSOC stack. It is the quotient of the energy produced in fuel cell mode and the energy expended in electrolysis mode. For system roundtrip efficiency the effect of BOP in both modes is also incorporated. The numerator expresses the total energy produced in fuel cell mode, while the denominator represents the total energy consumption in electrolysis mode [5], [9], [19]. An important note here is that Wendel et al. [9], [19] defined the cell roundtrip efficiency of both the stack and the system in terms of energy and not in terms of power. In order to ensure repeatable operation (i.e. cyclic operation with the same compositions for each cycle), Wendel stated that the total charge transfer in each mode must be equal (i.e. $q_{el} = q_{fc}$). The equal charge transfer rule as well as Eq. (2-12) will be utilized for roundtrip efficiency optimization which is conducted in Chapter 6.

Ni et al. [12] cite that detailed exergy analysis is an essential tool in order to pinpoint and quantify losses for each component of the plant. Consequently, improvements can be made for those specific components of the plant where thermodynamic irreversibilities are most prevalent. While energy efficiency is useful, a true thermodynamic analysis is better shown by employing the second law efficiency. Exergy quantifies the maximum available work of a substance that can be extracted when reversibly returns from its existing state to environmental conditions. During exergy analysis, a dead state needs to be defined which represents the environment. Exergy analysis determines the flows of potentially produced work or in other words, thermodynamic losses. Consequently, apart from roundtrip efficiency, energy and exergy efficiencies are also important metrics for the thermodynamic evaluation of stacks or systems. More details on exergy analysis and roundtrip efficiency calculation in this work will be given in Chapter 1 and also in Appendix H & I.

CHAPTER 3

LITERATURE STUDY

In this chapter, a literature review of scientific publications relevant to this work is presented in sections 3.1 and 3.2. In section 3.3 a summary and a critical review of sections 3.1 and 3.2 is taking place while an extended literature review can be seen in Table 3-1. Models, decisions and assumptions have been adopted from the literature presented in this chapter, while they have been effectively utilized towards the realization of this modeling endeavor. In section 3.4 a brief review in methanol synthesis will be mentioned. The closure of Chapter 3 contains a few words regarding the storage pressure of H_2 and CO_2 in section 3.5.

3.1 Steam electrolysis – Stacks and Systems

The need for high-temperature steam electrolysis has been identified by researchers many years ago. Doenitz et al. [28] recognized the need for future energy carriers and hydrogen could be a great candidate. They firmly believe that steam electrolysis for hydrogen production at higher temperatures will increase the efficiency of the process, compared to low-temperature water electrolysis. While low-temperature electrolysis efficiency is limited at 25-28%, process modeling studies revealed that high-temperature steam electrolysis can reach efficiencies of 40-50% depending on the primary source of energy.

De Saint et al. [7] proposed a rSOC system with steam electrolysis for substitute natural gas production (SNG) by using ProsimPlus 3™ software. Instead of producing just hydrogen as a fuel, the authors support the production of SNG by mentioning many advantages of SNG in comparison with H_2. Among those advantages, it is the higher volumetric energy density, reduced flammable range and a higher minimum energy to be provided for ignition, thus accounting for safety. In addition, when producing SNG the existing network can be utilized for its transport. Finally, its high versatility (i.e. energy carried, production of other chemicals etc.) makes it a suitable candidate for synthesis. For their modeling attempt, they conducted experiments and used regression methods on the experimental results to derive analytical equations which represent the polarization curves. Those equations were imported in their model. It seems that the higher the steam molar flow rate, the lesser is the steam conversion which results in reduced area specific resistance, mainly due to the drop of concentration losses. The results produce 67.5 Nm^3/h of SNG with a higher heating value of 10.75 kWh/Nm^3 accompanied with a respective 14.4 kWh/Nm^3 energy consumption. The electrolysis step consumes 90% of the total expended electricity. It is reported that higher steam conversion will maximize SNG production with a simultaneous reduction in the energy cost. In addition, an extensive economic analysis is proposed for the system, since the efficiency is much higher compared to a low-temperature system.

Rivera-Tinocco et al. [3], performed a techno-economic analysis of an electrolysis plant for methanol production either by using high temperature (SOEC) or low-temperature water electrolysis (PEM). The model has been realized in Aspen Plus. When performing low or high-temperature steam electrolysis, the reported efficiency values are 45.3% and 54.8% respectively. Despite the lower efficiency of the PEM electrolysis system, methanol cost is deduced to be 891 €/tn, while methanol cost reaches 5459 €/tn when high-temperature electrolysis is employed.

Mcelroy et al. [29] demonstrated also the idea of rSOC by performing experimental work for hydrogen production. The goals of the project were to perform 1000 hours of operation with less than 2% change in voltage (which accounts for degradation) either in fuel cell mode or electrolysis mode. Electrochemical voltage efficiency was also used to evaluate the process. The goal was 70% efficiency at 100 mA/cm^2 and 61.5% efficiency at 200 mA/cm^2. Sixteen cells were made for testing. The goals were achieved while the study showed eight cells achieving above 80% efficiency at 100 mA/cm^2 initially, while all cells tested at 200 mA/cm^2

exceeded 66% efficiency. At 100 mA/cm^2, 7 out of 16 cells achieved the goal of degradation (i.e. 2% degradation at 1000 hours of operation) while only 2 cells achieved the same goal at 200 mA/cm^2. Thermal storage techniques by using phase change materials (PCM) were evaluated, but the small size of the 1 kW stack contributed to the high specific area and high losses of the stack (491 W) rendering the strategy unable to satisfy thermal sufficiency of the stack. For thermal energy storage, lithium fluoride (LiF) was selected as the best choice of PCM since its melting temperature (848^{o}C) is within the optimum range, while it has the highest latent heat of fusion in both gravimetric and volumetric basis. Results concerning the heat losses were obtained by using Aspen Plus, Cosmos Works as well as experimental measurements. Finally, it was concluded that the proposed thermal energy storage is not suitable for this 1 kW stack due to the aforementioned reasons, however, this strategy can be implemented in large-scale systems in order to maintain the working temperature with a stand-alone thermal energy storage system.

Al-Musleh et al. [11] have proposed novel cycles for methane or methanol synthesis. The necessary hydrogen is produced through steam electrolysis while the synthesized molecules (i.e. methane or methanol) are reformed and electrochemically oxidized for electricity production. CO_2 is stored through liquefaction and the need for high-intensity refrigeration cycles. In this work, although the concept of the reversible solid oxide fuel cell is not referred, the concept is still relevant. Roundtrip efficiencies of 54-58% have been reported for the modeled cycles. In this work, no extensive exergy analysis has been conducted in order to identify specific pieces of equipment where there is ample room for improvement. On the other hand, a more complex process design has been employed with maximized utilization of streams through recycling. For example, a heat recovery steam generator (HRSG) has been employed for extra power generation, the produced heat from fuel cell operation is utilized for reforming, while the remaining gas stream after CO_2 separation is recycled back to the stack for enhanced power production. This complexity is justified because the system produces electricity in GWh levels, while the system studied in this work is on the scale of 100 kW. In addition, apart from CO_2 condensation, the authors are also employing condensed CH_4. While evaporation of one substance is facilitated through condensation of the other one, it is expected that condensation of both components at such low temperature (especially methane condensation which takes place at 100K) will induce significant refrigeration loads, which exacerbate roundtrip efficiency.

3.2 Co-electrolysis – Stacks and Systems

Hauck et al. [13] performed rSOC simulations using Aspen Plus. His reported results conclude that at his simulation conditions, the addition of CO_2 in the feed added a positive effect on the performance. In addition, overall performance can be increased by either increase of stack pressure or temperature, while varying inlet composition promotes the efficient operation of one mode and the inefficient operation of the other mode. For example, an increase in hydrogen content is beneficial for the performance of fuel cell mode while reducing the performance during electrolysis operation. The exact opposite behavior is observed when the steam content is enhanced.

Giglio et al. [24], [30] simulated the integration of a SOEC with a methanator for SNG production. System pressure was kept at 33 bar while an energy efficiency of 81.4% is reported. In their financial part of the study, they found that co-electrolysis along with maintenance costs contribute the most to CAPEX and OPEX while carbon capture, degradation, and electrolysis stack cost were also included in the calculations. By increasing the pressure of a co-electrolyzer, the thermoneutral voltage drops due to the presence of methanation which is an exothermic process and is promoted at higher pressures. Being exothermic in nature, it reduces the thermoneutral current density as pressure increases, leading to better thermal management of the stack. The reversible voltage still increases due to the presence of the logarithmic pressure term in the Nernst equation. In his two-part study,

Wendel et al. [27] state the significance of the thermoneutral voltage in increasing roundtrip efficiency. More specifically, it is stated that when the thermoneutral voltage is close to the reversible voltage, it can enhance roundtrip efficiency. In this study, thermoneutral voltage is not only affected by temperature as it is happening in steam electrolysis but because a number of reactions are taking place in the channel the broader definition of thermoneutral voltage is necessitated. For example, the endothermic mode of operation during electrolysis is also accompanied by a methanation reaction which acts as a heat source for electrolysis. In fuel cell mode, methane steam reforming acts as a heat sink for the exothermic electrochemical reactions and therefore providing better thermal management.

Bierschenk et al. [10], came to the same conclusion. Their study again is based on electricity storage *via* co-electrolysis but also on the in-channel formation of methane for improved thermal management and increased roundtrip efficiency. It is evident that by increasing stack pressure, reversible and thermoneutral voltage are closer. They propose rSOC operation at approximately 600°C and 10 bar during the electrolysis step. It is suggested that at low temperature and high pressure when using a carbonaceous fuel inlet, the heat of reaction during methanation can accommodate the endothermic energy supply of the electrolyzer. This means that less resistive heating is necessary to achieve thermoneutral operation. As a result, thermoneutral voltage drops and roundtrip efficiency is enhanced.

Perna et al. [4] in their modeling study of reversible solid oxide fuel cell with co-electrolysis also concluded that methane reforming reaction in fuel cell mode and methanation in electrolysis mode simplify stack thermal management. Moreover, while the temperature range of their study was 700-850°C, it was indicated that the highest stack roundtrip efficiencies are occurring at 700°C. Reported values of stack roundtrip efficiency are 67.7% when operating at 700°C down to 47.2% when operating at 850°C.

Jensen et al. [5] analyzed a rSOC system with CH_4 and CO_2 underground storage. They state that operation at high pressure and low temperature induces good thermal management of the stack and thus increasing roundtrip efficiency. A general rule for methane formation as stated in his work is that it is benefitted at higher pressure, lower temperature and lower H/C ratio (i.e. increased carbon content in feed stream of electrolyzer). Their results also state that methane content has a limited increase when pressure varies from 20 to 50 bar while at lower pressures (<15 bar), carbon deposition is initiated. The more carbonaceous material fed into the system, the more methane is produced, however, entering the coking region should be avoided which appears at an H/C ratio of less than 5.5. Operation at a low temperature (<650°C) is also necessary to avoid coking. A roundtrip efficiency of 70% has been reported in their work.

Alenazey et al. [31] performed experimental studies on anode supported SOEC stack. Experiments were conducted at a constant working temperature of 750°C with various inlet compositions (i.e. varying the ratio $CO_2/(H_2 + H_2O)$). Gas chromatography was employed for measuring the outlet composition after water condensation. The main findings from this work are that the higher the current density the more hydrogen is produced, which is expected. A linear increase of CO_2 conversion is also observed while increasing the current density. This phenomenon suggests that part of CO_2 is converted electrochemically. However, it is pointed out that the main contributor of CO_2 conversion is the effect of the reverse water gas shift reaction which occurs at high temperature. In addition, CO_2 concentration in fuel electrode did not play any significant role in the conversion suggesting that the major CO_2 quantity remains unconverted.

Wang et al. [32] observed that co-electrolysis is an energy-intensive process with limited efficiency. For the alteration of I-V curves and for higher efficiency conversion, they suggest the combination of co-electrolysis with simultaneous partial oxidation of CH_4 which is mildly exothermic. The partial oxidation will provide an extra energy source for the energy-intensive electrolysis, increasing efficiency and lowering applied voltage significantly. Those results were verified through thermodynamic modeling as well as experimental measurements.

Bidrawn et al. [33] performed experimental studies using a SOEC with a ceramic electrode "*based on* $La_{0.8}Sr_{0.2}Cr_{0.5}Mn_{0.5}O_3$ *(LSCM), infiltrated into an YSZ scaffold together with 0.5% Pd supported on 5 wt%*

$Ce_{0.48}Zr_{0.48}Y_{0.04}O_2$". At 1073K a total ASR of 0.36 Ωcm^{-2} was observed while the cell could handle pure CO_2 streams. In this study, it is proven that CO_2 can be reduced with the same efficiency as H_2O.

Leonard et al. [2] presented an Aspen Plus model with co-electrolysis in an electrolysis stack and production of methanol. The operating conditions used are 850°C/1 bar. The co-electrolysis model is validated by comparing data with experiments in similar conditions as proposed by Sun et al. [34] and their results are almost identical. The process flowsheet contains a CO_2 capture plant, a co-electrolysis section, a syngas compression section which leads to the methanol synthesis loop and the final purification step *via* distillation. Methanol synthesis has been modeled in a clever way, including in-situ methanol condensation. According to Bos and Brillman [35], internal methanol condensation will shift the gaseous methanol synthesis equilibrium to the forward direction, promoting its production. Pinch analysis is used to determine the effect of heat integration in power-to-methanol efficiency and a value of 53% is reported whereas an efficiency of 40.1% is reported when no heat integration is applied. The authors concur that by including the CO_2 capture system in the heat integration calculations, further improvement of power to methanol efficiency can be achieved.

Hansen et al. [25] analyzed a co-electrolysis system with possible coupling to methanol or methane production. In both cases, a pressurized stack was used and an LHV efficiency of 74.8-78.1% was reported for SNG production, while 75.8-80.1% was achieved for methanol production. The authors cite that pressurized operation can boost energy efficiency up to 3-4% due to the fact that the syngas compression section is relieved from excessive loads. When large amounts of CO_2 and H_2O are reduced, a major threat for CO_2 deposition takes place. While lower conversion rates are acceptable to avoid CO_2 deposition and increase stack lifetime, increased CO_2 incoming rates will increase catalyst inventory leading to early degradation.

Barelli et al. [36] proposed a system for the production of hydromethane by utilizing co-electrolysis. For hydromethane production, a multistage reactor system is proposed. Hydromethane, a mixture which consists mainly of H_2 and CH_4 is seen as an attractive energy storage option. Aspen Plus has been utilized to evaluate system performance. The system consists of a co-electrolysis and a methanation step. An overall efficiency of 60.2% and a LHV of 21.9 MJ/Sm^3 is reported. Another case study which involves steam electrolysis is worse compared to co-electrolysis resulting in an efficiency of 51.2% and LHV of 19.4 MJ/Sm^3. Finally, it is reported that since hydrogen mole fraction in the final product is in the range of 5-30%, hydromethane could be a potential fuel for transportation applications.

Fu et al. [37] did an economic assessment on producing syngas from high-temperature co-electrolysis for the synthesis of Fischer Tropsch fuels. Their findings report that high-temperature electrolysis has higher conversion efficiency compared to low-temperature (i.e. 87-93% while low-temperature efficiency is lower by 10-15% than previous range). They also reported that at thermoneutral mode, only 4% of total energy input is needed for heat in order to sustain the process. Finally, while the energy associated to provide electricity during electrolysis is a major contributor to the cost, cheap electricity provided by nuclear power plants can reduce the cost of production to 1.02€/l. To reach this competitive cost, it is suggested by the authors that CO_2 will be captured at concentrated sources and also produced O_2 will also be sold.

Ferrero et al. [1] conducted both experimental and simulation studies in a solid oxide reversible cell (rSOC). His model was validated using his own experimental data. It can be observed that his MATLAB model is in agreement with his experimental results. Additionally, it is observed that his data provide the same trend as explained by Kazempoor et al. [6]. The more the hydrogen content, the more beneficial the fuel cell operation and the more polarization losses occur in electrolysis mode, which reduces performance. This behavior is reversed by adding more steam to the feed composition. The developed electrochemical model is validated both from experimental data of the same work but also from I-V curves of commercial cells for H_2/H_2O mixtures [1].

Guan et al. [38] performed a 10 stack rSOC operation over 1000 hours. Hydrogen and methane were used as feed streams for fuel cell mode, while steam electrolysis was performed during electrolysis mode. Materials and electrode microstructure were optimized for reversible operation. In fuel cell mode, the stack ran successfully at a voltage of 0.7 V with 80% fuel utilization and 480 mW/cm^2 power density. During electrolysis

mode, the stack consumed 1.1 kW electrical power and produced more than 6 SLPM H_2. In the duration of the program, degradation rate was reduced down to 200 mΩcm^2/1000 hours. After a detailed cost evaluation, for large-scale hydrogen production, the cost would be approximately 2.7$/kg H_2 which is considered quite competitive.

Ebbesen et al. [39] performed experiments on Ni/YSZ solid oxide cells for co-electrolysis. While it is stated that electrochemical oxidation of both species is happening in-channel, it is also stated that water-gas shift (WGS) equilibrium is reached and CO is produced by means of reverse water gas shift reaction. Impurities on the reactant electrode seem to be the primary cause for cell degradation. Cells operated at 850^{o}C for hundreds of hours while a reported degradation rate of 0.003-0.006mV/h seems to be more than adequate for continuous operation.

Wendel in his Ph.D. thesis [19] thermodynamically analyzed a reversible solid oxide fuel cell system using co-electrolysis for a CH_4-H_2-CO mixture production by utilizing Engineering Equation Solver and gPROMS. A steady-state model for distributed (100 kW) as well as a bulk scale system (> 10 MW) is analyzed. Cost analysis is also performed for the two systems. For system analysis, roundtrip efficiency is considered the most important thermodynamic metric. The target goal of 80% roundtrip efficiency was not achieved, but 74% was achieved instead. According to Wendel, stack theoretical roundtrip efficiency can reach 100% through thermoneutral voltage minimization and operation close to reversible voltage, but practical operation at 5000A/m^2 indicates a RT efficiency of less than 75% which gives room for improvement by lowering cell resistance through material development. Apart from the stack efficiency penalty, the main contributors to increased energy penalty are the water vaporization and condensation step. Energy efficiency is heightened when steam is stored in the vapor phase, instead of condensing it. Additionally, storage compressors employed after the stack for underground storage induce further energy penalty in the process. Wendel indicates that a resistance of 0.2 Ωcm^2 should be achieved at low temperatures in order to enhance efficiency. Stack optimal operating conditions for the bulk scale system are reported to be 680^{o}C and 20 bar. The estimated cost for energy storage is 2.6 c/kWh for the bulk system of 250 MW and 8-11 c/kWh for distributed scale system. Only PHS systems are cheaper than the bulk energy storage system while the energy storage cost for distributed scale system is almost equal to that of red-ox batteries. Those results suggest that employment of reversible solid oxide systems can be a viable alternative for energy storage in the future.

3.3 Summary of Literature Review

From the literature review, the following conclusions can be drawn. A summary of an extended literature review can also be found in Table 3-1

- Doenitz et al. [28] and Fu et al. [37] support the use of high-temperature electrolyzers because they are more efficient than low-temperature electrolyzers. This is one of the reasons why in this project, high-temperature rSOCs are employed
- Guan et al. [38] performed testing on a 10 stack rSOC for over 1000 hours. Operation in either electrolysis or fuel cell mode has also been conducted for over 1000 hours by McElroy et al. [29] with less than 2% change in voltage, which accounts for cell degradation. Additionally, in their work, Ebbesen et al. [39] operated cells for hundreds of hours at 850^{o}C while the measured degradation rate was minimum (i.e. 0.003-0.006mV/h). While long term operation of reversible solid oxide fuel cells has not been proven yet, there is a considerable amount of scientific literature towards that direction
- For this study, the elaborate model of Hauck et al. [13] has been utilized for the modeling of each type of irreversibility. The same model has been utilized for electrolysis and for fuel cell operation as well. For the process modeling of the electrolysis stack, the model of Rivera-tinoco [3] was employed, while for

fuel cell operation, the model used by Barelli et al. [36] was implemented. The models will be analyzed in Chapter 4.

- When it comes to stack studies, more studies are referring to high-temperature co-electrolysis instead of steam electrolysis [4], [5], [10], [24], [27], [30]. A possible reason for that might be the fact that the lack of any heat sink/source such as methane steam reforming/methanation will lead to decreased roundtrip efficiencies. Even though in steam electrolysis roundtrip efficiency can be increased when operating closer to reversible voltage, the constant value of the thermoneutral voltage at a given temperature means that in order to operate close to reversible voltage, the heating requirement is enhanced. Apart from methanation, which can act as a heat source during co-electrolysis, Wang et al. [32] suggests the partial oxidation of methane as a heat source for the endothermic more of electrolysis. When electrolyzers are employed to produce synthetic fuels, Fischer-Tropsch fuels, SNG, Methanol, and DME have been investigated
- Authors who carried out simulation studies for fuel production prefer mainly pressurized stack operation not only due to the higher efficiencies that higher pressures can bring to the stack level but also due to the fact that pumping water results in lower CAPEX and OPEX rather than hydrogen/syngas compression after the stack. Generally, high pressures are induced by thermodynamics in all synthesis process synthesis routes according to Le Chatelier's principle and reaction stoichiometry
- Reversible solid oxide fuel cell stacks have already attracted attention for experiments, but thermodynamic system analysis of rSOC for electricity storage has mostly attracted attention of the research community in the last five years
- The research community is still uncertain about the oxidation/reduction of CO/CO_2 species while the dominant opinion is that CO/CO_2 conversion is mainly achieved through the WGS/RWGS route and not electrochemically. Ebbesen et al. [39] state that although CO oxidation is occurring in the channel, CO equilibrium composition is also been reached through reverse WGS. Alenazey et al. [31] pointed out that during SOEC operation CO_2 was reduced mainly due to reverse WGS. In addition, CO_2 concentration in fuel electrode did not play any significant role in the conversion suggesting that the major CO_2 quantity remains unconverted. On the other hand, Bidrawn et al. [33] found that CO_2 can also be efficiently reduced. In the present work, CO oxidation has been omitted and only the effect of H_2 oxidation and the effect of WGS/RWGS have been taken into account.
- Steam electrolysis or co-electrolysis for the ultimate goal of methanol synthesis has been only employed in these journal publications [2], [3], [25]. The concept of electricity storage *via* high-temperature electrolyzer-fuel cell operation with intermediate methanol synthesis has only been realized by Al-Musleh et al. [11]. Consequently, there is a gap of knowledge in rSOC to methanol systems for electricity storage. There have been no studies concerning the energy and exergy efficiency of each mode of operation separately in rSOC to methanol systems. The current thesis aims to provide more information about the system performance towards that direction
- Roundtrip efficiency for the rSOC-methanol case has only been examined by Al-Musleh et al. [11]. The process modeling adopted in the present work is simpler compared to that of Al-Musleh et al. mainly due to the fact that the power scale of this system is small (~100 kW). In contrast, energy and exergy analysis for this system as well as coupled modes of operation *via* a thermal energy storage system has never been proposed for the specific system. Consequently, thermodynamic analysis of the specific system from a different perspective and process changes towards a more efficient energy storage system summarize the novelty of this work
- In Chapter 6, a heat storage system will be necessitated for the enhancement of rountrip efficiency. The main inspiration of this heat storage system is derived from the work of Wendel [19]. Apart from high cell voltage during fuel cell operation and low cell voltage during electrolysis operation, the heat storage system will minimize the sweep gas flow rate during electrolysis mode which is detrimental for energy,

exergy and roundtrip efficiency as it will be explained in Chapter 5 & 6 of the present work. McElroy et al. have also been experimenting with latent heat storage materials such as LiF [29] in order to enhance system performance. While in small power scale systems (i.e. 1 kW) the large specific area induces a large percentage of heat losses, it was concluded that at a higher power scale system the strategy could potentially be effective since the specific area will be reduced, along with percentage heat losses from the latent heat storage system

- De Saint et al. [7] reported that electrolysis consumes 90% of the total electricity expended. Hansen et al. [25] achieved LHV efficiencies in the range of 75.8-80.1 for methanol production. A power-to-methanol efficiency of 53% has been achieved by Leonard et al. [2]. Those efficiency numbers will be compared with the results from the present work in Chapter 5
- When hydrogen content is enhanced during fuel cell mode, the beneficial operation in terms of power production has been observed [1], [13]. The same behavior takes place when steam content is enhanced when operating in electrolysis mode. Those observations are in accordance with theory. The results of the current work, which are presented in Chapters 5 & 6 are also in accordance with the aforementioned observations and the theory explained in Chapter 2

Table 3-1: A summary of existing literature study on electrolyzers, fuel synthesis systems through electrolysis and reversible solid oxide fuel cell systems for electricity storage

Unit/Groups	*Software*	*Field*	*Ref*
		EUROPE	
Politecnico Di Torino	Matlab	rSOC operation: Experimental and modeling study on Ni/YSZ supported cells in both modes	[1]
	Aspen Plus	Evaluation of alternative ways of producing SNG coupled with either steam electrolysis or co-electrolysis – Economic evaluation	[24], [30]
University of Perugia	Aspen Plus	System modeling: Integration of SOEC and methanation for production of hydromethane	[36]
University of Liege	Aspen Plus	Modeling study for electricity storage, from power to methanol	[2]
Mines, Paris Tech	Aspen Plus	Techno-economic analysis of power to methanol system by utilizing either co-electrolysis or steam-electrolysis	[3]
University of Cassino	Aspen Plus, numerical modeling	Performance assessment of rSOC for energy storage based on co-electrolysis	[4]
Technical University of Denmark	-	Energy storage system by utilizing rSOC and underground storage of CO_2 and CH_4- Storage Cost Estimation	[5]
	Mathematical	Modeling on co-electrolysis for syngas production. Discussion on the suitability for FT or SNG synthesis	[40]
	-	Thermodynamic analysis on coupling SOEC with DME production	[34]
	Suite Pro/II	Thermodynamic model analysis of CO_2 capture technology, high-temperature co-electrolysis and SNG production followed by economic analysis	[41]
	-	Experimental investigation of Ni/YSZ solid oxide cells for co-electrolysis	[39]
Haldor Topsoe, Denmark	Topsoe Software	High-temperature co-electrolysis system with coupling to methanol or methane production	[25]
University of Grenoble	ProsimPlus 3	Parametric study for an efficient integration of steam electrolysis and SNG synthesis	[7]
CEA, France	-	Experimental study of a button cell, 10 & 25 cell stack for steam electrolysis and co-electrolysis	[42]
	-	2-D multi-physics in-house model for SOEC performance for hydrogen production	[43]

Technische Universitat Munchen	Aspen Plus	A detailed simulation of rSOC	[13]
EIFER, Germany	Aspen Plus	Thermodynamic and economic assessment for FT-fuels by utilization of SOEC	[37]
University of Strathclyde	Matlab/ Simulink	Inverter models for high-quality electrical transformation for rSOC systems	[44]
University of Surrey	-	Dynamic modeling and optimal control of SOEC	[45]
University of Delft	Aspen Plus	System modeling and performance assessment by coupling SOEC and DME synthesis	[46]
		UNITED STATES	
School of Mines, Colorado	Mathematical	An in-depth modeling study on rSOC performance and economic evaluation. rSOC system based on co-electrolysis –Techno-economic analysis also conducted	[6], [9], [19], [27], [47]
	Mathematical	Modeling of Fischer-Tropsch production chain using high-temperature co-electrolysis – Economics also evaluated	[48]
	Mathematical	Performance assessment of rSOC – High detailed analysis of different irreversibilities in the stack	[49]
University of Illinois	-	Thermodynamic modeling and preliminary experiments for rSOC energy storage application	[10]
Purdue University	Aspen Plus	A novel electricity storage system using rSOC: From Power to Methane or Methanol	[11]
Northwestern University	-	Thermodynamic modeling and preliminary experiments for rSOC energy storage application	[50]
University of South Carolina	-	Experimental study on syngas production by a combination of SOEC and partial methane oxidation	[32]
University of Pensylvania	-	Experimental studies on CO_2 using SOEC with a ceramic electrode "*based on* $La_{0.8}Sr_{0.2}Cr_{0.5}Mn_{0.5}O_3$ *(LSCM), infiltrated into an YSZ scaffold together with 0.5% Pd supported on 5 wt%* $Ce_{0.48}Zr_{0.48}Y_{0.04}O_2$*".*	[33]
Columbia University	-	Thermodynamic study of high-temperature co-electrolysis – including energy and exergy analysis	[51]
	-	In-depth technical and economic analysis of methane-based rSOC	[52]
Department of Energy, USA	-	Experimental investigation of rSOC for long-term operation. Materials and electrode structure optimization for low degradation	[29], [38]
		ASIA	
KACST, Saudi Arabia	-	Experimental study on syngas production from co-electrolysis	[31]
UMPEDAC, Malaysia	Mathematical	Modeling of a novel system employing parabolic trough solar collectors, photovoltaic panels and rSOC for cogeneration purposes	[53]
University of Hong Kong	Mathematical	Parametric study of a high-temperature steam electrolyzer	[54], [55]
	Mathematical	Energy and exergy analysis of a high-temperature steam electrolysis	[12]
Shanghai Institute of Applied sciences	-	Experimental characterization of a cell during co-electrolysis by varying current density and inlet composition	[56]
Energy System Research Institute, Japan	-	Experimental investigation of rSOC as a standalone system or coupled with Mg-based metal hydride for hydrogen storage	[57]

3.4 Methanol Synthesis

Since methanol is the main chemical produced in the process chain, some more details will be given. The produced hydrogen from electrolysis can be combined to form methanol *via* the following main reactions [58]–[60]:

$$CO + 2H_2 \leftrightarrow CH_3OH \qquad \Delta H_R^0 = -90.7 kJ/mol_{CO}$$
$$CO_2 + 3H_2 \leftrightarrow CH_3OH + H_2O \qquad \Delta H_R^0 = -49.5 kJ/mol_{CO_2}$$
$$CO + H_2O \leftrightarrow CO_2 + H_2 \qquad \Delta H_R^0 = -41.2 kJ/mol_{CO_2}$$

Methanol is a very important commodity in the chemical industry mainly serving the role of either an intermediate product or transportation fuel [61]. Apart from those uses, methanol is also widely used as a solvent and as an energy storage medium. Methanol is an interesting candidate for synthesis since its energy density is quite high (either specific, 19.9 MJ/kg or volumetric energy density, 18.2 MJ/l) and therefore lower cost is associated with building storage tanks. In addition, its stability at environmental conditions facilitates storage and transportation, while its conversion to electricity can be achieved by using a combination of methanol steam reformer and fuel cell. Methanol synthesis *via* renewable energy technologies can close the carbon loop and scientists have envisaged the "Methanol Economy" where methanol will play a highly important role in the energy sector [2], [60]. As can be seen, the main reaction for methanol synthesis is an exothermic equilibrium reaction, therefore for its realization lower temperature is required in order to achieve a higher equilibrium composition in methanol. High pressure induces elevated equilibrium yield due to reaction stoichiometry and Le Chatelier's principle. In reality, pressures up to 50-100 bar and temperatures up to 490-560 K are used over a $Cu/ZnO/Al_2O_3$ [61]. Copper is also used as a catalyst for the direct conversion of CO_2 to methanol [25]. The catalyst provides fertile ground for an above 99% selectivity during conversion. Being exothermic by its nature, effective heat removal is necessitated, giving process engineers an extra source of heat for heat integration [61]. In the past, methanol was used to be produced at pressures close to 250-300 bar (BASF Germany, 1923), but due to lower operational cost, improvements on sulfur removal from syngas and developments in employing more active and cheaper catalysts, those very high pressures were replaced by the typical pressures mentioned before [61], [62].

Methanol synthesis reactors must provide a high reaction rate and high heat removal rate simultaneously [63]. Reactors for this process are categorized into adiabatic and isothermal reactors. Adiabatic reactors consist of multiple beds incorporated in one shell. They are cooled through cold gas shots by using the so-called *longzenes*. In this reactor scheme, the heat of reaction is captured, but the maldistribution of catalyst inside the beds can create large temperature gradients resulting either in high or low conversion to methanol. By combining the catalyst maldistribution and the unstable temperature profile of this type of reactor (i.e. sawtooth profile), temperature gradients are enhanced leading to reduced catalyst lifetime and activity [63]. Overall, regulating the reactor temperature of the adiabatic reactors is more difficult than tubular reactors, but the construction is simple. Lower conversion rates demand higher recycle flows and therefore higher compression cost. Isothermal reactors usually ensure higher methanol productivity, longer catalyst lifetime, lower byproducts and more economic operation since it includes a less intense recycle loop. The most commonly used type of isothermal reactor is the Lurgi reactor, which is similar to a shell and a tube reactor. The catalyst is placed in the tubes and water-steam acts as the cooling medium, which is placed in the shell. Temperature profiles are regulated through steam pressure adjustment. The produced steam can be reused in downstream processes such as the distillation process [64]. A process schematic regarding various cooling options for methanol synthesis reactor is provided below (see Figure 3-1). In the current thesis, a plug-flow reactor model will be utilized for the methanol synthesis, as it is the closest one to the tubular reactor. Regarding the kinetics of methanol synthesis, there is quite some ambiguity since different mechanisms have

been proposed for different feed compositions and process conditions. Generally the most predominant opinion is that methanol is produced mainly through CO_2 hydrogeneration [64], [65] but on the other hand Graaf et al. [66] state that CO hydrogenation has to be taken into account. Olah et al. [65] state that when CO is present before methanol synthesis, a water-gas shift reactor should be implemented first so that CO is converted to CO_2 before it is fed to the reactor. According to stoichiometry, CO requires 2 moles of H_2 in order for methanol to be produced, while CO_2 requires 3 moles of H_2, therefore it is believed that CO_2 hydrogenation to methanol is more expensive than CO hydrogenation [65]. Kinetics of the methanol synthesis system have been studied extensively in the literature for the last 45 years [66]–[73].

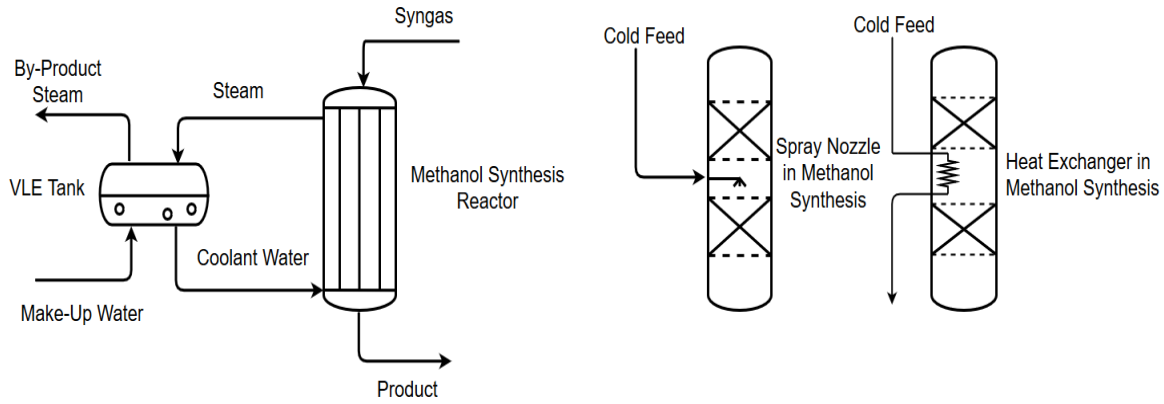

Figure 3-1: Cooling options during Methanol Synthesis (Left), Steam Production and utilization, (Right) Cooling through spraying or heat exchanging

Another aspect of methanol synthesis is the optimum feed composition. It has been agreed that the stoichiometric number $M = \frac{\dot{n}_{H_2} - \dot{n}_{CO_2}}{\dot{n}_{CO} - \dot{n}_{CO_2}}$ should slightly exceed 2. Hydrogen is the limiting compound. If the stoichiometric ratio is below 2, then conversion rates are declining. On the other hand, stoichiometric ratios way above 2 will lead to enhanced recycle streams and recycle train operation expenses. Therefore, to attain reasonable recycle loads and maximize selectivity the stoichiometric ratio should be slightly above 2. In the case where only H_2 and CO_2 are provided to the methanol synthesis reactor, a mole ratio of H_2/CO_2=1/3 is equivalent to M=2 [63]. Recycle stream of the product is necessary since carbon conversion for a unique pass is in the range of 50-80% [35], [63].

In the current work, a sensitivity analysis will be performed in order to examine the effect of methanol synthesis pressure and temperature on system performance. The pressure and temperature in this sensitivity analysis range from 50-150 bar and 460-540 K respectively. In any case, a stoichiometric number of 2 is always utilized which ensures the maximization of methanol production. For the maximization of carbon conversion, a recycle loop has also been employed in this study. Finally, the kinetics from Van de Bussche and Froment have been incorporated in the reactor model [67]. These kinetic equations for methanol synthesis are based on CO_2 hydrogenation.

3.5 Storage of Carbon Dioxide and Hydrogen

In the present work, storage of chemicals is also considered important since it will influence thermodynamic efficiencies. Gaseous storage is expected to occupy more space and therefore more capital cost, but on the other hand liquefaction of gases such as H_2 and CO_2 demand the application of very low temperatures or very high pressures resulting in the use of intense refrigeration systems and higher operational cost. A brief summary of storage methods for CO_2 and H_2 is mentioned.

Comparing hydrogen and hydrocarbons, it can be seen that on a mass basis hydrogen has a larger specific energy density of 142 MJ/kg compared to approximately 47 MJ/kg for liquid hydrocarbons. However, this comes at a cost of the necessary volume for storage needed since hydrogen is an ultra-low density gas compared to liquid hydrocarbons (i.e. 1 kg of hydrogen occupies $11m^3$ at ambient conditions) [74], [75]. Hydrogen storage requires either very low temperatures since its boiling point is 20.3 K at atmospheric pressure. Hydrogen can also be stored as a gas at high pressures (~700bar) and ambient temperature [76]. It has been stated that compression at higher pressures consumes half the energy compared to cryogenic techniques. Standard pressures for hydrogen storage are between 100-200 bar.

Captured carbon dioxide can be stored efficiently by pressurizing it at 80-150 bar. In that pressure range, it is a liquid with 900 kg/m^3 density [77]. Another way is its liquefaction which happens at low temperatures (-78.46^{o}C) [78].

In the current thesis, pressurized hydrogen and carbon dioxide will be employed. Sensitivity analysis has been carried out for the storage pressure of both components (i.e. 100-700 bar for hydrogen, 80-160 bar for CO_2). However, the results of this sensitivity analysis have been omitted in Chapter 5 & 6, because there are not any substantial variations in the examined efficiencies.

CHAPTER 4

SYSTEM MODELING IN ASPEN PLUS

In this chapter, an overview of the process design of each mode of operation is given. Then each mode of operation is explained in detail along with its corresponding model. Aspen Plus is utilized for process modeling. Each block, represents a unitary function, such as compressor, turbine, reactor or heater/cooler and by combining blocks the modeler can simulate various process design chains. For heat integration, it is necessary to couple Aspen Plus with Aspen Energy Analyzer. Aspen Energy Analyzer utilizes the pinch technology to determine the minimum hot and cold utility for optimum heat integration. A brief overview on how to work with Aspen Energy Analyzer is given in the introduction of Chapter 5. It is also possible to import manual heat exchanger networks and see their effect on heat integration.

4.1 System Modeling

4.1.1 Electrolysis Mode – Process Flow Diagram

Hydrogen and water are drawn from their respective storage tanks. Initially, the hydrogen which is stored in a highly pressurized storage tank is heated and then expanded in order to generate electricity. Water, which is drawn from its respective storage tank at atmospheric pressure is entering the system. The water is pumped to stack pressure and then it is evaporated at the stack operating temperature before it is mixed with hydrogen. The resulting mixture is entering in the steam electrode. After the steam electrolysis, the outlet stream mainly consists of hydrogen and small amounts of steam, depending on steam utilization. The steam content is condensed and removed from the system and a highly pure hydrogen stream is obtained for downstream processing. The removed water returns to the water storage tank. The hydrogen is then pressurized at methanol synthesis pressure. The CO_2 stream is being drawn from its respective storage tank. In order to exploit its high pressure, the stream is heated up and expanded for electricity production before it mixes with hydrogen. Outlet pressure of CO_2 expander corresponds to the methanol synthesis pressure. Afterwards, the mixture of hydrogen and CO_2 is entering the methanol synthesis reactor. In the reactor effective conversion to methanol takes place. A recycle loop has also been employed in order to enhance the carbon conversion. The recycle loop contains unreacted gases which are recirculated and mixed with the initial H_2/CO_2 mixture. A small purge stream is necessary in order to avoid excessive reactant accumulation in the reactor. The methanol and water content of the product stream is condensed and separated. Dissolved gases in the methanol-water mixture are further removed in a separate flash column. The resulting methanol-water mixture is finally separated in a conventional distillation column in order to obtain high purity methanol. The bottom product, which is mainly water, returns to the water storage tank. The purge gas and the light gases separated from the methanol-water mixture are combusted in an afterburner. The exhaust gases are cooled down in order to exploit the heat of combustion. For the effective removal of produced oxygen during electrolysis, as well as for the balancing of stack thermal requirements, a sweep gas flow is provided. The sweep gas flow is compressed and heated prior to the rSOC stack and afterwards, a small portion is separated in order to provide the necessary oxidant in the afterburner where the combustion of the light gases and the purge stream is taking place. The remaining sweep gas flow is then expanded and cooled down before its exit to the environment. In order to cool down the system, a pump which runs on cooling water has been employed.

A schematic overview of the whole process can be seen in Figure 4-1.

*For the sake of saving space the three stage hydrogen expander has been represented with two stages in Figure 4-1

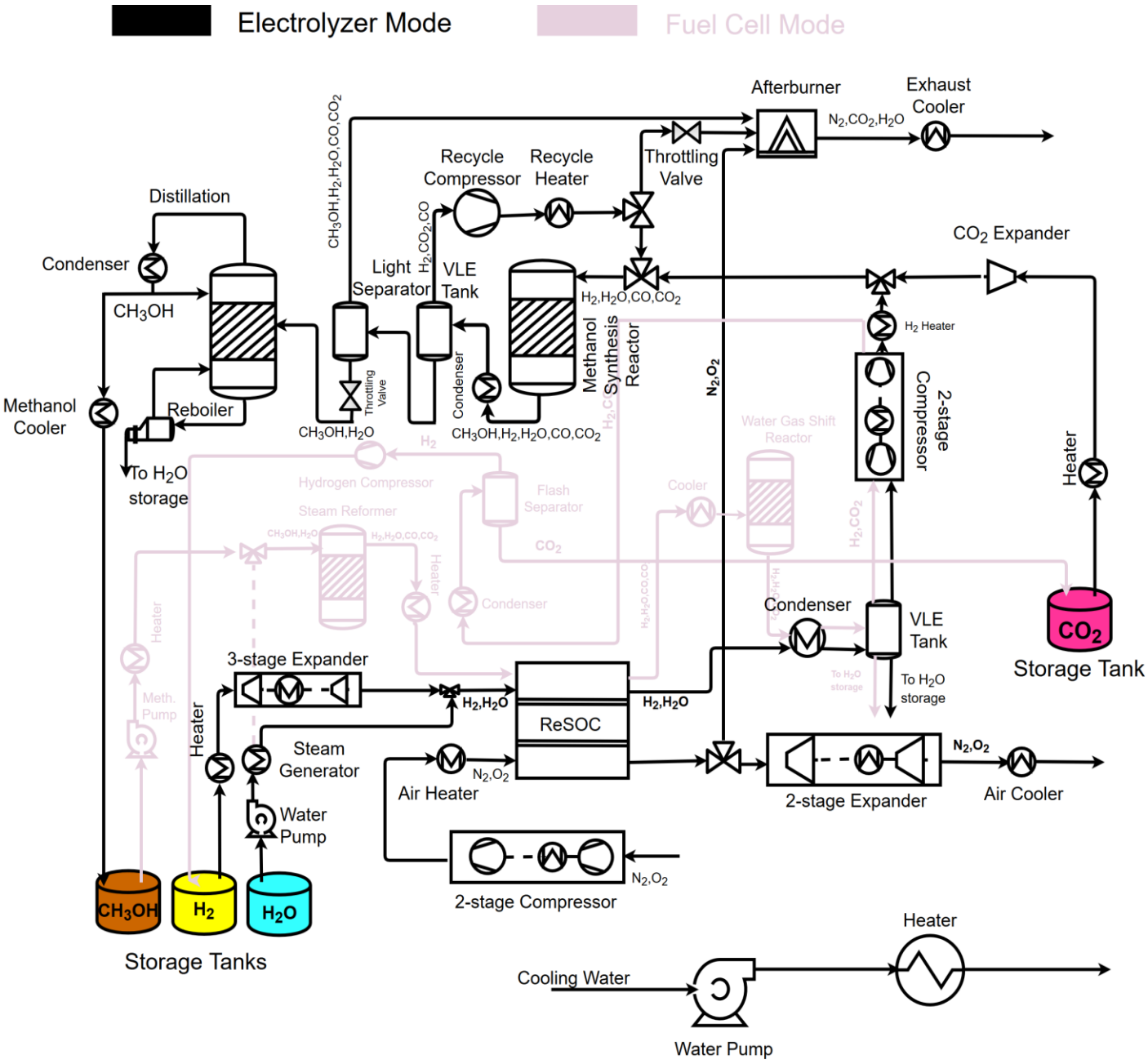

Figure 4-1: Conceptual Process Design of Electrolysis Mode

4.2.1 Fuel Cell Mode – Process Flow Diagram

Initially, methanol and water are extracted from their respective storage tanks. Each stream is separately pumped at stack pressure and evaporated before they mix. The mixture enters the methanol steam reformer at an appropriate temperature and the outlet stream contains mainly H_2, CO_2, CO, and H_2O. This stream is led for electrochemical oxidation and power production in the rSOC stack. The oxidized stream contains again the same components which have to be separated. First of all, the stream is entering a low-temperature WGS reactor where elimination of CO takes place. The remaining steam is then condensed, while the water returns to its storage tank. The resulting stream now consists of H_2 and CO_2. The stream is pressurized to CO_2 storage pressure, while CO_2 condensation takes place at low temperature. After the removal of CO_2 in an equilibrium

tank, the hydrogen stream is further pressurized and led to its storage tank. In order to provide the required oxidant which is used during the electrochemical conversion, as well as for the effective heat removal from the rSOC stack, an oxidant flow is provided. Again the oxidant train includes compression and heating steps prior to the stack, while after the stack the oxidant stream is expanded and cooled down before its exit to the environment. Due to the low temperature of CO_2 condensation, an intense vapor-compression refrigeration system has been utilized. External cooling at above ambient temperatures is also needed therefore a pump with cooling water has been employed in order to cover this extra cooling need. An overview of the system can be seen in Figure 4-2. Although a simplified version of the refrigeration system is shown in Figure 4-2, a more elaborate explanation will follow in the current chapter.

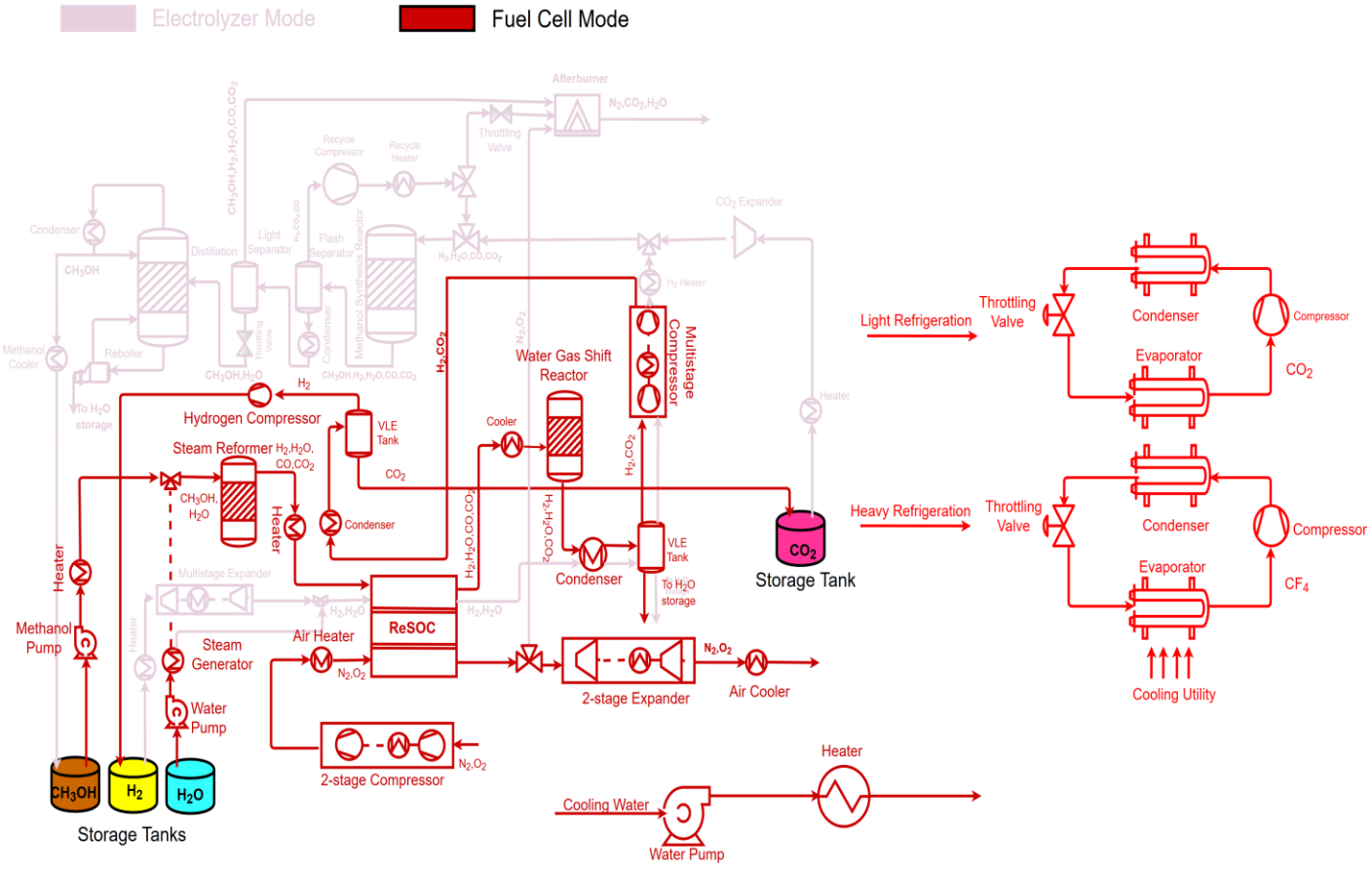

Figure 4-2: Conceptual Process Design of Fuel Cell Mode

4.2 Steam Electrolysis and Methanol Synthesis (Charging Mode)

4.2.1 Electrolysis stack modeling

For stack modeling, the model used by Rivera-Tinoco et al. [3] was employed. The main components of the model are:

- Stoichiometric reactor: In this reactor, the reaction at the fuel electrode takes place with a user-defined steam utilization
- Splitter block: The splitter block is responsible for the separation of oxygen. It substitutes the role of the electrolyte which represents the transport of oxide ions from the fuel electrode to the oxygen electrode.

It is assumed that oxygen is completely separated and transported to the oxygen electrode. The other stream from the splitter consists of a H_2O-H_2 mixture.

- A mixer is used to simulate the mixing of generated oxygen with the sweep gas stream for oxygen removal

Fortran code is employed for the calculation of reversible and thermoneutral voltage. Consequently, the first thing to do was to find the relation between ΔG & ΔH as a function of temperature. According to Eq. (2-3), a change in Gibbs free energy can be calculated when a change of enthalpy and entropy is known during electrolysis. Details of ΔH and ΔS were taken from [23]. A summary is provided in Appendix A. A 2nd order polynomial was regressed on the final plots of ΔG and ΔH in order to maximize accuracy.

In this study, every kind of loss will be modeled separately and plugged into the model. Fortran code was employed to implement the model described by Hauck et al. [13]. This model is elaborated in Appendix B.

As it has already been mentioned in 0, an electrolyzer can either operate in exothermic, thermoneutral or endothermic mode. For example, if there is operation in endothermic mode, apart from electricity, the addition of thermal energy is a prerequisite. In contrast, when operating in exothermic mode, removal of thermal energy is necessitated. For this purpose, a heater block has been incorporated in the system modeling. This block can operate either as a heater or a cooler depending on the type of electrolysis operation (i.e. endothermic or exothermic). For a better understanding of electrolysis stack process modeling, consult Figure 4-3.

For the calculation of heat generation, the electrical power requirement (ΔG) is subtracted from the total energy requirement (ΔH). If the difference is positive, the stack requires additional heat for operation and vice versa. Electrical power consumed is provided by Eq. (2-2) while the total power required (i.e. electrical plus thermal power) is calculated as:

$$P_{total} = \dot{n}_{H_2O,reacting}\Delta H(T) = U_{f,H_2O}\dot{n}_{H_2O}\Delta H(T) \qquad \text{Eq. (4-1)}$$

where U_{f,H_2O} is the steam utilization, $\dot{n}_{H_2O}$ is the inlet steam molar flow rate and ΔH is the molar enthalpy required for steam electrolysis at the specific stack temperature.

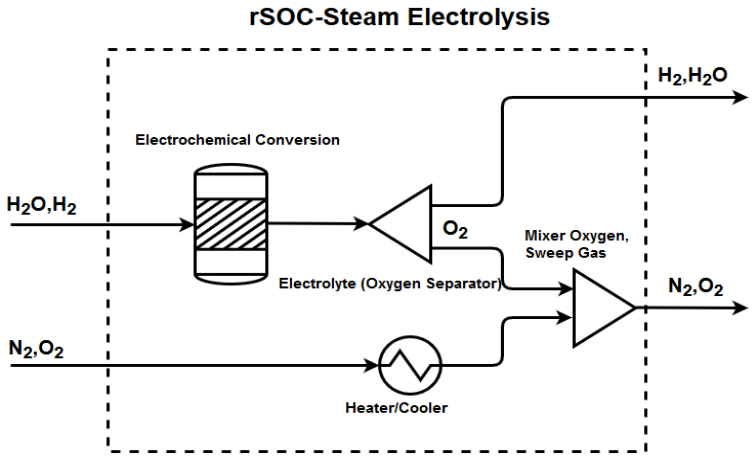

Figure 4-3: Steam electrolysis stack modeling, exothermic/endothermic mode. Exothermic mode – Sweep gas enters the stack at a lower temperature and vice versa

Stack inlet sweep gas stream is initially at temperature $\pm 60^o C$ from the stack temperature, depending on the mode of operation. It is not possible to cool down the stack for example with an air stream which enters the stack at ambient temperature because in reality, stack temperature will drop below the desirable limits due to excessive cooling. This, in turn, results in the disruption and ceasing of electrochemical reactions. In addition,

excessive thermal gradients will induce mechanical integrity problems. A maximum difference of $\pm 200^{o}C$ is used in the study as stated by Wendel [19].

Finally, the Nernst equation (Eq. (2-5)) has been utilized in order to include dependency of reversible voltage on stack pressure and stack feed composition. For I-V and power curves produced by the electrolysis stack, the reader is advised to see Appendix C.

4.2.2 Feed stream preparation to electrolysis

The stack inlet is constituted by mainly steam and a small amount of hydrogen. Both components are drawn from the corresponding storage tanks and they have to be conditioned before entering the stack as shown in Figure 4-4. The model consists of a triple-staged expander at the H_2 side, while a pump and a water evaporator are incorporated at the water side. A certain criterion has been used to select the number of stages during compression and expansion and the reader is suggested to refer to Appendix G.

This model is capable of:

- Conditioning each stream individually before they mix. This means that both hydrogen and steam are entering the stack at stack conditions (i.e. same pressure and temperature)
- Producing electricity by exploiting its high storage pressure by employing a triple expansion stage

The outlet temperature of the three heaters on the hydrogen side is determined in such a way that the outlet temperature of the third expander is equal to the stack temperature. Pressure ratio is equal for each stage for work output maximization. It has to be noted that for water evaporation, a large amount of heat input is necessary.

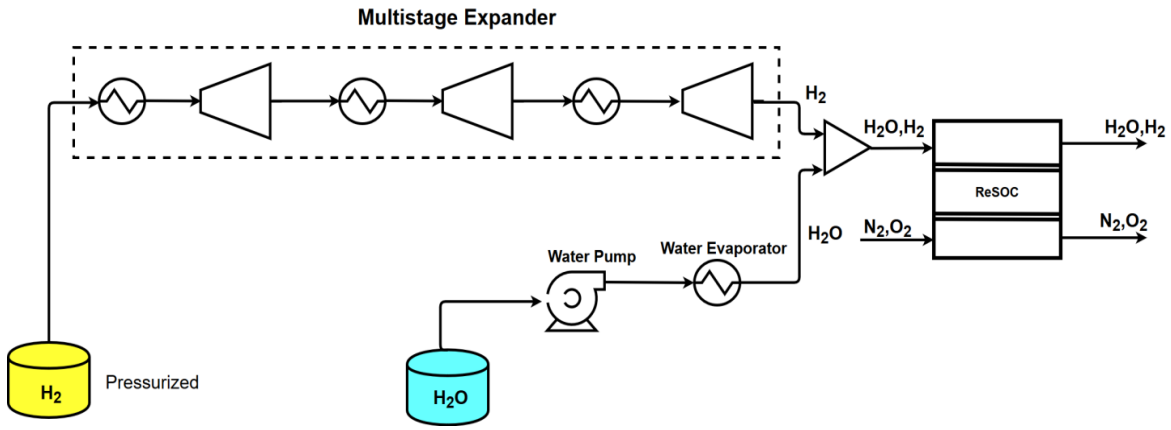

Figure 4-4: Feed stream preparation for steam electrolysis. Pressurized hydrogen is expanded while water is pumped and heated up to desired levels

4.2.3 Feed stream preparation to Methanol Synthesis

Before the methanol synthesis step, the outlet hydrogen-steam mixture has to be conditioned and mixed with a CO_2 stream at appropriate pressure and temperature before entering the methanol synthesis reactor. The model is constituted by a cooler and an equilibrium tank for water condensation and removal, a double staged compressor for hydrogen compression accompanied by a final heater for final temperature tuning. The CO_2 side consists of a single heater and expansion stage in order to exploit the highly pressurized stream and

produce work output, before entering the methanol synthesis reactor (see also Figure 4-5). In summary, this model is able to:

- Successfully recuperate energy from CO_2 expansion and provide the necessary pressure and temperature before the methanol synthesis reactor
- Separate water as much as possible before entry in hydrogen compression and methanol synthesis section. The equilibrium composition of methanol synthesis is negatively impacted by the presence of steam. In addition, the presence of condensed water can damage the compressor blades and reduce equipment lifetime
- Compress and heat hydrogen in order to match the pressure and temperature of methanol synthesis
- Provide CO_2 and H_2 at an optimum ratio (i.e. $H_2/CO_2=3$)

The outlet temperature of the H_2O condenser is regulated in a way that the mole fraction of H_2O in the gas stream is equal to 0.002, while it is ensured that the intercooler temperature does not fall below the dew point of the mixture in order not to cause the formation of condensates in the compression train. A final important note is that CO_2 flow rate is based on hydrogen generation rate. In any case, a molar ratio of $CO_2/H_2=1/3$ is ensured in order to maximize methanol production [63].

4.2.4 Methanol Synthesis Loop

In this section, the mixture of H_2 and CO_2 is effectively converted into methanol in a plug-flow reactor which implements Langmuir-Hinshelwood-Hougen-Watson (LHHW) Kinetics by Van De Bussche and Froment [67]. The equations of the kinetic model and the relevant parameters to be determined are shown below. Because the carbon conversion is low per pass [35], [63], a recycle loop ensures higher carbon conversion. To avoid excessive reactant concentration at the inlet of the reactor, a purge stream has been implemented. Methanol and water are separated through condensation with a subsequent equilibrium tank while the rest of the unreacted gases are being recycled in the recycle loop (see also Figure 4-6).

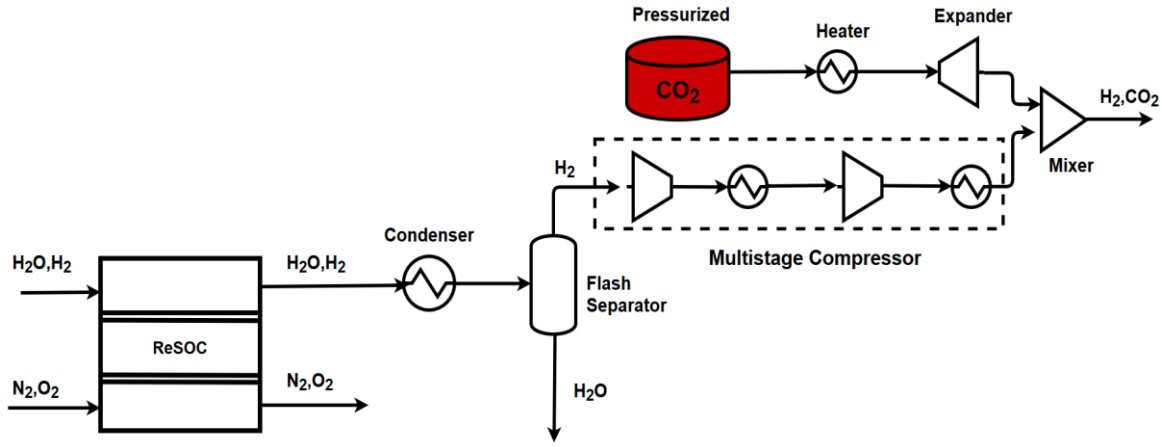

Figure 4-5: Hydrogen compression and mixing with CO_2 feed stream-Preparation to methanol synthesis. Prior to hydrogen compression, water is removed through condensation

The kinetic model is summarized in the two following equations:

$$r_{MeOH} = \frac{k'_{5a}K'_2K_3K_4K_{H_2}p_{CO_2}p_{H_2}[1-\left(\frac{1}{K^*}\right)\frac{p_{H_2O}p_{CH_3OH}}{p_{H_2}^3 p_{CO_2}}]}{(1+\frac{K_{H_2O}}{K_8K_9K_{H_2}}\frac{p_{H_2O}}{p_{H_2}}+\sqrt{K_{H_2}p_{H_2}}+K_{H_2O}p_{H_2O})^3} \quad \text{Eq. (4-2)}$$

$$r_{RWGS} = \frac{k'_1 p_{CO_2}[1-K_3^*\frac{p_{H_2O}p_{CO}}{p_{CO_2}p_{H_2}}]}{1+\frac{K_{H_2O}}{K_8K_9K_{H_2}}\frac{p_{H_2O}}{p_{H_2}}+\sqrt{K_{H_2}p_{H_2}}+K_{H_2O}p_{H_2O})} \quad \text{Eq. (4-3)}$$

where expressions of all k-values are provided in Table 4-1. Those values correspond to the preexponential factor and the activation energy of the Arrhenius equation (Eq. (4-4)):

$$k(i) = A(i)e^{\frac{B(i)}{RT}} \quad \text{Eq. (4-4)}$$

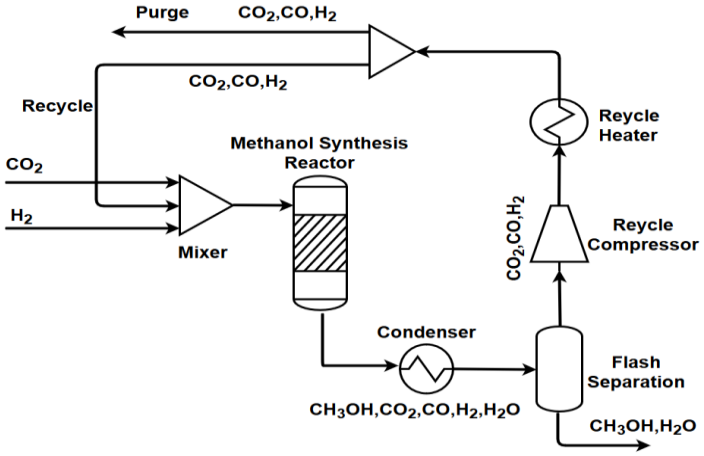

Figure 4-6: Methanol Synthesis Loop. Methanol/Water mixture separated through condensation. Recycle of unreacted gases

Table 4-1: k values - Parameter estimation

$\sqrt{\mathbf{K_{H_2}}}$	A	0.499
	B	17.197
$\mathbf{K_{H_2O}}$	A	$6.62 \cdot 10^{-11}$
	B	124.119
$\frac{\mathbf{K_{H_2O}}}{\mathbf{K_8K_9K_{H_2}}}$	A	3453.38
	B	-
$\mathbf{k'_{5a}K'_2K_3K_4K_{H_2}}$	A	1.07
	B	36.696
$\mathbf{k'_1}$	A	$1.22 \cdot 10^{10}$
	B	-94.765

By default, the methanol/water mixture is separated at methanol synthesis pressure through condensation. This will allow a low workload of the recycle compressor which accounts only for the pressure drop inside the equipment. In addition, at higher pressure, the mixture will condense at a higher temperature which will lessen the cooling load of the condenser prior to the vapor-liquid equilibrium tank. For validation of the methanol synthesis kinetic model, consult Appendix D.

4.2.5 Downstream Processing

The downstream processing section consists of a second flash separator which will separate the light dissolved gas from the water/methanol mixture. This light stream along with the purge stream from the methanol synthesis loop are mixed and led to the afterburner for combustion and heat utilization. In this schematic, the oxidant is provided from the outlet of the sweep gas electrode. Since the oxygen content is higher in the sweep gas compared to typical atmospheric air, reduced flow rate will be needed to burn this combustible mixture. Especially, when operating in thermoneutral mode where sweep gas flow rate is almost zero, almost pure oxygen is provided to the afterburner as oxidant stream. A distillation column completes the separation of water/methanol mixture into almost pure methanol and water (see also Figure 4-7).

The model is built in such a way that the oxidant, the purge stream, and the "light gases" stream are provided at the same pressure before they enter the afterburner. As a direct consequence, the afterburner and the light separator also operate at stack pressure.

4.2.6 Sweep Gas Route

Finally, the process is completed by formulating the sweep gas stream route. Inlet sweep gas flow passes through a double-stage compressor and heated to the necessary levels in order to provide or remove heat from the stack. Afterwards, it is mixed with the separated oxygen and produces an oxidant stream which a bit richer in oxygen (or a lot richer in oxygen when operating close to the thermoneutral point). Then, the stream is split into two parts. One part will provide the necessary amount of oxidant in the afterburner, while the second part is expanded in a double-stage expander and cooled down in order to provide work and heat output (see also Figure 4-8). Compression and expansion stages have been modeled with equal pressure ratios for work minimization and maximization respectively.

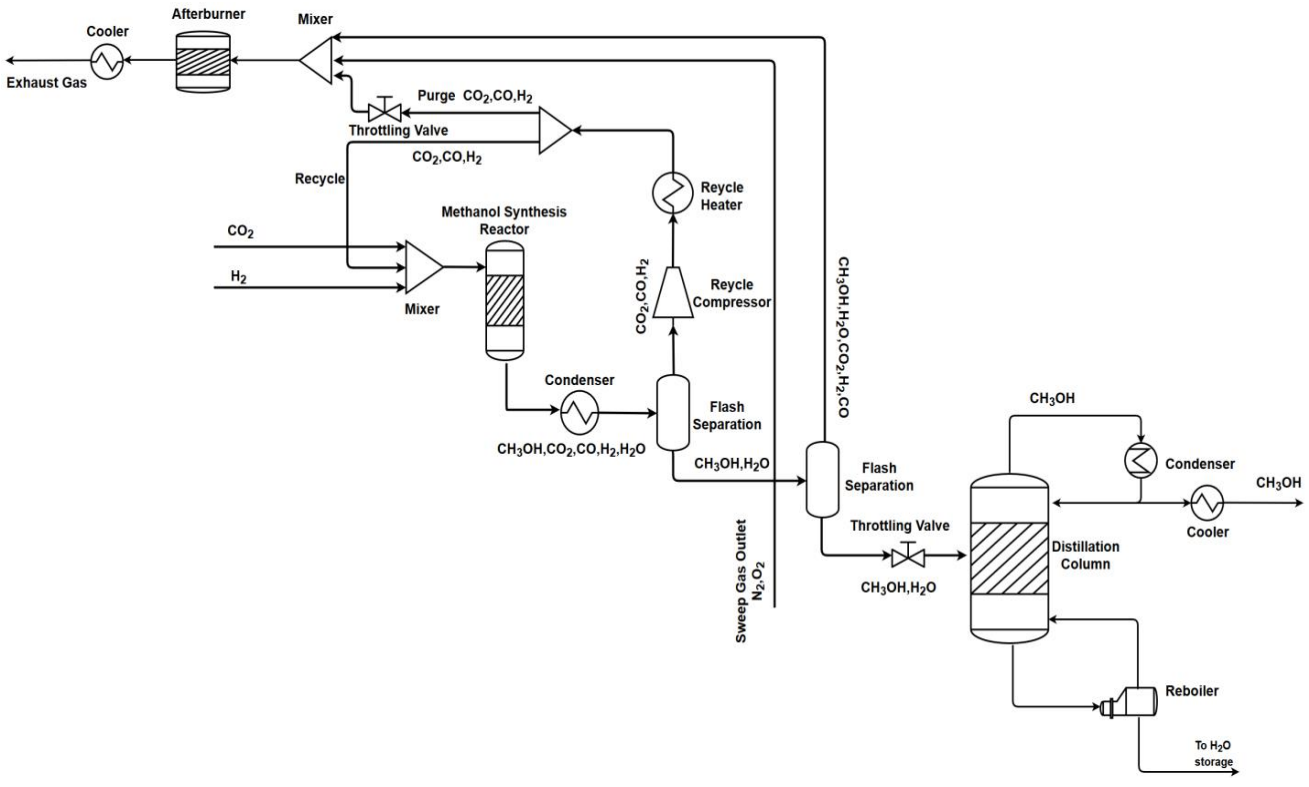

Figure 4-7: Methanol synthesis Loop and downstream processing

4.2.7 Cooling System

After pinch analysis of the system, the minimum hot and cold utility must be supplied to the system for its optimum heat integration scheme. Since the lowest temperature of the system is the environmental temperature, ambient water can be pumped and used for the cooling of the system, therefore the simple cooling system will consist of a pump and a heat exchanger which incorporates the cooling duty of the system as shown in Figure 4-9. It must be noted that the hot utility will be provided as electricity so no more equipment is necessitated in the existing model.

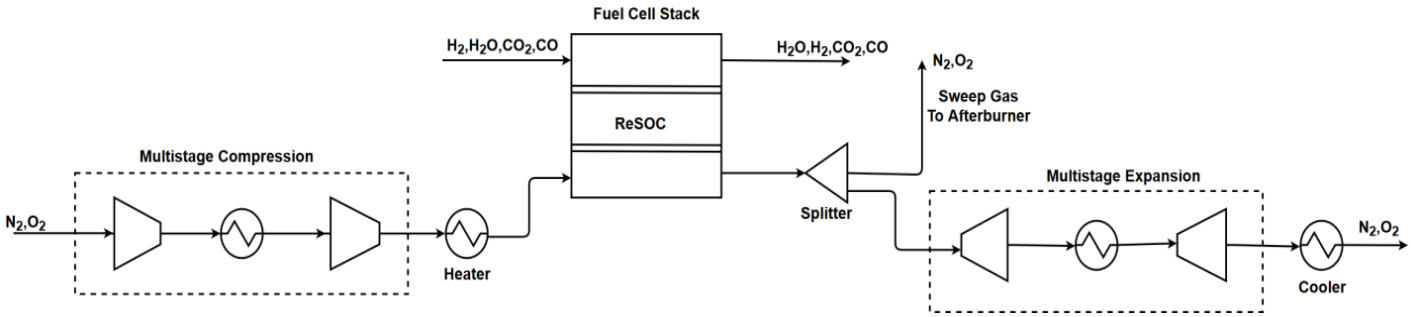

Figure 4-8: Sweep gas Compression - Expansion train

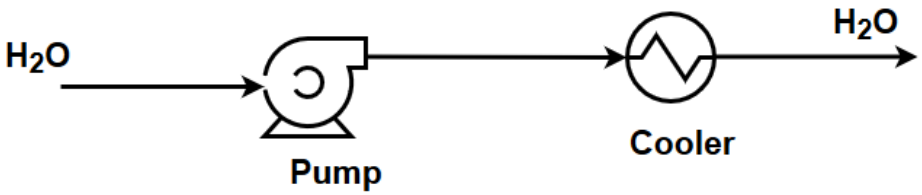

Figure 4-9: Cooling System for Electrolysis

4.3 Electricity Production through Fuel Cell Operation (Discharging Mode)

4.3.1 Fuel Cell Stack

The main concept used is the same as in the electrolysis stack. However, there are also some major changes. In reality, electrochemical conversion of both H_2 and CO takes place, but a very good approximation is the simulation of electrochemical conversion of H_2 while CO is mainly converted *via* the water-gas shift reaction as it has been explained during the literature review (see Chapter 3). Therefore apart from the stoichiometric reactor which simulates electrochemical conversion of H_2 to H_2O, two extra reactors have been incorporated to model WGS/RWGS reaction before and after the electrochemical reaction, based on the modeling work of Barelli et al. [36]. Employment of equilibrium reactors based on the minimization of Gibbs free energy is a reasonable choice since WGS/RWGS is considered to be a fast reaction and equilibrium composition can be achieved in the fuel electrode. CO electrochemical reaction is considered very slow compared to WGS reaction and therefore has not been modeled separately, due to the reasons mentioned in [39]. Oxygen also flows in the opposite way. For the electrochemical reaction, the necessary amount of oxygen is removed from the oxidant stream. Fuel cells only operate in exothermic mode (i.e. produce heat), and therefore a sweep gas cooler is incorporated to remove the heat which is produced by the three blocks (i.e. one stoichiometric reactor and two equilibrium WGS reactors). For the complete process modeling, please see Figure 4-10. The heat produced by the rSOC is effectively accommodated in the oxidant flow. The necessary oxidant flow rate is regulated internally by the model.

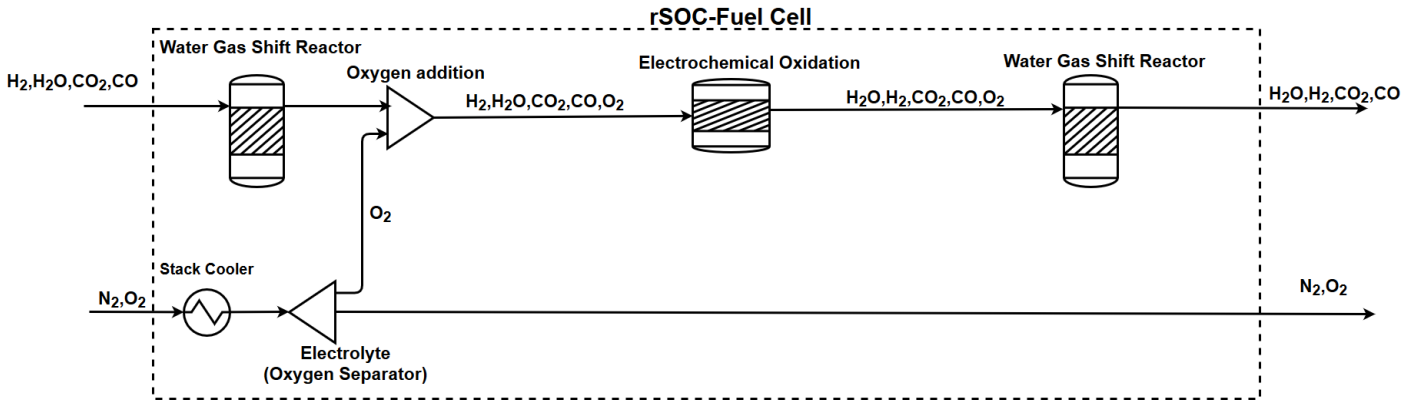

Figure 4-10: Fuel Cell modeling in Aspen Plus

For the modeling of various types of losses, again, the model proposed by Hauck et al [13] is utilized. In order to estimate the necessary heat removal, the following calculations have been performed. The total power produced (i.e. electricity plus heat) is estimated at first by Eq. (4-1). Electrical power produced is then estimated by Eq. (2-2). By subtracting the electrical power produced from the total power produced, a first estimation of the necessary heat removal is performed. Apart from that, heat dissipation through overpotential losses is added for the final estimation as shown below:

$$Q_{diss} = \Delta V_{OP} I = \Delta V_{OP} i A_{tot} \qquad \text{Eq. (4-5)}$$

where Q_{diss} is the extra heat dissipated through overpotential losses and ΔV_{OP} is the voltage overpotential.

4.3.2 Feed stream preparation and methanol steam reforming

Again, the feed mixture has to be preconditioned before fed into the fuel cell stack. Methanol and water streams are drawn from their respective storage tanks. Afterwards, they are pressurized and preheated separately before they mix. The next step is the methanol steam reforming, which has been modeled with an equilibrium reactor, followed by subsequent heating before entering the rSOC stack. For the methanol steam reforming the following reactions have been utilized as stated in [79]:

$$CH_3OH + H_2O \leftrightarrow CO_2 + 3H_2 \qquad \Delta H = 49.7 kJ/mol$$
$$CH_3OH \leftrightarrow CO + 2H_2 \qquad \Delta H = 90.2 kJ/mol$$
$$CO + H_2O \leftrightarrow CO_2 + H_2 \qquad \Delta H = -41.2 kJ/mol$$

Methanol is advantageous in terms of reforming temperature. Compared to other fuels, which are reformed at high temperatures (i.e. 700°C), methanol is reformed at a temperature range of 200-300°C, which translates into lesser heating load. Another design choice implemented here is the reforming process under stack pressure since it is cheaper to pump liquid water and methanol rather than compressing the reformate stream. Therefore, stack pressure and reformer operating pressure are equal.

An additional important note is that reforming methanol at low temperature would not produce a H_2/CO stream, but a H_2/CO_2 stream. The main reason is that WGS/RWGS is also promoted during steam reforming. The low temperature of the process will yield extra CO_2 (i.e. the forward exothermic reaction occurs). At higher reforming temperature, extra CO will be yielded through the backward endothermic reaction. Consequently, if

more CO was present, WGS reaction would be promoted in the stack. However, in this study, CO_2 content is considerably higher at stack inlet which promotes the RWGS and the creation of CO in the rSOC stack.

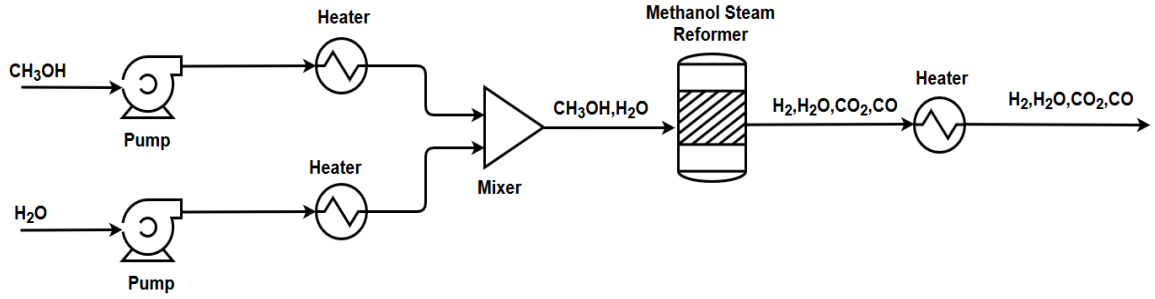

Figure 4-11: Feed preparation and methanol steam reforming before rSOC stack

4.3.3 Separation Train

The outlet gas from the fuel electrode has to be separated into its constituents before keeping them into their respective storage tanks. The idea that was developed is summarized in Figure 4-12. At the beginning of the separation train, a water-gas shift reactor has been added to convert H_2O and CO into CO_2 and H_2. Afterwards, it is ensured that only a minor amount of water vapor will exist in the outlet vapor stream of the first flash separator. Also, the corresponding intercooler ensures that the stream is not cooled below its dew point in order to avoid condensation in the second stage of compression. The second flash separator ensures a highly pure hydrogen stream product. Finally, it is preferred to perform the second separation at high pressure. When performing condensation at high pressure, the mixture must be cooled down at higher temperature and hence, it is energetically advantageous and will reduce the cooling load of the process. According to Wang et al. [20], condensation of CO_2 stream can be used when the CO_2 content of the gas stream is above 15% in volume so the employment of an intense refrigeration system is justified. The condensation route has also been employed by Al-Musleh et al. [11].

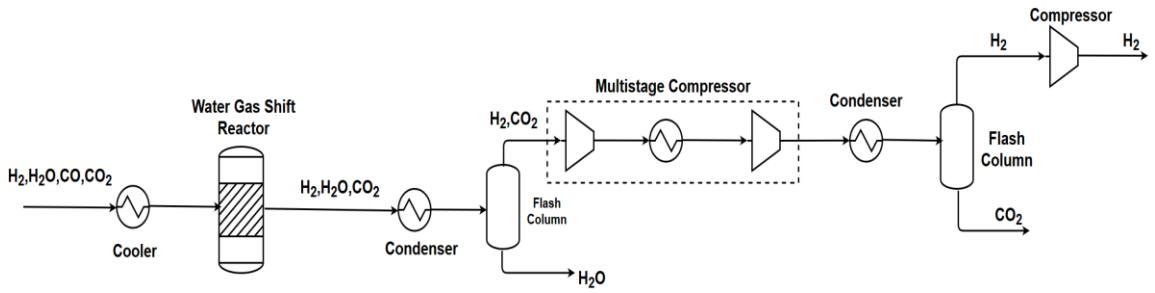

Figure 4-12: Separation Train and Storage

4.3.4 Sweep Gas Route

The principle is exactly the same as described in section 4.2.6. The differences here are the following:

- Oxygen is removed from the sweep gas stream, while in electrolysis oxygen is added
- No afterburner has been incorporated

The compression and expansion trains are being composed of the exact same modules as has been for the electrolysis model (see Figure 4-13).

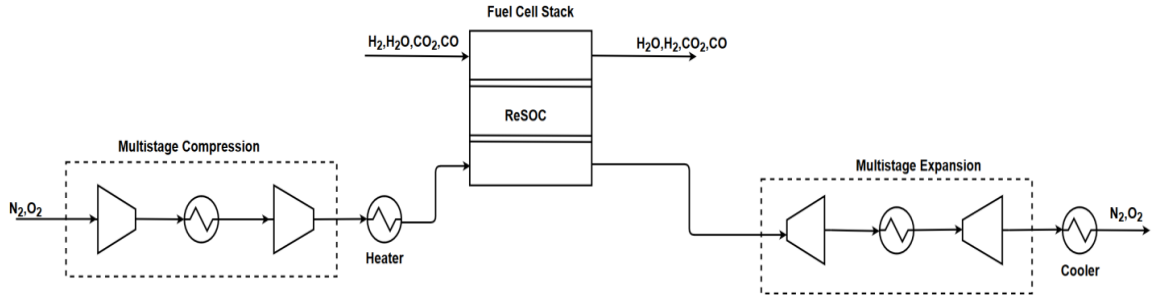

Figure 4-13: Oxidant Compression and expansion train

4.3.4 Refrigeration Cycle

In section 4.3.3, it has been denoted that the system will require very low temperatures for the condensation of CO_2 in order to be stored separately from H_2. Ambient cooling water cannot be employed in this case as it was employed during electrolysis. An intense refrigeration system will operate as shown in Figure 4-14.

The refrigeration system consists of two separate cycles and the working fluid is different for each cycle. For the bottom (i.e. heavy) refrigeration cycle, carbon tetrafluoride (CF_4) is used as a refrigerant, while the upper (i.e. light) refrigeration cycle employs CO_2 as a refrigerant. Due to very high pressure ratios in the light refrigeration cycle, it has been modeled as a triple compression stage vapor compression cycle with two intermediate vapor-liquid equilibrium tanks. By employing three stages, CO_2 enters the evaporator at quite low quality (i.e. close to 0). Consequently, less mass flow rate of CO_2 is required in order to receive the condenser duty of the heavy refrigeration cycle and this, in turn, alleviates the compressors from excessive duty, increasing the overall coefficient of performance (COP) and the efficiency of the refrigeration system. CO_2 could possibly cover the whole temperature range but the refrigeration system would end up very complex in order to be made efficient (i.e. many more compression stages), due to the fact that CO_2 at very low temperatures exists at extremely low pressures. Instead, CF_4 was chosen due to the fact that if a refrigeration cycle operates between -100^{o}C and -50^{o}C, the necessary pressure ratio is approximately 6, while for the same temperature range, CO_2 must be pressurized at quite large pressure ratios (in the order of 30), which reduces the COP.

Ambient cooling water can be employed though for cooling when temperatures are above ambient. A system as seen in Figure 4-9 will also be used here to receive loads of cooling streams. In total, the cooling duty will be split into two parts. One part includes coolers where temperatures are above ambient, while for sub-ambient temperatures an intense refrigeration cycle will be utilized as already mentioned.

4.4 Energy & Exergy Analysis

Exergy is defined as the maximum obtainable work from a source of energy, using the environment as the reference state (i.e. reservoir of heat and matter). While energy is conserved in all processes, exergy degrades, which means that thermal interactions, friction, mixing, and other irreversibilities account for exergy losses and the reduced availability of conversion to useful work due to an increase in entropy. In this analysis, differences in the quality of energy are taken into account. The environment has to be defined exactly in order to perform exergy analysis. The definition of the environment includes reference compounds as well as their partial pressure (see Table 4-2). Scientific literature providing details on exergy analysis of systems is provided by T.J.

Kotas [80] while only the minimum knowledge needed for the case study will be presented here for better understanding (see Appendix H & Appendix I).

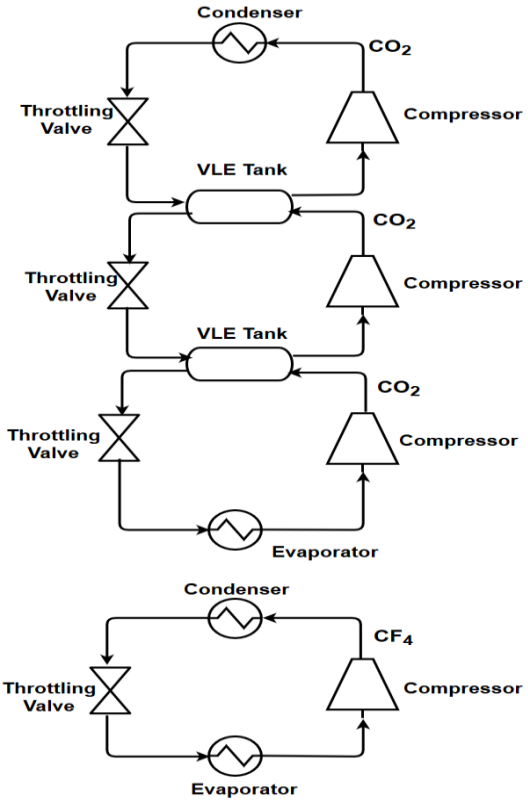

Figure 4-14: Refrigeration system for fuel cell model

4.4.1 Environment Definition

The reference pressure and temperature which define the environment are: $p_0 = 1.01325$ bar, $T_0 = 298.15$ K. The environmental compounds as well as their respective partial pressures have been proposed by Szargut et al [80].

Table 4-2: Environmental Definition by Szargut et al. [80]

Reference Compound	Equilibrium Partial Pressure (bar)
Ar	0.00907
CO_2	0.000294
D_2O	0.00000137
H_2O	0.0088
He	0.0000049
Kr	0.00000098
N_2	0.7583
Ne	0.0000177
O_2	0.204
Xe	0.000000088

For the specific project, only N_2, O_2, H_2O and CO_2 are relevant compounds and the rest can be ignored since every compound can be reduced to the abovementioned ones. Chemical exergy of CF_4 is not included in this study. Exergy losses of the refrigeration system are given as a total amount and not in a component-wise manner.

4.4.2 Energy and Exergy Efficiency Definitions for the existing systems

For the exergy efficiency of the electrolysis system, the modeler must include thermomechanical and chemical exergies of inlet and outlet streams. In addition, input and output exergies as electricity as well as exergies for compensation of the hot and cold utility (Q_H & Q_C) must be included in the definition. To specify the definition for each mode, one has to identify which stream is the product stream. In addition, it has to be understood that thermomechanical and chemical exergy cannot be added or subtracted with an electrical exergy term. Particularly, in electrolysis, the desired product is the methanol. Therefore, in the numerator only thermomechanical and chemical exergies can be included and in the denominator, the electrical exergies will add up (positive is equivalent to energy consumption and vice versa). Instead of taking into account only the exergy of the methanol stream, all the outlet flows have been considered as product in the present work. For example, the bottom product of the distillation column is also stored and utilized in fuel cell mode. Therefore its total exergy is also included in the definition. Exergy of the sweep gas outlet and the afterburner exhaust have also been taken into account, while those two streams are disposed to the environment, but in reality, their values are almost negligible. This will give a minor boost to the exergy efficiency (~1-1.5%) in the electrolysis mode. On the other hand, during fuel cell operation the identified product is the stack produced electricity and therefore the numerator will only contain terms of electrical exergy, while the denominator will contain terms of thermomechanical and chemical exergy. The same reasoning is applied to the formulation of energy efficiency as well. Energy derived from fuel cannot be added with electrical energy. The exact definitions employed in the current study can be seen below (Eq. (4-6)-Eq. (4-9)).

More specifically, in both systems, the hot utility is directly considered to be compensated by electricity. In the electrolysis system, the cooling utility is compensated by pumping cooling water through the system, therefore, the equivalent exergy induced into the system is the work of the pump. Work from or to the stack, as well as from system turbomachinery is considered as 100% exergy since electricity can be converted into other forms of energy reversibly if the process is designed meticulously.

For the energy efficiency in the case of electrolysis, the energy input of hydrogen and the energy output of methanol is included while all other streams are excluded from the definition since their LHV is equal to 0. Moving to fuel cell mode, the methanol stream is considered as an energy input to the system, while hydrogen is considered an energy output. Consequently, only the fuel streams are included in the definitions while all other streams are ignored. Stack electricity, as well as energy provided to compensate for the hot and cold utility, is also included in the definition.

An important note is that the work from turbomachinery (i.e. summation of electricity production and consumption from system expanders and compressors) can be either positive or negative. If it is positive, it means that the electricity is consumed and vice versa. For a better understanding of the definitions, consult Figure 4-15 & Figure 4-16.

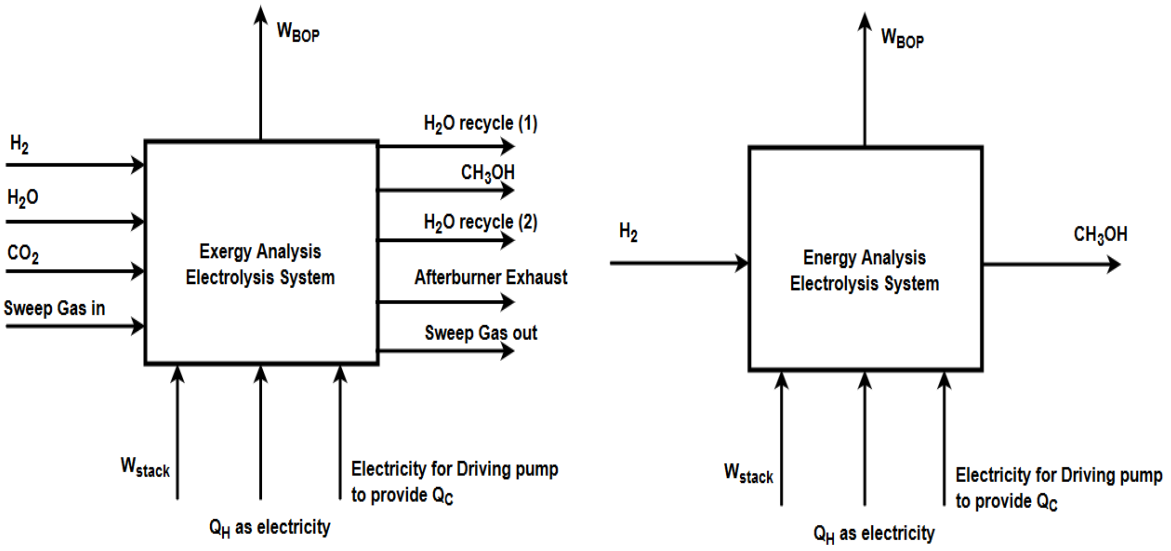

Figure 4-15: Exergy and Energy Analysis of Electrolysis System

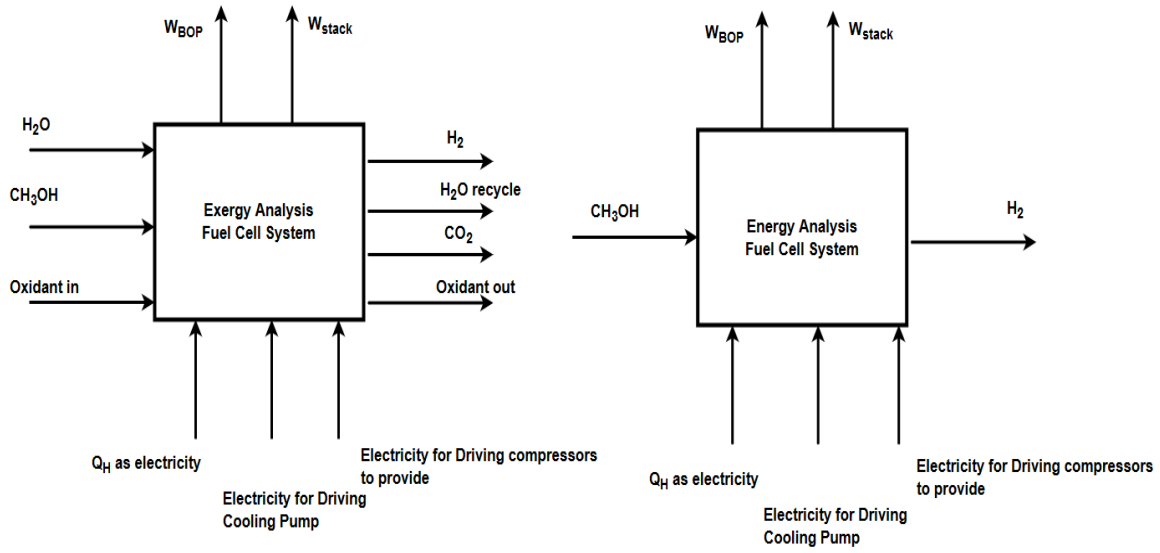

Figure 4-16: Exergy and Energy Analysis of Fuel Cell System

Electrolysis-Exergy Efficiency

$$n_{ex} = \frac{Ex_{TM\&CH,out} - Ex_{TM\&CH,in}}{Ex_{turb} + Ex_{Q_H} + Ex_{Q_C} + Ex_{stack,in}} \quad \text{Eq. (4-6)}$$

where:

$$E_{TM\&CH,in} = Ex_{H_2} + Ex_{H_2O} + Ex_{CO_2} + Ex_{SG,in}$$

$$E_{TM\&CH,out} = Ex_{CH_3OH} + Ex_{H_2O,rec(1)} + Ex_{Afterburn,exhaust} + Ex_{H_2O,rec(2)} + Ex_{SG,out}$$

$$Ex_{Q_H} = Q_H$$

$$Ex_{Q_C} = W_{cooling,pump}$$

$$Ex_{stack,in} = P_{stack}$$

$$Ex_{turb} = \sum W_{Comp,el} + \sum W_{Exp,el}$$

Electrolysis-Energy Efficiency

$$n_{en} = \frac{En_{CH_3OH} - En_{H_2}}{W_{turb} + W_{stack} + Q_H + W_{Cooling,pump}} \quad \text{Eq. (4-7)}$$

where:

$$En_{CH_3OH} = \dot{m}_{CH_3OH} \cdot LHV_{CH_3OH}$$

$$En_{H_2} = \dot{m}_{H_2} \cdot LHV_{H_2}$$

$$W_{turb} = \sum W_{Comp,el} + \sum W_{Exp,el}$$

Fuel Cell-Exergy Efficiency

$$n_{ex} = \frac{Ex_{stack,out} - Ex_{turb} - Ex_{Q_H} - Ex_{Q_C}}{Ex_{TM\&CH,in} - Ex_{TM\&CH,out}} \quad \text{Eq. (4-8)}$$

where:

$$Ex_{TM\&CH,in} = Ex_{H_2O} + Ex_{CH_3OH} + Ex_{SG,in}$$

$$Ex_{TM\&CH,out} = Ex_{H_2} + Ex_{H_2O,rec} + Ex_{CO_2} + Ex_{SG,out}$$

$$Ex_{Q_H} = Q_H$$

$$Ex_{Q_C} = W_{Refrigeration} + W_{cooling,pump}$$

$$Ex_{stack,out} = P_{stack}$$

$$Ex_{turb} = \sum W_{Comp,fc} + \sum W_{Exp,fc}$$

Fuel Cell-Energy Efficiency

$$n_{en} = \frac{W_{stack} - W_{turb} - Q_H - W_{Refrigeration} - W_{cooling,pump}}{En_{CH_3OH} - En_{H_2}} \quad \text{Eq. (4-9)}$$

where:

$$En_{H_2} = \dot{m}_{H_2} \cdot LHV_{H_2}$$

$$En_{CH_3OH} = \dot{m}_{CH_3OH} \cdot LHV_{CH_3OH}$$

$$W_{turb} = \sum W_{Comp,fc} + \sum W_{Exp,fc}$$

4.5 Roundtrip Efficiency

Apart from the exergy efficiency, the system should be examined for its roundtrip efficiency. As mentioned in 0, roundtrip efficiency is defined in Eq. (2-12), where V_{fc} and V_{el} refer to the operating cell voltage during fuel cell and electrolysis mode respectively, q_{fc} and q_{el} correspond to the total charge transferred during fuel cell and electrolysis operation. Finally, $E_{BOP,fc}$ and $E_{BOP,el}$ is the total energy generated during fuel cell mode and the total energy expended in electrolysis mode by the BOP. The significance of this metric is to evaluate how much energy is recovered in fuel cell mode for each unit of energy consumed in electrolysis mode. For repeatable operation between the two modes, the equal charge transfer rule is also applied in the current study:

$$q_{fc} = q_{el} \leftrightarrow j_{fc}A_{tot}t_{fc} = j_{el}A_{tot}t_{el} \leftrightarrow j_{fc}t_{fc} = j_{el}t_{el} = a$$

where A_{tot} is the total active electrode area, j_{fc} or j_{el} corresponds to the current density in fuel cell or in electrolysis mode and t_{fc} or t_{el} is the time operation in fuel cell or electrolysis mode respectively. The equal charge transfer rule alternatively states that if n moles of H_2 are oxidized during fuel cell operation, then n moles of steam are reduced during electrolytic operation. Despite the fact that the equal charge transfer rule can act as initial tool to connect the time of operation in each mode, it does not ensure that methanol produced in the electrolysis mode is adequate for consumption in the fuel cell mode .

Importing the abovementioned relation into Eq. (2-12) results to Eq. (4-11):

$$n_{RT,sys} = \frac{V_{fc}A_{tot} - \frac{W_{BOP,fc}}{j_{fc}}}{V_{el}A_{tot} + \frac{W_{BOP,el}}{j_{el}}} \qquad \text{Eq. (4-10)}$$

Therefore in order to maximize roundtrip efficiency, the numerator has to be maximized in fuel cell mode while the denominator has to be minimized in electrolysis mode.

Finally, for each mode, the total work required by BOP has to be defined.

In electrolysis mode:

$$W_{BOP,el} = \sum W_{Comp,el} + \sum W_{Exp,el} + Q_{H,el} + W_{cooling,pump,el}$$

The work of BOP in electrolysis mode includes the electricity requirement by the compressors, the electricity generation by the expanders, the hot utility and the cold utility which is compensated by a cooling water pump. If $W_{BOP,el}$ is positive it means that BOP consumes electricity and vice versa. An important reminder is that the hot utility (denoted as Q_H) will be provided in form of electricity in the present study.

In fuel cell mode:

$$W_{BOP,fc} = \sum W_{Comp,fc} + \sum W_{Exp,fc} + Q_{H,fc} + W_{cooling,pump,fc} + W_{refrigeration,fc}$$

The work of BOP in fuel cell mode consists of the same terms as in the electrolysis mode. The extra term $W_{refrigeration,fc}$ corresponds to the total electricity consumption of the compressors in the refrigeration system. If $W_{BOP,fc}$ is positive it means that the BOP consumes electricity and vice versa. In both modes, compressor work is considered positive and expander work is considered negative. Eq. (4-10) is also given in a

way, that if $W_{BOP,fc}$ is negative the numerator is further maximized, while if $W_{BOP,el}$ is negative, the denominator is minimized.

Apart from the maximization of roundtrip efficiency, it has to be ensured that enough methanol is produced during electrolysis mode, in order to be consumed in fuel cell mode. A criterion will be developed in Chapter 6, in order to ensure methanol adequacy.

4.6 Summary

In this chapter, the electrolysis and fuel cell operation were elaborated. To sum it up, the electrolysis mode consists of the feed section, the rSOC stack, the hydrogen pressurization section, the methanol synthesis reactor where a mixture of H_2 and CO_2 is effectively converted into methanol, and the separation train where pure methanol is finally obtained. The system also includes an afterburner where purge and light gases are combusted, a sweep gas compression-expansion train for the effective removal of oxygen but also for stack thermal balancing, and finally, a cooling system which is based on coolant water.

The fuel cell mode consists of the feed section, the methanol steam reformer, the rSOC stack, and the separation train. The separation train consists of a WGS reactor, a water condenser, a CO_2 condenser and storage compressors. For the CO_2 condensation, which takes place at low temperatures, an intense refrigeration system is employed. An oxidant compression-expansion train is also employed during the fuel cell operation for the provision of the required amount of oxidant as well as for stack thermal balancing. The cooling system which is based on coolant water is also employed in the fuel cell operation to cool down streams at above ambient temperatures.

Finally, in this chapter, the metrics of energy, exergy as well as roundtrip efficiency were analyzed. It was clarified that during the electrolysis mode the useful product is the methanol, while during fuel cell operation, electricity generation should be of utmost priority. The abovementioned statement was clearly incorporated into the definition of energy and exergy efficiencies (Eq. (4-6)-Eq. (4-9)). The roundtrip efficiency which was initially introduced in section 2.5 was further elaborated here. By importing the equal charge transfer equation into the roundtrip efficiency definition, Eq. (4-10) emerged. Eq. (4-10) is a very useful form of the roundtrip efficiency because the numerator can be separately maximized by using the existing fuel cell model, while the denominator can be minimized by using the existing electrolysis model.

CHAPTER 5

THERMODYNAMIC OPTIMIZATION FOR ENERGY AND EXERGY EFFICIENCY – RESULTS AND DISCUSSION

In this chapter, for each of the processes (i.e. Electrolysis Mode or Fuel Cell mode), a set of base case conditions is initially defined. Various system parameters are varied simultaneously to the see the effect on various system parameters, such as energy, exergy efficiency, hot and cold utility as well as electricity consumed (or produced) by the stack, electricity consumed (or produced) by system turbomachinery, methanol production etc. The process has been carried out by using a combination of Aspen Plus, Aspen Energy Analyzer and Microsoft Excel software and no optimization software has been utilized. This means that optimization takes place through trial and error and not through specialized software which performs multivariable optimization. In the current work, an initial subset of parameters is examined and optimized. For the next set of parameters, the optimum values from the previous sensitivity analysis are kept and optimization of the new set of parameters occurs. This procedure continues till all the parameters have been optimized.

Next, the results of the "perfectly heat integrated" modes are presented. A "perfectly heat integrated" mode refers to the minimization of the external hot and cold utility required to balance the energy needs. Those values can be obtained without manually importing a heat exchanger network. The pinch technology is utilized in this case. By feeding the inlet and outlet temperatures as well as the duties of each heater and cooler in the Energy Aspen Analyzer software, the hot and cold composite curves are formed automatically, while the software identifies the minimum hot and cold utility of the system.

Afterwards, manual heat exchanger networks will be imported for the base case and optimized case. The results of the "perfectly heat integrated" cases and the cases with manually imported heat exchanger networks will be compared in order to see the effect of manual heat integration in system efficiency. In addition, elaborated exergy flow diagrams will be shown for the cases where the heat exchanger network has been imported manually. From the exergy flow diagrams, identification of the components which contribute significant portions of the total exergy losses will be identified, while the reduction in exergy losses of those components will be clarified when moving from the base case to the optimized case conditions.

Apart from the exergy efficiency optimization, an optimization procedure for system roundtrip efficiency will complete the thermodynamic evaluation. For roundtrip efficiency maximization, it will be shown that strategies such as thermal coupling of both modes are necessary. Roundtrip efficiency optimization will be analyzed in Chapter 6.

Moreover, it has to be mentioned that when referring to electricity produced/consumed by system turbomachinery, the author only refers to the total summation of electricity produced or consumed by expanders and compressors respectively, while external duty for heaters and coolers is referred as hot and cold utility respectively. Whenever electricity from turbomachinery is negative, it means that electricity is removed from the system which is equivalent to electricity generated. Consequently, the most negative values correspond to the highest electrical work produced by the system turbomachinery and vice versa. In addition, the current density range is set to be between 3000-10000 A/m^2 in the current work.

Finally, a major assumption is used for the water cooling system. It is assumed that the pressure drop that the cooling water pump has to overcome for the whole system is 5 bar.

5.1 System Exergy and Energy efficiencies & Optimization for electrolysis mode

In this section, the base case parameters and assumptions for the electrolysis model will be presented and then the optimization process and corresponding results will follow.

5.1.1 Base Case Parameters – Electrolysis mode

The base case parameters for the electrolysis mode are summarized in Table 5-1. Finally, it has to be mentioned that sweep gas removes or provides the heat to the rSOC stack. The temperature difference is 60 K at the stack inlet and 10 K at the stack outlet. During endothermic operation, the stack needs heat so the sweep gas temperature is higher than the stack temperature at the stack inlet. At exothermic mode, the stack has to remove heat and the sweep gas temperature is lower than the stack temperature, at the stack inlet. For these process conditions, the energy and exergy efficiencies of the system are 52.40% and 59.48% respectively. These values can be considered as the starting point of the optimization process. Although the efficiencies are at reasonable levels, there is still room for improvement. The most negative aspect is the excess sweep gas flow rate accompanied with low capabilities of heat integration when operating at high stack pressure. Hence, during the optimization process, the increased hot utility of the system will be addressed. The initial value of the system hot utility is approximately 63 kW.

Table 5-1: Base Case Parameters - Electrolysis

Parameter	***Value***	***Parameter***	***Value***
Number of cells (-)	1300	Pressure of feed CO_2 stream (bar)	150
Electrode area per cell (m^2)	0.01	Temperature of feed CO_2 stream (K)	298.15
Stack pressure (bar)	5	Length of PFR (m)	40
Stack temperature (K)	973.15	Number of tubes (-)	5000
Steam utilization (-)	0.8	Tube Diameter (m)	0.02
Oxidant inlet pressure (bar)	1	Porosity of catalyst (-)	0.5
Oxidant inlet temperature (K)	298.15	Density of catalyst (kg/m^3)	2000
Flow rate of feed water (mol/s)	0.5	Inlet pressure (bar)	50
Pressure of feed water (bar)	1	Constant reactor temperature (K)	480
Temperature of feed water (K)	298.15	Outlet pressure of throttling valve leading to distillation (bar)	1.2
Flow rate of feed H_2 (mol/s)	0.125	Molar Reflux ratio	1.5
Pressure of feed H_2 (bar)	200	Light Recovery (Purity %)	0.99
Temperature of feed H_2 (K)	298.15	Heavy Recovery (Purity %)	0.01

Parameter	***Value***	***Parameter***	***Value***
Isentropic eff. of pumps and compressors (-)	0.85	Mole fraction of N_2 in feed sweep gas stream (-)	0.79
Isentropic eff. of turbines (-)	0.75	Mole fraction of O_2 in feed sweep gas stream (-)	0.21
Mechanical Losses of components	0.95	Mole fraction of water to syngas compression	0.01
Mole fraction of feed water (-)	1	Mole fraction of water to recycle compressor	0.002
Mole fraction of feed CO_2 (-)	1	Fraction of flow going to purge	0.01
Mole fraction of feed H_2 (-)	1	Partial Condenser of distillation column	0.05
Afterburner cooled exhaust gases temperature (^oC)	770.4		

5.1.2 Optimization of Electrolysis mode and Results

Effect of stack pressure and temperature

After the initialization of the above values into the electrolysis model, the optimization procedure is initiated. Firstly, **stack pressure** and **temperature** are varied. The pressure is varied in the range of *1-40 bar*, while the temperature is varied from *923.15-1123.15 K (i.e. 650°C-850°C)*. Both exergy and energy efficiencies follow the same trend. By looking at Figure 5-1 & Figure 5-2, one can declare the following statements.

- Exergy and energy efficiencies rise as temperature increases, while they decline at higher temperature
- The temperature at which the peak is met increases with an increase of stack pressure
- The higher the stack pressure the higher the peak efficiency
- If the operator desires to pick a temperature operating window, it is beneficial to operate at low pressure since the gradient of the low-pressure curve is low before and after the maximum point. On the other hand, if someone wants to operate at one specific point (which is more difficult), it is advised to operate at high stack pressure and the peak temperature
- In this study of the stack pressure and temperature at the specific range of both parameters, exergy efficiency varies from 27-76%, which means that those parameters play a crucial role in system efficiency, and they have to be regulated strictly, especially when operating at high pressures

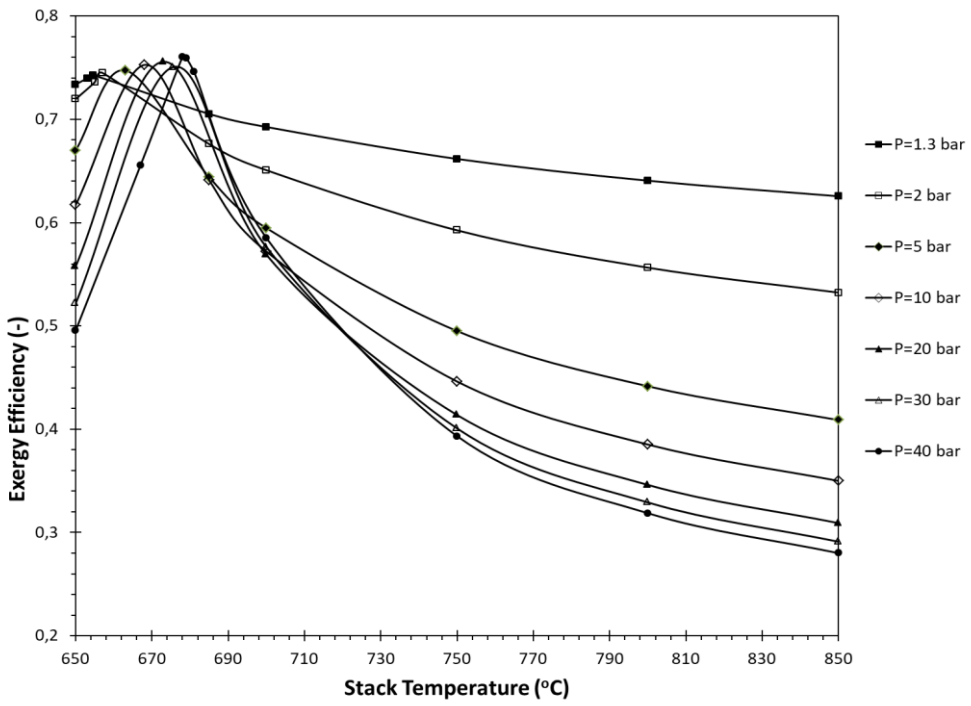

Figure 5-1: Exergy efficiency - Process Conditions, See Base Case - Vary stack P_s, T_s

A question that may be asked is: "What is so special about the peak operating point?". By observing Figure 5-3, it can be seen that the peak coincides with the thermoneutral point of operation. The plot below has been drawn for a constant current density (~6000 A/m^2). It can be seen that by increasing the pressure, the reversible voltage increases, and therefore in order to cross the thermoneutral voltage at the same current density, lower overpotential losses are required. Lower overpotential losses can be achieved by operation at higher stack temperature. It can also be observed that the thermoneutral voltage slightly increases with an increase in temperature.

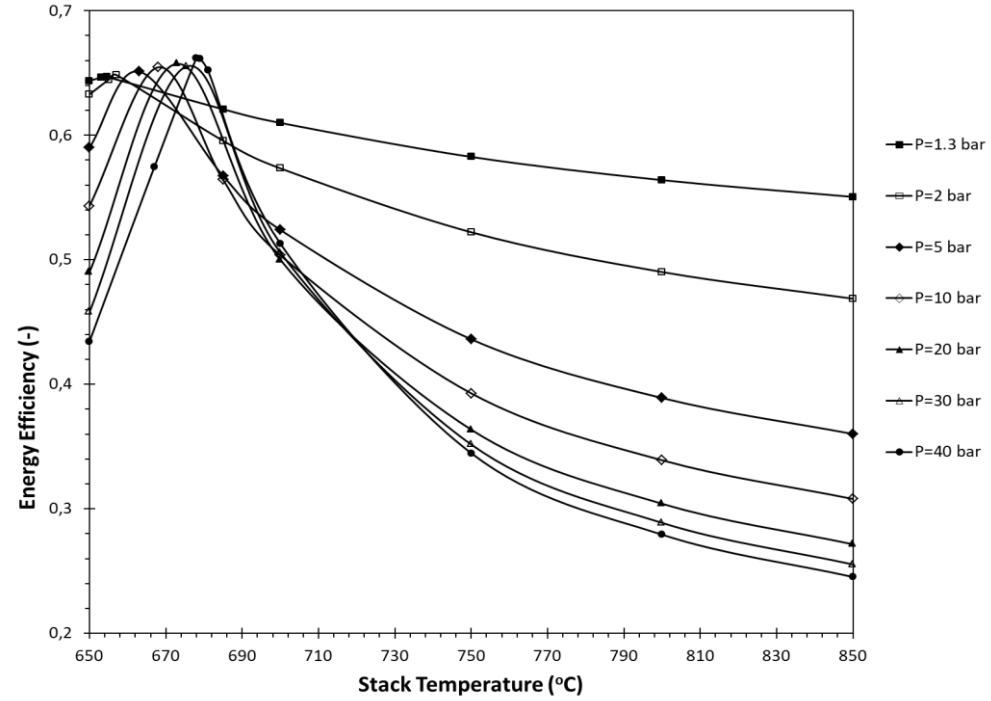

Figure 5-2: Energy efficiency - Process Conditions, See Base Case - Vary stack P_s, T_s

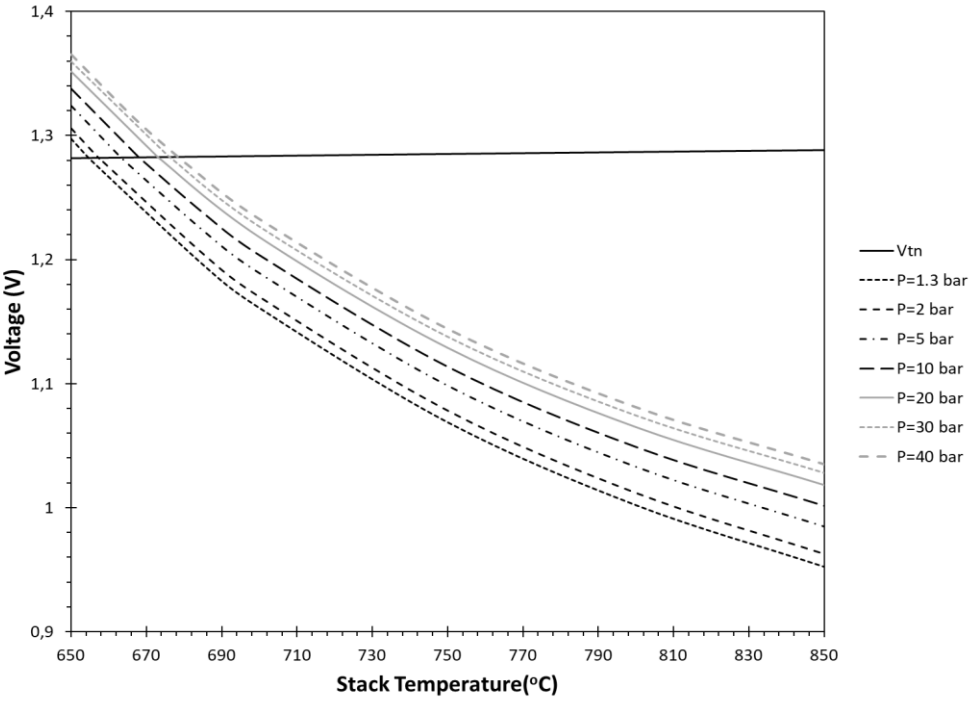

Figure 5-3: Thermoneutral Voltage as a function of T, Cell Voltage as a function of P_s, T_s

It has to be understood that at the thermoneutral point of operation, no sweep gas stream exists while far away from thermoneutral operation elevated sweep gas flow exists. Therefore the conclusion here is that increased sweep gas flows play a detrimental role in system exergy and energy efficiencies. The sweep gas section includes mainly heaters/coolers, compressors and turbines. When sweep gas flow rate is reduced, hot and cold utility is minimized. This means that the system hot and cold utility mainly depend on the sweep gas flow rate. Enhanced sweep gas flow rate results in heightened hot and cold utility due to the compression intercooler, stack preheater, expansion reheater, and oxidant cooler. When stack pressure is low, this means that the pressure ratio of the two-stage sweep gas compressor and expander is very low. A low pressure ratio

indicates a slight increase in temperature during compression and a slight decrease in temperature during expansion, alleviating the intercooler and the reheater from excessive duties. In contrast, at high stack pressure, compression and expansion pressure ratio is high and temperature increase and decrease are high respectively, therefore the intercooler and reheater are heavily loaded. It can be seen that hot and cold utility rises dramatically when stack pressure is higher. Another important reason on why hot and cold utility increase excessively at high stack pressure when diverging from the thermoneutral point of operation is the fact that at lower stack pressure there are more opportunities for better heat integration between the sweep gas pre-stack heater and the final cooler. This can be seen in Table 5-2. From the last row of Table 5-2, it can be seen that at lower stack pressure, a larger temperature difference of the heated cold stream can be recovered through heat integration. The same conclusion can be drawn also for the hot fluid. Alternatively, from the ideal Brayton cycle with recuperation, low pressure ratio results to heightened efficiencies compared to high pressure due to the fact that at high pressure ratio, recuperation is not that effective. In every conceivable case, the coupling of the pre-stack heater and final sweep gas cooler is possible since the flow rate of the sweep gas cooler is always greater than the flow rate of sweep gas inlet due to oxygen production from the stack. Oxygen production corresponds to an increase in $\dot{m}c_p$ of the expanded sweep gas stream, making this heat integration possible. A pinch of 10 K has been taken into account in Table 5-2. The final result is summarized in Figure 5-4 & Figure 5-5. Enormous temperature difference can be covered internally at lower stack pressure, while at higher stack pressure the system is unable to do so and requires more external cold utility.

Table 5-2: Qualitative representation of better heat integration at a low stack pressure

Stack Pressure (bar)	1.3	2	5	10	20	40
Cold Fluid In (°C)	38,4	61,4	115,1	160,4	210	264,2
Cold Fluid Out (°C)	676,1	638,2	563,7	512,2	464,9	421,4
Hot Fluid In (°C)	686,1	648,2	573,7	522,2	474,9	431,4
Hot Fluid Out (°C)	48,4	71,4	125,1	170,4	220	274,2
Cold Fluid Diff. (°C)	637,7	576,8	448,6	351,8	254,9	157,2

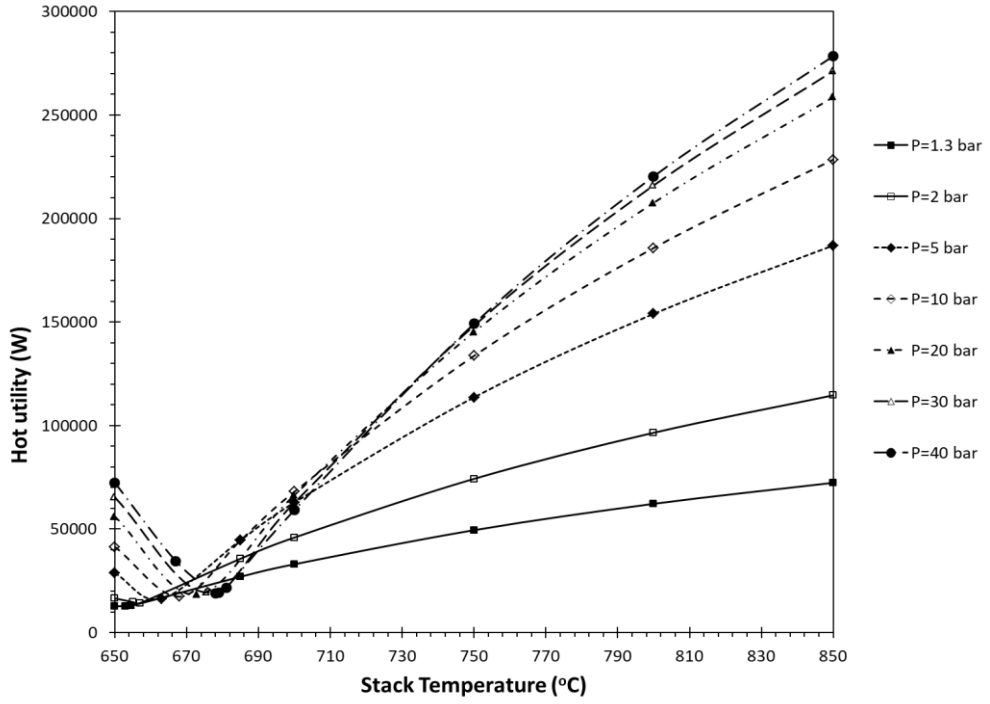

Figure 5-4: Hot Utility- Process Conditions, See Base Case - Vary stack P_s, T_s

Moving on to the next system parameter, electricity produced by turbomachinery also depends mainly on sweep gas compressors and expanders. It is also expected that sweep gas expanders will produce more work in every conceivable case since the mass flow rate of sweep gas is increased due to oxygen production from the stack but also due to the effect that the inlet temperature to the expansion train is very high. Those are the main reasons why the system turbomachinery produces electricity in almost every case, especially at high sweep gas flow rates (i.e. away from thermoneutral mode operation). It is also expected that by increasing the stack pressure and therefore the pressure ratio of the sweep gas compressor and expander, the turbomachinery will produce more net electricity. The result is depicted in Figure 5-6.

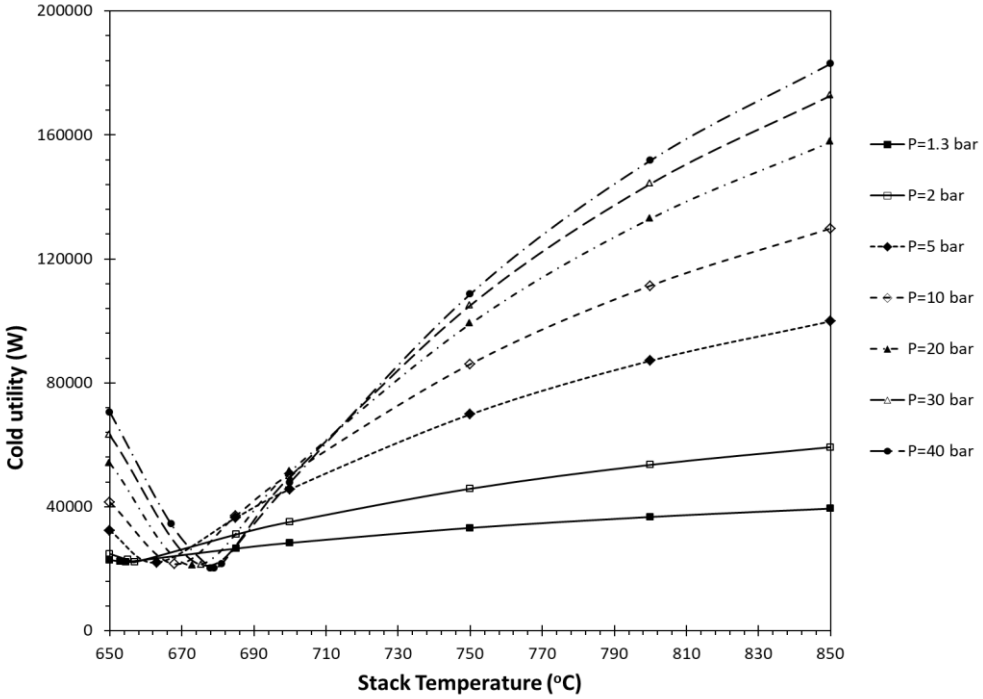

Figure 5-5: Cold Utility- Process Conditions, See Base Case - Vary stack P_s, T_s

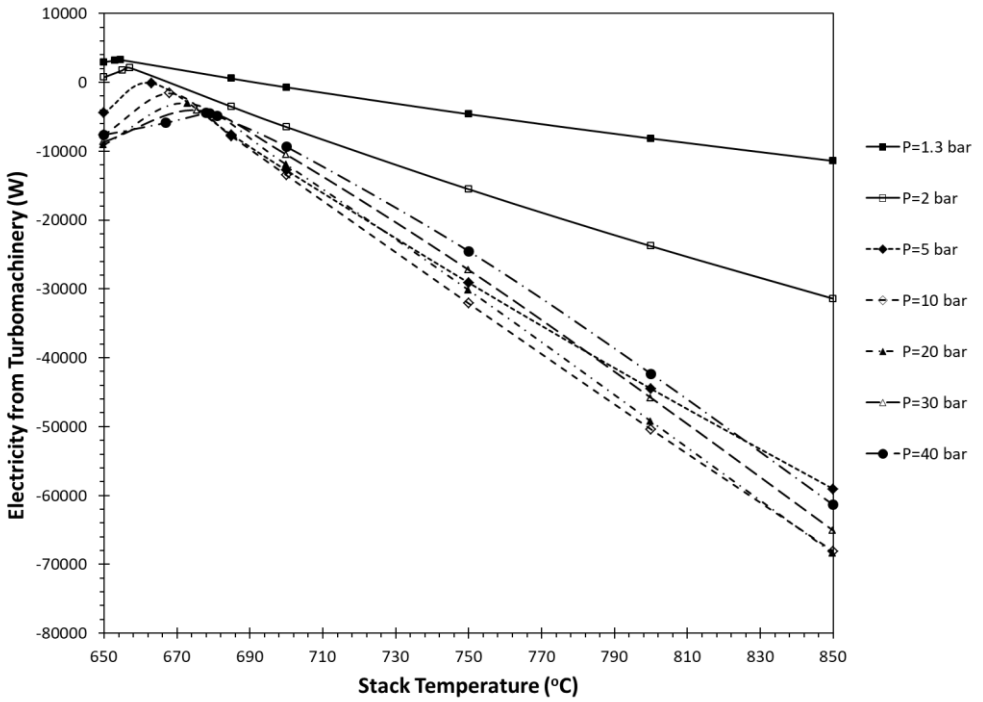

Figure 5-6: Electricity produced from BOP - Process Conditions, See Base Case - Vary stack P_s, T_s

Comparing the effect of heaters/coolers and compressors/expanders, it can be seen that the effect of hot and cold utility is much more prevalent, especially at high pressures where there is a rapid increase of both utilities. This increase is the main contributor to exergy and energy efficiencies reduction. At high stack pressure, both efficiencies reduce substantially when operating in either endothermic or exothermic mode. However, this reduction is milder when the stack pressure is lower. In general, exergy and energy efficiencies follow the trend of hot and cold utility.

As far as the electricity consumption by the stack is concerned, the explanation of the trend is simple. Current density for this sensitivity analysis remains constant and therefore what determines electricity consumption is solely cell voltage. By increasing stack temperature, ΔG^o is reduced for steam electrolysis and therefore the reversible voltage is also reduced. Higher temperature also leads to lower overpotential losses, ending up at lower cell voltage. That is the reason why an increase in temperature results in less power consumption. On the other hand, an increase in pressure results in risen cell voltages and since current density is fixed, the stack electricity needs are heightened (see Figure 5-7).

Another question which arises is: "Why the true maximum of the exergy and energy efficiencies lies at higher stack pressure?". To answer this question, one has to remember that the light separator (i.e. light gases separator) operates also at stack pressure so while varying the stack pressure, the pressure of flash separation also varies. It is well understood that while flash separation takes place at high pressure, the separation will be less effective. Flashing at higher pressure has two distinct effects:

- Fewer gasses are led to the afterburner where they are converted to lower quality gases (such as H_2O and CO_2)
- More gasses are led to the distillation column and still remain in their high-quality state (i.e. fuels such as CH_3OH, H_2, and CO have higher molar chemical exergy than their oxidized states such as CO_2 and H_2O)

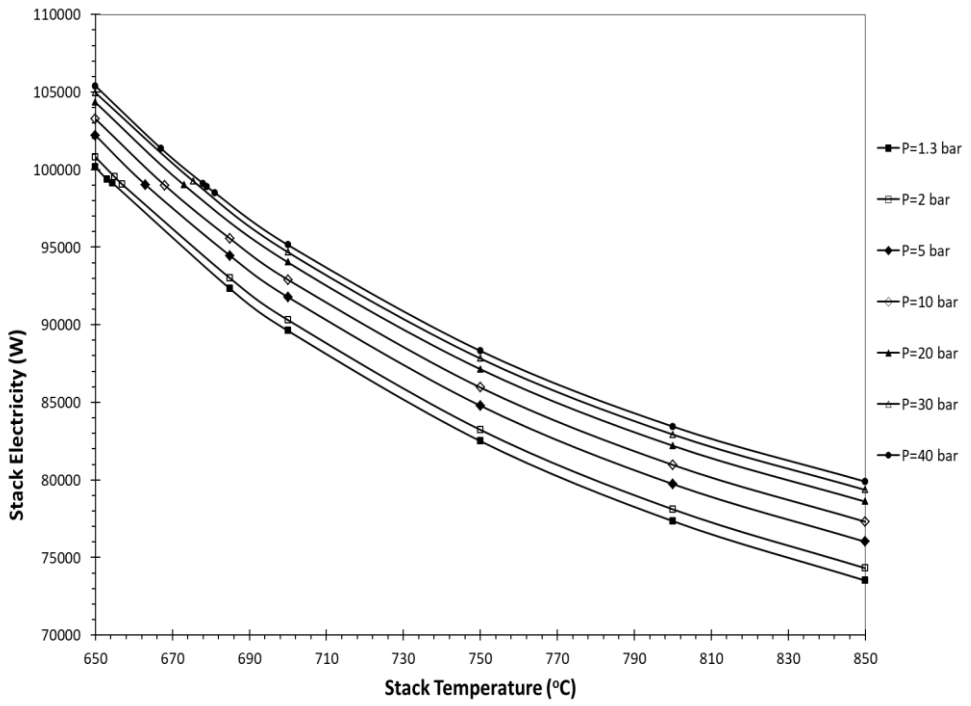

Figure 5-7: Stack Electricity Requirement- Process Conditions, See Base Case - Vary stack P_s, T_s

Hence, flashing at higher pressures more methanol of less purity will be stored. Even though purity will be less, "high quality" products will give a distinct push to the exergy efficiency which maximizes at higher pressures. Methanol produced and methanol purity as a function of stack pressure are depicted in Figure 5-8. A final note is that methanol production is not dependent on stack temperature, but on steam utilization. Steam utilization

determines the hydrogen flow rate at the rSOC outlet and CO_2 incoming flow is always determined so that $CO_2/H_2=1/3$. Energy efficiency is also maximized at higher stack pressure due to increased stored methanol flow.

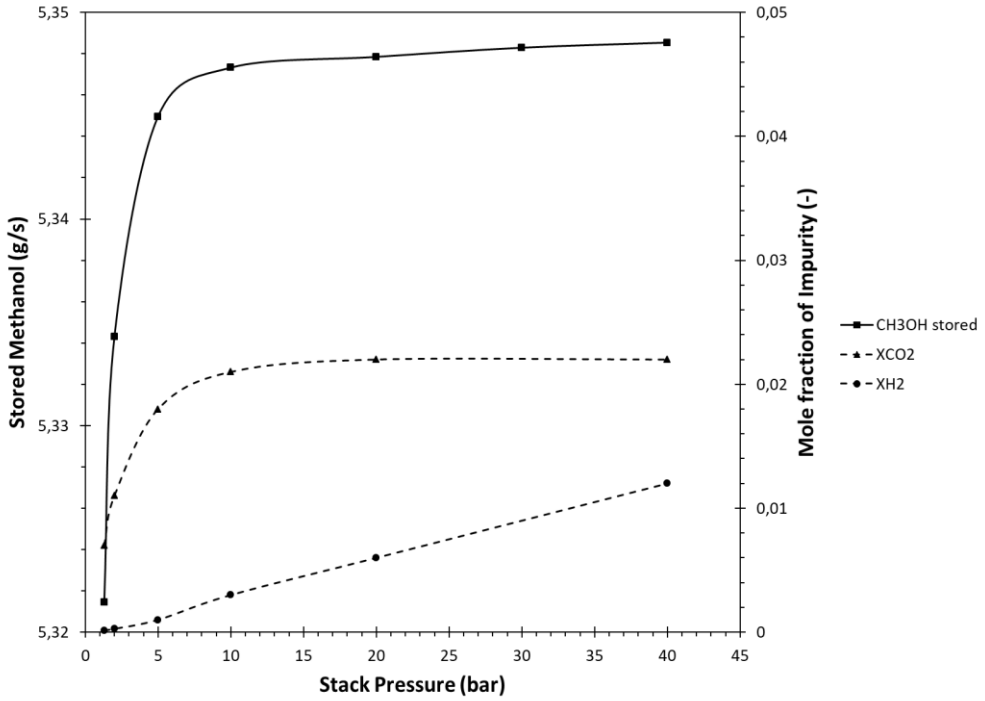

Figure 5-8: Methanol flow rate stored and impurities as a function of stack pressure

Effect of steam flow rate & Steam Utilization

Next, the effect of **H_2O molar flow rate** and the **steam utilization** is investigated. Steam utilization ranges from *0.3-0.9* whiles steam molar flow rate ranges from *0.4-1 mol/s* in this study. It must be noted that both parameters affect current density which ranges between 2000-9000 A/m^2. Also, the steam flow rate affects the ratio between H_2O and H_2 since the H_2 flow rate is kept constant. This ratio has a clear impact on the determination of cell voltage. It is important that the reader keeps in mind that the thermoneutral point of operation is the optimum one. A sensitivity analysis will be performed, while keeping constant stack pressure and temperature (i.e. 40 bar, 951.15 K from previous analysis). The results of the analysis are being shown below.

It can be seen that both parameters greatly affect exergy and energy efficiencies (Figure 5-9 & Figure 5-10). This happens because they directly affect cell reversible voltage and current density. Those parameters affect the mode of the electrolysis stack and the significance of the sweep gas flow minimization can be observed through this analysis again. More specifically:

- For every H_2O molar flow rate there is an ascending part followed by a peak and finally a descending part
- For every H_2O molar flow rate, the maximum point of each curve takes place at different steam utilization. More specifically, while steam molar flow rate increases, the optimum steam utilization decreases
- The true maximum occurs at the highest steam molar flow rate (i.e. maximum H_2O/H_2 feed)

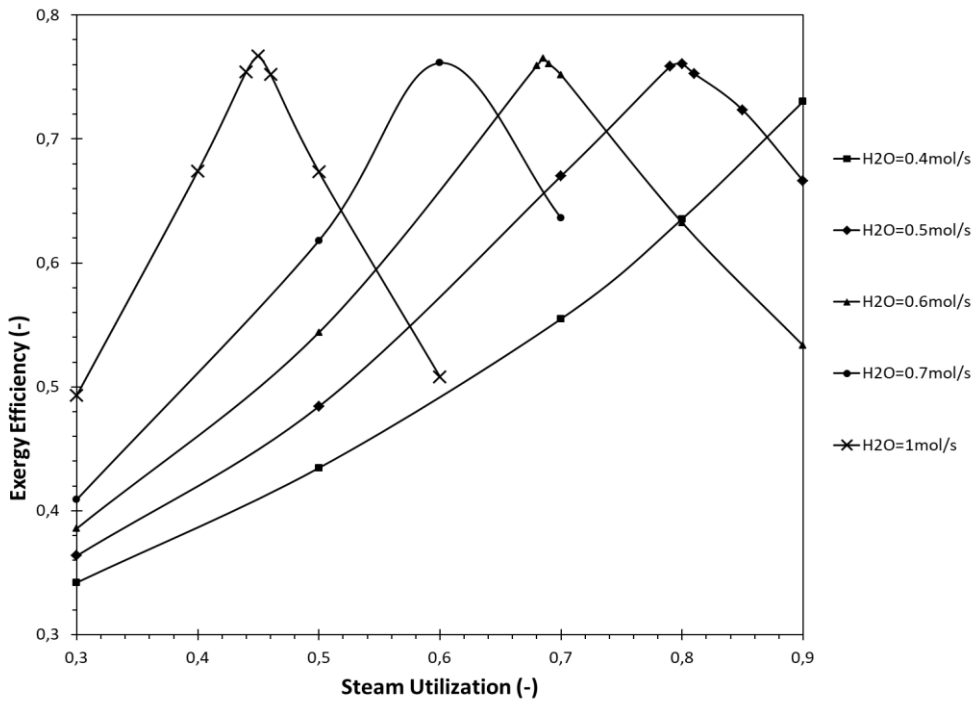

Figure 5-9: Exergy Efficiency - Process Conditions, See Base Case, fix P_s=40bar, T_s=951.15K, Vary Steam Utilization and steam feed flow rate

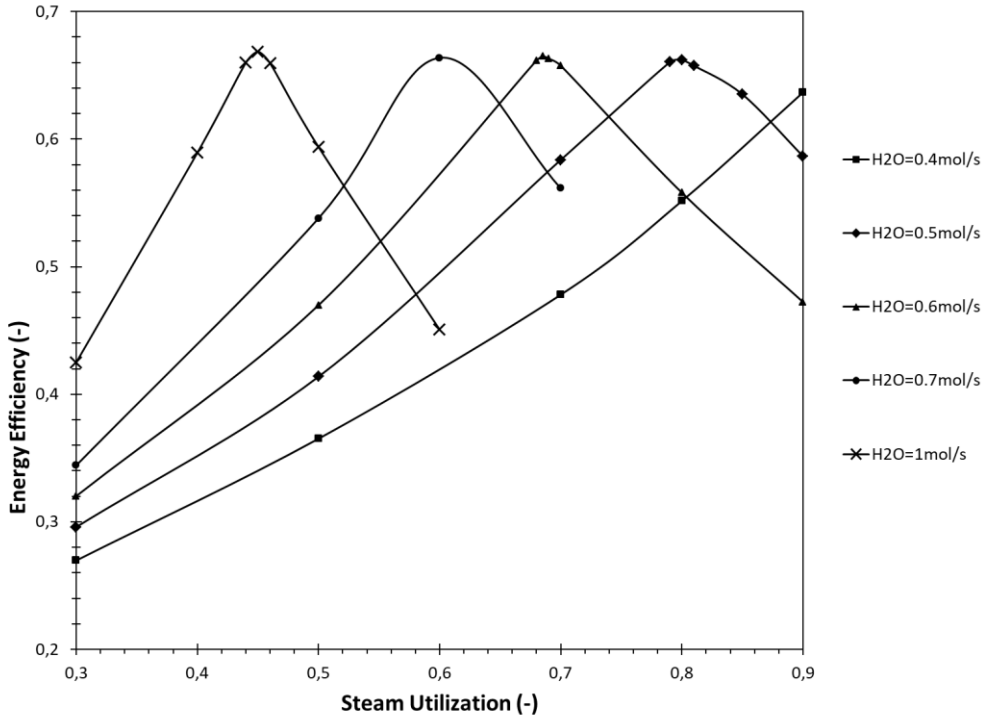

Figure 5-10: Energy Efficiency - Process Conditions, See Base Case, fix P_s=40bar, T_s=951.15K, Vary Steam Utilization and steam feed flow rate

It is well understood that by increasing H_2O/H_2 ratio, the reversible voltage decreases according to Eq. (2-5). That is the reason why the thermoneutral point will be reached at higher current densities. Higher current densities imply that higher $\dot{n}_{H_2O} \cdot U_f$ is required. Indeed, as the steam flow rate increases, a corresponding increase in $\dot{n}_{H_2O} \cdot U_f$ is observed, despite the fact that thermoneutral operation occurs at lower steam utilization. The product $\dot{n}_{H_2O} \cdot U_f$ is calculated for the maximum point of each curve in Table 5-3:

Table 5-3: Product ($n_{H2O}U_{f,steam}$) for the optimized point of exergy and energy efficiencies and for each steam molar flow rate

Steam Molar flow rate $(\dot{n}_{H_2O})$	***Steam Utilization*** $(U_{f,steam})$	***Product*** $(\dot{n}_{H_2O} \cdot U_{f,steam})$
0.4	0.9	0.36
0.5	0.8	0.4
0.6	0.685	0.411
0.7	0.6	0.42
1	0.45	0.45

It can be inferred that increased current density (i.e. higher product $\dot{n}_{H_2O} \cdot U_f$), is accompanied by enhanced H_2 production and therefore heightened methanol production. Increased current density also imposes greater electricity consumption by the stack. This explains the similar trend of electrical power consumption and methanol produced while varying steam molar flow rate and steam utilization as it is depicted in Figure 5-11 & Figure 5-12.

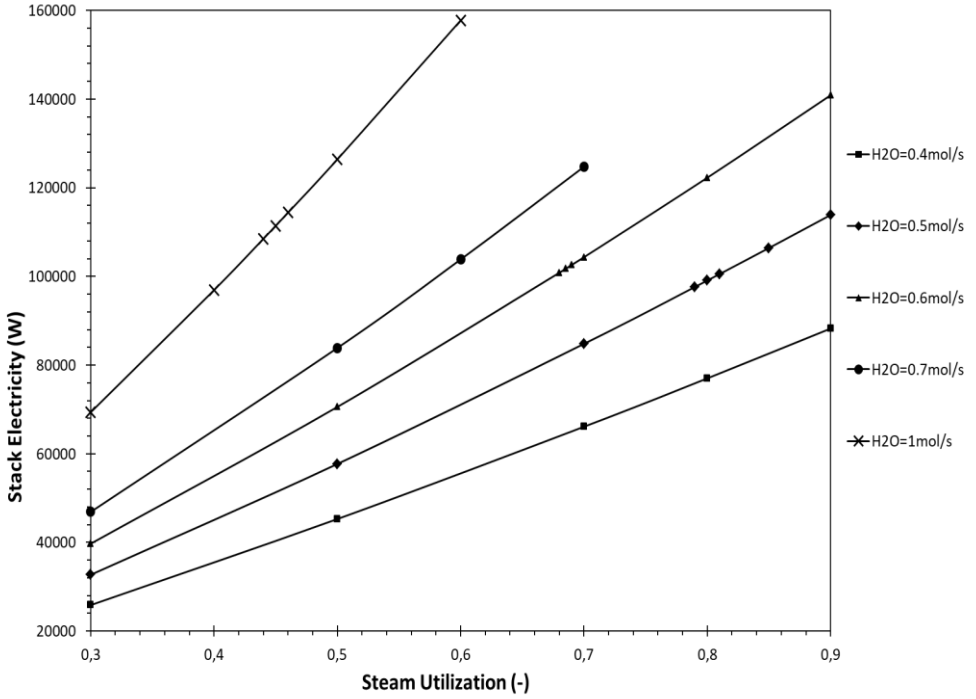

Figure 5-11: Stack Electricity Requirement - Process Conditions, See Base Case, fix P_s=40bar, T_s=951.15K, Vary Steam Utilization and steam feed flow rate

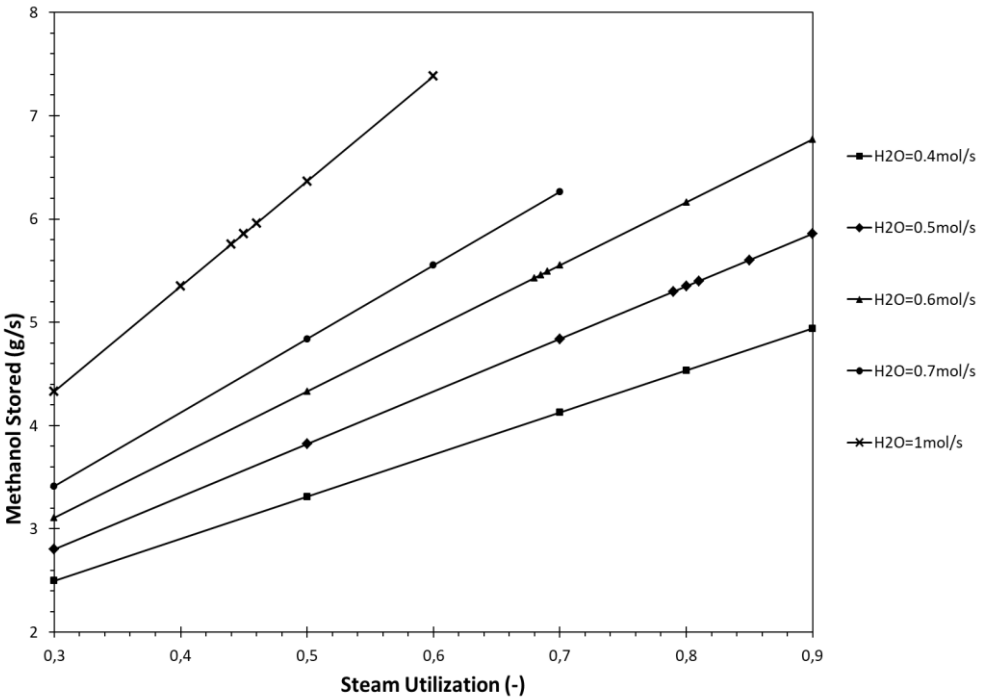

Figure 5-12: Stored Methanol flow rate - Process Conditions, See Base Case, fix P_s=40bar, T_s=951.15K, Vary Steam Utilization and steam feed flow rate

At a steam molar flow rate of 1 mol/s and steam utilization of 0.45 the corresponding current density is approximately 6700 A/m^2. For the maximization of exergy efficiency, one could continue increasing steam molar flow rate and decreasing steam utilization while preserving thermoneutral operation till the current density reaches 10000 A/m^2 which is considered as the upper limit in the current work. The true maximum of the optimization lies there, however, the procedure will stop here and values of 1 mol/s and 0.45 will be adopted for the rest of the simulations due to the fact that the increase will not be substantial.

It is plausible that the electricity produced from turbomachinery is minimized at thermoneutral operation. In general, when moving away from thermoneutral operation and the sweep gas flow rate increases, it becomes the dominant factor in determining the electricity produced by system turbomachinery. The reader must also reminisce that the sweep gas train always produces net electricity in every conceivable case. Therefore, divergence from thermoneutral operation always gives a boost to the net electricity produced by the turbomachinery. When the sweep gas flow rate is negligible (i.e. thermoneutral operation), electricity produced by the turbomachinery is mainly determined by the rest of expanders and compressors. Electricity produced is still positive since the pressurized content of components such as H_2 and CO_2 is exploited through expansion while the compression section includes H_2 pressurization before the methanol synthesis and the slight consumption by the recycle compressor to compensate for the reactor pressure drop (see Figure 5-13).

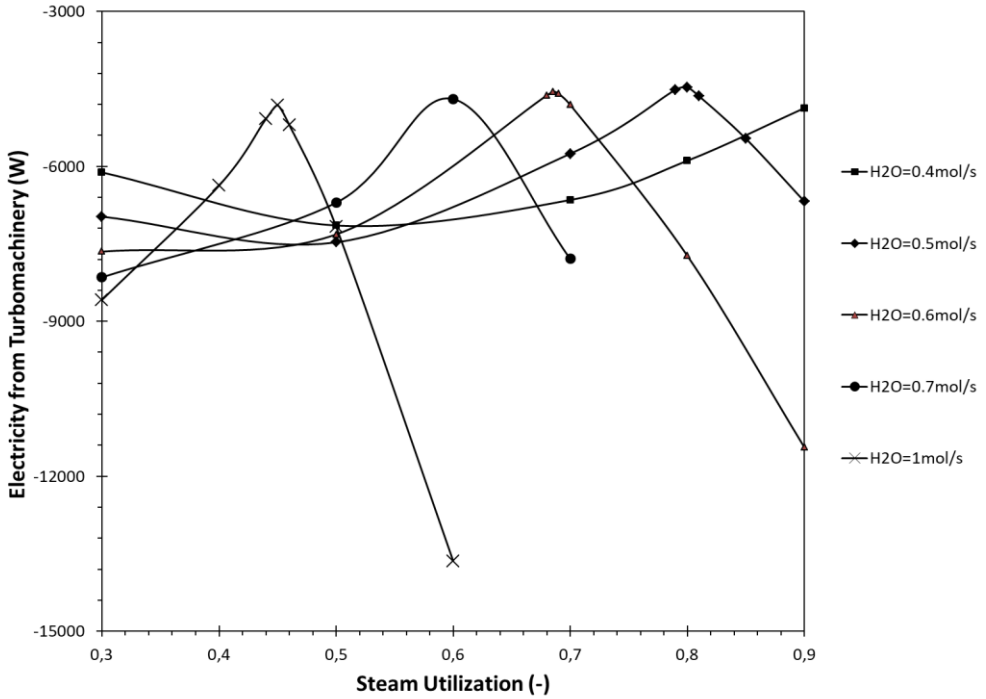

Figure 5-13: Electricity produced from turbomachinery - Process Conditions, See Base Case, fix P_s=40bar, T_s=951.15K, Vary Steam Utilization and steam feed flow rate

Regarding the hot and cold utility, it is clear that moving away from thermoneutral operation increases their values. Since stack pressure and temperature is the same during this sensitivity analysis, pressure ratio and temperatures in all heaters and coolers remain the same. However, it is the increased flow rate of sweep gas which enhances both utilities. For example, a cold stream is heated up from 50°C to 300°C (i.e. in sweep gas compression section) while a hot stream with greater $\dot{m}c_p$ (i.e. in sweep gas expansion section) is cooled down from 260°C to 40°C. Assuming a pinch temperature difference of 10K, the cold stream will be heated up from 50°C till 250°C, while the hot stream will cool down from 260°C to 60°C. The cold stream needs to be heated from 250°C to 300°C and it needs external hot utility, while the hot stream needs to be cooled down from 60°C to 40°C with external cold utility. In every case, this temperature difference remains the same, but the sweep gas flow rate increases when diverging from thermoneutral operation and in order to cover the same temperature difference for the cold and hot stream, more hot and cold utility is needed respectively (see Figure 5-14 & Figure 5-15). Electricity produced from turbomachinery affects efficiency in a minor way. More specifically, electricity produced from system turbomachinery is minimized at the thermoneutral point of operation while it is increased when diverging from it. The increased methanol production and electricity from turbomachinery at high steam utilizations and high steam molar flow rates are not enough to counteract the excessive increase of the hot and cold utility. This is also the reason why the exergy and energy efficiencies graph mainly follows the trend imposed by the hot and cold utility.

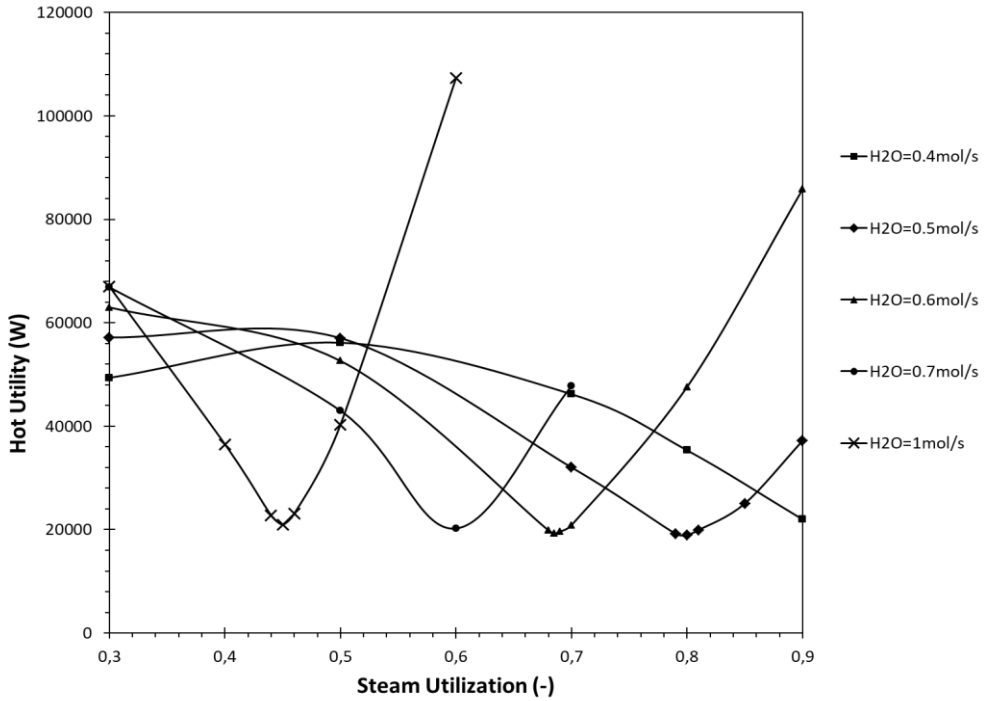

Figure 5-14: Hot Utility - Process Conditions, See Base Case, fix P_s=40bar, T_s=951.15K, Vary Steam Utilization and steam feed flow rate

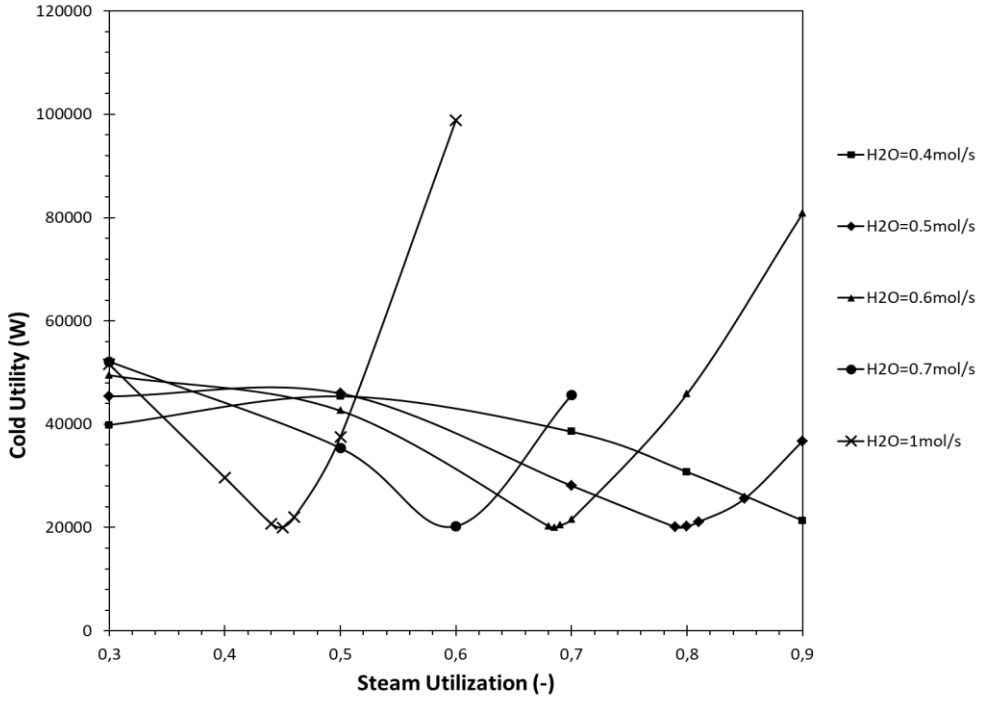

Figure 5-15: Cold Utility - Process Conditions, See Base Case, fix P_s=40bar, T_s=951.15K, Vary Steam Utilization and steam feed flow rate

Effect of Hydrogen flow rate

Afterwards, **the hydrogen molar flow rate** will be varied. Specifically, a range of *0.05-1 mol/s* is examined. It is expected that the four defined parameters from the optimization analysis (i.e. stack pressure, temperature, steam utilization, and steam molar flow rate) along with the constant flow rate of hydrogen will constitute an optimum set of parameters since they characterize a thermoneutral point of operation. The main question is, what is going to happen if the hydrogen molar flow rate diverges from the constant value already

used? In that case, thermoneutral operation is not achieved and a decrease in exergy efficiency is expected as shown (see Figure 5-16 & Figure 5-17).

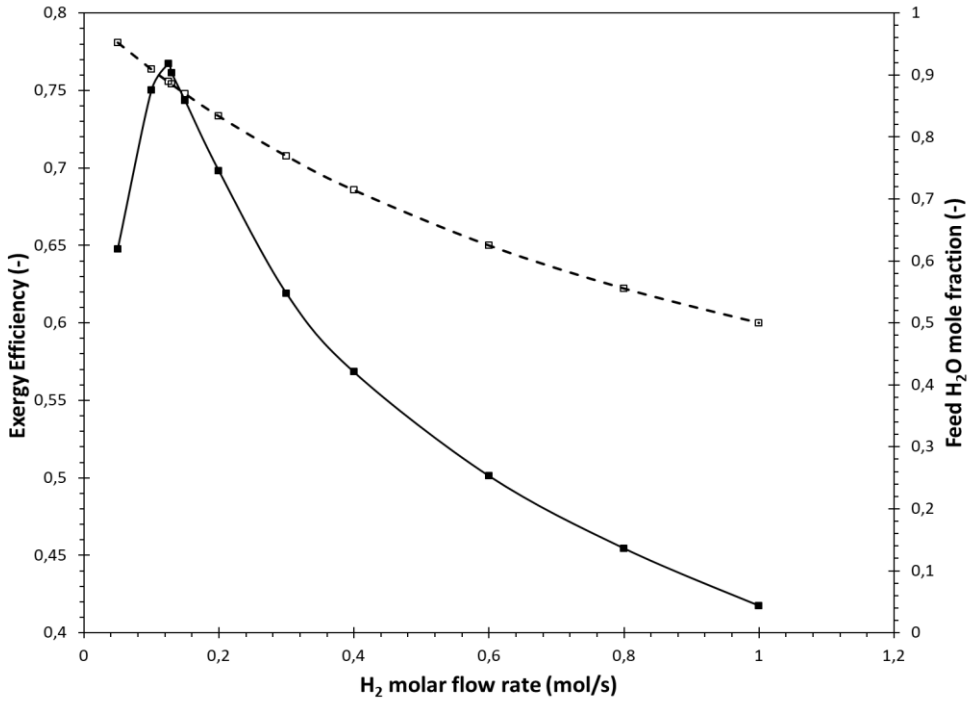

Figure 5-16: Exergy Efficiency - Process Conditions, See Base Case, fix P_s=40bar, T_s=951.15K, n_{H2O}=1mol/s, $U_{f,steam}$=0.45, Vary Hydrogen molar flow rate

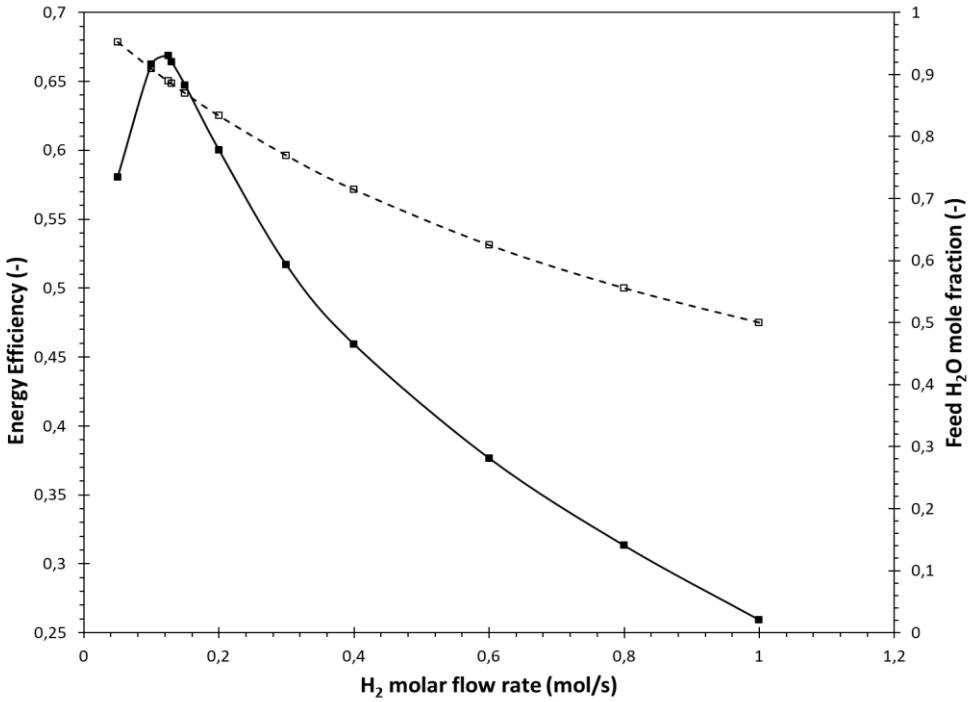

Figure 5-17: Energy Efficiency - Process Conditions, See Base Case, fix P_s=40bar, T_s=951.15K, n_{H2O}=1mol/s, $U_{f,steam}$=0.45, Vary Hydrogen molar flow rate

The author enhanced the hydrogen molar flow rate in such a way that a minimum steam mole fraction at stack inlet is 0.5. If the steam mole fraction is further reduced, then the stack inlet stream is not suitable for

electrochemical reduction but for oxidation. That is the reason why the molar flow rate of hydrogen is limited at 1 mol/s. Additional observations from the graphs are the following:

- Electricity from turbomachinery is minimized when operating at the thermoneutral point. Non-thermoneutral operation renders dominance of the sweep gas expansion section which produces more valuable electricity due to increased sweep gas flow rate (see Figure 5-18).

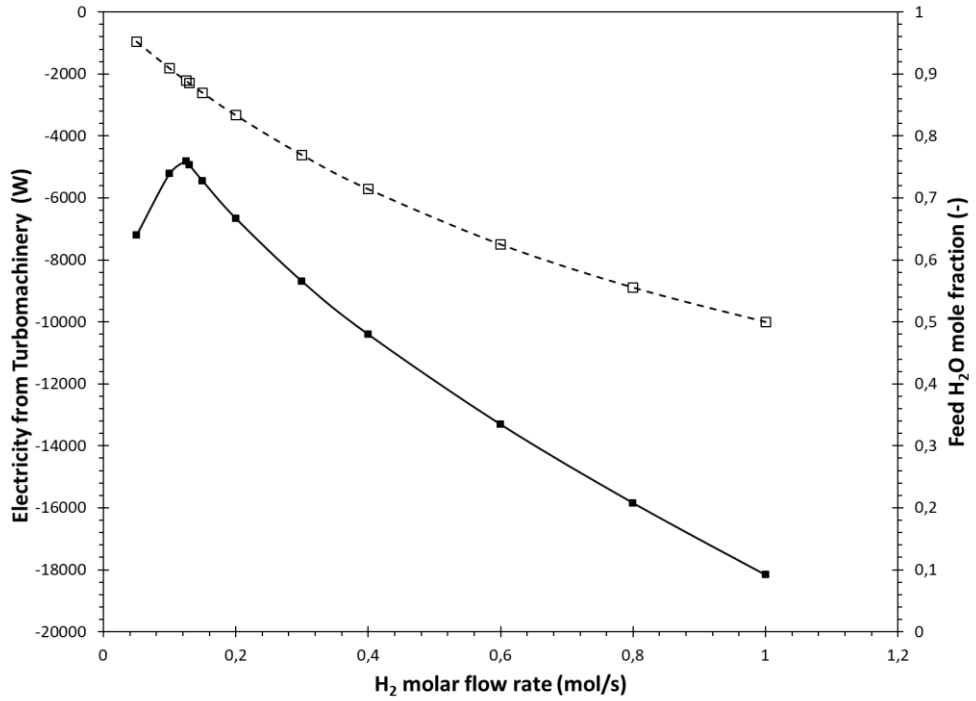

Figure 5-18: Electricity produced from turbomachinery - Process Conditions, See Base Case, fix P_s=40bar, T_s=951.15K, n_{H2O}=1mol/s, $U_{f,steam}$=0.45, Vary Hydrogen molar flow rate

- Cold and hot utility are also minimized when operating at the thermoneutral point (see Figure 5-19 & Figure 5-20). The reason behind the increase of hot and cold utility away from thermoneutral operation is the same as in the previous sensitivity analysis. By moving slightly away from the thermoneutral operation, the increase of sweep gas flow rate becomes important which imposes excessive duties on heaters and coolers.

- It should be clear that during this sensitivity analysis, current density remains constant since steam utilization and steam molar flow rate remain constant. An increase of hydrogen molar flow rate also increases the reversible cell voltage. This means that in order to achieve the same current density, a higher operating voltage is required which will give heightened electrical consumption. The shape of the curve which corresponds to the stack electrical consumption is not random. It follows a logarithmic form. This is due to the fact that reversible cell voltage is proportional to $\ln(x_{H_2})$ which is proportional to $\ln(\dot{n}_{H_2})$ since the steam molar flow rate remains constant (Figure 5-21).

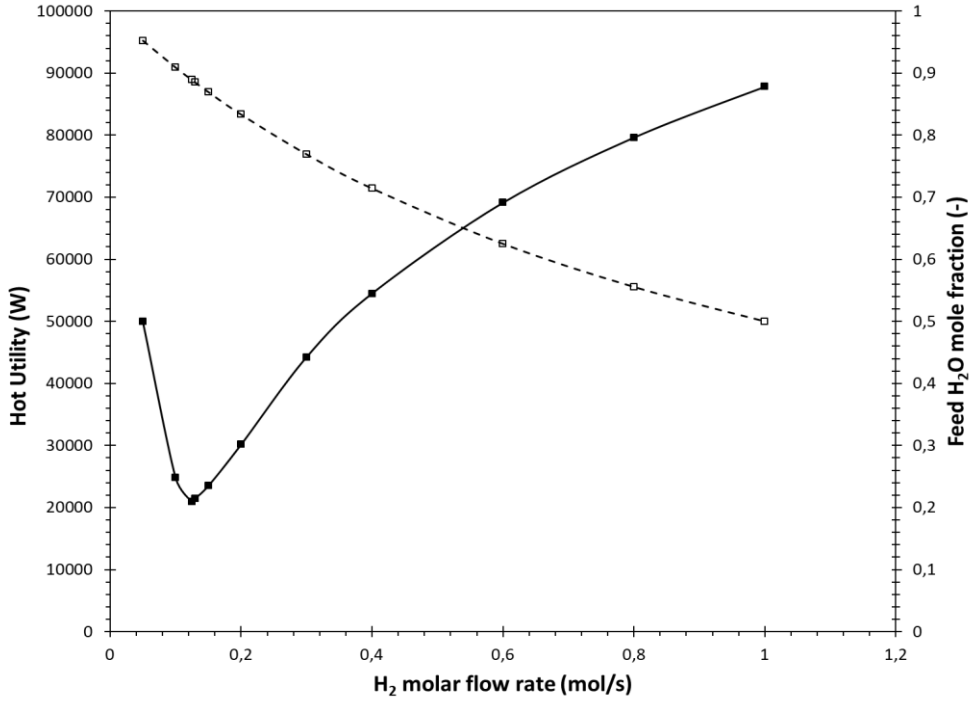

Figure 5-19: Hot Utility - Process Conditions, See Base Case, fix P_s=40bar, T_s=951.15K, n_{H2O}=1mol/s, $U_{f,steam}$=0.45, Vary Hydrogen molar flow rate

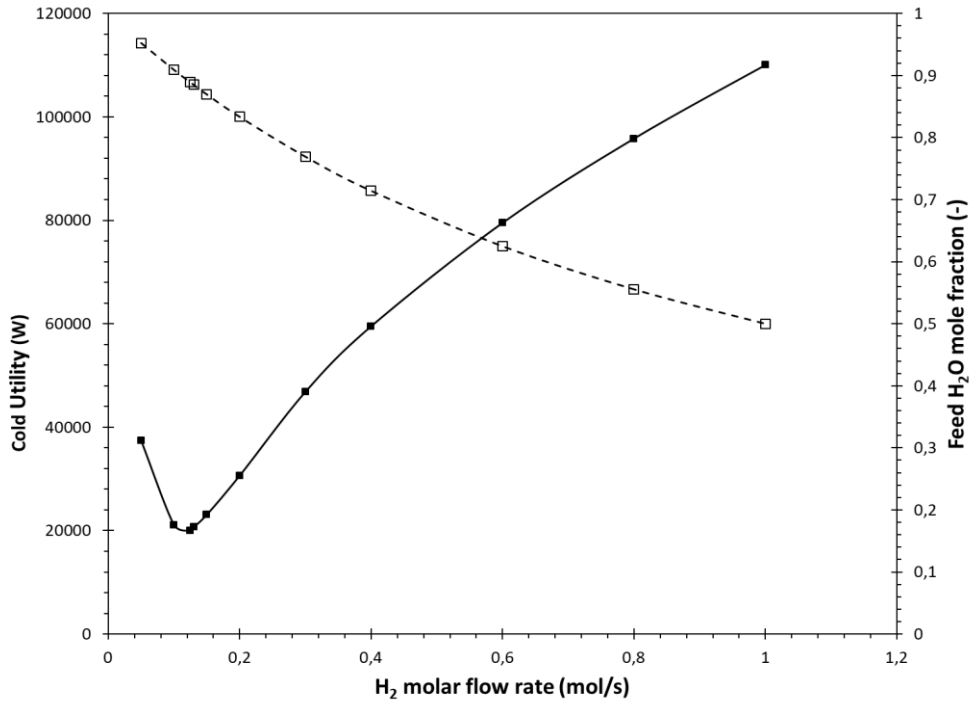

Figure 5-20: Cold Utility - Process Conditions, See Base Case, fix P_s=40bar, T_s=951.15K, n_{H2O}=1mol/s, $U_{f,steam}$=0.45, Vary Hydrogen molar flow rate

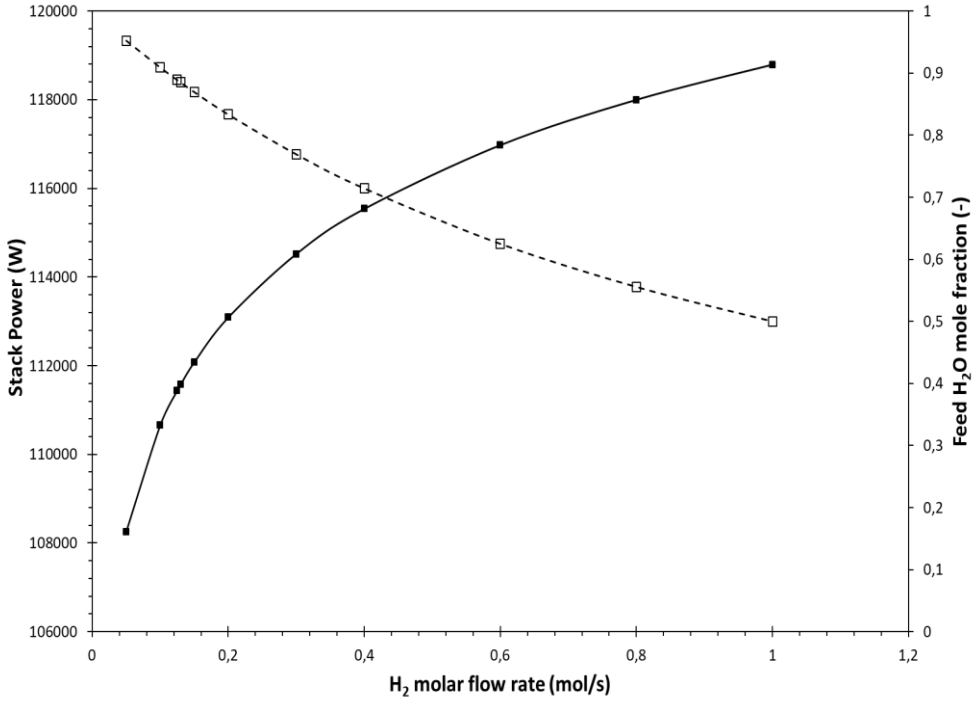

Figure 5-21: Stack Electricity Requirement - Process Conditions, See Base Case, fix P_s=40bar, T_s=951.15K, n_{H2O}=1mol/s, $U_{f,steam}$=0.45, Vary Hydrogen molar flow rate

- The increase of stored methanol flow rate as a function of hydrogen molar flow rate is linear as expected (see Figure 5-22). If the feed flow of hydrogen is increased, then the total flow of hydrogen at stack outlet is enhanced, which leads to heightened methanol production. Since kinetics are involved in the methanol synthesis reactor, if someone excessively increases hydrogen molar flow rate, the specified geometry of the reactor will not be able to reproduce this linear relation because residence time will drop rapidly

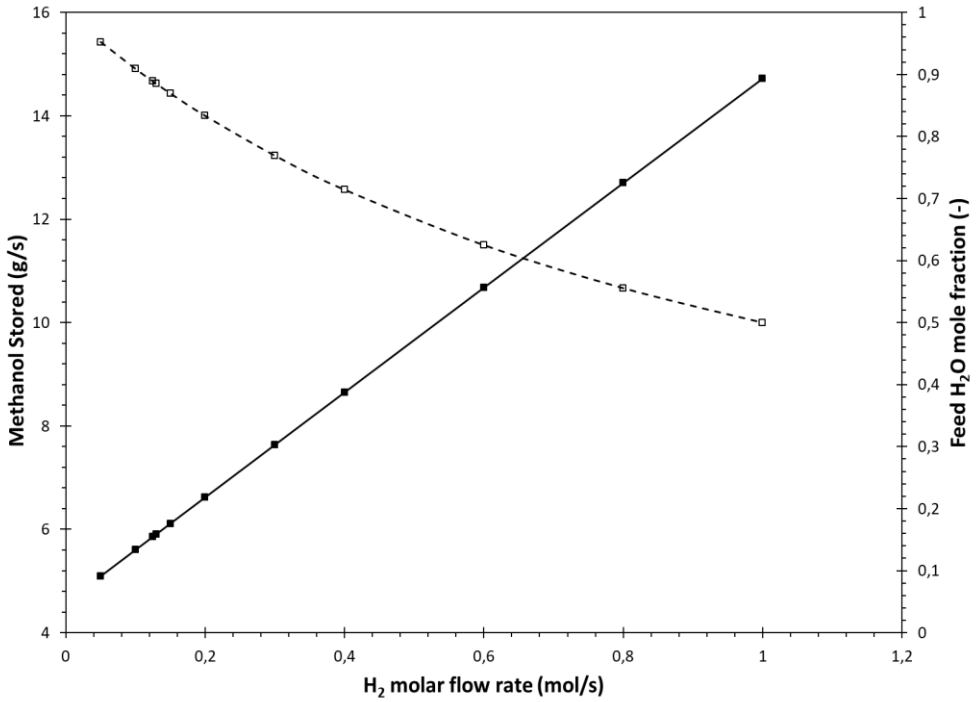

Figure 5-22: Stored Methanol flow rate- Process Conditions, See Base Case, fix P_s=40bar, T_s=951.15K, n_{H2O}=1mol/s, $U_{f,steam}$=0.45, Vary Hydrogen molar flow rate

Effect of Pressure and Temperature in Methanol Synthesis Reactor

Next, the sensitivity analysis will shift to **pressure and temperature of the methanol synthesis reactor**. Methanol synthesis technology is well-established but the intricate details of the reactions are still unknown. Generally, it is accepted that methanol formation is realized through CO_2 hydrogenation under 50-100 bar and temperatures up to 490-560 K over a $Cu/ZnO/Al_2O_3$ catalyst [61]. A range of *50-150 bar* and *460-540 K* is examined in this study. The reaction scheme is the following:

CO Hydrogenation:	$CO + 2H_2 \leftrightarrow CH_3OH$	$\Delta H_R^0 = -90.7 kJ/mol_{CO}$
CO_2 Hydrogeneration:	$CO_2 + 3H_2 \leftrightarrow CH_3OH + H_2O$	$\Delta H_R^0 = -49.5 kJ/mol_{CO_2}$
WGS:	$CO + H_2O \leftrightarrow CO_2 + H_2$	$\Delta H_R^0 = -41.2 kJ/mol_{CO_2}$

The above-mentioned reaction is strongly exothermic and the forward reaction is favored under high pressure. “Strongly exothermic” is also equivalent to “the reaction is favored at low temperatures”. Therefore, it is expected that the lower the temperature and the higher the pressure, the better the methanol yield. On the other hand, at lower temperature, the kinetics are sluggish even though the equilibrium yield is better. Bulky equipment and thus expenditure is needed for the realization of methanol synthesis at very low temperature. At low temperature (i.e. 460 K), it is observed that the higher the pressure, the less the stored methanol. At that temperature, the reaction rate of WGS reaction is also limited, resulting in more steam in the products. The increase of partial pressure of steam in the product stream results in decreased stored methanol and higher pressures seem to magnify this effect. Since in the existing reactor model the kinetic equations from the work of Van de Bussche and Froment are imported [67], the size of the reactor is defined as can be seen in Table 5-1. Reactor parameters are constant throughout the simulation. The reactor is simulated as a multi-tubular plug flow reactor.

Delving more into detail, the highest methanol yield is obtained when operating at 150 bar and 500°C (Figure 5-23) but this is not the point where maximum exergy and energy efficiencies are obtained (Figure 5-24 & Figure 5-25). Therefore again there is an interplay between hot utility (Figure 5-26), cold utility (Figure 5-27) and electricity produced from system turbomachinery (Figure 5-28).

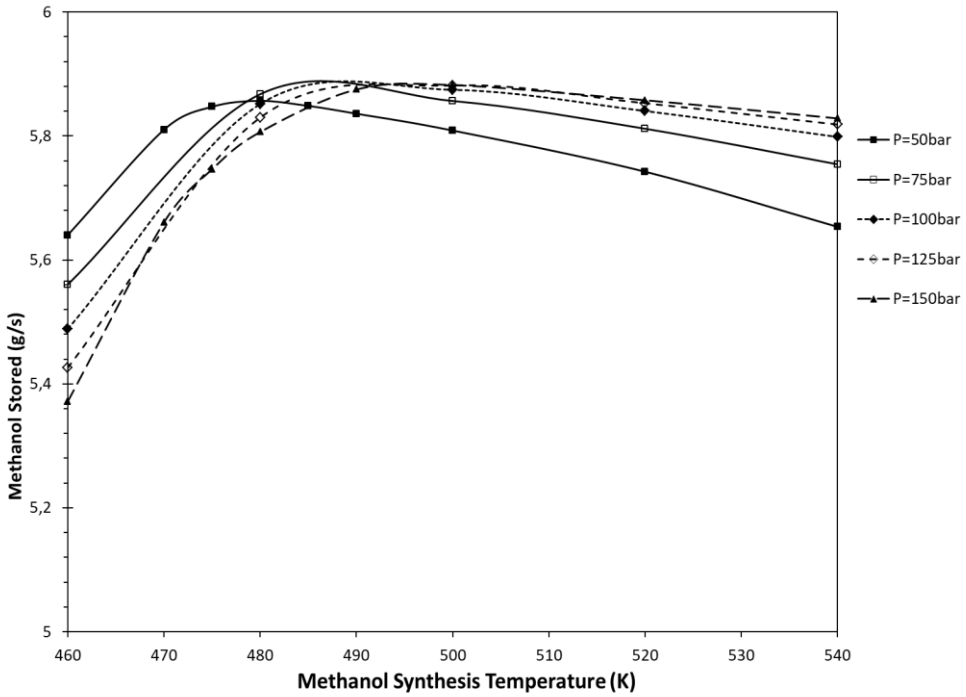

Figure 5-23: Stored Methanol flow rate - Process Conditions, See Base Case, fix P_s=40bar, T_s=951.15K, n_{H2O}=1mol/s, $U_{f,steam}$=0.45, n_{H2}=0.125mol/s, P_{CO2}=160bar, P_{H2}=700bar, Vary methanol synthesis pressure and temperature

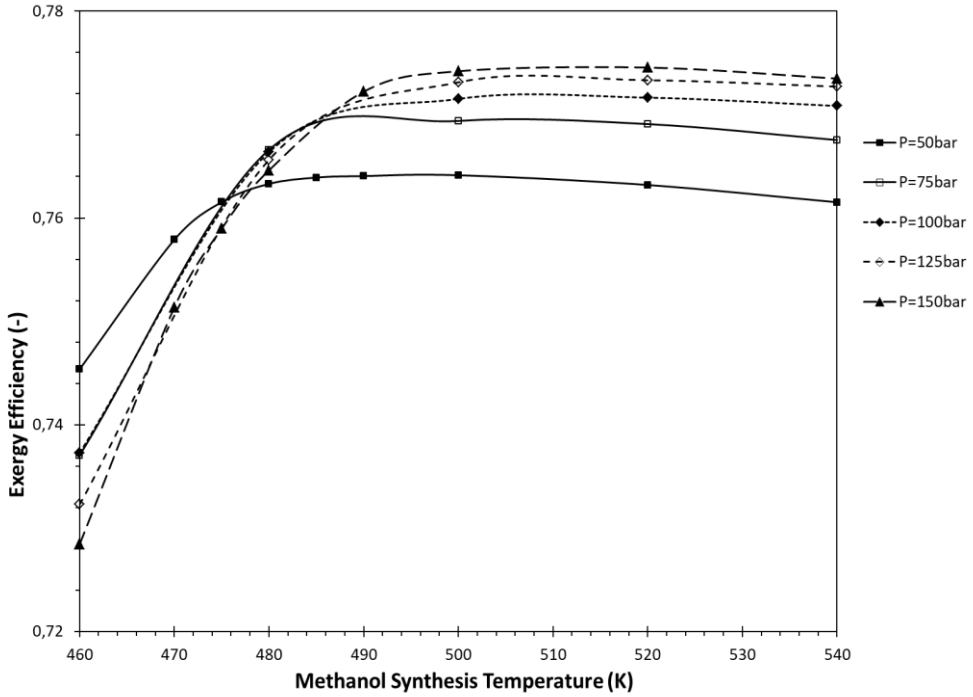

Figure 5-24: Exergy Efficiency - Process Conditions, See Base Case, fix P_s=40bar, T_s=951.15K, n_{H2O}=1mol/s, $U_{f,steam}$=0.45, n_{H2}=0.125mol/s, P_{CO2}=160bar, P_{H2}=700bar, Vary methanol synthesis pressure and temperature

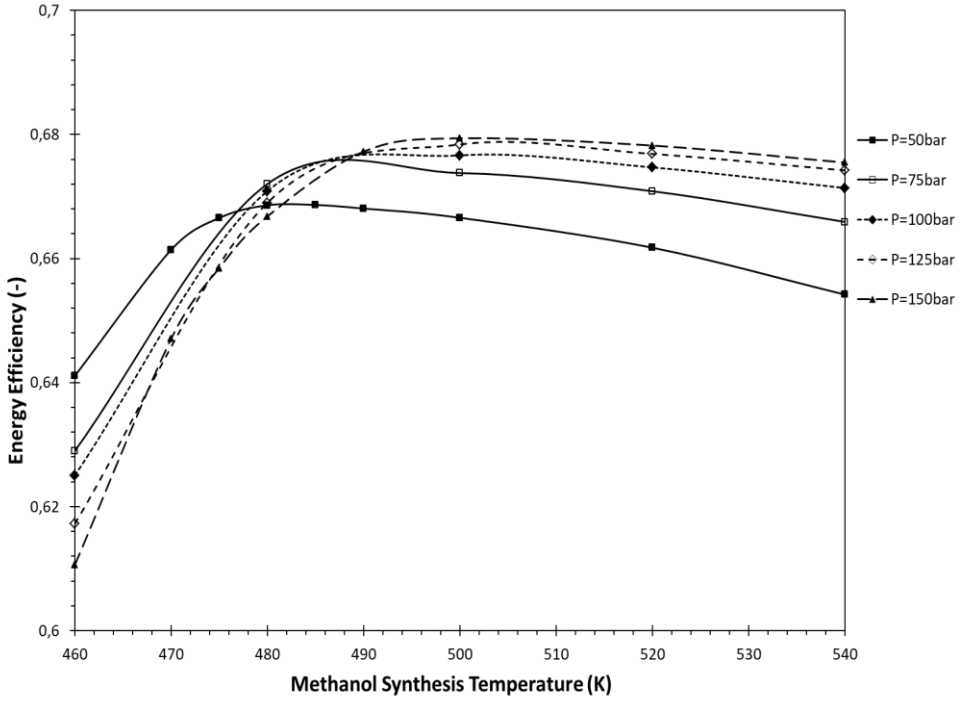

Figure 5-25: Energy Efficiency - Process Conditions, See Base Case, fix P_s=40bar, T_s=951.15K, n_{H2O}=1mol/s, $U_{f,steam}$=0.45, n_{H2}=0.125mol/s, P_{CO2}=160bar, P_{H2}=700bar, Vary methanol synthesis pressure and temperature

More specifically:

- The hot utility decreases with an increase in pressure. That occurs mainly due to efficient methanol conversion which reduces the recycle flow through the recycle heater, causing the hot utility to drop. The recycle heater can be heat integrated with the product condenser. Depending on the pinch point selected (i.e. 10 K), at every pressure, the pinch difference has to be covered externally. Since in every

case, the same temperature difference must be covered, the heat duty is mainly determined by the recycle flow of unreacted gases through the recycle heater (see Figure 5-26).

- On the other hand, at a constant pressure, the hot utility (see Figure 5-26) rises till a specific temperature and then drops again. At most, it has to do with the product condenser duty. Whenever the conversion is inefficient, for example at very low and very high temperature (i.e. 460°C or 540°C), the product mixture consists mainly of H_2, CO, and CO_2, and when the condenser is tasked to condense the product mixture, more heat of condensation is released, giving more opportunities for heat integration and lowering the hot utility. When the conversion is efficient, then the condenser releases less duty to the environment during condensation since the product consists mostly of methanol and water and the mixture will condense at a higher temperature. The last case is beneficial for reducing condenser duty, but on the other hand, less heat is released and therefore, hot utility increases

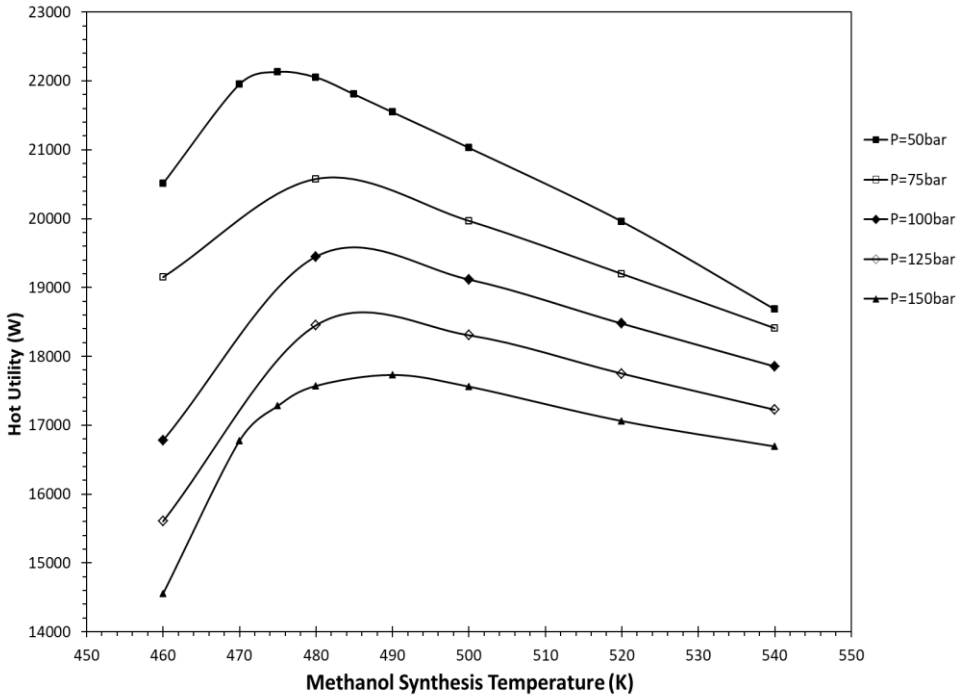

Figure 5-26: Hot Utility - Process Conditions, See Base Case, fix P_s=40bar, T_s=951.15K, n_{H2O}=1mol/s, $U_{f,steam}$=0.45, n_{H2}=0.125mol/s, P_{CO2}=160bar, P_{H2}=700bar, Vary methanol synthesis pressure and temperature

- When trying to explain why cold utility drops (see Figure 5-27) at every pressure with an increase of temperature one would come to the following conclusion. There are two factors that have opposite effects. At low temperature, methanol synthesis reactor duty desires to lower system cooling utility due to poor conversion, but on the other hand, poor conversion increases cooling utility from condensation because condensation will occur at even lower temperature when a stream contains mostly H_2, CO_2, and CO rather than H_2O and CH_3OH. At low temperature, the cooling utility is increased due to inefficient conversion. As temperature increases, methanol reactor cooling duty will increase slightly while condensation duty falls abruptly as shown in Table 5-4 rendering the condensation duty as the dominant factor for determining the cold utility

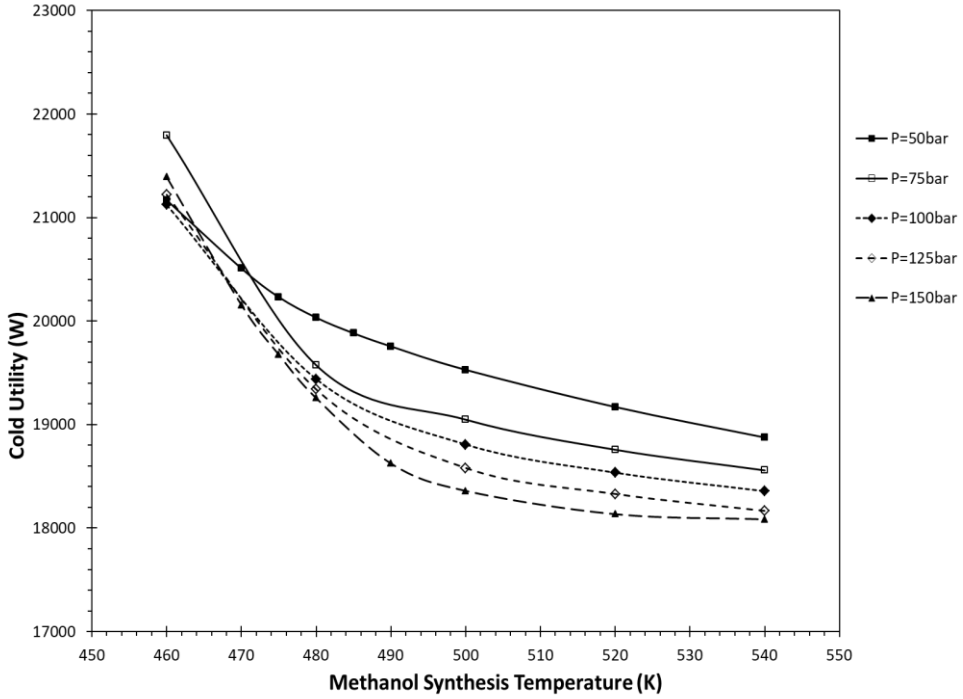

Figure 5-27: Cold Utility - Process Conditions, See Base Case, fix P_s=40bar, T_s=951.15K, n_{H2O}=1mol/s, $U_{f,steam}$=0.45, n_{H2}=0.125mol/s, P_{CO2}=160bar, P_{H2}=700bar, Vary methanol synthesis pressure and temperature

- As pressure increases, the electricity produced from turbomachinery is reduced due to enhanced power consumption for the compression of H_2 and also less work produced from the CO_2 expansion stage due to decreased pressure ratio. Electricity produced by system turbomachinery is almost unaffected when varying the reactor temperature (see Figure 5-28)

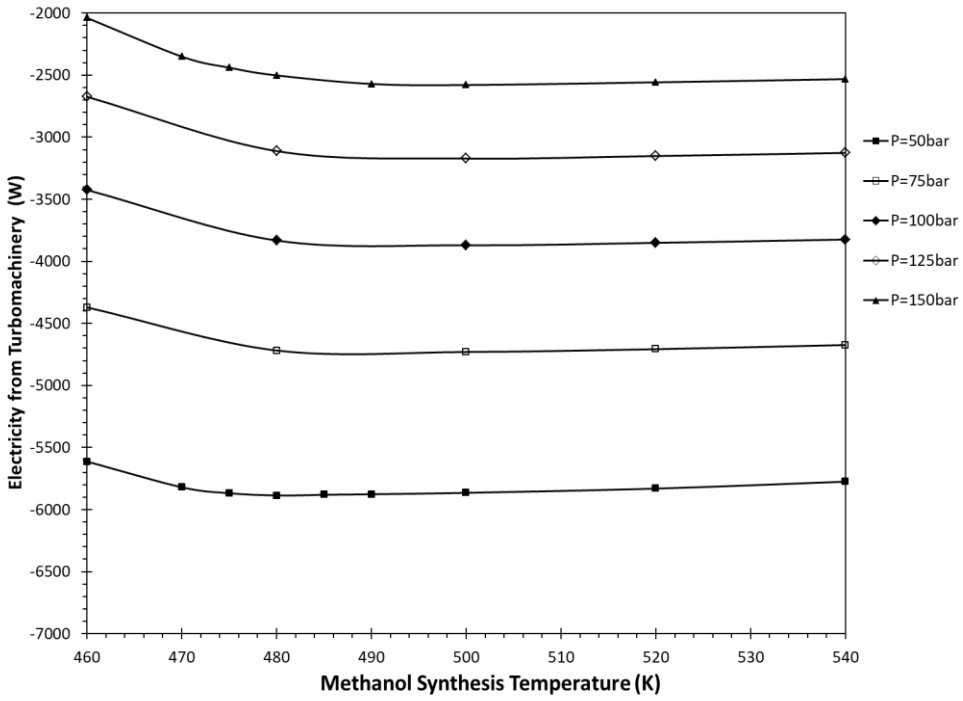

Figure 5-28: Electricity produced from turbomachinery - Process Conditions, See Base Case, fix P_s=40bar, T_s=951.15K, n_{H2O}=1mol/s, $U_{f,steam}$=0.45, n_{H2}=0.125mol/s, P_{CO2}=160bar, P_{H2}=700bar, Vary methanol synthesis pressure and temperature

Table 5-4: Cooling duty of methanol reactor and product condenser at 150 bar and varying temperature

Pressure	*150 bar*	
Temperature (K)	*Methanol Reactor (kW)*	*Condensation Duty (kW)*
460	11.72	41.70
480	12.01	24.92
500	12.33	22.35
520	12.23	25.20
540	12.14	28.67

Before reporting the process conditions of the optimized case, it has to be noted that additional sensitivity analyses have been conducted as well. Those analyses regard the following:

- CO_2 and H_2 storage pressure (80-160 bar & 100-700 bar respectively)
- Fractional recovery for the heavy and light component of the distillation column (0.001-0.05 & 0.9-0.999 respectively)
- Isentropic efficiency for compressors and expanders (0.75-0.95 for both types of components)
- Stack inlet temperature of the sweep gas stream (40-200^{o}C)

These sensitivity analyses had minor impact on the exergy and energy efficiencies and therefore the results are omitted. However, the change of these magnitudes during the transition from the base case to the optimized case is stated in the section below. The impact of those changes in the optimized energy and exergy efficiencies is also incorporated in the final values.

5.1.3 Optimized Case Parameters – Electrolysis mode

Table 5-5 contains the process parameters which constitute the optimized case for electrolytic operation.

Table 5-5: Optimized Case Parameters - Electrolysis

Parameter	*Value*	*Parameter*	*Value*
Number of cells (-)	1300	Pressure of feed CO_2 stream (bar)	160
Electrode area per cell (m^2)	0.01	Temperature of feed CO_2 stream (K)	298.15
Stack pressure (bar)	40	Length of PFR (m)	40
Stack temperature (K)	951.15	Number of tubes (-)	5000
Steam utilization (-)	0.45	Tube Diameter (m)	0.02
Oxidant inlet pressure (bar)	1	Porosity of catalyst (-)	0.5
Oxidant inlet temperature (K)	298.15	Density of catalyst (kg/m^3)	2000
Flow rate of feed water (mol/s)	1	Methanol Synthesis pressure (bar)	150
Pressure of feed water (bar)	1	Constant reactor temperature (K)	520
Temperature of feed water (K)	298.15	Outlet pressure of throttling valve leading to distillation (bar)	1.2
Flow rate of feed H_2 (mol/s)	0.125	Molar Reflux ratio	1.5
Pressure of feed H_2 (bar)	700	Light Recovery (Purity %)	0.999
Temperature of feed H_2 (K)	298.15	Heavy Recovery (Purity %)	0.001
Parameter	*Value*	*Parameter*	*Value*
Isentropic eff. of pumps and compressors(-)	0.95	Mole fraction of N_2 in feed sweep gas stream (-)	0.79
Isentropic eff. of turbines (-)	0.95	Mole fraction of O_2 in feed sweep gas stream (-)	0.21
Mechanical Losses of components	0.95	Mole fraction of water to syngas compression	0.01
Mole fraction of feed water (-)	1	Mole fraction of water to recycle compressor	0.002
Mole fraction of feed CO_2 (-)	1	Fraction of flow going to purge	0.01
Mole fraction of feed H_2 (-)	1	Partial Condenser of distillation column	0.05
Afterburner cooled exhaust gases temperature (^oC)	770.4		

During the transition from the base case to the optimized case energy efficiency has been increased from 52.4% in the base case to 68.74%, while exergy efficiency has also been increased from 59.48% to 77.67%. As it was mentioned in the base case, excessive hot utility (~63 kW) was responsible for the initial energy and exergy efficiencies. After the optimization process, the hot utility decreased from 63 kW to 19 kW.

5.2 System Exergy and Energy efficiencies & Optimization for fuel cell mode

In this section, the base case parameters and assumptions for the fuel cell model will be presented and then the optimization process and corresponding results will follow.

5.2.1 Base Case Parameters – Fuel Cell mode

Previously, in electrolysis mode, the base case conditions were already producing decent results. Hence, approximately the same process conditions will also be used in fuel cell operation. The rSOC stack remains the same as in the electrolysis mode. This means that the rSOC stack comprises by 1300 cells while the active electrode area per cell is 0.01 m^2. As far as the pressure is concerned, the pressure remains the same (i.e. 5 bar) as it was in the base case conditions during electrolysis mode. Pressurized fuel cell operation is beneficial for power production according to the Nernst equation. In addition, during the electrolysis optimization, it was seen that thermoneutral operation was beneficial for the energy and exergy efficiencies. Consequently, in the

fuel cell mode, it is expected that the lower the voltage drop, which will lead to less oxidant flow rate, will also be beneficial for fuel cell operation. Less voltage drop can be achieved through higher stack temperature or lower current densities. In the case where current density is fixed and temperature is increasing, then cell voltage will also increase which results in higher electricity production by the stack. For those reasons, the stack temperature in this base case has been increased by 50 K compared to the electrolysis base case. The base case parameters for fuel cell operation are summarized in Table 5-6. Since the rSOC stack during fuel cell operation necessitates heat removal, the sweep gas stack inlet stream is regulated to enter the stack at 60^{o}C *below* stack temperature. This temperature difference is again justified by the work of Wendel [19]. For this configuration, energy and exergy efficiencies are negative (i.e. energy efficiency of -91.35% and exergy efficiency of -83.73%). Those negative efficiencies are better justified in the first optimization step in section 5.2.2. This means that in order to satisfy the balance of plant in electricity needs, external electricity is required, while the stack is unable to generate electricity adequately. Therefore, despite the fact that the base case conditions in electrolysis were producing decent results, it seems that the efficiencies are abruptly reduced during fuel cell operation. These values can be considered as the starting point of the optimization process. Again, increased oxidant flow and high stack pressure induce excessive hot utilities (~193 kW) in the system. In addition, the refrigeration system also plays an important role in reducing both efficiencies.

Table 5-6: Base Case Parameters – Fuel Cell Mode

Parameter	***Value***	***Parameter***	***Value***
Number of cells (-)	1300	Temperature of feed CH_3OH (K)	298.15
Electrode area per cell (m^2)	0.01	Flow rate of feed H_2O (mol/s)	0.25
Stack pressure (bar)	5	Pressure of feed H_2O (bar)	1
Stack temperature (K)	1023.15	Temperature of feed water (K)	298.15
Fuel utilization (-)	0.8	Reforming Temperature (K)	523.15
Inlet oxidant pressure (bar)	1	Pressure of H_2 storage (bar)	700
Inlet oxidant temperature (K)	298.15	Pressure of CO_2 storage (bar)	160
Flow rate of feed methanol (mol/s)	0.25	Temperature of Water Gas Shift Reaction (K)	523.15
Pressure of feed methanol (bar)	1		
Parameter	***Value***	***Parameter***	***Value***
Isentropic eff. of pumps and compressors (-)	0.85	Mole fraction of O_2 in feed sweep gas stream (-)	0.21
Isentropic eff. of turbines (-)	0.75	Mole fraction of water to double stage compression (-)	0.005
Mechanical Losses of components	0.95	Mole fraction of CO2 to final hydrogen stream (-)	0.01
Mole fraction of feed water (-)	1	CF_4 Evaporator Temperature (Ref. Cycle) (^{o}C)	-109
Mole fraction of feed CH_3OH(-)	1	CO_2 condenser Tempereature (Ref. Cycle) (^{o}C)	30
Mole fraction of N_2 in feed oxidant stream (-)	0.79		

5.2.2 Optimization of Fuel Cell mode and Results

Effect of stack pressure and temperature

After the initialization of the above values into the electrolysis model, the optimization procedure is initiated. Firstly, **stack pressure** and **temperature** are varied. The pressure is varied in the range of *1-8 bar*, while the temperature is varied from *923.15-1123.15 K*. The results are depicted in the graph below. By observing the resulting figures, one can make the following conclusions:

- Exergy and energy efficiencies follow the same trend (see Figure 5-29 & Figure 5-30)
- There is a pressure of 1.2 bar where the maximum energy and exergy efficiencies are obtained for the whole temperature range

- The higher the stack temperature the better the system performance
- At high stack pressure, exergy and energy efficiencies are negative. This means that in order to sustain the process the system requires electricity from external sources (i.e. net electricity production is negative)

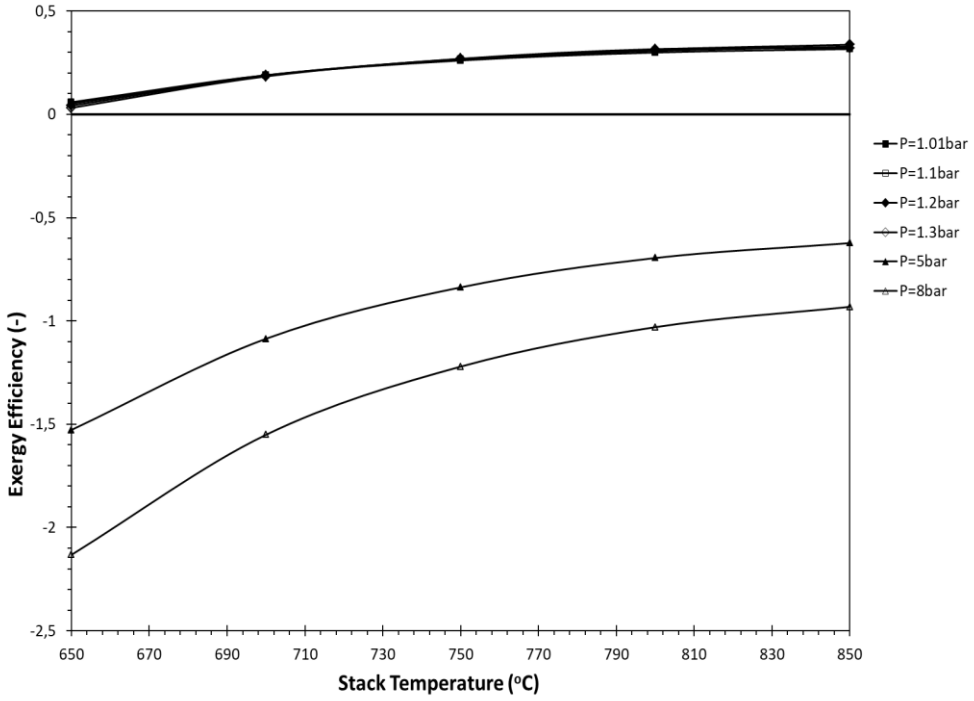

Figure 5-29: Exergy efficiency - Process Conditions, See Base Case - Vary stack P_s, T_s

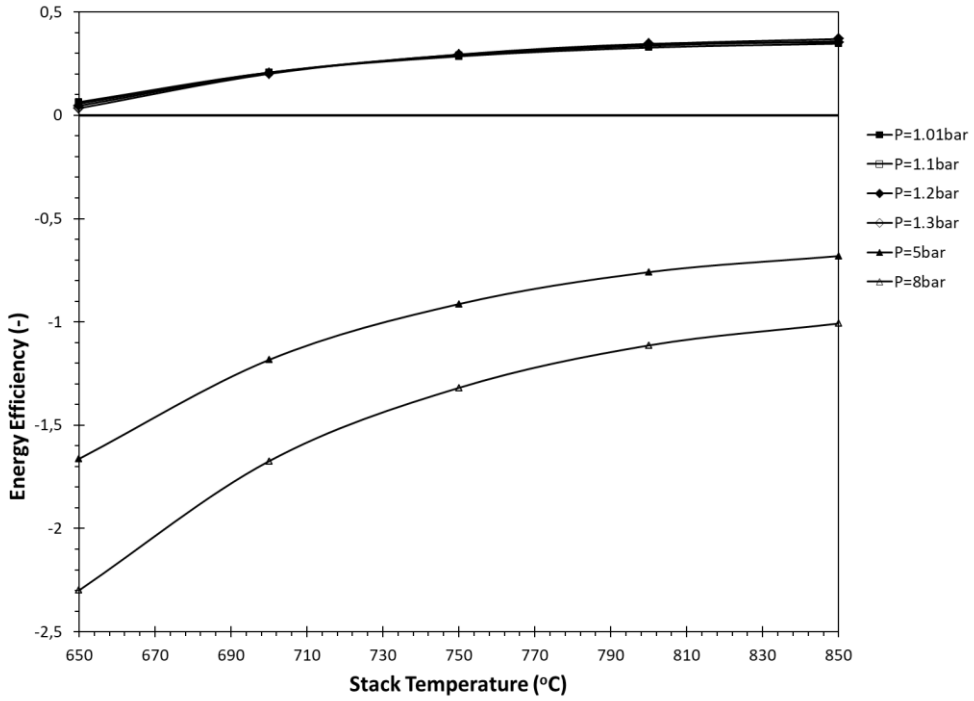

Figure 5-30: Energy efficiency - Process Conditions, See Base Case - Vary stack P_s, T_s

First of all, the reader must also reminisce from the analysis of the electrolysis system, that the more thermoneutral is the operation, the better the obtained performance. Since in fuel cell operation there is no

thermoneutral operation, it is plausible that beneficial operation is equivalent to reduced heat generation by the stack and therefore decreased flow rate of oxidant. During this analysis, stack operates at an *almost constant current density* (methanol steam reformer and stack operate at the same pressure and reforming pressure has a distinct effect on H_2 yield which in turn affects slightly the current density) which means that the higher the temperature of operation, the higher the cell voltage. By minimizing the overpotential losses, the necessary heat removal from the stack is also reduced. Other observations that can be made from the results are:

- With the increase in pressure, hot and cold utilites increase enormously. This increase results in decreased exergy and energy efficiencies (Figure 5-31 & Figure 5-32). In reality, for power production from the system, the user needs to operate at low pressure and high temperature, otherwise, the balance of plant itself consumes more electricity than the stack produces. The reason is that the intercooler must provide more cooling in the intercooler stage at higher pressure ratio (which is on the low-temperature side) and higher reheat duty (which is at the high-temperature side). The low intercooler temperature side and high-temperature side of the expansion reheater are the most important sides since those regions contribute to the cold and hot utility. This can be seen in Table 5-7. Additionally, as it has been seen in Table 5-2, there are better chances of heat integration at reduced stack pressure. Again, the ideal Brayton cycle with recuperation can be utilized in order to verify the results from Table 5-2
- An increase in stack temperature decreases cold and hot utility due to fewer overpotential losses. Fewer overpotential losses are equivalent to reduced oxidant flow rate. As it has been seen already in electrolysis, a large sweep gas flow rate is detrimental for hot and cold utility. The same situation is encountered here for the oxidant flow rate (Figure 5-31 & Figure 5-32).

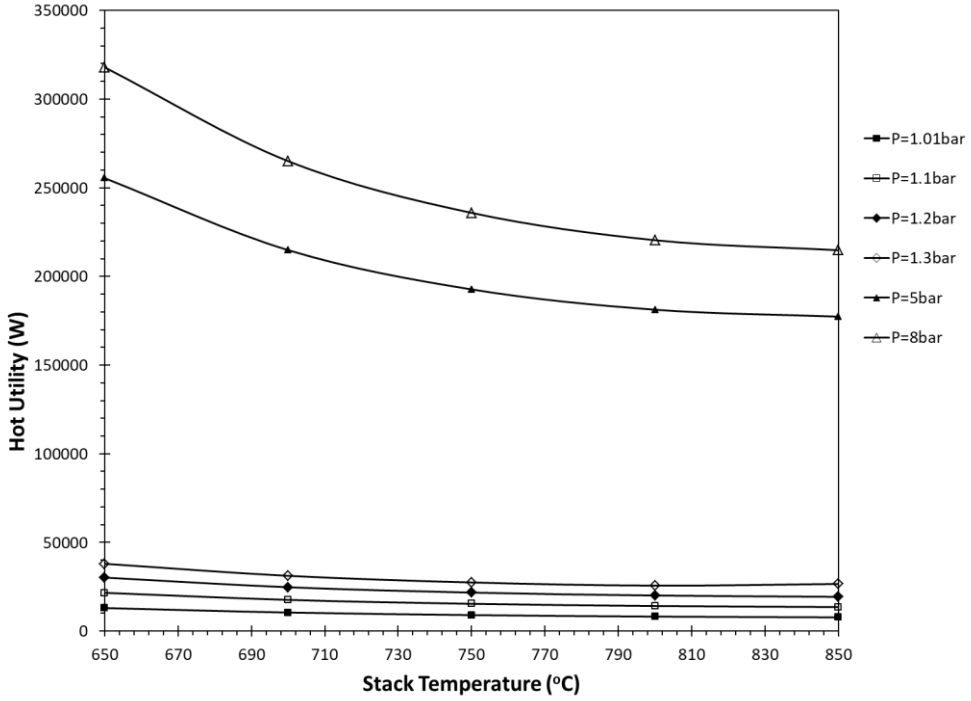

Figure 5-31: Hot Utility - Process Conditions, See Base Case - Vary stack P_s, T_s

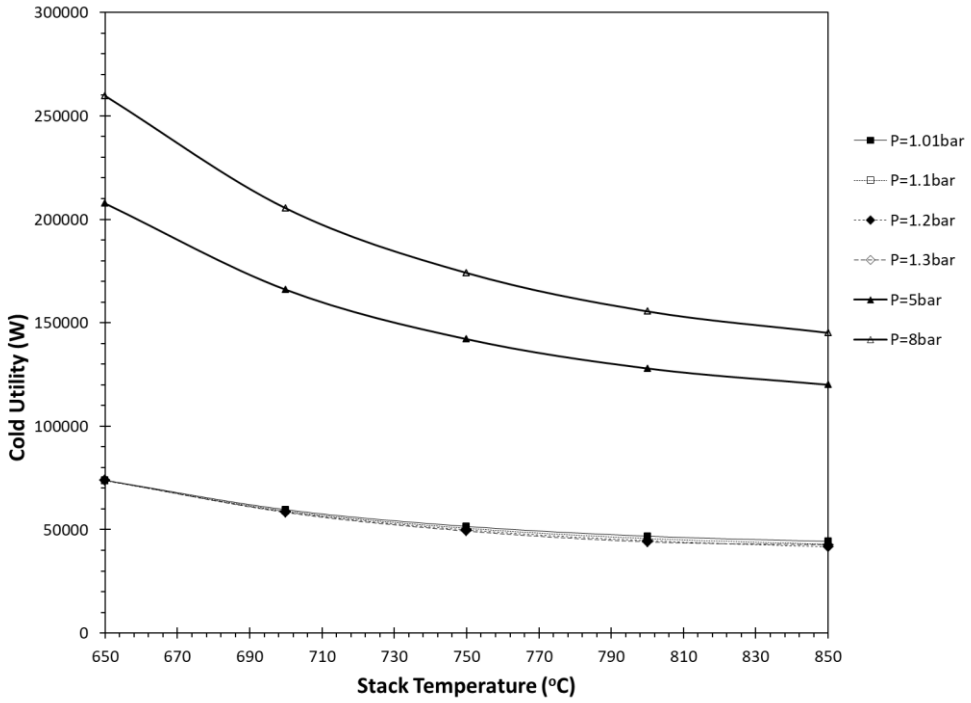

Figure 5-32: Cold Utility - Process Conditions, See Base Case - Vary stack P_s, T_s

Table 5-7: The effect of stack pressure in oxidant flow rate and intercooler/reheater duty (at T_{stack}=923.15K)

Stack Pressure	1.3 bar	8 bar
Reheater Duty (kW)	37.71	180.19
Intercooler Duty (kW)	-13.99	-116.39
Oxidant flow rate (kmol/hr)	129.16	118.75

- With an increase in stack pressure, stack electricity is also increased. Enhanced stack power produced at higher pressure is reasonable and derives directly from the Nernst equation with an increase of the reversible voltage. Since current density is almost constant in this simulation, a heightened reversible cell voltage will result in increased operating cell voltage and therefore elevated power production. An increase in stack temperature also decreases overpotential losses which leads to enhanced power production, despite the fact that reversible voltage is decreased (see Figure 5-33)
- An increase in stack temperature enhances H_2 flow rate led to storage. The higher the stack temperature, the more prevalent is the effect of RWGS in the stack. Consequently, more hydrogen is converted to H_2O by the combination of RWGS and the electrochemical oxidation. The "unconverted hydrogen" which is in the form of high-temperature steam, is converted back to hydrogen through low-temperature WGS reaction which is exothermic and favored at lower temperatures. High stack pressure leads to decreased hydrogen storage due to reduced hydrogen yield from the methanol steam reformer. Maximum hydrogen flow to storage occurs at 1.2 bar which is the result from methanol steam reforming, three WGS reactors and one intermediate hydrogen oxidation (Figure 5-34)

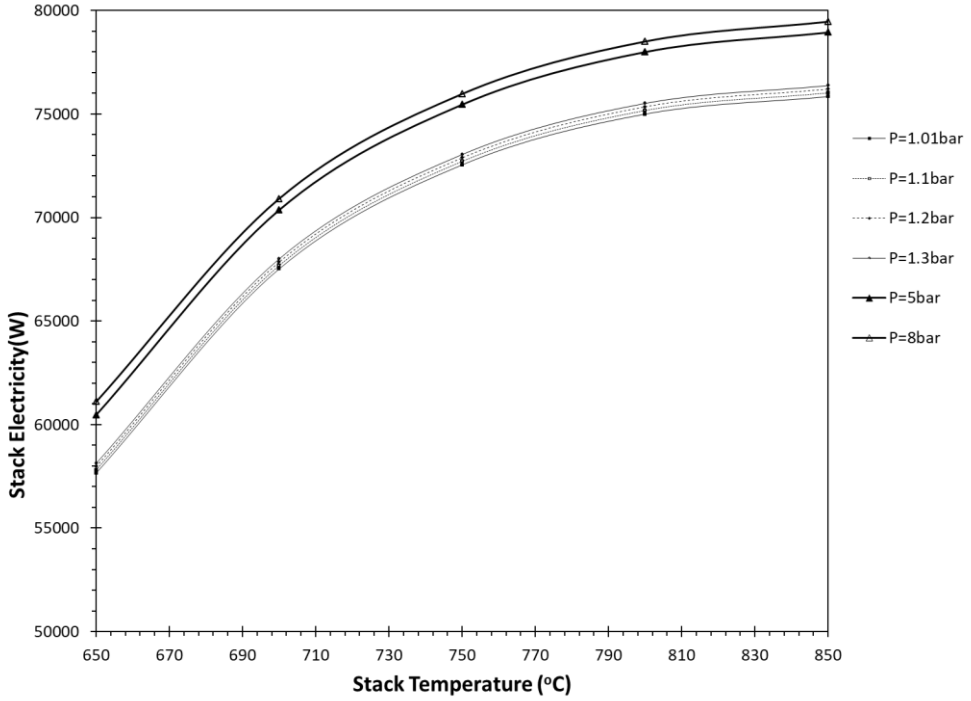

Figure 5-33: Electricity produced by stack - Process Conditions, See Base Case - Vary stack P_s, T_s

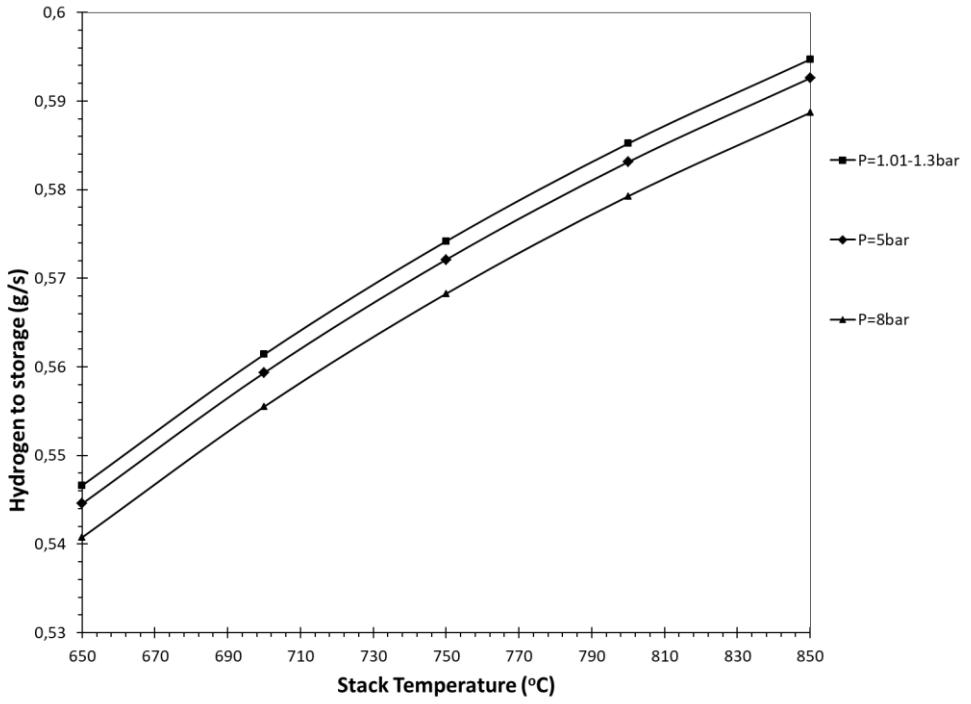

Figure 5-34: Stored Hydrogen flow rate - Process Conditions, See Base Case - Vary stack P_s, T_s

- Despite the fact that oxidant flow rate is lessened in the oxidant expansion section compared to the oxidant compression section, the initially higher temperatures in the expansion section are responsible for the net electricity production from system turbomachinery when stack pressure is higher than 1.2 bar. When stack pressure is less than 1.2 bar, then sweep gas compression and expansion train can be omitted in the calculations since the pressure ratio will be minimum, while the electricity consumption will be dominated by the H_2 storage compressors (see Figure 5-35)

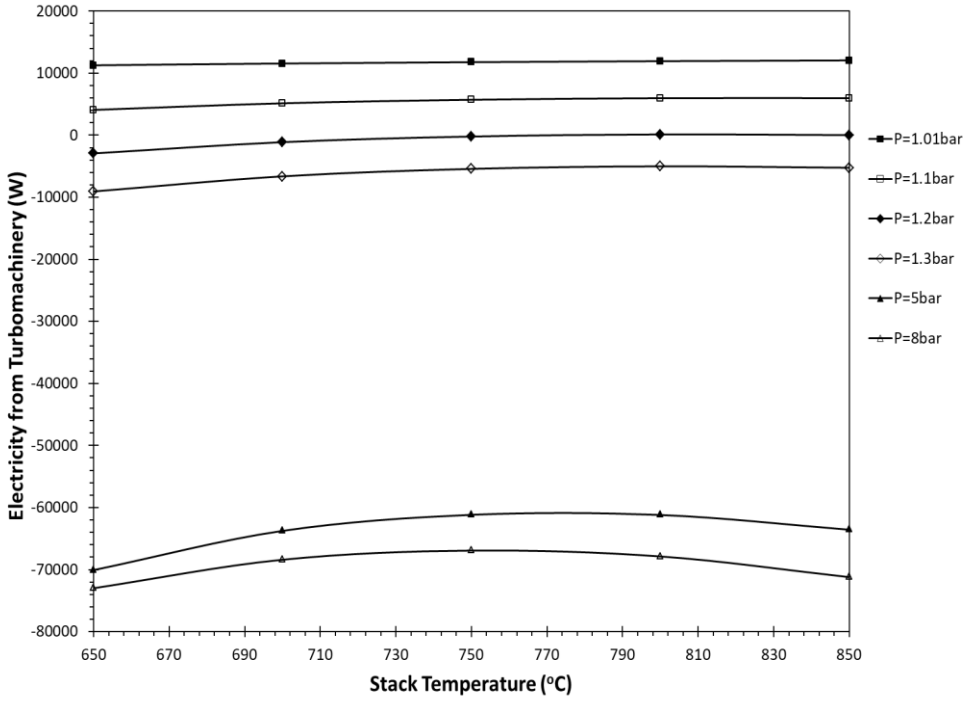

Figure 5-35: Electricity produced by turbomachinery - Process Conditions, See Base Case - Vary stack P_s, T_s

Effect of fuel Utilization, steam and methanol flow rate

In this case, **fuel utilization** and **steam flow rate** are varied. The model runs in such a way that methanol and steam flow rate are equal due to the stoichiometry of methanol steam reforming which imposes a 1:1 ratio steam-to-methanol. The examined range varies from *0.1-0.35 mol/s*. Steam utilization varies from *0.25-0.95*. It is obvious that those parameters affect the current density which varies from 2000-8000 A/m^2.

By observing the results related to the exergy and energy efficiencies (see Figure 5-36 & Figure 5-37), one can observe that by increasing fuel utilization, exergy and energy efficiencies increase. If the fuel utilization is decreased enormously, decreased power production by the stack will be unable to electrically sustain the process, leading to negative energy and exergy efficiencies. In addition, if fuel utilization is constant and feed flow rates are increased, this will lead to enhanced current densities, which necessitate larger oxidant flows to remove the growing dissipated heat, resulting in reduced energy and exergy efficiencies.

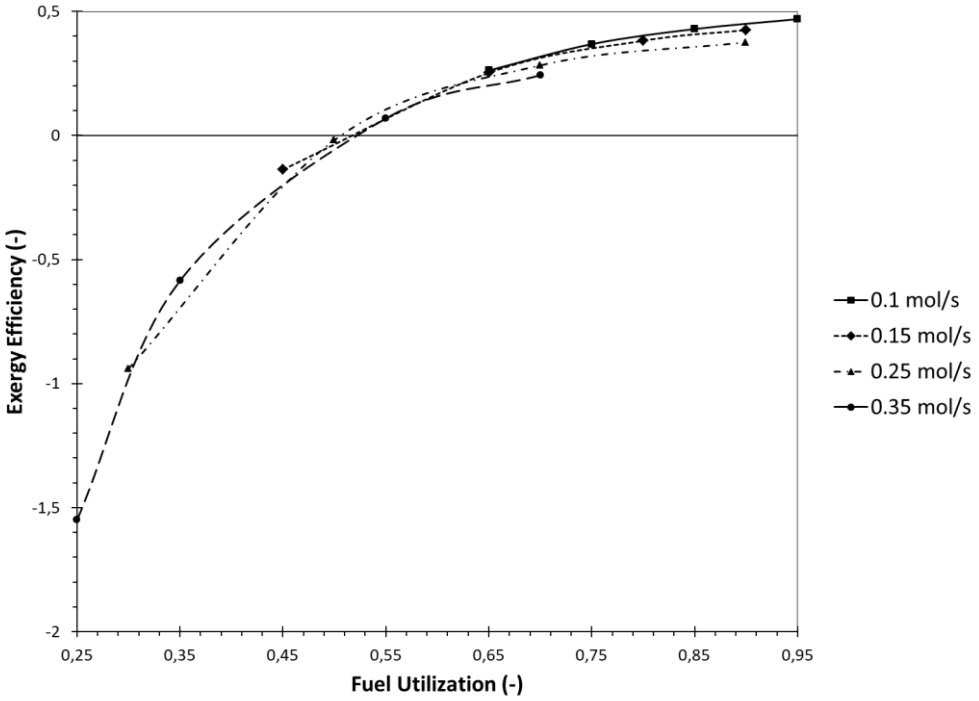

Figure 5-36: Exergy efficiency - Process Conditions, See Base Case and Fix P_s=1.2bar, T_s=1123.15K, Vary Steam (and Methanol) flow rate and Fuel Utilization

Other observations that can be made from the resulting figures are:

- By enhancing fuel utilization, less electricity is expended from system turbomachinery (see Figure 5-38). One reason for less power consumption from system turbomachinery is due to the fact that higher fuel utilization results in heightened steam formation and less hydrogen led to the storage compressors, alleviating their duty. In addition, the higher the current density and the feed steam flow rate, the more the current density of the stack and the more the oxidant flow rate. Despite the fact that the compression and expansion train operate at negligible pressure ratio ($p_{stack} = 1.2\ bar$), enlarged oxidant flows still affect the results distinctly

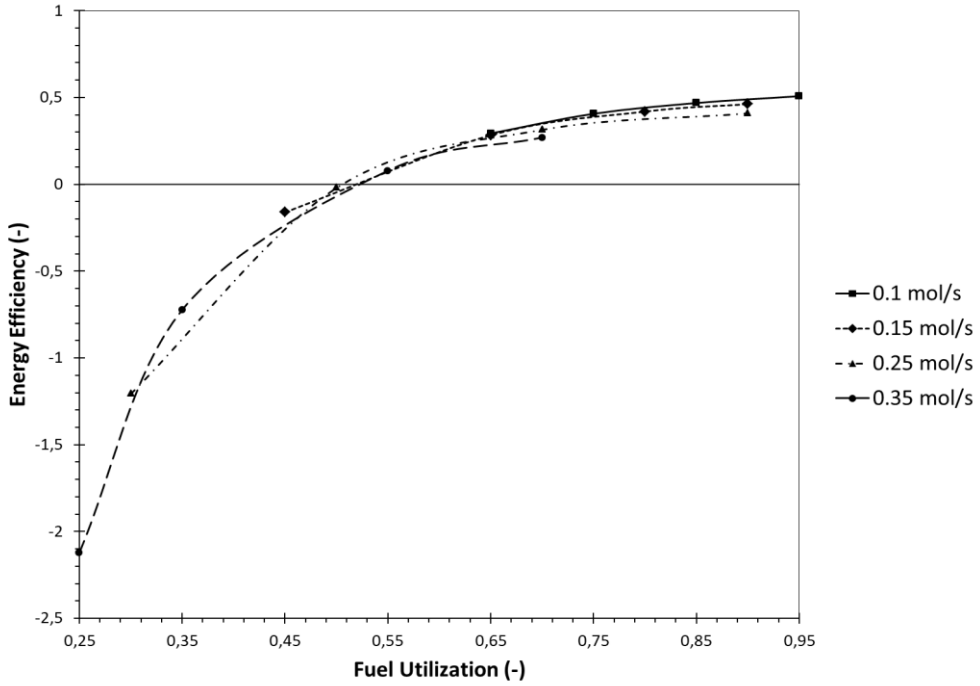

Figure 5-37: Energy efficiency - Process Conditions, See Base Case and Fix P_s=1.2bar, T_s=1123.15K, Vary Steam (and Methanol) flow rate and Fuel Utilization

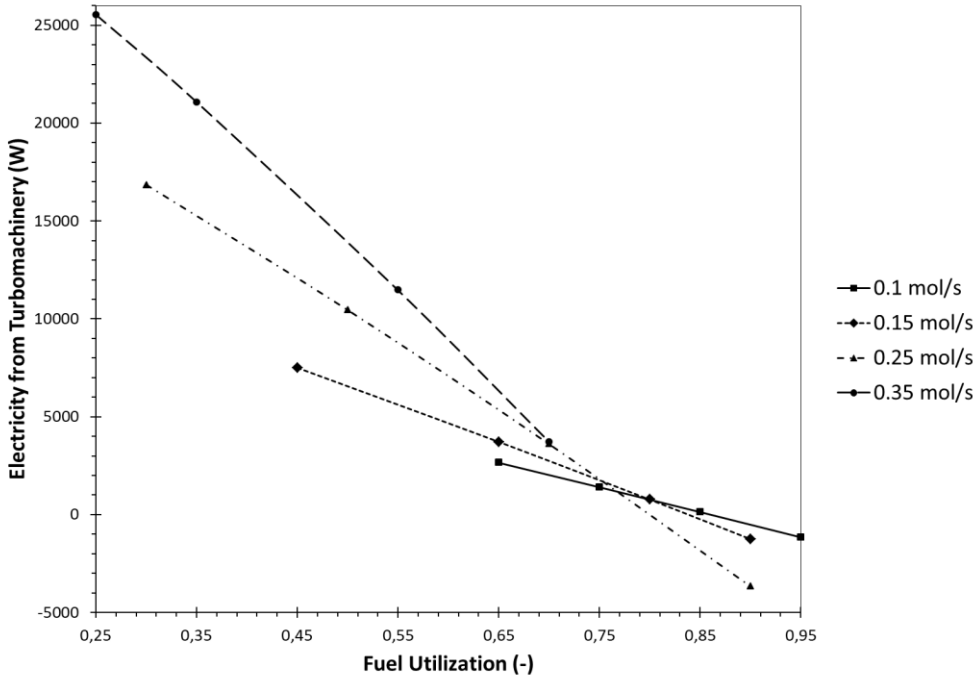

Figure 5-38: Electricity produced by turbomachinery - Process Conditions, See Base Case and Fix P_s=1.3bar, T_s=1123.15K, Vary Steam (and Methanol) flow rate and Fuel Utilization

- Of course, increased fuel utilization leads to enhanced current density, and more power is produced from the stack (see Figure 5-39)

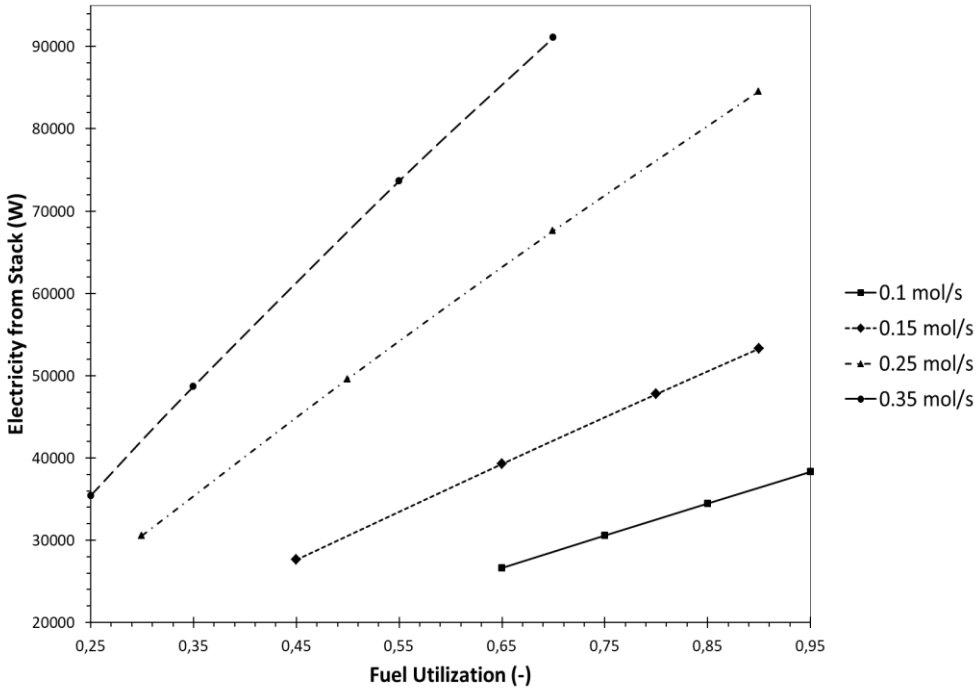

Figure 5-39: Electricity produced by stack - Process Conditions, See Base Case and Fix P_s=1.2bar, T_s=1123.15K, Vary Steam (and Methanol) flow rate and Fuel Utilization

- Less hydrogen is led to storage when fuel utilization is increasing due to heightened electrochemically converted hydrogen to H_2O (see Figure 5-40). Despite the fact that more steam is provided to the low-temperature WGS, extinction of CO still results in increased steam content even after the WGS and therefore less H_2 is stored. It has already been mentioned that less hydrogen stored alleviates the storage compressors from excessive duty

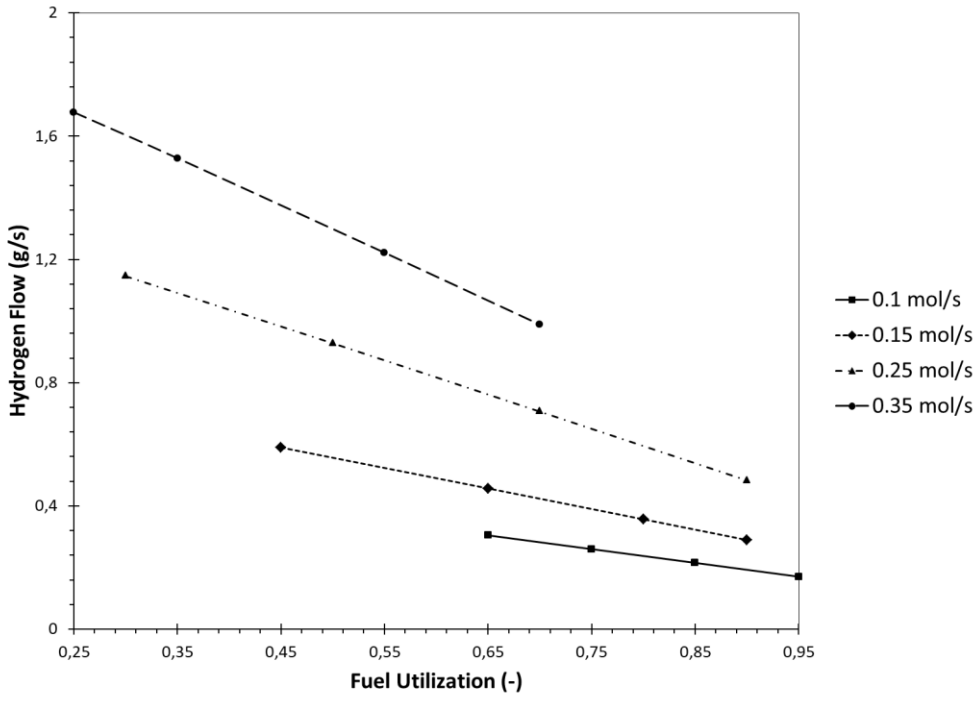

Figure 5-40: Stored Hydrogen flow rate- Process Conditions, See Base Case and Fix P_s=1.2bar, T_s=1123.15K, Vary Steam (and Methanol) flow rate and Fuel Utilization

- Hot and cold utilities are both increased by either fuel utilization enhancement or growth of feed flow rate (i.e. water and methanol flow rate). Increased fuel utilization or feed steam molar flow rate, enhance current density and therefore, oxidant flow rate which dominates on the hot and cold utility (see Figure 5-41 & Figure 5-42). After a specific current density (which is proportional to the product $\dot{n}_{H_2,stack}U_f \sim \dot{n}_{H_2O,feed}U_f$), oxidant flow rate still grows, but simultaneously more oxidant is consumed by the electrochemical reactions due to increased fuel utilization. This decrease in flow rate during the expansion section results in inability of internal heat integration and increased utilities

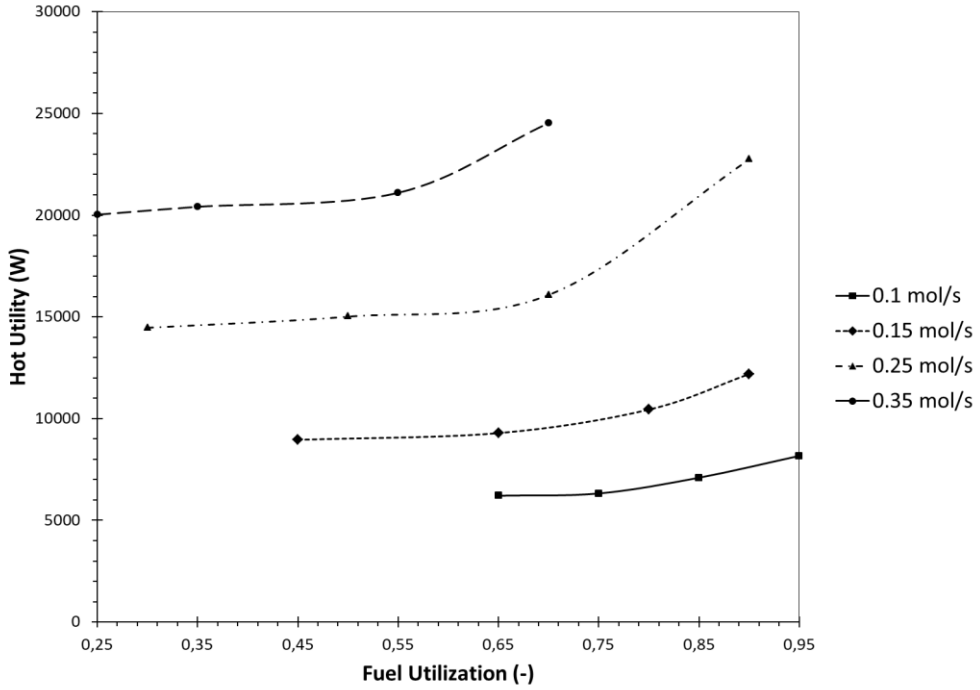

Figure 5-41: Hot Utility - Process Conditions, See Base Case and Fix P_s=1.2bar, T_s=1123.15K, Vary Steam (and Methanol) flow rate and Fuel Utilization

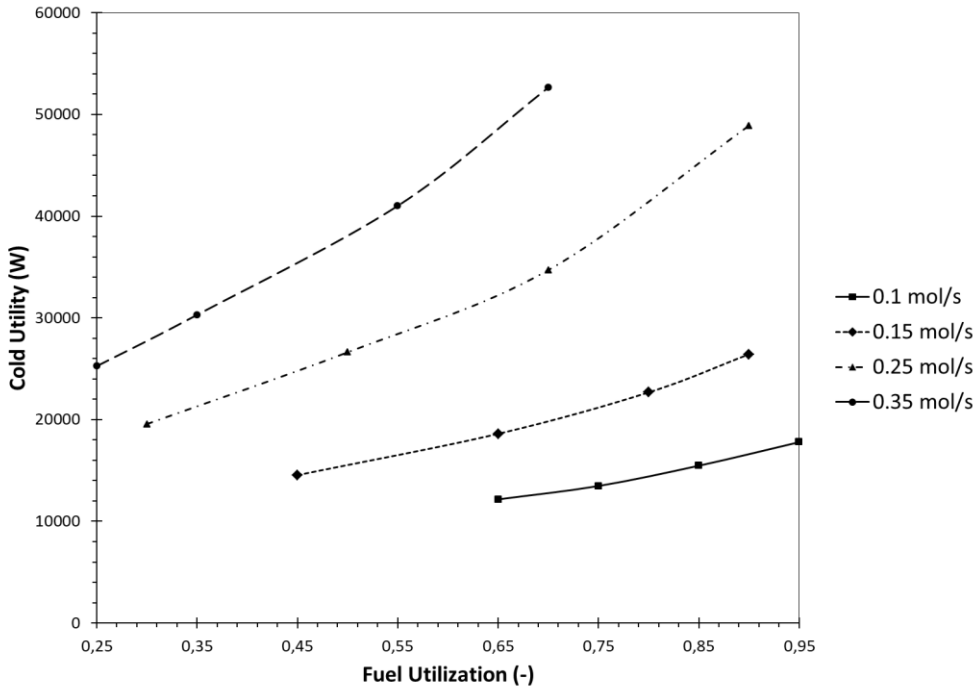

Figure 5-42: Cold Utility - Process Conditions, See Base Case and Fix P_s=1.2bar, T_s=1123.15K, Vary Steam (and Methanol) flow rate and Fuel Utilization

Effect of steam reforming temperature

Steam reforming temperature affects the equilibrium composition of the methanol steam reformer and hence, the efficiencies. WGS reaction also takes place along with methanol decomposition. Those three reactions are the main reactions in methanol steam reforming and are shown below [79]:

$$CH_3OH + H_2O \leftrightarrow CO_2 + 3H_2 \qquad \Delta H = 49.7 kJ/mol$$
$$CH_3OH \leftrightarrow CO + 2H_2 \qquad \Delta H = 90.2 kJ/mol$$
$$CO + H_2O \leftrightarrow CO_2 + H_2 \qquad \Delta H = -41.2 kJ/mol$$

This set of reactions increases the hydrogen yield when operating at low temperature and low pressure as depicted in Figure 5-43 & Figure 5-44.

Apart from the equilibrium composition, the trend energy, and exergy efficiencies (see Figure 5-45 & Figure 5-46) is mainly determined by system hot and cold utility (Figure 5-47 & Figure 5-48). At low temperature, exergy and energy efficiencies remain almost constant, reaching their maximum values. After a certain methanol steam reforming temperature, hot and cold utility rises linearly. Hot utility rises due to the fact that the steam and methanol heaters before the steam reformer are unable to satisfy their thermal needs internally and therefore external heat is required. In addition, heat coupling of the methanol steam reformer and the external WGS reactor is no longer possible at elevated reforming temperatures. This effect will impact hot and cold utility negatively. Stored hydrogen flow rate increases with an increase of methanol steam reforming temperature. This will give a boost to the intercooler duty during hydrogen storage, which will further enhance cold utility.

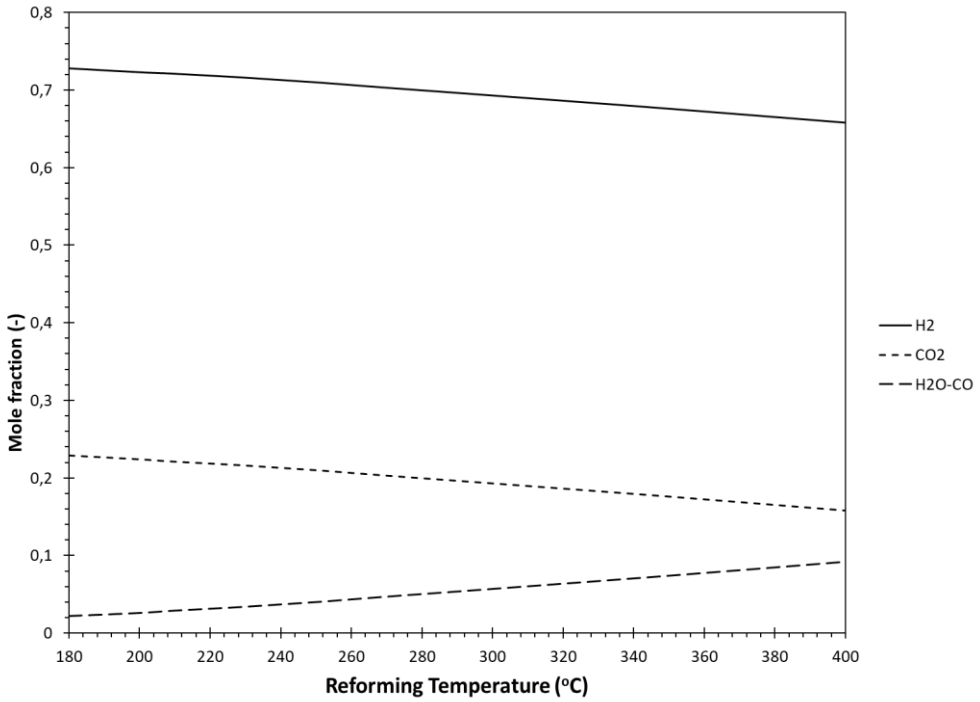

Figure 5-43: Methanol Steam Reforming – Outlet Composition Breakdown for varying temperature (p=1.2 bar)

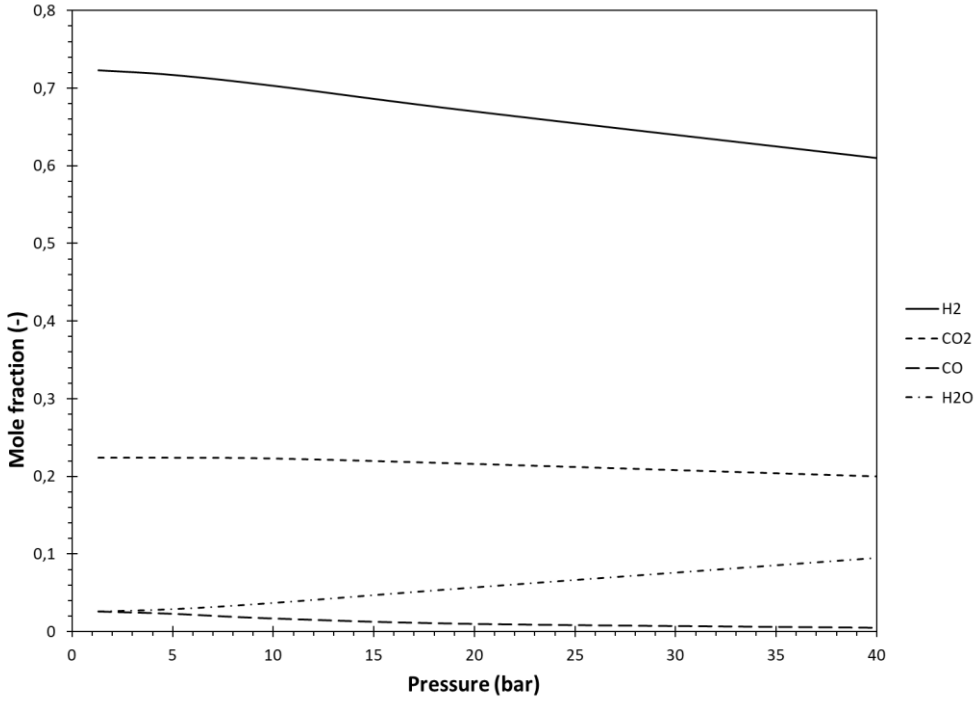

Figure 5-44: Methanol Steam Reforming – Outlet Composition Breakdown for varying pressure (T=1123.15 K)

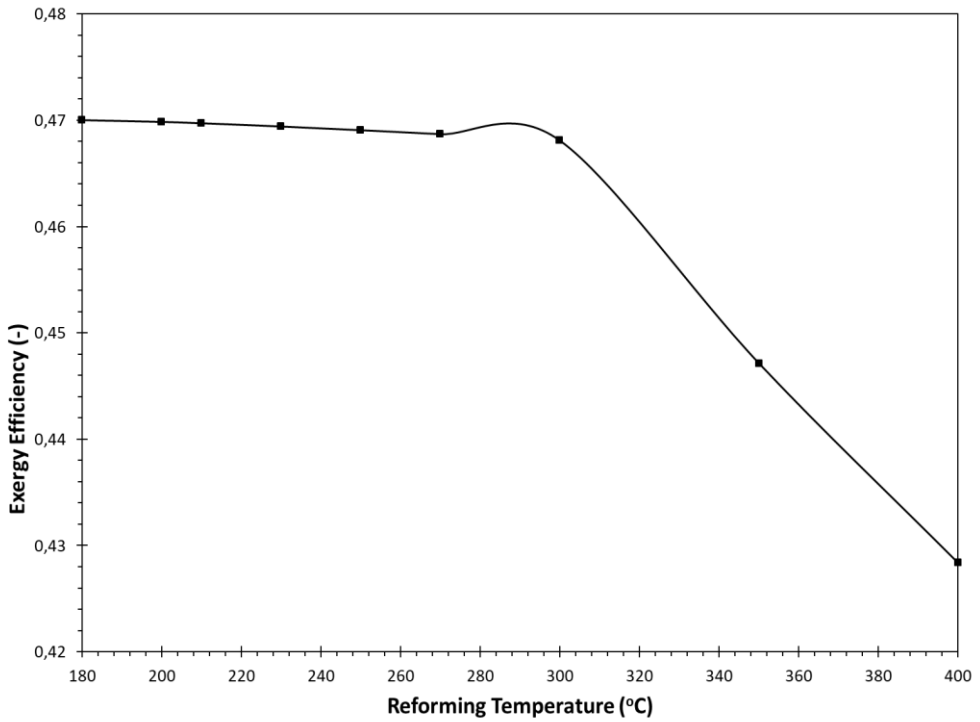

Figure 5-45: Exergy Efficiency - Process Conditions, See Base Case and Fix P_s=1.2bar, T_s=1123.15K, U_f=0.95, n_{H2O}=0.1mol/s, Vary methanol steam reforming temperature

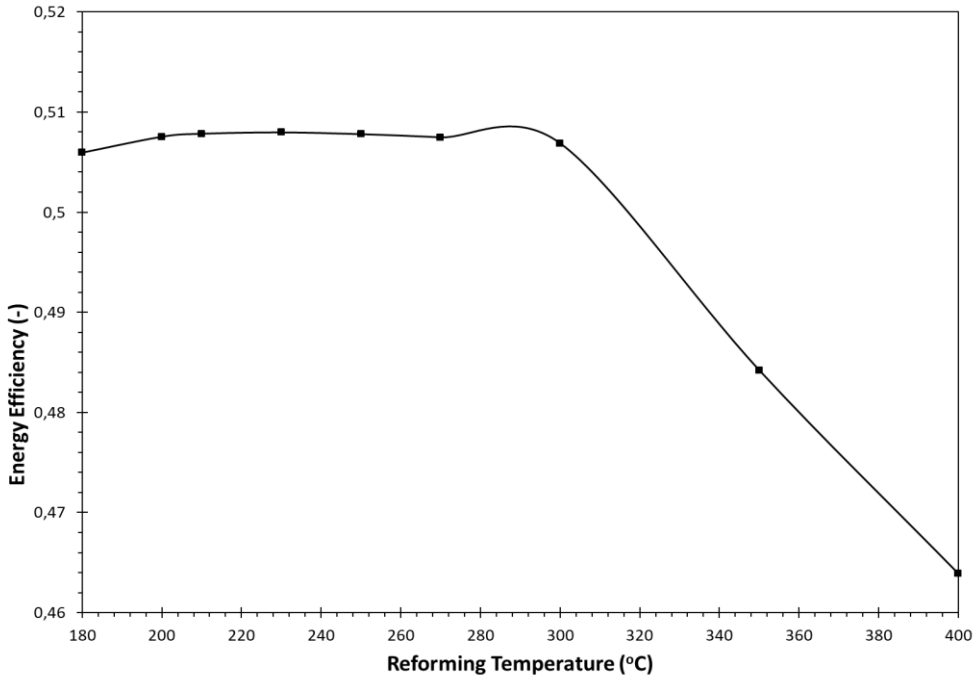

Figure 5-46: Energy Efficiency - Process Conditions, See Base Case and Fix P_s=1.2bar, T_s=1123.15K, U_f=0.95, n_{H2O}=0.1mol/s, Vary methanol steam reforming temperature

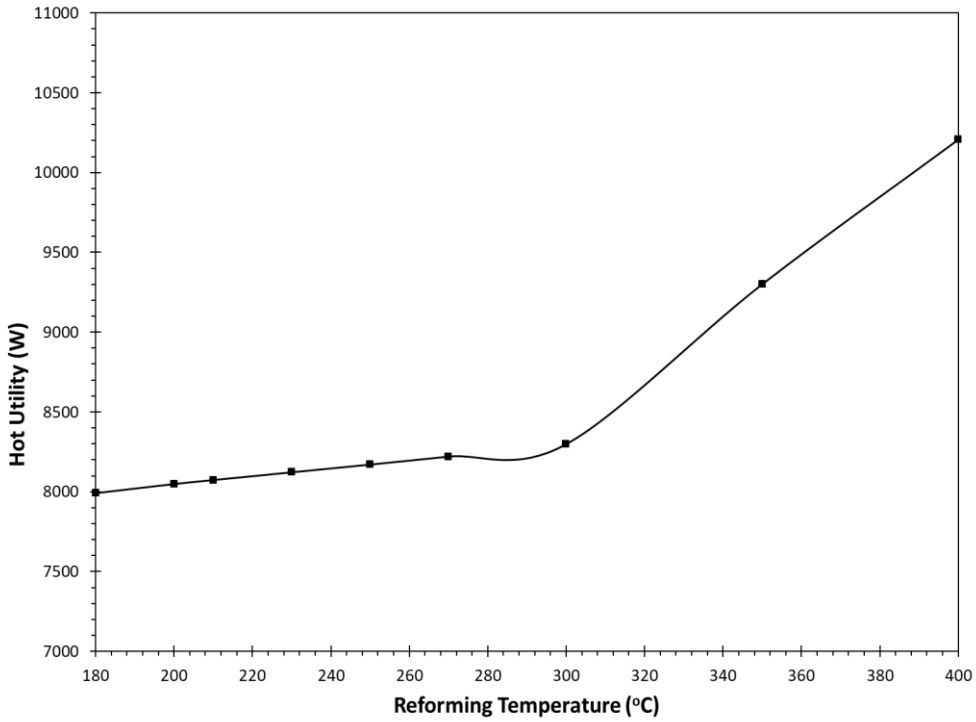

Figure 5-47: Hot Utility - Process Conditions, See Base Case and Fix P_s=1.2bar, T_s=1123.15K, U_f=0.95, n_{H2O}=0.1mol/s, Vary methanol steam reforming temperature

Other observations that can be made are the following:

- Electricity from the stack slightly increases with an increase of reforming temperature. By increasing the steam content before the stack, RWGS which takes place in the stack has a lesser effect, therefore hydrogen which is electrochemically converted is increased (increasing current density), and

additionally an increased H_2/H_2O ratio also increases reversible voltage and thus operating voltage. Those two factors contribute to a small growth of stack electricity (see Figure 5-49)

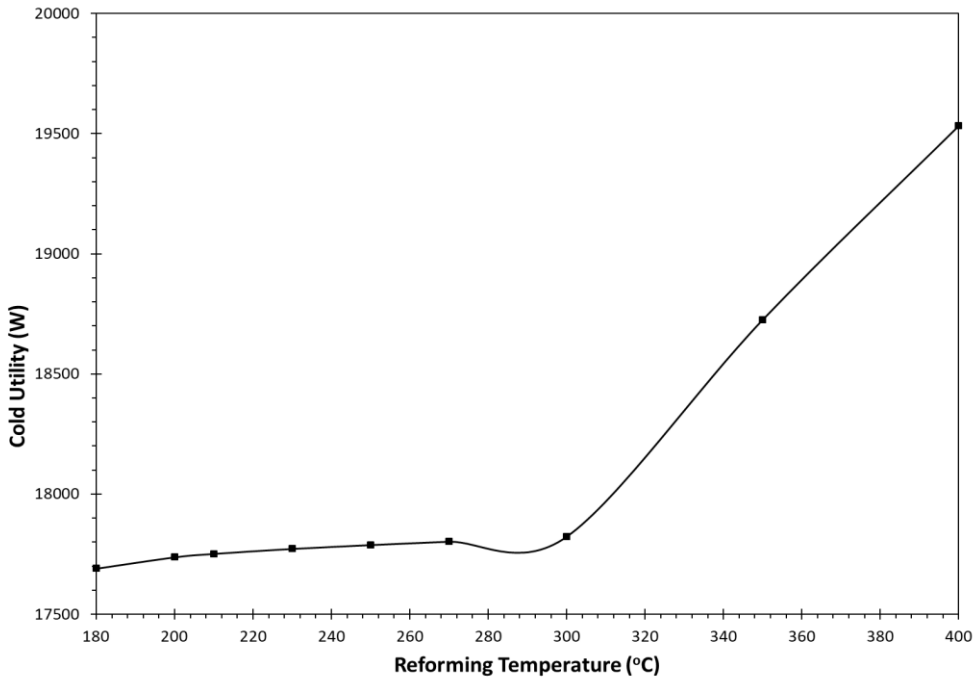

Figure 5-48: Cold Utility - Process Conditions, See Base Case and Fix P_s=1.2bar, T_s=1123.15K, U_f=0.95, n_{H2O}=0.1mol/s, Vary methanol steam reforming temperature

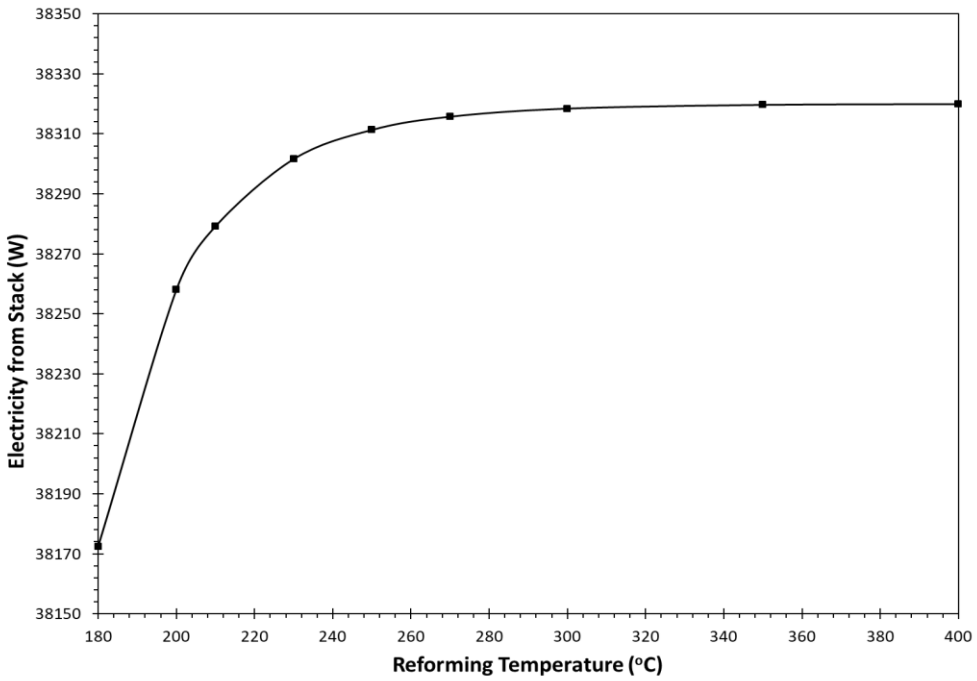

Figure 5-49: Electricity Produced by Stack - Process Conditions, See Base Case and Fix P_s=1.2bar, T_s=1123.15K, U_f=0.95, n_{H2O}=0.1mol/s, Vary methanol steam reforming temperature

- As reforming temperature increases, steam content prior to the stack increases. After the first WGS reactor, the hydrogen flow which is led for electrochemical reaction is increased and therefore current density is also enhanced. Finally, enhanced current density leads to slightly higher oxidant flow which results in slightly increased electricity from the turbomachinery (see Figure 5-50)

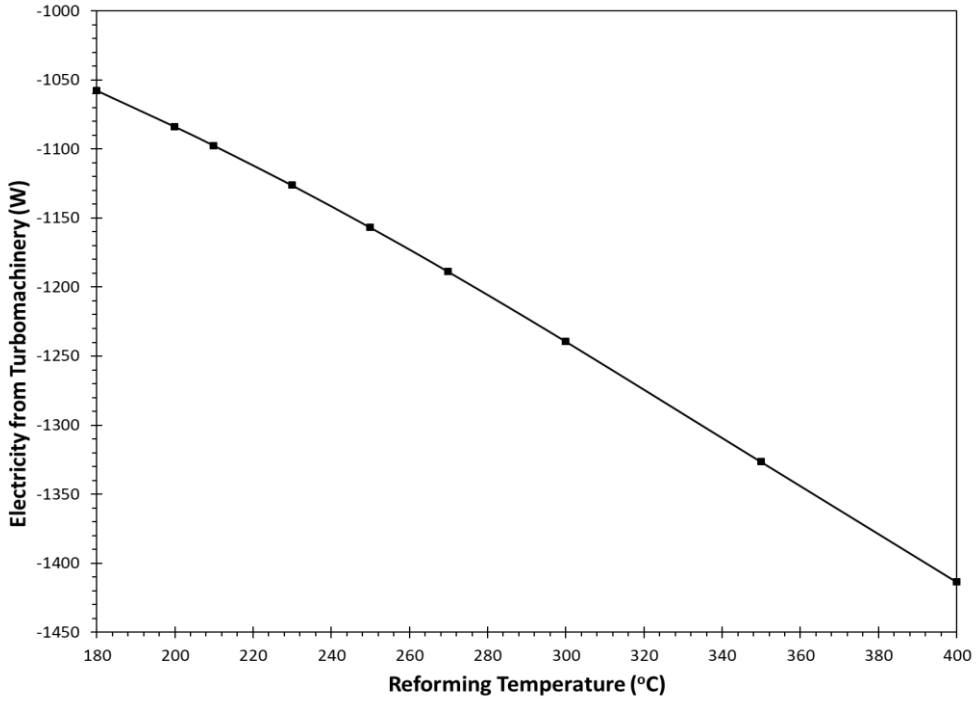

Figure 5-50: Electricity produced by turbomachinery - Process Conditions, See Base Case and Fix P_s=1.2bar, T_s=1123.15K, U_f=0.95, n_{H2O}=0.1mol/s, Vary methanol steam reforming temperature

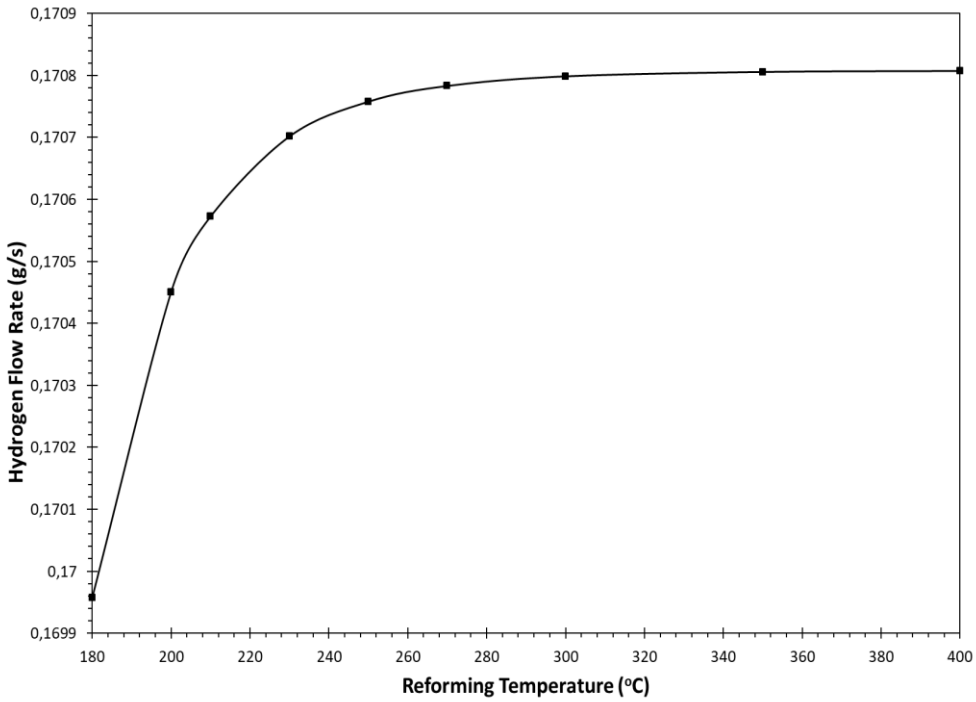

Figure 5-51: Stored hydrogen flow rate - Process Conditions, See Base Case and Fix P_s=1.2bar, T_s=1123.15K, U_f=0.95, n_{H2O}=0.1mol/s, Vary methanol steam reforming temperature

- A slight overall increase of hydrogen stored is also observed with an increase in reforming temperature. In the range of 180-400°C, the increase is equal to 0.001 g/s. The higher the temperature of steam reforming, the more the CO content led to WGS reactor, and therefore more hydrogen will be produced and stored (see Figure 5-51)

Effect of isentropic efficiency of turbomachinery

The effect of isentropic efficiency of turbomachinery in exergy and energy efficiencies is shown in Figure 5-52 & Figure 5-53. It is obvious that by increasing the isentropic efficiency of the turbomachinery, both efficiencies will increase. However, a separate section is made because their impact is much more significant in fuel cell mode compared to electrolytic operation.

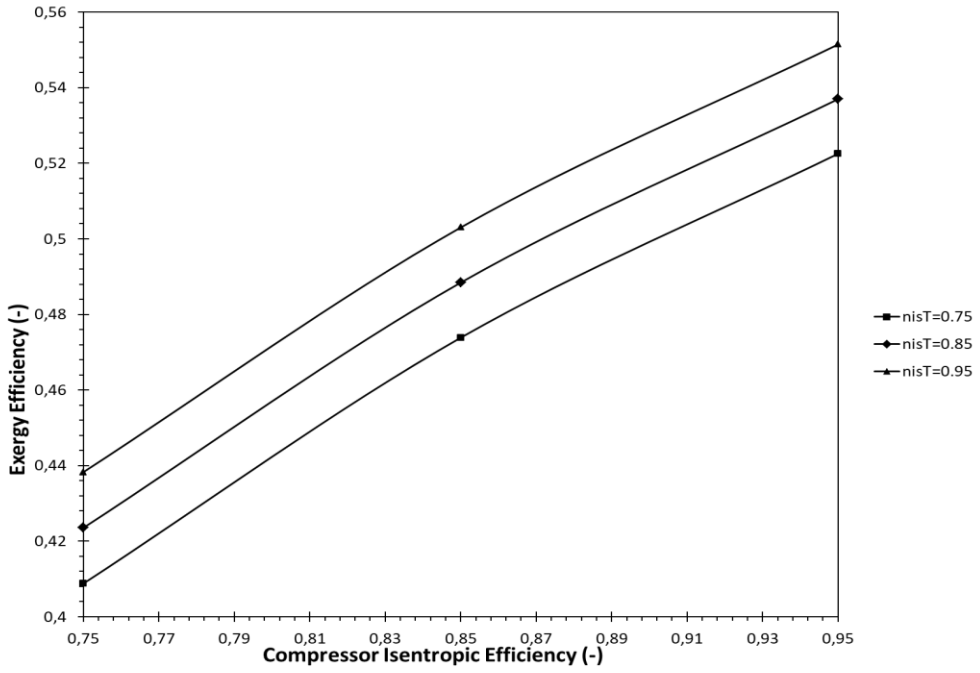

Figure 5-52: Exergy Efficiency- Process Conditions, See Base Case and Fix P_s=1.2bar, T_s=1123.15K, U_f=0.95, n_{H2O}=0.1mol/s, T_{ref}=180^{o}C, T_{WGS}=400^{o}C, Vary $n_{is,C}$ & $n_{is,T}$

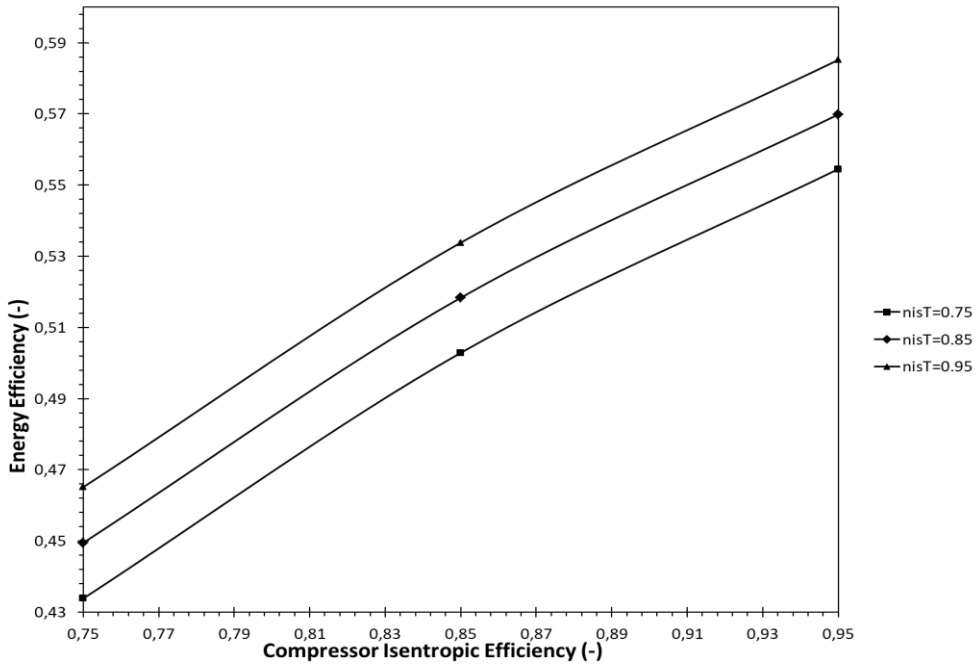

Figure 5-53: Exergy Efficiency- Process Conditions, See Base Case and Fix P_s=1.2bar, T_s=1123.15K, U_f=0.95, n_{H2O}=0.1mol/s, T_{ref}=180^{o}C, T_{WGS}=400^{o}C, Vary $n_{is,C}$ & $n_{is,T}$

Other observations that can be made are:

- Electricity production from system turbomachinery is increased when isentropic efficiencies are higher (see Figure 5-54)

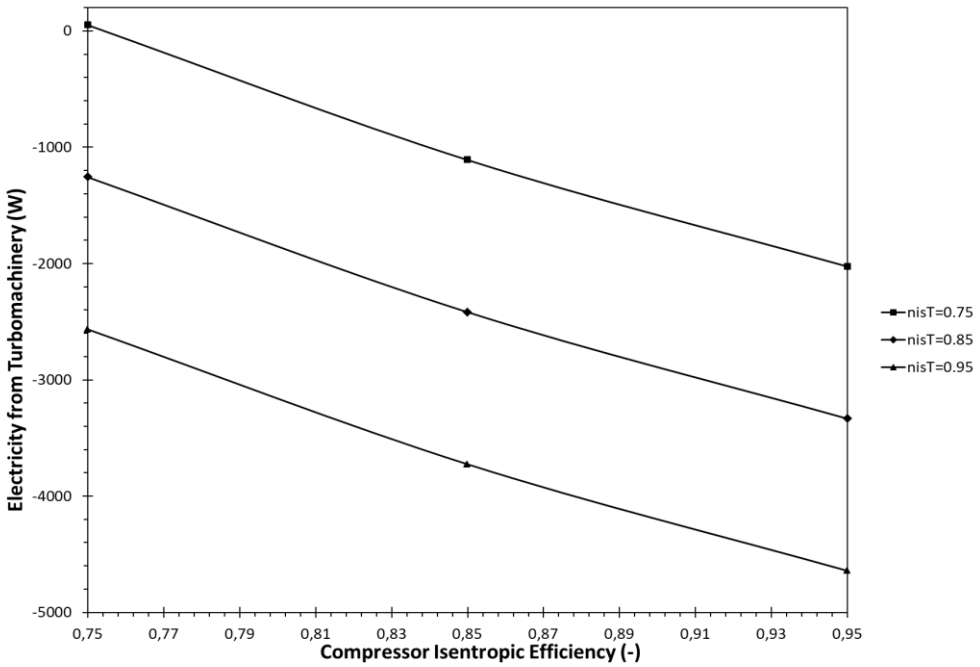

Figure 5-54: Exergy Efficiency- Process Conditions, See Base Case and Fix P_s=1.2bar, T_s=1123.15K, U_f=0.95, n_{H2O}=0.1mol/s, T_{ref}=180^{o}C, T_{WGS}=400^{o}C, Vary $n_{is,C}$ & $n_{is,T}$

- Cooling utility decreases either with an increase of either the isentropic efficiency of compressors or expanders (see Figure 5-55).

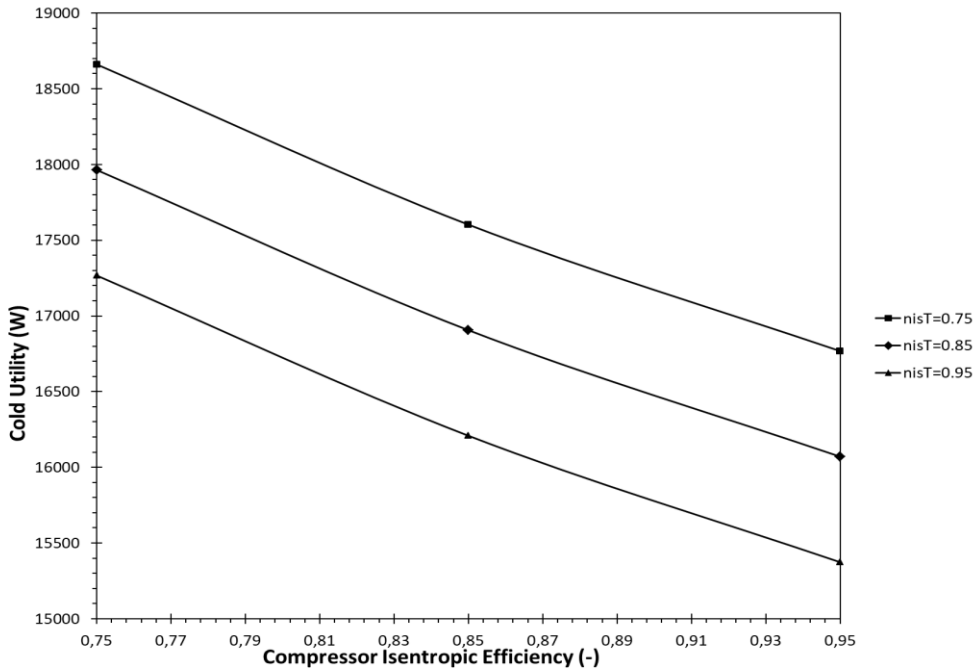

Figure 5-55: Exergy Efficiency- Process Conditions, See Base Case and Fix P_s=1.2bar, T_s=1123.15K, U_f=0.95, n_{H2O}=0.1mol/s, T_{ref}=180^{o}C, T_{WGS}=400^{o}C, Vary $n_{is,C}$ & $n_{is,T}$

The increase in temperature during compression is lower when it is done more efficiently and therefore less cooling duty is demanded in the intercooling stage. Also, highly efficient expansion leads to lower temperatures of the exhaust streams and therefore less temperature difference must be covered externally.

- Hot utility only increases when isentropic efficiency of expanders increases while it is not affected by compressor isentropic efficiency (not shown here). When expanding efficiently, the outlet stream has lower temperature and the reheater necessitates more external heat

Before reporting the process conditions of the optimized case, it has to be noted that additional sensitivity analyses have been conducted as well. Those analyses regard the following:

- Temperature of external WGS reactor (200^{o}C-400^{o}C)
- Stack inlet temperature of the oxidant stream (40-200^{o}C)

These sensitivity analyses had a minor impact on the exergy and energy efficiencies and therefore the results are omitted. However, the change of these magnitudes during the transition from the base case to the optimized case is stated in the section below. The impact of those changes in the optimized energy and exergy efficiencies is also incorporated in the final values.

5.2.3 Optimized Case Parameters – Fuel Cell mode

Table 5-8 contains the process parameters which constitute the optimized case for fuel cell mode.

Table 5-8: Optimized Case Parameters – Fuel Cell Mode

Parameter	*Value*	*Parameter*	*Value*
Number of cells (-)	1300	Temperature of feed CH_3OH (K)	298.15
Electrode area per cell (m^2)	0.01	Flow rate of feed H_2O (mol/s)	0.1
Stack pressure (bar)	1.2	Pressure of feed H_2O (bar)	1
Stack temperature (K)	1123.15	Temperature of feed water (K)	298.15
Fuel utilization (-)	0.95	Reforming Temperature (K)	453.15
Inlet oxidant pressure (bar)	1	Pressure of H_2 storage (bar)	700
Inlet oxidant temperature (K)	298.15	Pressure of CO_2 storage (bar)	160
Flow rate of feed methanol (mol/s)	0.1	Temperature of Water Gas Shift Reaction (K)	673.15
Pressure of feed methanol (bar)	1		
Parameter	*Value*	*Parameter*	*Value*
Isentropic eff. of pumps and compressors(-)	0.95	Mole fraction of O_2 in feed sweep gas stream (-)	0.21
Isentropic eff. of turbines (-)	0.95	Mole fraction of water to double stage compression (-)	0.005
Mechanical Losses of components	0.95	Mole fraction of CO2 to final hydrogen stream (-)	0.01
Mole fraction of feed water (-)	1	CF_4 Evaporator Temperature (Ref. Cycle) (^{o}C)	-109
Mole fraction of feed CH_3 OH(-)	1	CO_2 condenser Tempereature (Ref. Cycle) (^{o}C)	30
Mole fraction of N_2 in oxidant gas stream (-)	0.79		

Overall, this transition from base case to the optimized case gives rise to energy efficiency from -91.35 % to 60.22%. The same goes for exergy which is enhanced from -83.73% to 56.78%. In the meanwhile, the hot utility reduced from approximately 193 kW to 2.5 kW. Now the main reason that hinders both efficiencies from reaching higher values, is the refrigeration system which consumes a considerable amount of electricity due to its low COP (approximately 0.42).

5.3 Exergy and Energy percentage breakdown of the "perfectly heat integrated" base case and optimum case for electrolysis and fuel cell operation

In this subsection, a comparison of the base case and the optimized case for electrolytic operation will be presented through exergy and energy breakdown as presented in Table 5-9 & Table 5-10 and from Figure 5-56 to Figure 5-63. In this "perfectly heat integrated" case it is impossible for an exergy flow diagram to be drawn since the optimum configuration of the heat exchanger network is not known, rather than the minimum hot and cold utilities. The same information for fuel cell operation is also presented in Table 5-9 & Table 5-10 and also from Figure 5-64 till Figure 5-71.

Table 5-9: Exergy and Energy Inlet Breakdown for Electrolysis and Fuel Cell Operation

Inlet Breakdown		Base	Optimized
Electrolysis	Energy Inlet (kW)	188.30	162.01
	Exergy Inlet (kW)	200.67	181.24
Fuel Cell	Energy Inlet (kW)	378.93	73.96
	Exergy Inlet (kW)	408.72	85.25

Table 5-10: Exergy and Energy Outlet Breakdown for Electrolysis and Fuel Cell Operation

Outlet Breakdown		Base	Optimized
Electrolysis	Energy Outlet (kW)	119.15	122.28
	Exergy Outlet (kW)	14222	152.86
Fuel Cell	Energy Outlet (kW)	20527	59.46
	Exergy Outlet (kW)	226.81	68.07

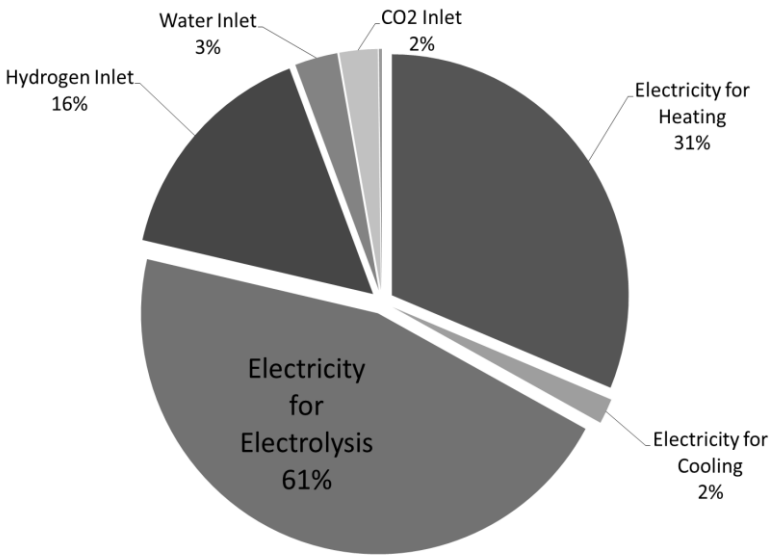

Figure 5-56: Exergy Inlet Percentage Breakdown – Electrolytic operation (Base Case)

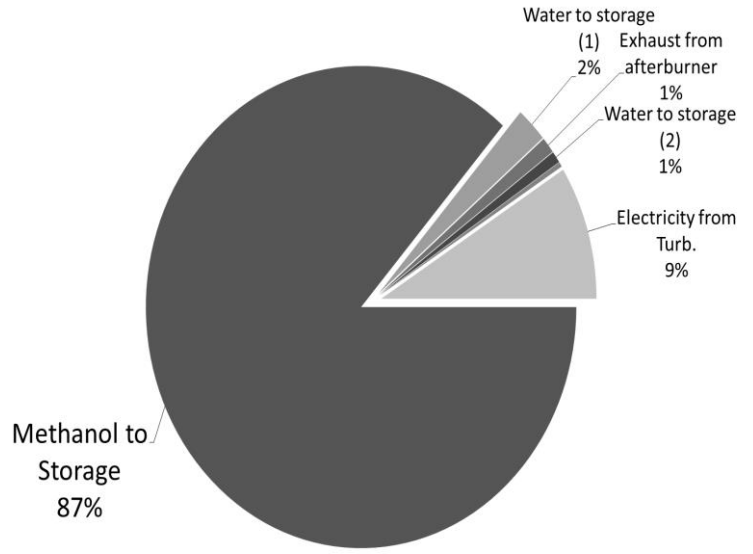

Figure 5-57: Exergy Outlet Percentage Breakdown – Electrolytic operation (Base Case)

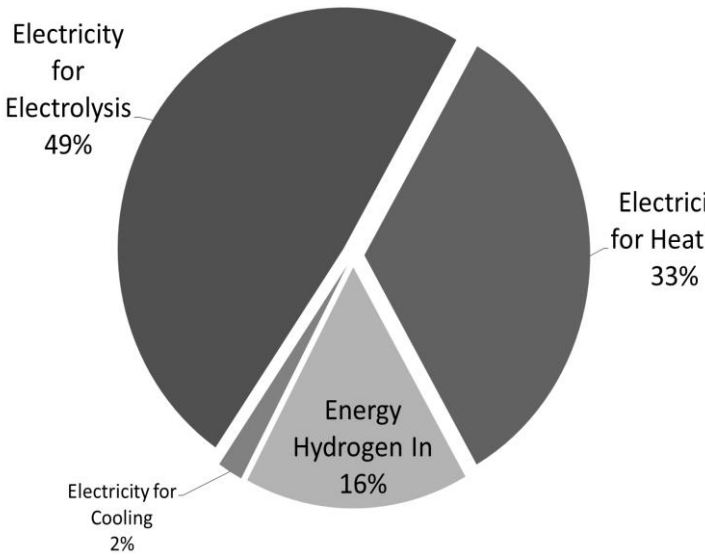

Figure 5-58: Energy Inlet Percentage Breakdown – Electrolytic operation (Base Case)

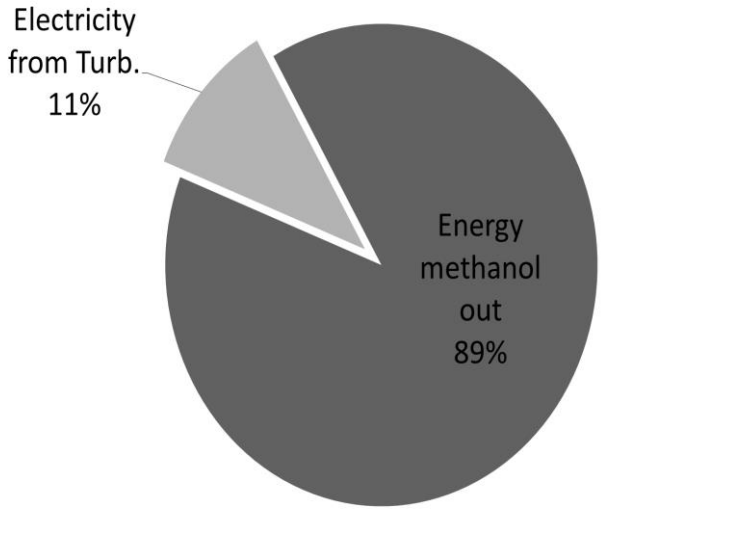

Figure 5-59: Energy Outlet Percentage Breakdown – Electrolytic operation (Base Case)

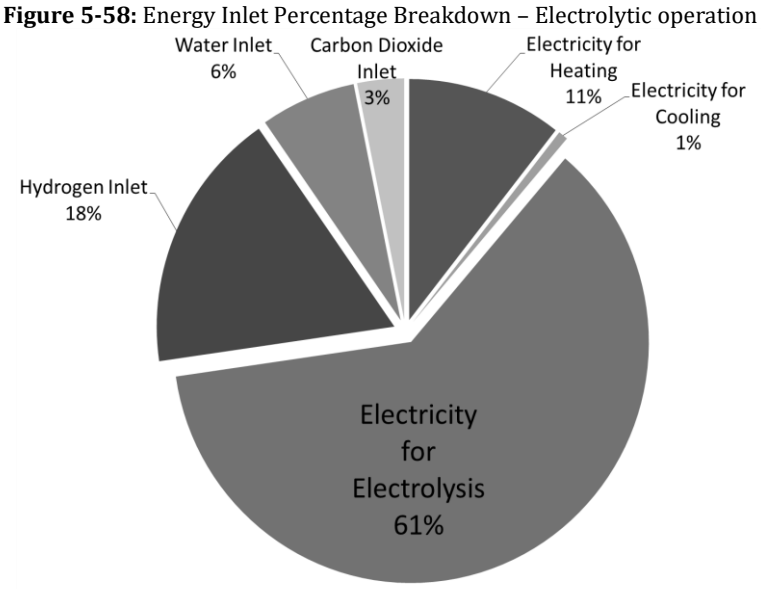

Figure 5-60: Exergy Inlet Percentage Breakdown – Electrolytic operation (Optimized Case)

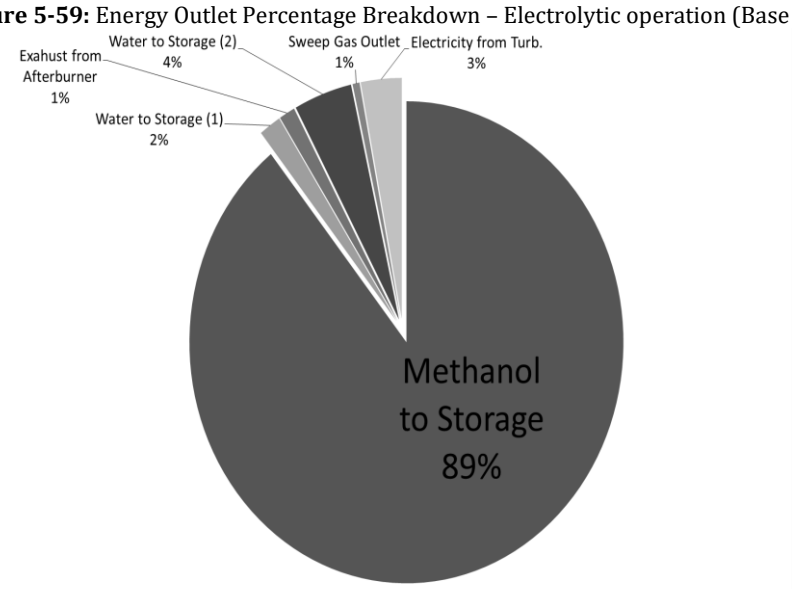

Figure 5-61: Exergy Outlet Percentage Breakdown – Electrolytic operation (Optimized Case)

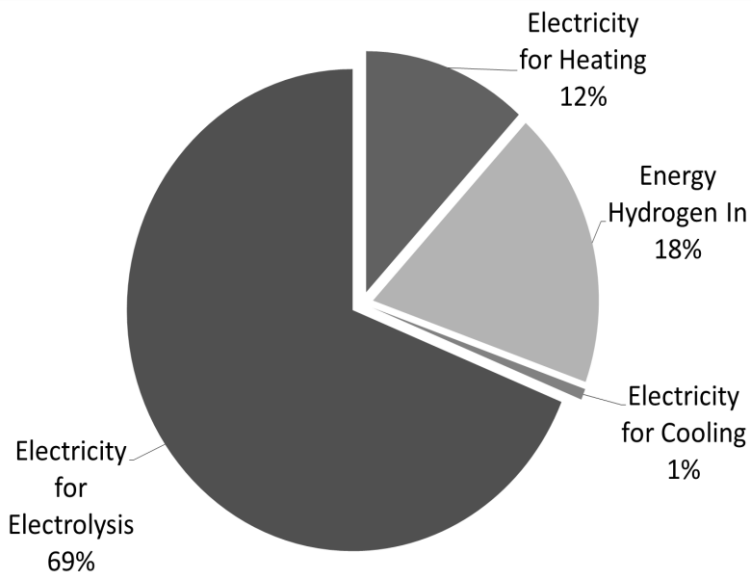

Figure 5-62: Energy Inlet Percentage Breakdown – Electrolytic operation (Optimized Case)

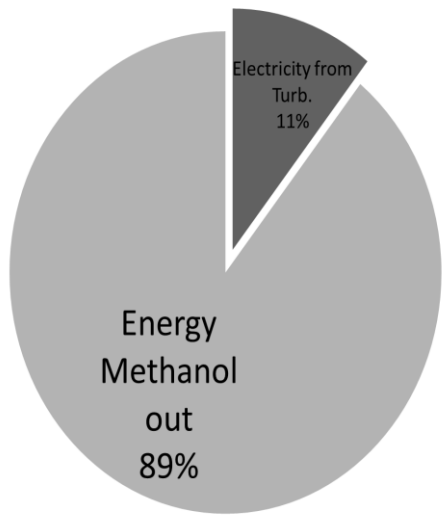

Figure 5-63: Energy Outlet Percentage Breakdown – Electrolytic operation (Optimized Case)

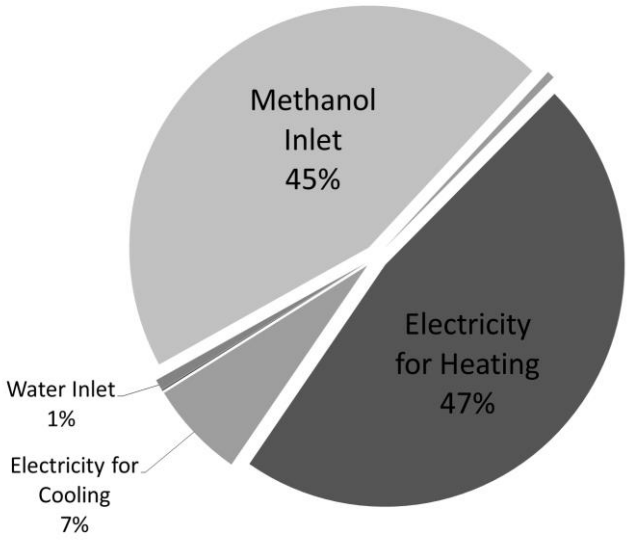

Figure 5-64: Exergy Inlet Percentage Breakdown – Fuel Cell operation (Base Case)

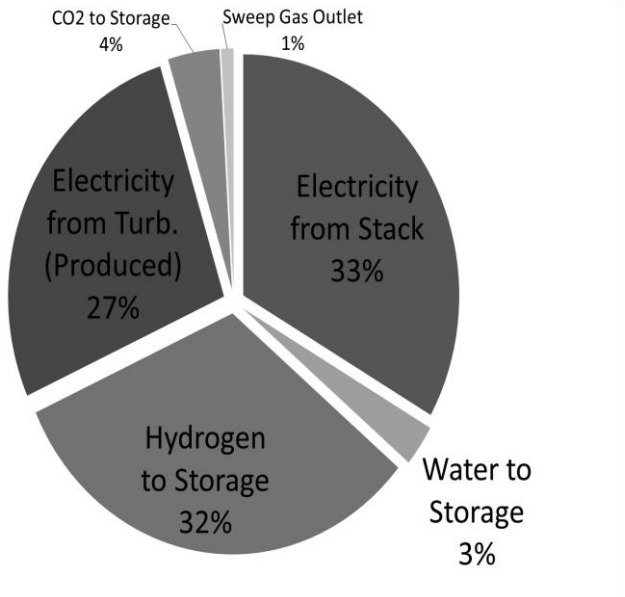

Figure 5-65: Exergy Outlet Percentage Breakdown – Fuel Cell operation (Base Case)

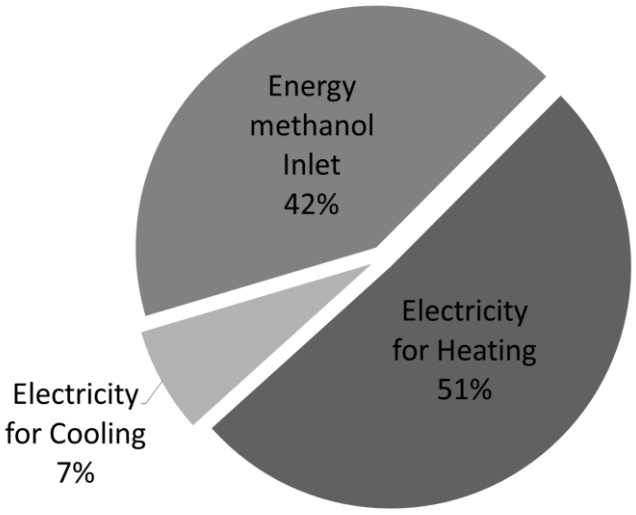

Figure 5-66: Energy Inlet Percentage Breakdown – Fuel Cell operation (Base Case)

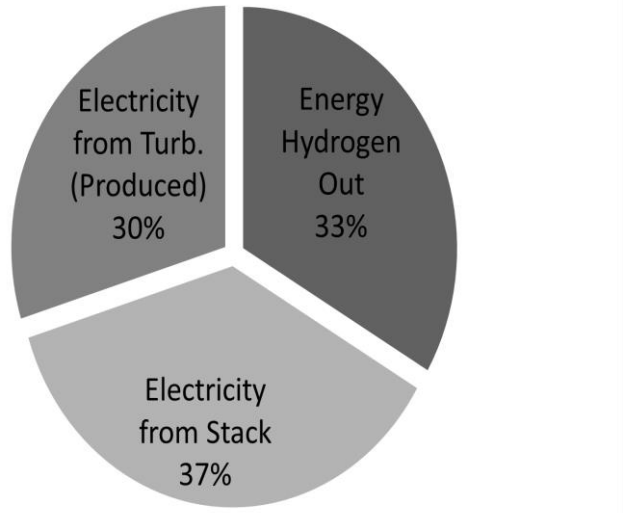

Figure 5-67: Energy Outlet Percentage Breakdown – Fuel Cell operation (Base Case)

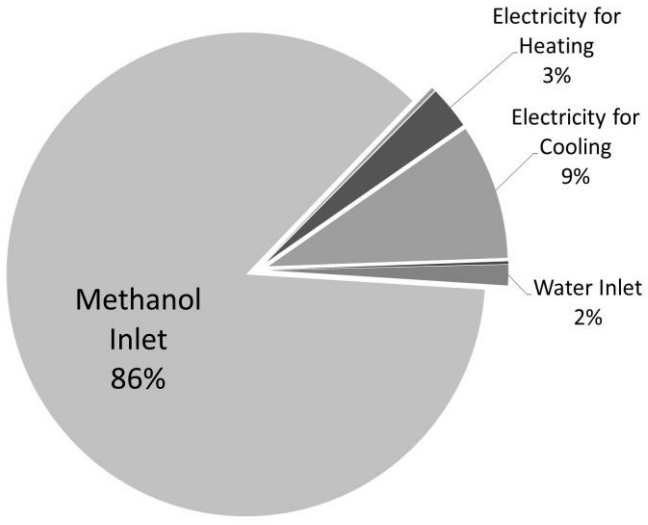

Figure 5-68: Exergy Inlet Percentage Breakdown – Fuel Cell operation (Optimized Case)

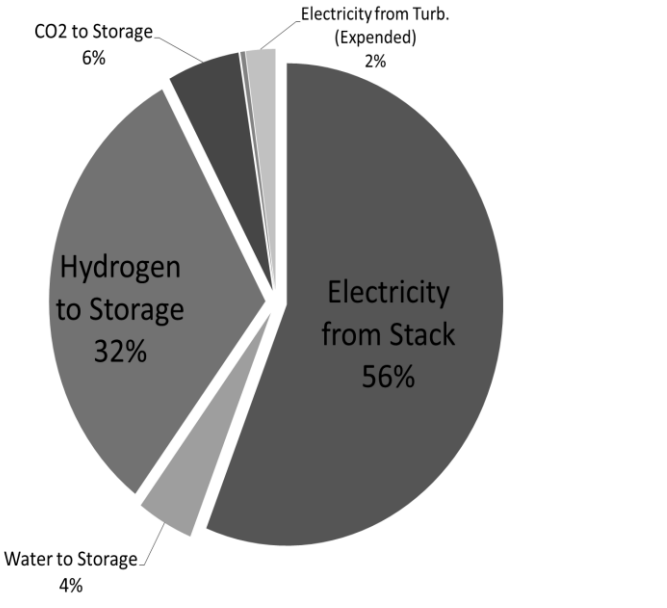

Figure 5-69: Exergy Outlet Percentage Breakdown – Fuel Cell operation (Optimized Case)

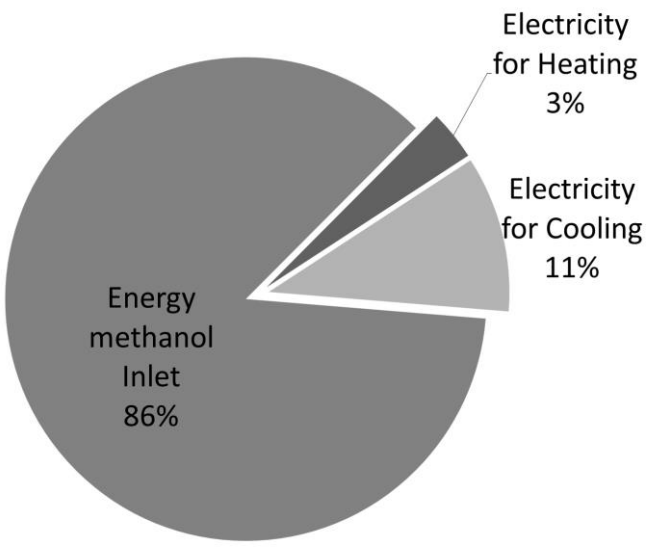

Figure 5-70: Energy Inlet Percentage Breakdown – Fuel Cell operation (Optimized Case)

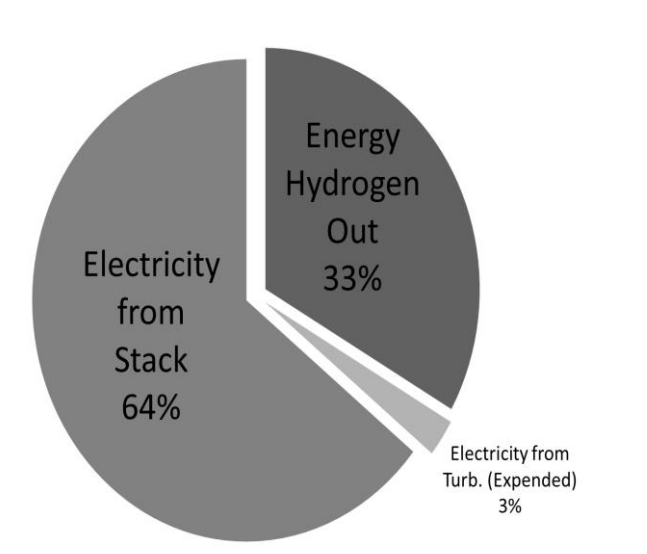

Figure 5-71: Energy Outlet Percentage Breakdown – Fuel Cell operation (Optimized Case)

5.4 A feasible heat integration scheme – Exergy flow Diagrams

Achieving the "perfect heat integrated" process is a tedious task for the process engineer because the heat exchanger network has to be designed manually for its realization. In fact, numerous heat exchangers (HEX) will be needed for the perfect heat integration and this will give an excessive rise in capital cost. The objective of the present study is not to define the heat exchanger network which minimizes the cold and hot utility but to define a set of heat exchangers and see their effect on system energy and exergy efficiency. It is obvious therefore that hot and cold utility will not be minimized anymore while energy and exergy efficiency will drop compared to the "perfectly heat integrated" case. In the present study, a set of seven heat exchangers will be defined based on the optimized case conditions. This set of heat exchangers is also extended in the base case. An important note is that there are some heat exchangers which are thermodynamically feasible in the optimized case but not in the base case due to heat transfer inability (i.e. hot temperature lower than cold temperature), and therefore the number of HEXs can be reduced in the base case. By defining a relatively small number of well-placed heat exchangers, the system becomes economically viable. In addition, the reader will be able to discern the role of a proper heat exchanger network in system energy and exergy efficiency. Finally, thorough exergy flow diagrams can be drawn which unlock the possibility of pinpointing excess amount of exergy losses. Pinpointing the exact components for excess exergy losses means that in these components there is ample space for thermodynamic improvement. HEX network is a design process where design freedom exists, however, with a certain number of heat exchangers a decent amount of heat should be transferred. In the present study, the HEX network is designed meticulously in order to satisfy as much as possible the streams with high heating/cooling capacity (i.e. $\dot{m}c_p$) and then moving on with other streams in descending order of heating/cooling capacity. Finally, the HEX network for each mode is only using the BOP components of the specific mode. Hence, during electrolytic operation only the BOP components of the electrolysis mode will be heat integrated and the same is applied for the fuel cell operation.

5.5.1 Electrolysis Mode – Base Case Scenario

The detailed 7-HEX network applied is shown in Figure 5-72. The temperature of each stream at each subsection is written on the specific stream while the unit is in Celsius. The duty of each HEX is depicted with orange letters on top of each HEX while numbering is shown with orange letters at the bottom of each HEX. For the base case, exergy losses are approximately 119.65 kW. In addition, a pie-chart summarizing the exergy losses is given in Figure 5-73. For the base case scenario, energy and exergy efficiencies are 36.87% and 42.01% respectively. The respective efficiency values for the perfectly heat integrated case are 52.40% and 59.48%. For a more analytical view of the exergy flow diagram, see Appendix E.

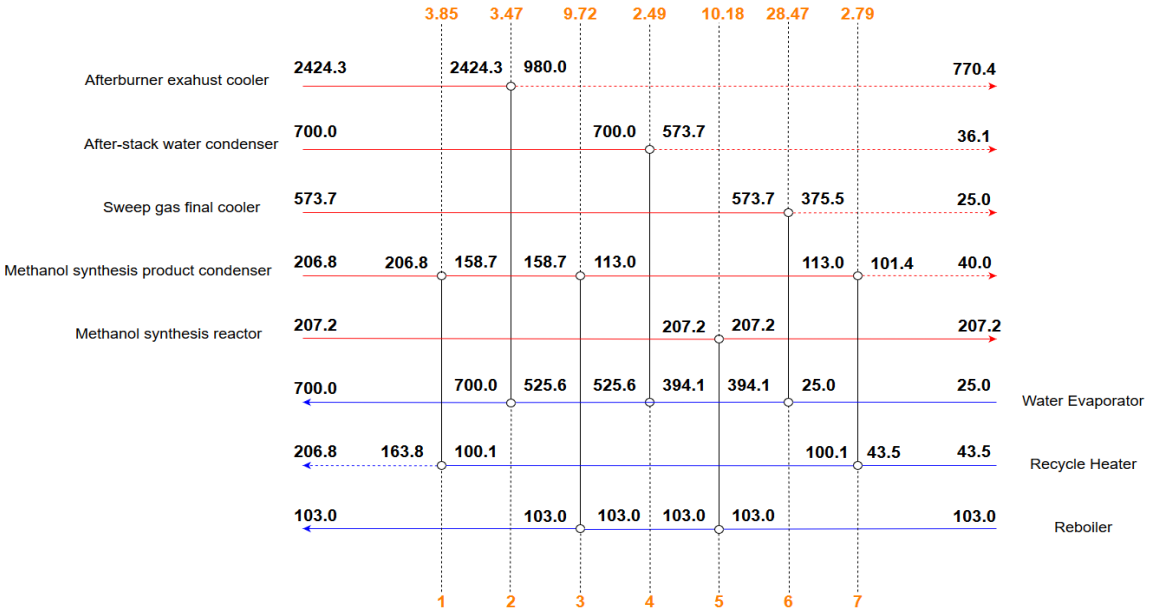

Figure 5-72: Heat Exchanger Network – Electrolysis (Base Case)

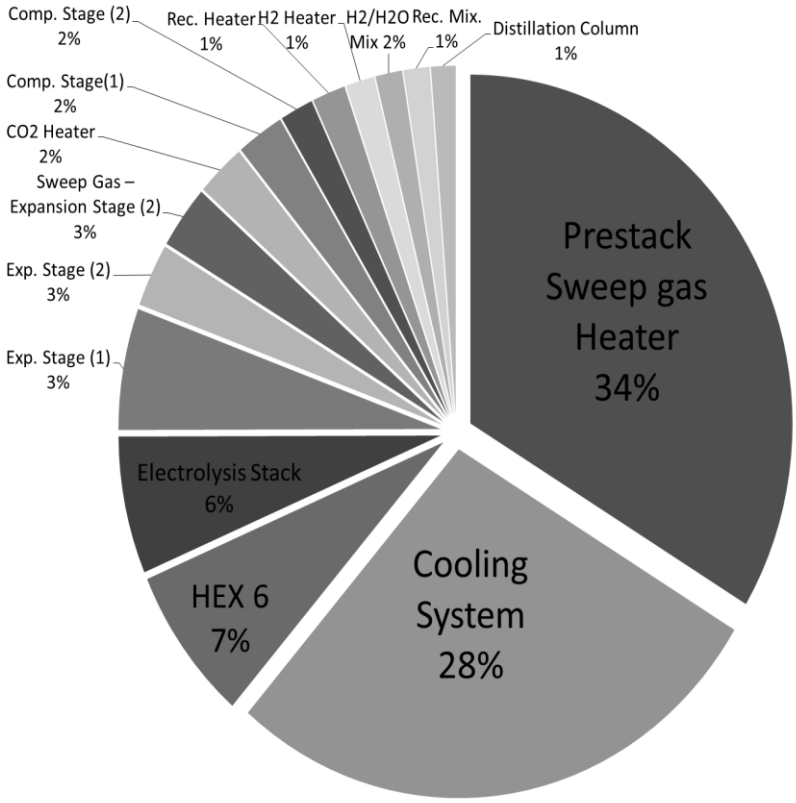

Figure 5-73: Per component contribution (%) in total exergy loss – Electrolysis (Base Case)

5.5.2 Electrolysis Mode – Optimum Scenario

The detailed 7-HEX network applied is shown in Figure 5-74. Color coding and numbers/units are the same as explained in subsection 5.5.1. In this case, the total amount of exergy losses is 43.62 kW. Moreover, Figure 5-75 summarizes the contribution of each component to the total exergy losses. For the optimum

scenario, energy and exergy efficiencies are 61.49% and 69.37% respectively, while for the perfectly heat integrated case they are 68.74% and 77.67%.

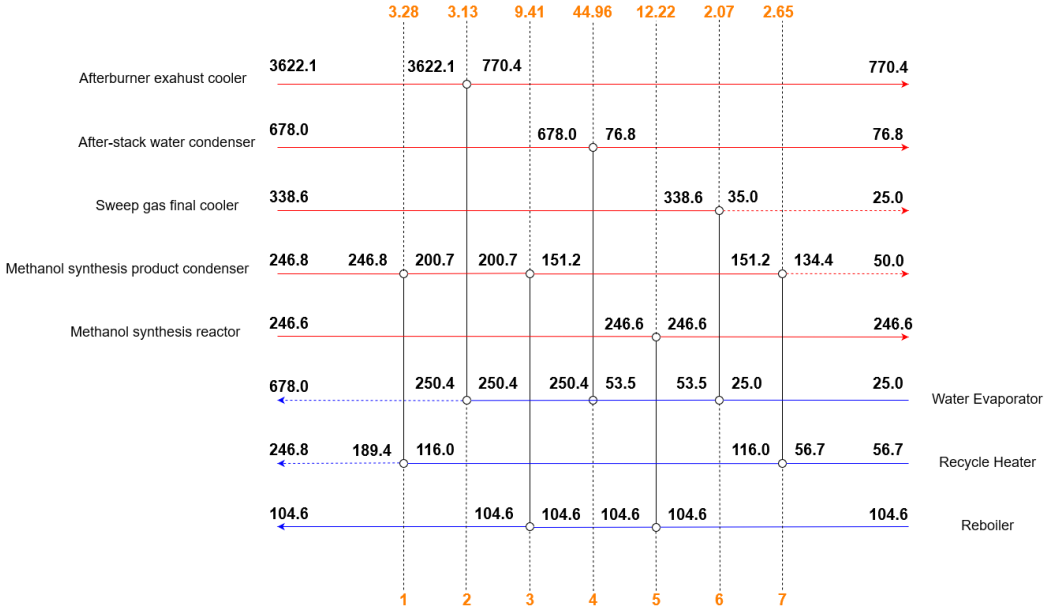

Figure 5-74: Heat Exchanger Network – Electrolysis (Optimized Case)

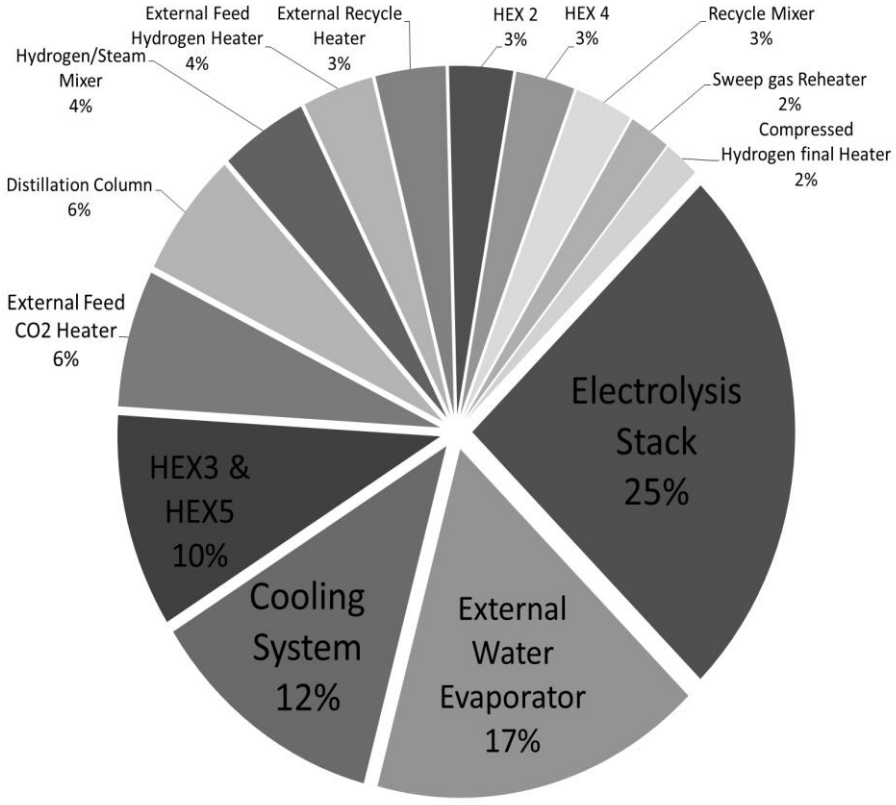

Figure 5-75: Per component contribution (%) in total exergy loss – Electrolysis (Optimized Case)

Before finishing this subsection, a direct comparison of exergy losses will be presented and the improvements per component will be shown in Table 5-11. The most striking improvement is the elimination of exergy losses in the prestack sweep gas heater. Secondly, exergy losses due to the cooling system have been

drastically reduced. Moreover, exergy losses of HEX6 and sweep gas reheater have almost been neutralized. All exergy losses attributed to sweep gas compressors and expanders have been effectively nullified due to the elimination of sweep gas flow rate. On the other hand, electrolysis stack exergy losses have been increased. The rest of the differences are of minor significance. For a more analytical view of the exergy flow diagram, see Appendix E.

Table 5-11: Direct comparison of exergy losses per component between base/optimized case (Electrolysis Mode)

Component	Exergy loss (kW)	
Case	**Base**	**Optimized**
Prestack Sweep gas Heater	39.66	-
Cooling System	32.65	5.32
HEX 6	8.5	-
Electrolysis Stack	7.5	11.14
Sweep gas Reheater	6.64	0.92
Sweep Gas – Expansion Stage (1)	3.46	-
Sweep Gas – Expansion Stage (2)	3.46	-
HEX 3 & HEX 5	2.92	4.41
External Feed CO_2 Heater	2.81	2.83
Sweep Gas – Expansion Stage (1)	1.97	-
Sweep Gas – Expansion Stage (2)	1.97	-
External Recycle Heater	1.71	1.56
External Feed Hydrogen Heater	1.58	1.58
Hydrogen/Steam Mixer	1.54	1.95
Distillation Column	1.45	2.60
Hydrogen/Carbon Dioxide/Recycle Mixer	1.12	1.30
HEX 2	0.62	1.42

5.5.3 Fuel Cell Mode – Base Case Scenario

The detailed 7-HEX network, which is degraded down to a 5-HEX network for the fuel cell base case, is shown in Figure 5-76. Color coding and numbers/units are the same as explained in subsection 5.5.1.

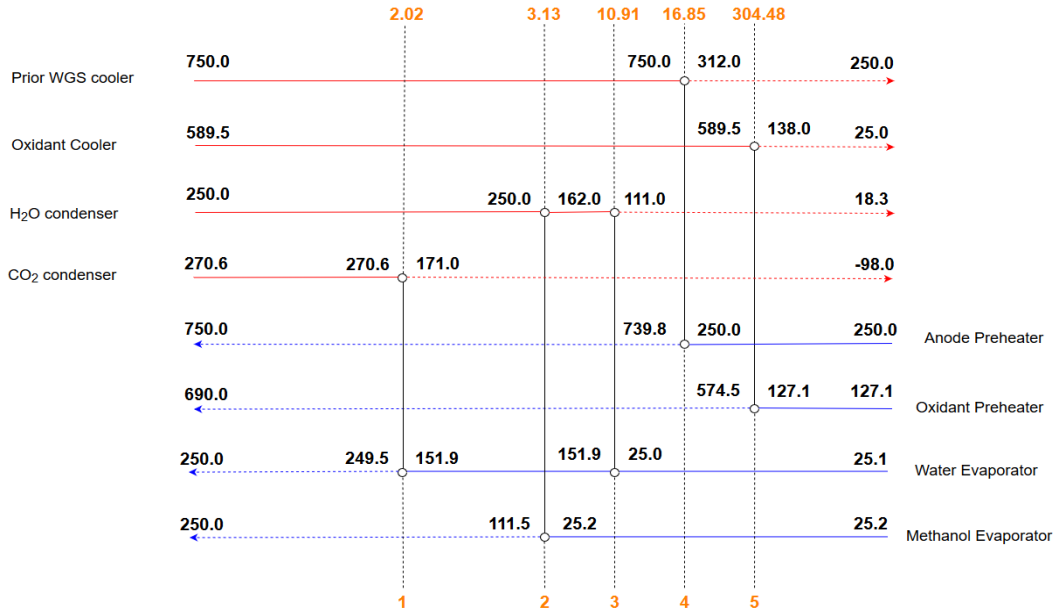

Figure 5-76: Heat Exchanger Network – Fuel Cell (Base Case)

In this case, the total amount of exergy losses is 194.87 kW. Moreover, Figure 5-77 summarizes the contribution of each component to the total exergy. For this base case scenario, energy and exergy efficiencies are -105.95% and -97.08% respectively, compared to -91.35% and -83.73% of the perfectly heat integrated base case. The same for the perfectly heat integrated case are -8. For a more analytical view of the exergy flow diagram, see Appendix F.

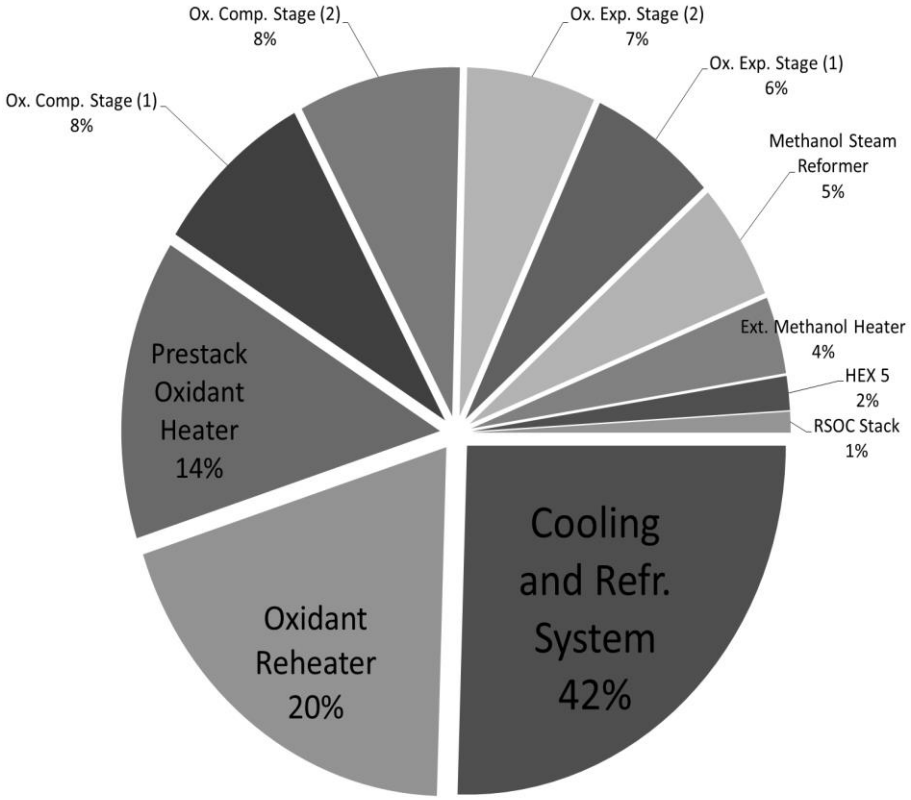

Figure 5-77: Per component contribution in total exergy loss –Fuel Cell (Base Case)

5.5.4 Fuel Cell Mode – Optimum Scenario

The detailed 7-HEX network is shown in Figure 5-78. Color coding and numbers/units are the same as explained in subsection 5.5.1. In this case, the total amount of exergy losses is 24.19 kW. Moreover, Figure 5-79 summarizes the contribution of each component to the total exergy losses. For the optimum scenario, energy and exergy efficiencies are 50.88% and 47.94% respectively. The same efficiencies for the perfectly heat integrated case are 60.22% and 56.78%. Before finishing this subsection, a direct comparison of exergy losses will be performed and the improvements per component will be shown in Table 5-12. The most striking improvement is a huge elimination of exergy losses of the cooling and refrigeration system. Oxidant flow reduction eliminates completely the vast exergy losses in the prestack oxidant heater. Exergy losses referring to oxidant train components such as oxidant compressors, expanders, and the oxidant reheater are also eliminated due to oxidant flow minimization. Exergy losses of methanol steam reformer have also been drastically reduced. The rest of the differences are of minor significance. It is also worth noting that feed flow rates have been lessened during the transition from base case to the optimized case. For a more analytical view of the exergy flow diagram, see Appendix F.

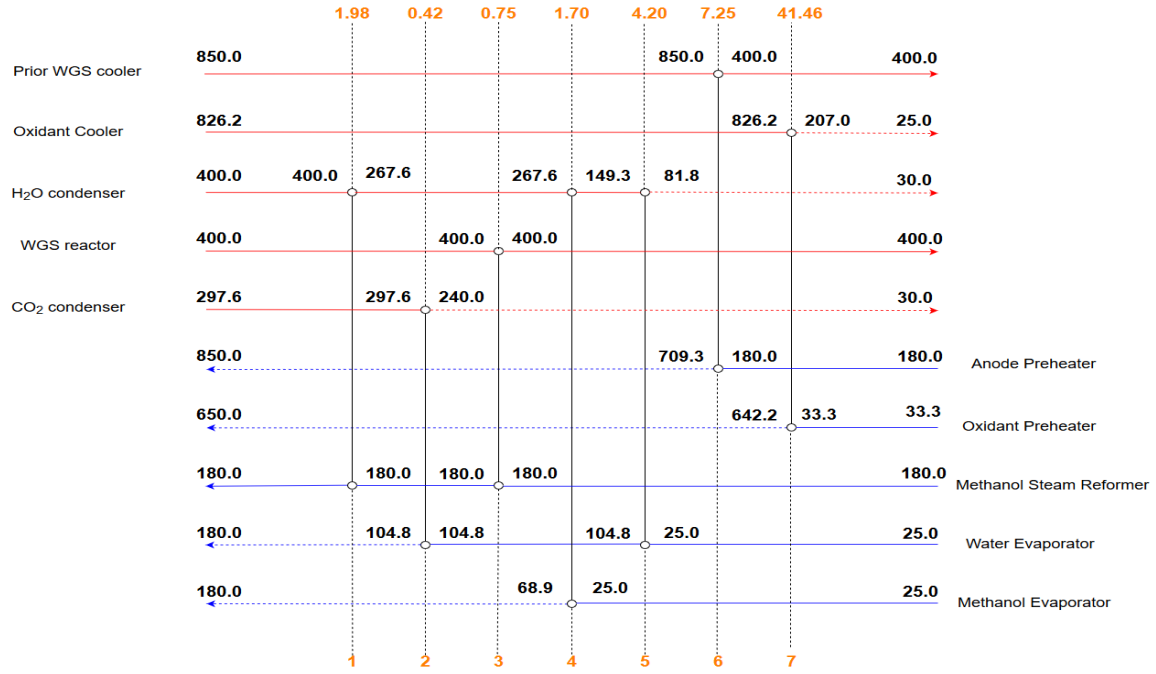

Figure 5-78: Heat Exchanger Network – Fuel Cell (Optimized Case)

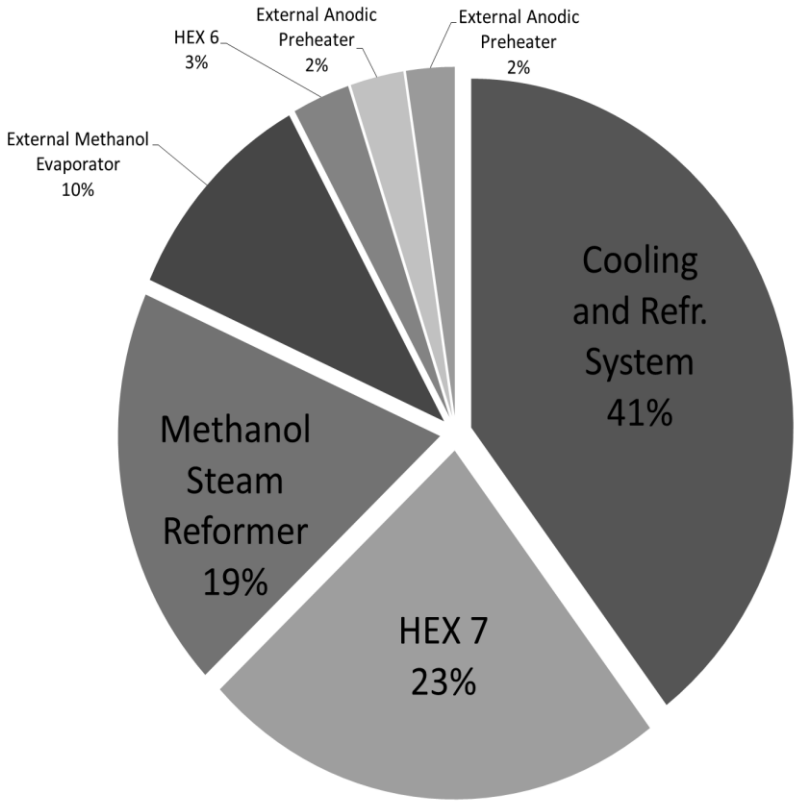

Figure 5-79: Per component contribution (%) in total exergy loss – Fuel Cell (Optimized Case)

Table 5-12: Direct comparison of exergy losses per component between base/optimized case (Fuel Cell Mode)

Component	Exergy loss (kW)	
Case	Base	Optimized
Cooling and Refrigeration System	50.26	9.48
Oxidant Reheater	38.58	0.64
Prestack Oxidant Heater	27.47	-
Oxidant Compression Stage (1)	16.21	-
Oxidant Compression Stage (2)	16.21	-
Oxidant Expansion Stage (1)	12.92	-
Oxidant Expansion Stage (2)	12.86	-
Methanol Steam Reformer	10.72	4.46
External Methanol Evaporator	7.06	2.48
HEX 5 (Base) – Hex 7 (Optimized)	3.11	5.59
rSOC Stack	1.9	-

5.5 Other metrics and comparison with scientific literature

In the optimized case of electrolytic operation, the electrolysis operation consumes 84.5% of the total input electricity while De Saint et al. [7] reported a value of 90%. This difference can be justified due to the fact that in this work the hot utility is solely provided by electricity while in their work, the hot utility is supplied by means of heat. To generate that specific amount of heat, they performed calculations for the respective electricity consumption. Hence, the electricity consumption to cover the hot utility is lessened in their work.

LHV efficiency achieved in this work is 74.7% while Hansen et al. [25] achieved 75.8-80.1% for methanol production. Again it is suspected that LHV efficiency is lowered due to the fact that the hot utility is converted solely by electricity. If a typical Rankine Cycle which converts heat into electricity is assumed to have 40% efficiency, it means that 2.5 kW of heat can be produced by 1 kW of electricity. If this assumption is taken into account, the LHV efficiency reaches 80.6% in this work, which is in accordance with the reported results by Hansen et al. [25]. LHV efficiency is equivalent to the existing energy efficiency if the inlet chemical energy of the hydrogen stream is ignored.

Finally, in this work, power-to-methanol efficiency (which is equivalent to the energy efficiency used in this work) was calculated to be 68.74% for the optimized electrolysis case, while Leonard et al. [2] reported a maximum value of 50.3%. Leonard et al. performed co-electrolysis instead of steam electrolysis for the production of methanol. In addition, partial heat integration was achieved in their work. For the partially heat integrated case presented in the current work, power-to-methanol efficiency is still 61.49%. Their efficiency is still lower because in their work the CO_2 is captured in-situ, while in the current study a certain amount of CO_2 exists in the system.

5.6 Summary

In this chapter, the optimization of both electrolysis and fuel cell mode of operation was presented in terms of energy and exergy efficiencies. While the base case conditions provided a quite efficient system during electrolytic operation, the adoption of those conditions in fuel cell mode reduced the energy and exergy efficiency abruptly. The system was first studied as a whole by employing the pinch technology which minimizes the system hot and cold utility and the respective results and process conditions were reported. The base case and the optimized case conditions have been reported in Table 5-1 & Table 5-5 respectively. The same, have also been reported for fuel cell operation in Table 5-6 & Table 5-8. During the transition from the base case to the optimized case in electrolysis mode, the energy efficiency increased from 52.4% to 68.74%,

while the exergy efficiency has also been increased from 59.48% to 77.67%. The same increase was also observed in fuel cell operation. The energy efficiency increased from -91.35% to 60.22%, while the exergy efficiency was enhanced from -83.73% to 56.78%. The lower efficiencies of the base case were prevailing due to high system hot utility. Initially, increased sweep gas/oxidant flow rate and high stack pressure led to high hot utilities. After the optimization of the fuel cell mode, the efficiencies were still limited due to the operation of an intense refrigeration cycle for the CO_2 condensation, while the hot utility is minimized in both modes. In sections 5.3 and 5.4 there is a complete energy and exergy analysis of the base and the optimized case for each mode.

Afterwards, a manual HEX network was implemented in each mode based on the optimized process conditions. This HEX network was also expanded in the base case conditions. In this case, the efficiencies were reduced because the hot and cold utilities were higher compared to their minimized values obtained from pinch analysis. More specifically, from base case to optimized case in electrolysis mode, the energy and exergy efficiencies increased from 36.87% to 61.49%, and from 42.01% to 69.37% respectively. The increase in energy and exergy efficiencies is also reported during fuel cell operation. For the energy efficiency there was an increase from -105.95% to 50.88% while the same for the exergy efficiency was from -97.08% to 47.94%. Apart from the negative effect of the manually imported heat exchanger network in both efficiencies, it was made possible to see in which components the major exergy losses took place for each mode but also how these exergy losses changed during the transition from the base case to the optimized case. A summary of those results can be found in Table 5-11 & Table 5-12, while the respective exergy flow diagrams are shown Appendix E & F. Finally, the optimized cases were compared to results obtained from the scientific literature.

CHAPTER 6

THERMODYNAMIC OPTIMIZATION FOR ROUNDTRIP EFFICIENCY– RESULTS AND DISCUSSION

While exergy efficiency is a strong measure of the thermodynamic irreversibility of the system, roundtrip efficiency is also a significant metric which is examined by the research community [4], [5], [10], [11], [19]. Some differences from the exergy efficiency are the following:

- Each of the operating modes (i.e. fuel cell or electrolysis mode) can be decoupled and exergy can be optimized separately for each mode. However, this decoupling does not take into account the time of operation for each mode. In roundtrip efficiency, time of operation is included because all the terms are expressed in energy and not in power. In addition, exergy efficiency optimization does not take into account the fact that the methanol produced in electrolysis mode might not be sufficient for consumption in fuel cell mode. To include the time of operation in each mode, the equal charge transfer rule will be employed
- Roundtrip efficiency includes only terms of electrical power consumption/production, while exergy efficiency also contains terms related to the exergy content of streams. It is simply the ratio of energy recovered and energy stored and it does not characterize the reversibility of the process

Eq. (4-10) can be split into two parts. The numerator is totally dependent on fuel cell operation while the denominator is only dependent on electrolysis mode. An optimization process it again initiated for each mode. The electrolysis model will be utilized to minimize the denominator while the fuel cell model will be employed to maximize the numerator. At the end of the calculations, a methanol adequacy criterion must be formulated in order to ensure sufficient production/consumption of methanol when switching from electrolysis to fuel cell mode.

6.1 RT Optimization – Electrolysis Mode

In this section, minimization of the term $V_{el}A_{tot} + \frac{W_{BOP,el}}{j_{el}}$ (i.e. denominator of Eq. (4-10)) will occur by following the exact same process as followed for exergy efficiency maximization during electrolysis mode. For a revision of the term $W_{BOP,el}$, the reader is advised to revisit section 4.5. According to the previous base case conditions mentioned in Table 5-1 the starting point of the denominator is 24.47 Vm^2. When stack pressure and temperature are varied, it can be seen that RT denominator follows the same trend with system hot utility (see Figure 5-4 & Figure 6-1) which seems to be the dominant term. Again, thermoneutral operation is necessitated for the minimization of RT denominator. The same trend continues to happen when varying steam utilization, steam molar flow rate and hydrogen flow rate. It seems that the trend of RT denominator mainly depends on the hot utility(see Figure 5-14 & Figure 6-3 / Figure 5-19 & Figure 6-2). Of course, cell voltage affects the result quite significantly, but not as much as hot utility. The results so far indicate that thermoneutral operation leads to minimization of RT denominator.

Afterwards, the stack operation parameters (i.e. cell voltage and current density) remain the same in all the analysis. From now and on, the differences are becoming smaller. The results do not follow solely the trend of hot utility, but electricity produced/consumed by system turbomachinery is also becoming an important factor. The interplay of those two factors is giving out the trend in the final result. Pump power is not differing that much in these sensitivity analyses so it is hardly playing any role. More specifically, minimization of the RT

denominator occurs at 50 bar/540 ^{o}C when varying the methanol synthesis temperature and pressure (Figure 6-4). It should be reminded that the RT efficiency is not a function of methanol production. All trends regarding system BOP and hot utility are explained in detail in Chapter 5.

More sensitivity analyses (as mentioned in section 5.1.2) have been conducted for further minimization of RT denominator but their effect is minimal and therefore the respective results have been omitted. After the whole analysis, the minimized obtained value of the denominator is 18.34 Vm^2.

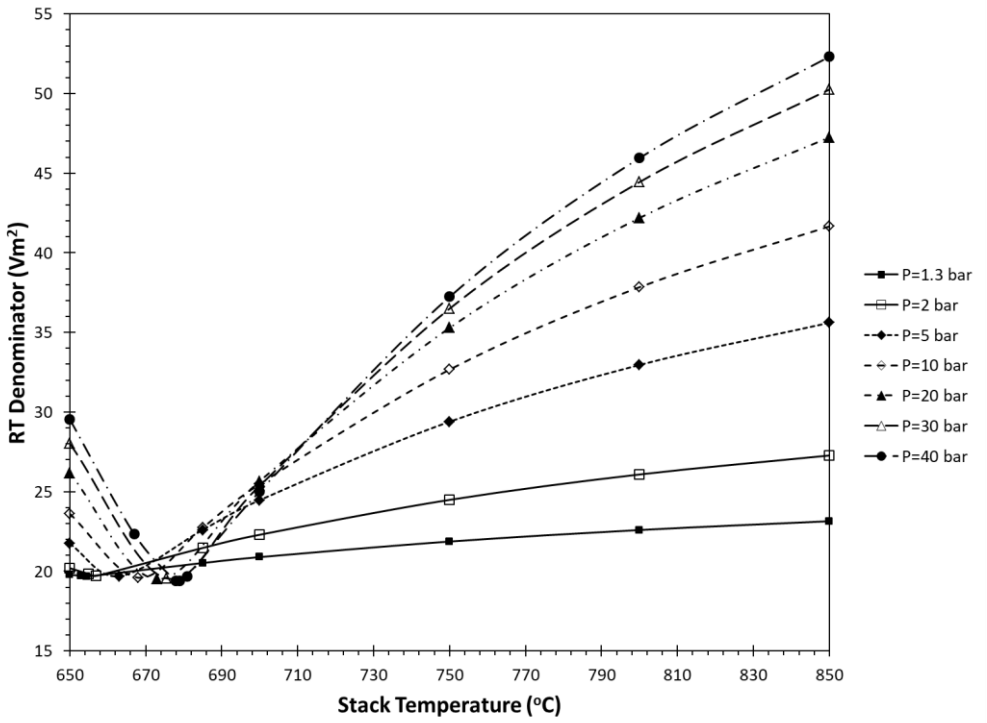

Figure 6-1: RT Denominator - Process Conditions, See Base Case - Vary stack P_s, T_s

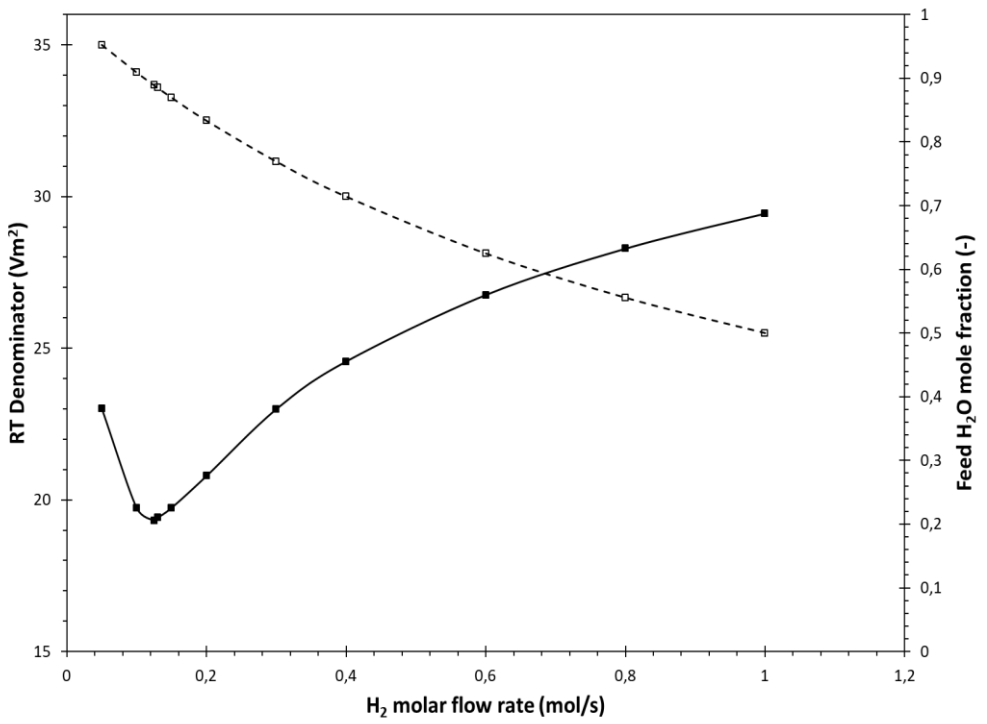

Figure 6-2: RT Denominator- Process Conditions, See Base Case, fix P_s=40bar, T_s=951.15K, n_{H2O}=1mol/s, $U_{f,steam}$=0.45**,** Vary Hydrogen molar flow rate.

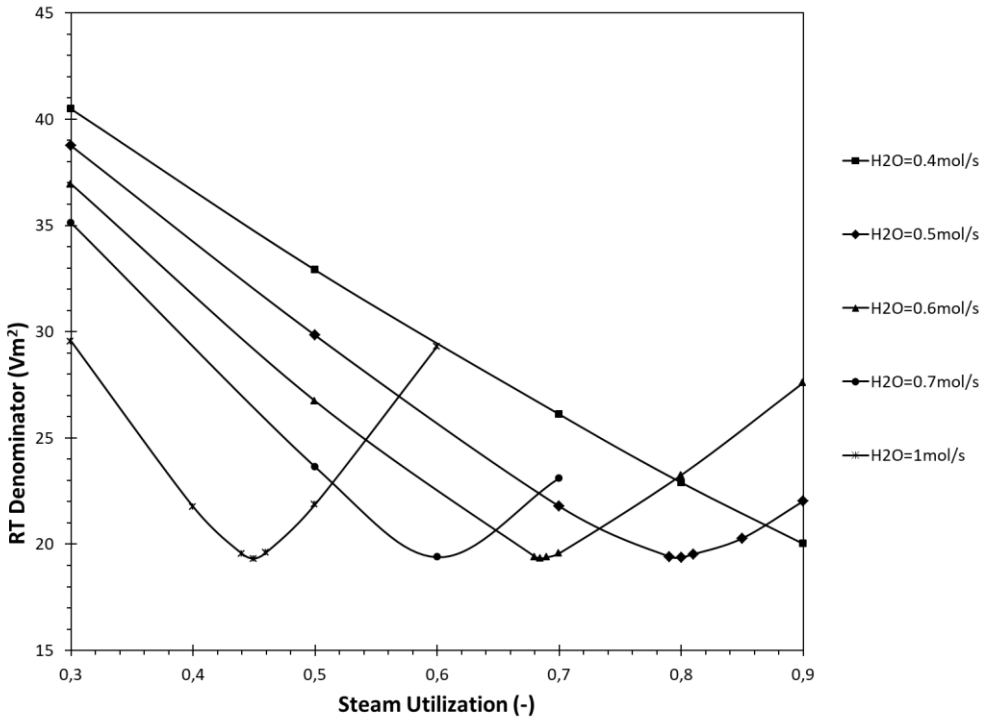

Figure 6-3: RT Denominator- Process Conditions, See Base Case, fix P_s=40bar, T_s=951.15K, Vary Steam Utilization and steam feed flow rate

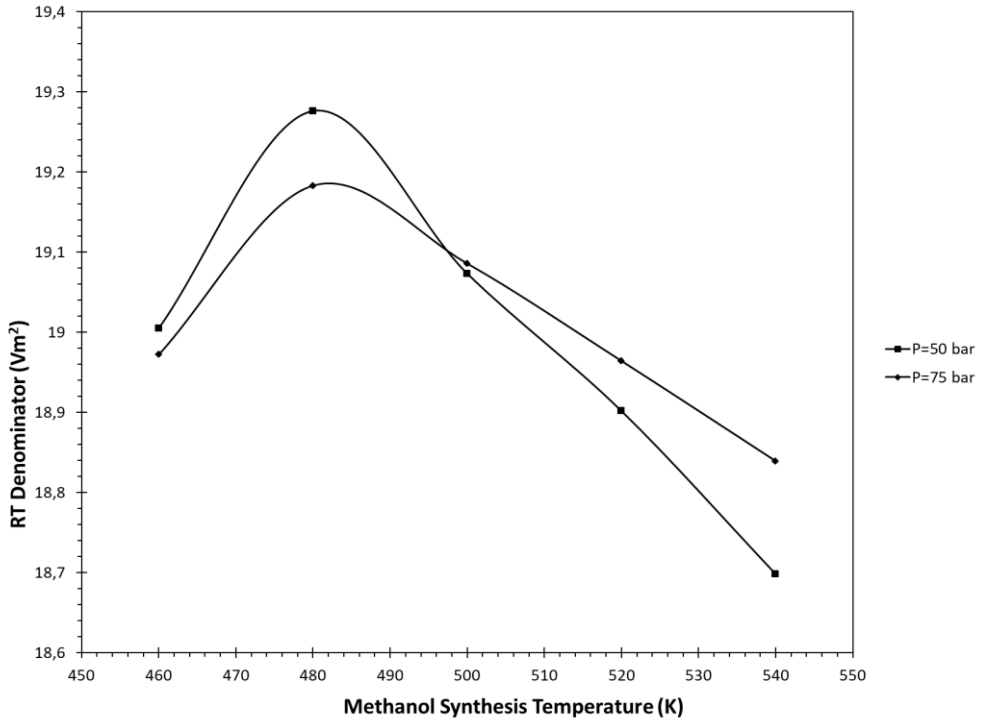

Figure 6-4: RT Denominator - Process Conditions, See Base Case, fix P_s=40bar, T_s=951.15K, n_{H2O}=1mol/s, $U_{f,steam}$=0.45, n_{H2}=0.125mol/s, P_{CO2}=80bar, P_{H2}=100bar, Vary methanol synthesis pressure and temperature

6.2 RT Optimization – Fuel Cell Mode

In this section, maximization of the term $V_{fc}A_{tot} - \frac{W_{BOP,fc}}{j_{fc}}$ (i.e. numerator of Eq. (4-10)) will occur by following the exact same process as followed for the exergy efficiency maximization during fuel cell operation. For a revision of the term $W_{BOP,fc}$, revisit section 4.5. Again, the optimization process begins with base case process parameters (see Table 5-6). The initial starting point of the numerator is -12.24 Vm^2. Again, this negative number signifies that the system BOP consumes more electricity than it is produced from the stack and system turbomachinery. Initially, stack pressure and temperature are varied. It is observed that the final trend of RT numerator is predominantly following the system hot utility (see Figure 6-5). Again, operation at low overpotentials (i.e. high temperature) results in less oxidant flow while external cooling and heating duties are reduced. Next, fuel utilization and steam (plus methanol) flow rate are varied. In this range, the RT numerator is increased by increasing fuel utilization or by reducing flow rates of feed streams. The trend of this graph is the same as the exergy efficiency trend during the same optimization step (see Figure 5-36 & Figure 6-7).

Afterwards, methanol steam reforming temperature is varied and RT numerator is maximized when methanol steam reforming temperature is 180°C (see Figure 6-6). Finally, Figure 6-8 outlines the significance of isentropic efficiencies of system turbomachinery. It is prevalent that the higher the efficiencies of either expanders or compressors, the more the increase of RT numerator. The effect is very strong when varying compressor isentropic efficiency because it enhances the COP of the refrigeration system. For once, more it is shown that the quality of the refrigeration system is significant in determining the RT numerator. Also, since the oxidant flow rate is not negligible as in the electrolytic operation, the effect of efficient oxidant expansion is also affecting quite significantly the RT numerator.

All trends regarding the electricity produced/consumed by system turbomachinery, hot utility and hydrogen stored are explained in detail in Chapter 5. More sensitivity analyses have been conducted (as mentioned in section 5.2.2) for further minimization of RT denominator but their effect is minimal and therefore the respective results have been omitted. After the whole analysis, the maximum value of the numerator is 8.57 Vm^2.

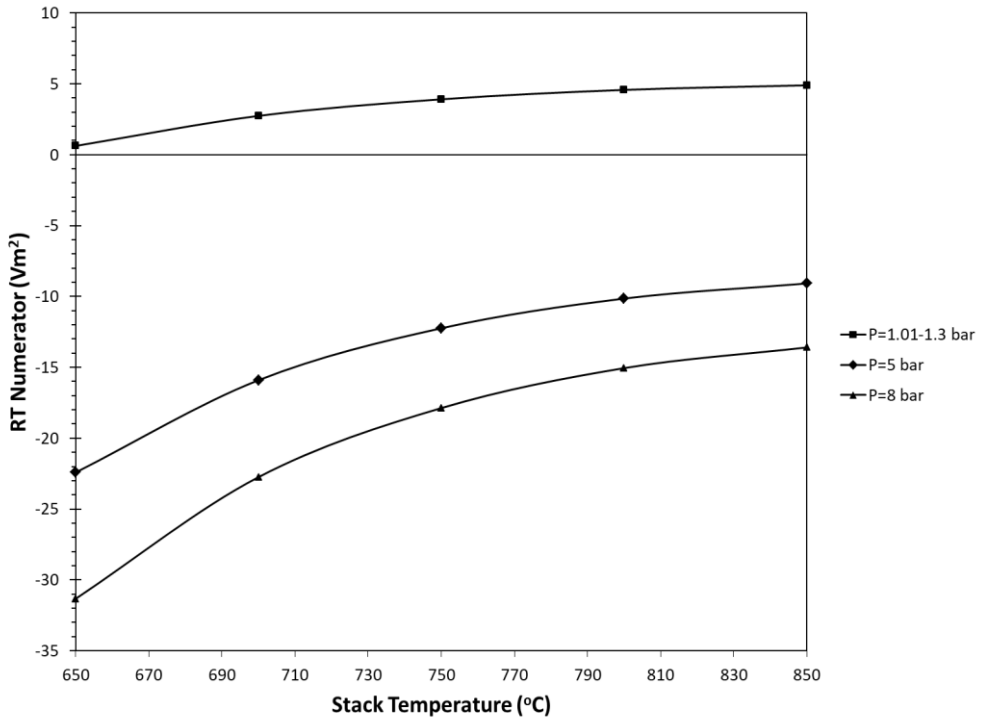

Figure 6-5: RT Numerator - Process Conditions, Vary Stack Pressure and Temperature

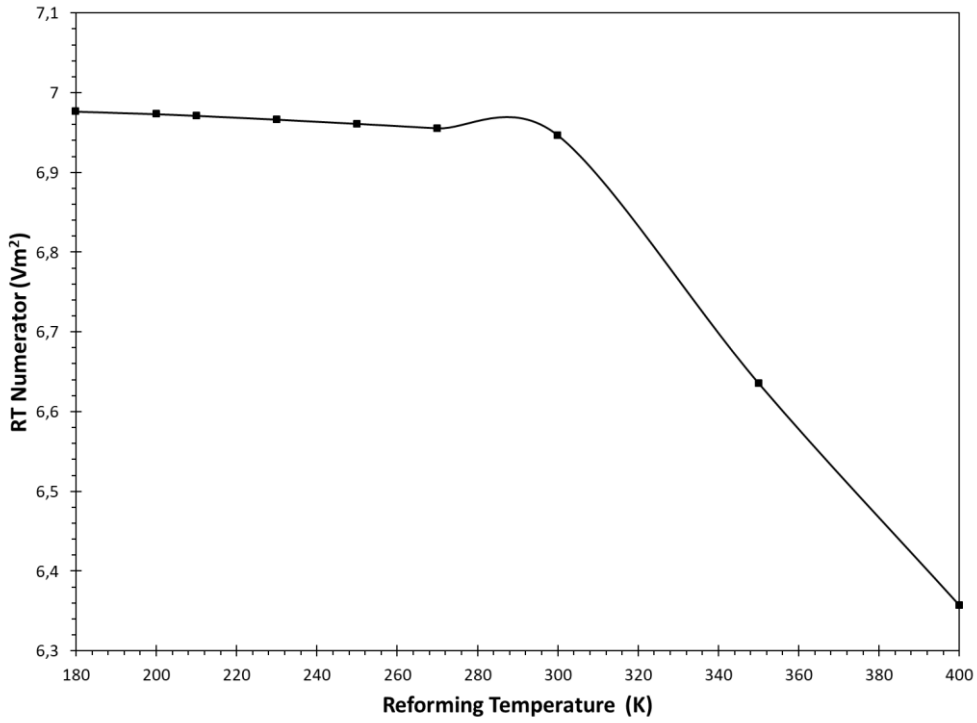

Figure 6-6: RT Numerator - Process Conditions, See Base Case and Fix P_s=1.2bar, T_s=1123.15K, U_f=0.95, n_{H2O}=0.1mol/s, Vary Methanol Steam Reforming Temperature

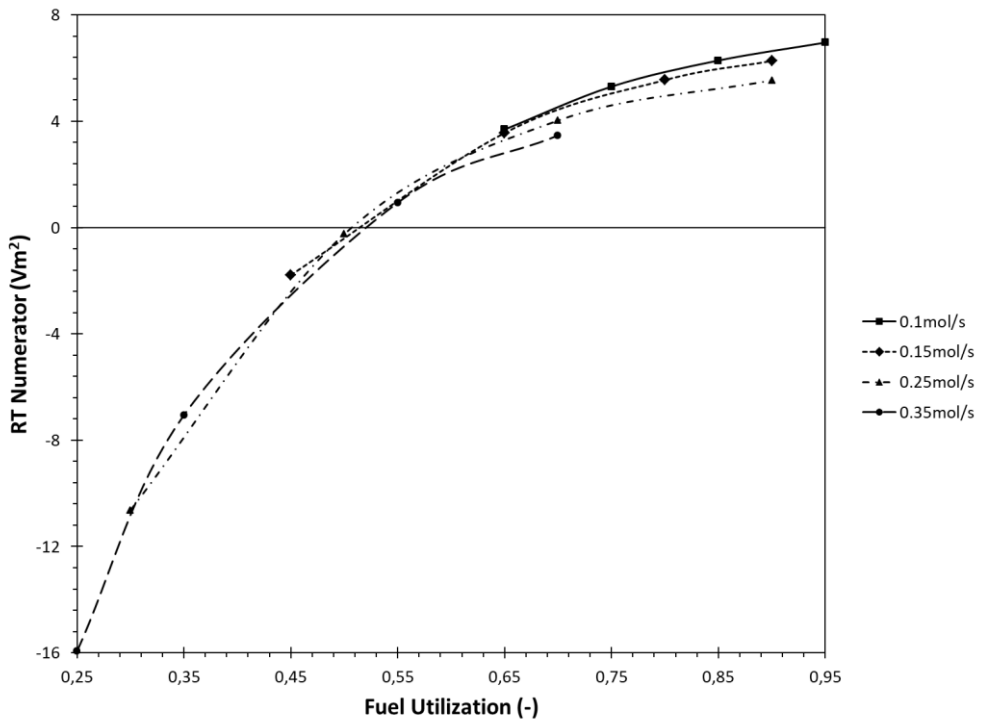

Figure 6-7: RT Numerator - Process Conditions, See Base Case and Fix P_s=1.2bar, T_s=1123.15K, Vary Fuel Utilization and Steam Molar Flow Rate

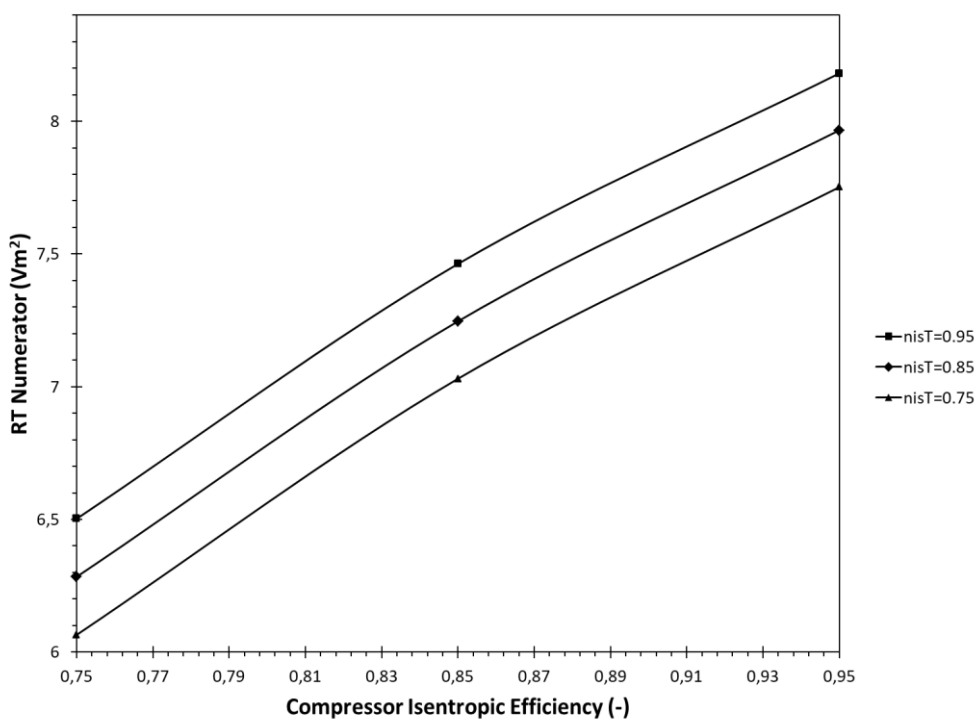

Figure 6-8: RT Numerator - Process Conditions, See Base Case and Fix P_s=1.2bar, T_s=1123.15K, U_f=0.95, n_{H2O}=0.1mol/s, T_{reform}=180°C,T_{WGS} =400°C, Vary $n_{is,C}$ & $n_{is,T}$

6.3 The need for Thermal Coupling between the modes and the effect on Roundtrip Efficiency

If both optimized modes were coupled (with a numerator of 8.57 and a denominator of 18.34), a roundtrip efficiency of 46.7% would be achieved. Roundtrip efficiency is quite low despite all the optimization steps. Apart from that, is enough methanol produced during the electrolysis step to be utilized in fuel cell mode? A criterion is developed here to see if the two modes can be coupled (see Eq. (6-1)). This criterion involves the charge transfer criterion and methanol production/consumption in one rule. If the following criterion occurs, then mode coupling can take place.

$$\frac{\dot{m}_{meth,el}}{j_{el}} > \frac{\dot{m}_{meth,fc}}{j_{fc}} \qquad \text{Eq. (6-1)}$$

By using the data from Table 6-1, the criterion does not apply.

Table 6-1: Current Density and Stored Methanol flow rate for each mode (1st Attempt)

Operating Mode	Current Density (A/m²)	Stored Methanol/Required (g/s)
Electrolysis	6680	5.14
Fuel Cell	3145	3.2

Consequently, in this case, it is impossible to couple these two modes for repeatable operation, since methanol production from electrolysis mode is not enough for fuel cell operation under these process conditions. Overall, a system has been proposed where roundtrip efficiency is very low and mode coupling cannot take place.

So far, both models run under the assumption that excess heat addition/removal is provided by a sweep gas or oxidant air stream. In addition, enhanced sweep gas or oxidant flow rate decreases the performance in every possible criterion (i.e. energy, exergy, roundtrip efficiency). According to Eq. (4-10), further minimization of the denominator can happen when operating in endothermic mode instead of thermoneutral mode. Of course, this is accompanied by excess hot and cold utility due to the large sweep gas flow rate. The increased utilities are also enhanced by inability of thermal coupling at high stack pressure according to the recuperated gas turbine theory. The idea proposed in the current work is a thermal energy storage system where the electrolysis stack will be capable of operation in endothermic mode with minimal sweep gas flow. The thermal energy storage system will be fed from excess heat removed from fuel cell mode and it will be deployed directly to the stack during electrolysis operation. In this scenario, cell voltage during electrolysis mode will be minimized without being accompanied by excess hot and cold utility. In other words, fuel cell operation functions under minimal overpotential which maximizes roundtrip efficiency. On the other hand, electrolysis operation runs under very high overpotential which limits the increase of roundtrip efficiency. The purpose of the heat energy storage system is to thermally couple both modes, while enabling them to operate under small overpotential losses and minimal sweep gas flow rate, in order to maximize roundtrip efficiency. It is prevalent that:

- Operating in endothermic mode, slightly below V_{tn}, will require a small amount of heat, but operating cell voltage will not be low enough for roundtrip maximization
- Operating in endothermic mode, quite below $V_{tn,}$ would maximize roundtrip efficiency, but maybe the excessive heat requirement could not be accommodated solely by heat removal during fuel cell operation

A conceptual design of this heat storage system can be visualized in Figure 6-9.

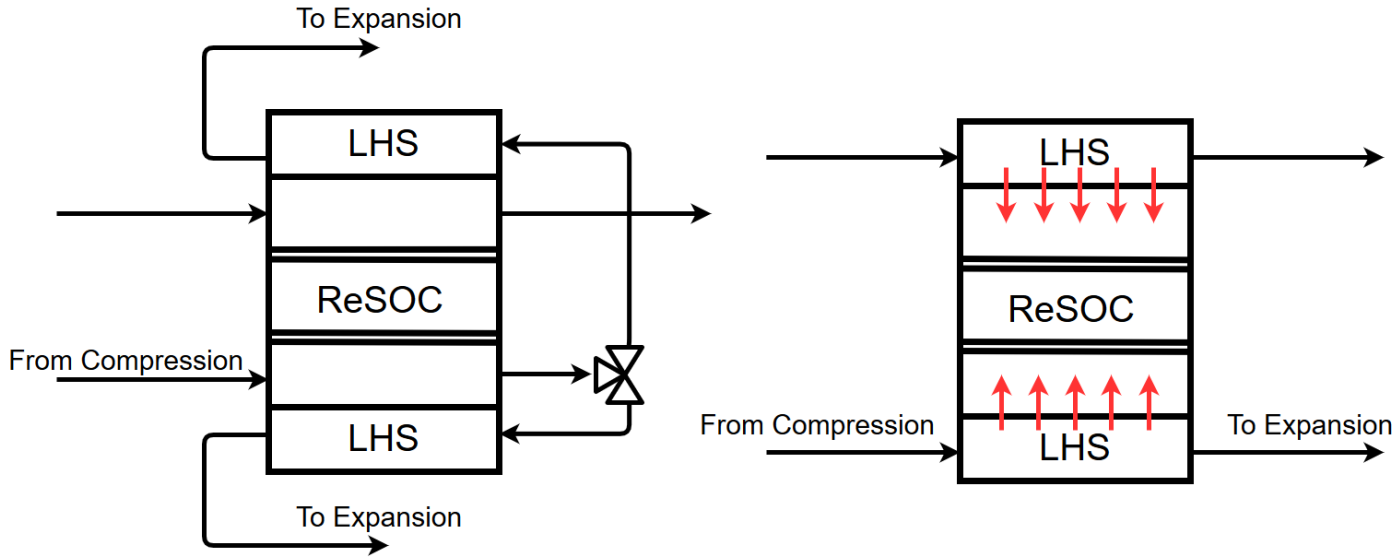

Figure 6-9: Conceptual process design of heat storage system. (Left) Charging during FC exothermic operation, (Right) Discharging during endothermic electrolytic operation

In steam electrolysis, thermoneutral voltage depends only on temperature which means that it is approximately constant (1.282-1.288 V in the examined temperature range). If an exothermic reaction was taking place, thermoneutral voltage would be reduced. This happens during co-electrolysis where exothermic methanation occurs as it has been extensively mentioned in Chapter 3. This means that operation close to reversible voltage could be easily achieved since thermoneutral voltage would be reduced, resulting also to heat requirement minimization and roundtrip efficiency maximization.

The process of optimizing starts with the fuel cell mode running in optimized process conditions where maximization of RT numerator takes place (mentioned at the end of this chapter). The process design changes in such a way that after the stack outlet, the oxidant stream is cooled down slightly before the expansion section. Optimized process conditions include maximum stack temperature which is ideal for heat storage and transfer to a lower temperature rSOC stack during electrolysis. Specifically, rSOC stack operates at 1123.15 K during fuel cell operation. After inserting the cooler, the numerator of roundtrip efficiency is modified as shown in Table 4-2 for different cooling temperatures.

For now, the heat storage material can be assumed to be a PCM. The temperature of a PCM remains constant during evaporation. This latent heat storage system will be attached to the stack walls enabling heat charging and discharging without the use of an intermediate fluid. Therefore the simulated cooler in fuel cell mode will be, in reality, inside the stack.

Table 6-2: Results for fuel cell operation with an in-channel cooling system for heat storage

Cell Voltage during Fuel Cell operation (V)	0.93355	**Current Density during Fuel Cell Operation (A/m²)**	3145
Cooling Temperature (K)	**Heat Stored (W)**	**Total Electricity Consumption from BOP (kW)**	**RT Numerator (Vm²)**
973.15	12562	13.96	7.70
1023.15	8108	9.77	9.03
1073.15	3617	10.09	8.93

The PCM, of course, will operate at a slightly lower temperature than the cooling temperature. A cooling temperature of 1023.15 K is picked because a considerable amount of heat can be stored (~8.1 kW) while simultaneously maximizing the numerator of roundtrip efficiency. The reason why 973.15 K is not chosen is due to the fact that electrolysis stack can only be coupled when operating at 923.15 K. In the examined pressure range (1-10 bar), operation at 923.15 K is an exothermic one, so this case is excluded.

Next, the electrolysis mode is re-optimized. Starting with optimized process conditions where minimization of RT denominator takes place, the rSOC stack will be reconfigured for the maximization of roundtrip efficiency. At first, stack pressure and temperature are varied. It is seen that by increasing the temperature (while operating under same current density), decreases cell voltage, but increases required heating duty. Heightened heat duty is reasonable since the difference between thermoneutral voltage and cell voltage is larger at higher temperature. By increasing the pressure, the reversible voltage and thus the operating cell voltage are enhanced without affecting the thermoneutral voltage. Therefore, the combination of these effects will lower the required heat demand of the rSOC stack during electrolytic operation due to decreased difference between V_{tn} and V_{cell}. An additional restriction for temperature is that stack temperature during electrolysis mode should be lower than the melting point of the PCM for successful mode coupling. The results from the first step are summarized in Table 6-3. It has to be noted that when the cooling temperature is higher, less heat is stored in the PCM and more heat requirement has to be covered through enhanced sweep gas flow in electrolysis mode. That is the reason why at higher cooling temperatures the roundtrip efficiency drops.

Table 6-3: Re-optimizing electrolysis stack for thermal coupling, Vary stack pressure and temperature

Operating Pressure (bar)	Operating Temp. (K)	Heat Required (W)	Cell Voltage (V)	Coupled When Cooling Temperature is (K)	RT Efficiency (%)
1.3	973.15	9452.59	0.92057	1023,15	50.79
1.3	973.15	9452.59	0.92057	1073,15	48.15
1.3	1023.15	16695.60	0.901838	1073,15	47.55
2	973.15	8761.31	0.929601	1023,15	51.00
2	973.15	8761.31	0.929601	1073,15	47.94
2	1023.15	15968.96	0.911332	1073,15	46.66
5	973.15	7285.07	0.94881	1023,15	51.61
5	973.15	7285.08	0.94881	1073,15	48.16
5	1023.15	14417.04	0.931528	1073,15	45.36
10	973.15	6165.60	0.963341	1023,15	51.38
10	973.15	6165.60	0.963341	1073,15	48.74
10	1023.15	13240.11	0.946806	1073,15	44.69

After deciding for pressure and temperature of the stack, steam fuel utilization and steam molar flow rate has to be decided. It is plausible that operating at the lower limit of current density (~3000 A/m^2) will lower operating cell voltage and thus enhance roundtrip efficiency. But what about the heating load required? The model for heating load is given in the following equations (Eq. (6-2)-Eq. (6-5)):

$$j = -2FU_{F,st}\dot{n}_{H_2O}/A_{tot} \quad \text{Eq. (6-2)}$$

$$P_{el} = -V_{cell}jA_{tot} \quad \text{Eq. (6-3)}$$

$$P_{total} = U_{F,st}\dot{n}_{H_2O}\Delta H_{el} \quad \text{Eq. (6-4)}$$

$$P_{Heat} = P_{total} - P_{el} = U_{F,st}\dot{n}_{H_2O}\Delta H_{el} + V_{cell}jA_{tot} = U_{F,st}\dot{n}_{H_2O}(\Delta H_{el} - 2FV_{cell})$$
$$\leftrightarrow P_{Heat} = 2FU_{F,st}\dot{n}_{H_2O}(V_{tn} - V_{cell}) \quad \text{Eq. (6-5)}$$

From Eq. (6-5) it can be seen that by increasing the product $U_{F,st}\dot{n}_{H_2O}$, heat requirement will also increase. However, it should also be noted that V_{cell} affects the heat requirement, which is also a function of the steam molar flow rate and stack pressure. Enhanced steam content lowers reversible voltage and thus operating cell voltage. On the other hand, the difference between cell voltage and thermoneutral voltage is increased by giving excess heating requirements. Therefore, fine tuning has to be made in order to keep current density at ~3000 A/m^2, while maximizing roundtrip efficiency and simultaneously having enough heat to provide to the system (in this case 8.1 kW). The results shown in Table 6-4 are in agreement with the abovementioned theoretical observations.

Table 6-4: Roundtrip efficiency when electrolysis operates at 5 bar/973.15 K, Vary Fuel Utilization and steam molar flow rate (j=3000 A/m^2)

Fuel Utilization (-)	$\dot{n}_{H_2O}$(mol/s)	Heating Load (kW)	RT Efficiency (%)
0.5	0.4	7.27	54.99
0.35	0.58	7.92	55.46
0.95	0.21	6.23	54.01

Also, from Table 6-3 it seems that a pressure of 5 bar leads to maximization of roundtrip efficiency and optimization should continue with 5 bar. But does this stack pressure lead to optimized roundtrip efficiency? In total, there are three parameters (pressure, steam utilization and, steam molar flow rate), for the fine tuning of the current density (~3000 A/m^2) and the heat requirement (~8.1 kW) of the rSOC stack during endothermic electrolytic operation. Hence, there are many solutions to the abovementioned problem. For example, it can be seen in Table 6-5, that for different rSOC stack pressure, a fine-tuning of steam utilization and steam molar flow rate is leading to the same operating stack parameters which satisfy the criteria of current density and stack heat requirement.

Table 6-5: Stack Tuning by varying stack pressure, steam utilization, and steam molar flow rate

Stack Pressure (bar)	Steam Utilization (-)	Steam Molar Flow Rate (mol/s)	Heating Duty (W)	Reversible Voltage (V)	Cell Voltage(V)	Current Density (A/m^2)
5	0.31	0.65	8079	0.9378	1,0757	2991,04
10	0.22	0.92	8094	0.9378	1,0762	3004,40

The stack parameters remain the same, but does this mean that the system roundtrip efficiency remains the same for the two cases? Indeed, operating voltage is playing a major role in determining roundtrip efficiency but the final operating pressure will be judged in terms of minimization of electricity consumption (i.e. BOP parasitic loads). Simulations showed the following results:

- At a lower stack pressure, the electricity consumption due to turbomachinery is enhanced due to enlarged electricity consumption during the hydrogen compression step before the methanol synthesis, despite the fact that feed hydrogen expanders produce more work due to increased pressure ratio
- At a lower pressure, cooling duty is enhanced due to the fact that steam condensation temperature is also reduced at lower stack pressure.
- At a lower stack pressure, hot utility is increased. Despite the fact that more water is heated in the evaporator at higher pressure, this extra heat does not participate in the hot utility at all since it can be heat integrated. The increase in hot utility occurs due to the fact that at lower stack pressure, hydrogen heaters during its multistage expansion consume more heat (i.e. a higher pressure ratio needs a bigger reheat duty)

Consequently, higher stack pressure (i.e. 10 bar) is the clear winner. In total, the optimized parameters when adding the thermal energy storage system are as follows (see Table 6.6).

A final check will be performed on methanol adequacy as it has already been performed during the start of subsection 6.3. The necessary data are provided in Table 6-7.

The criterion proposed during the beginning of this subsection (see **Eq. (6-1**)) is still not satisfied but the two hand sides are very close to each other compared to the initial case. Therefore, mode coupling with the proposed process conditions does not only maximize roundtrip efficiency but also methanol requirements are almost met. If the methanol requirements are met, then a cyclic operation of the system can be performed.

Table 6-6: Optimum electrolysis stack configuration for thermally coupled modes. Optimum Roundtrip Efficiency

Fuel Cell Mode	**Electrolysis Mode**				
Cooling Temperature (K)	Stack Pressure (bar)	Stack Temperature (K)	Steam Utilization (-)	Steam Molar Flow Rate (mol/s)	Roundtrip Efficiency (%)
1023.15	10	973.15	0.22	0.92	56.72

Table 6-7: Current Density and Stored Methanol flow rate for each mode (2nd Attempt)

Operating Mode	**Current Density (A/m²)**	**Methanol Produced/Required (g/s)**
Electrolysis	3004	2.93
Fuel Cell	3145	3.20

6.4 Proposed Process conditions for RT maximization

Table 6-8 summarizes the process conditions for electrolysis mode while Table 6-9 is showing the process conditions for fuel cell operation for the maximization of roundtrip efficiency.

Table 6-8: Optimized Electrolysis Conditions for Maximum RT efficiency

Parameter	*Value*	*Parameter*	*Value*
Number of cells (-)	1300	Pressure of feed CO_2 stream (bar)	80
Electrode area per cell (m^2)	0.01	Temperature of feed CO_2 stream (K)	298.15
Stack pressure (bar)	10	Length of PFR (m)	40
Stack temperature (K)	973.15	Number of tubes (-)	5000
Fuel utilization (-)	0.22	Tube Diameter (m)	0.02
Oxidant inlet pressure (bar)	1	Porosity of catalyst (-)	0.5
Oxidant inlet temperature (K)	298.15	Density of catalyst (kg/m^3)	2000
Flow rate of feed water (mol/s)	0.92	Methanol Synthesis pressure (bar)	50
Pressure of feed water (bar)	1	Constant reactor temperature (K)	540
Temperature of feed water (K)	298.15	Outlet pressure of throttling valve leading to distillation (bar)	1.2
Flow rate of feed H_2 (mol/s)	0.125	Molar Reflux ratio	1.5
Pressure of feed H_2 (bar)	100	Light Recovery (Purity %)	0.9
Temperature of feed H_2 (K)	298.15	Heavy Recovery (Purity %)	0.001
Parameter	***Value***	***Parameter***	***Value***
Isentropic eff. of pumps and compressors(-)	0.95	Mole fraction of N_2 in feed sweep gas stream (-)	0.79
Isentropic eff. of turbines (-)	0.75	Mole fraction of O_2 in feed sweep gas stream (-)	0.21
Mechanical Losses of components	0.95	Mole fraction of water to syngas compression	0.01
Mole fraction of feed water (-)	1	Mole fraction of water to recycle compressor	0.002
Mole fraction of feed CO_2 (-)	1	Fraction of flow going to purge	0,01
Mole fraction of feed H_2 (-)	1	Partial Condenser of distillation column	0.05
Afterburner cooled exhaust gases temperature (^oC)	770.4		

Table 6-9: Optimized Fuel Cell Conditions for Maximum RT efficiency

Parameter	*Value*	*Parameter*	*Value*
Number of cells (-)	1300	Temperature of feed CH_3OH (K)	298.15
Electrode area per cell (m^2)	0.01	Flow rate of feed H_2O (mol/s)	0.10
Stack pressure (bar)	1.2	Pressure of feed H_2O (bar)	1
Stack temperature (K)	1123.15	Temperature of feed water (K)	298.15
Fuel utilization (-)	0.95	Reforming Temperature (K)	453.15
Inlet oxidant pressure (bar)	1	Pressure of H_2 storage (bar)	100
Inlet oxidant temperature (K)	298.15	Pressure of CO_2 storage (bar)	80
Flow rate of feed methanol (mol/s)	0.10	Temperature of Water Gas Shift Reaction (K)	673.15
Pressure of feed methanol (bar)	1		
Parameter	***Value***	***Parameter***	***Value***
Isentropic eff. of pumps and compressors(-)	0.95	Mole fraction of O_2 in feed sweep gas stream (-)	0.21
Isentropic eff. of turbines (-)	0.95	Mole fraction of water to double stage compression (-)	0.005
Mechanical Losses of components	0.95	Mole fraction of CO2 to final hydrogen stream (-)	0.01
Mole fraction of feed water (-)	1	CF_4 Evaporator Temperature (Ref. Cycle) (^oC)	-109
Mole fraction of feed CH_3 OH(-)	1	CO_2 condenser Tempereature (Ref. Cycle) (^oC)	30
Mole fraction of N_2 in feed oxidant stream (-)	0.79		

Finally, temperature difference between either sweep gas (in electrolysis) or oxidant (in fuel cell) stack inlet and stack temperature is 200 K.

6.5 Summary

In this chapter, the maximization of roundtrip efficiency was presented. Initially, optimization took place by maximizing the numerator of Eq. (4-10) while utilizing the existing fuel cell mode and also by minimizing the denominator of Eq. (4-10) while employing the existing electrolysis mode. After the optimization procedure, a roundtrip efficiency of 46.7% was obtained. Further countermeasures were discussed in order to enhance the roundtrip efficiency.

It was observed that during electrolytic operation, the rSOC stack consumed a significant amount of power while parasitic electrical consumption by the system BOP was minimized. However, according to the definition provided in Eq. (4-10), roundtrip efficiency can be further enhanced if both stack power consumption and parasitic electrical consumption by the system BOP were reduced during steam electrolysis. In order to achieve that, it was recognized that an endothermic mode of electrolytic operation was necessitated. Simultaneously, the sweep gas flows had to be eliminated in order to minimize the parasitic loads from the BOP. Therefore the required heat during endothermic operation had to be provided by other means, instead of enhanced sweep gas flows. The solution to the problem was the adoption of a latent heat storage system where it is charged during the exothermic operation of the rSOC stack in fuel cell mode. The stored heat can then be deployed in order to cover the heat requirements of the rSOC during electrolytic operation while keeping the sweep gas flow at a minimum. Finally, after this process change, the roundtrip efficiency was further enhanced from 46.7% to 56.72%.

CHAPTER 7

CONCLUSIONS & RECOMMENDATIONS

7.1 Conclusions

To sum it up, an electrical energy storage system employing a rSOC accompanied by intermediate methanol synthesis was presented in Chapter 4. A thorough system exergy and energy analysis has been conducted and the results are reported in Chapter 5 while, roundtrip efficiency optimization has been performed in Chapter 6 along with the respective results. The research questions presented in the introductory chapter will be addressed below:

- In the models presented in Chapter 5, where all excess heat removed/added was accomplished through sweep gas/oxidant flow rate regulation, energy and exergy efficiency is maximized when sweep gas/oxidant flow rate was kept at a minimum. In electrolysis mode, the optimum point of operation was the thermoneutral one which almost eliminates sweep gas flow rate. During fuel cell operation, there is no thermoneutral point of operation and therefore lower current density resulted in lower heat removal requirements which enabled lower oxidant flow. While oxidant flow rate (or high current density) is detrimental for the performance in fuel cell mode, the rSOC stack should also produce enough power to electrically sustain the energy needs of the system
- Maximization of stored methanol flow rate, during electrolysis mode, is achieved at 150 bar/500^{o}C by using the proposed reactor configuration. Exergy and energy efficiencies maximization is achieved at 150 bar/520^{o}C which does not correspond to the maximization of stored methanol flow. The reason why this mismatch exists is that at 150 bar/520^{o}C the hot and cold utilities are lower compared to the same at 150 bar/500^{o}C.
- Exergy and energy efficiencies, in fuel cell mode, depend highly on fuel utilization and steam & methanol flow rate. It has been shown that at low steam & methanol flow rates accompanied with very high fuel utilization maximize energy and exergy efficiency. Reduced feed flow rates enable low hot and cold utilities and minimized hydrogen flow rates to storage. On the other hand, high fuel utilization enables high stack power and lower electricity consumption by the storage compressors of the system. Low fuel utilization minimizes power generation and the system requires external electricity in order to sustain the process (denoted by negative energy efficiency). Finally, by keeping fuel utilization constant and increasing the feed flow rates, the respective increase in current density will give rise to the oxidant flow. This increase in oxidant flow results in decreased energy and exergy efficiencies
- Exergy and energy efficiencies, in fuel cell mode, also depend on reforming pressure and temperature. It was shown that at lower pressure and lower temperature, minimization of the hot and cold utilities resulted in an enhancement of both efficiencies. During the simulations, stack pressure and reforming pressure are equal and that is mainly the reason why the maximization of both efficiencies occurs at low pressure (i.e. 1.2 bar)
- Exergy and energy efficiencies, in fuel cell mode, also highly depend on WGS reactor temperature. Lower temperature results in higher hydrogen yield, while higher temperature yields more CO. CO has a higher chemical exergy value compared to H_2 and therefore it is beneficial to operate at a higher temperature (i.e. 400^{o}C) when operating the WGS reactor. Therefore, it is more beneficial to store impure H_2 with small quantities of CO rather than pure H_2

- The highest energy and exergy values achieved were 68.74% and 77.67% respectively, for electrolysis mode. The optimized process conditions are given in Table 5-5
- The highest energy and exergy values achieved were 60.22% and 56.78% respectively, for fuel cell mode. The optimized process conditions are given in Table 5-8. The maximum values are mainly restrained by the operation of an intense refrigeration system for the CO_2 condensation
- The effect of a manually imported HEX network of seven heat exchangers in each mode has the following distinct effect in exergy and energy efficiencies (see Table 7-1). As expected, the efficiencies are reduced when manually importing a HEX network compared to the efficiencies obtained when utilizing the pinch technology. All relevant process conditions have been reported in Chapter 5
- From the exergy flow diagram, in base case electrolysis, the main exergy losses originate from the pre-stack sweep gas heater, the cooling system, the sweep gas reheater, the heat exchanger between sweep gas and feed water stream , as well as the rSOC stack. Sweep gas turbomachinery induce high exergy losses in total as well in the base case, showing decreased efficiencies of the sweep gas train at heightened sweep gas flow rates. From base case to optimum case, most of the abovementioned exergy losses have mostly been eliminated completely with the exception of the electrolysis stack where exergy losses have been heightened. A more detailed view can be seen in Table 5-11
- From the exergy flow diagram, in base case fuel cell mode, the main exergy losses arise from the cooling and refrigeration system, the oxidant reheater, the pre-stack oxidant heater, oxidant reheater as well as the methanol steam reformer and oxidant turbomachinery (both compressors and expanders). From base case to optimum case, most of the abovementioned exergy losses have been drastically reduced. The rSOC stack does not contribute significantly to the total exergy losses in either case. A more detailed view can be seen in Table 5-12

Table 7-1: Energy and Exergy Efficiency for all cases

		Electrolysis Mode	Fuel Cell Mode
Perfect Heat Integration			
Base Case	Energy Efficiency(%)	52.40	-91.35
	Exergy Efficiency(%)	59.48	-83.73
Optimized Case	Energy Efficiency(%)	68.74	60.22
	Exergy Efficiency(%)	77.67	56.78
7 HEX Network			
Base Case	Energy Efficiency(%)	36.87	-105.95
	Exergy Efficiency(%)	42.01	-97.08
Optimized Case	Energy Efficiency(%)	61.49	50.88
	Exergy Efficiency(%)	69.37	47.94

Next, it became clear that roundtrip efficiency is also a very important metric for the evaluation of an energy storage system. While energy and exergy efficiencies during electrolysis mode are focused on the production of the intermediate product, the roundtrip efficiency is decoupled from any intermediates while it purely expresses the ratio of energy generation to energy consumption in both modes. Energy and exergy efficiency characterizes each mode separately but it does not ensure the coupling of both modes. In contrast, roundtrip efficiency incorporates the time of operation in each mode through the equal charge transfer rule. By incorporating the time of operation in each mode, a criterion regarding methanol adequacy can also be formulated. It has to be ensured that the total methanol production in electrolysis mode is higher than the methanol consumption in fuel cell mode.

The integration of a thermal energy storage system is important for the maximization of roundtrip efficiency since it will enable endothermic mode of operation combined with minimal sweep gas flow rate. Endothermic mode of operation enables reduced cell voltage which is closer to the reversible and therefore enabling RT maximization. The heat storage system is charged by heat removal from the exothermic fuel cell mode. The stored heat is then deployed when there is a switch to endothermic electrolysis operation.

After careful optimization and tuning, a maximum roundtrip efficiency of 56.72% has been achieved. In addition, the methanol adequacy criterion is almost fulfilled (see Table 6-7). Scientific literature proposed values of roundtrip efficiency from 48.2% to 54.3% [11], and therefore a clear improvement of system performance is shown.

7.2 Recommendations for further research

Process design options which may potentially drive the existing system into higher exergy and roundtrip efficiencies will be proposed.

- First of all, during fuel cell operation, it has been clearly seen that the refrigeration system consumes a lot of electricity and hence, it increases parasitic BOP electricity loads, which reduce roundtrip efficiency. The first idea for CO_2 removal from a H_2/CO_2 stream would be *via* absorption, instead of condensation. During absorption, the main energy requirement is the regeneration of the solvent. The temperature of regeneration is approximately 100-140^{o}C, which means that the energy requirement can be partly satisfied through heat integration. A physical solvent will be utilized in this case since the molar composition of the specific stream in H_2 and CO_2 is approximately ~50/50 [20]. This results in lower heat of regeneration since CO_2 is absorbed through physical bonding while no chemical reaction takes place. More specifically, the heat of regeneration is 0.9-1.6 MJ/kgCO_2 for a physical solvent, instead of 2.0 MJ/kgCO_2 when using the typical monoethanolamine (MEA, 30 wt%) aqueous solution [81]. This process is slightly exothermic (compared to chemical absorption) and excessive cooling duties in the absorber column will be avoided. The Absorber column will typically operate at a temperature between 40-60^{o}C. This means that the column can be cooled down *via* cooling water instead of an intense refrigeration cycle. Commercial physical solvents include Selexol® and Rectisol®. Assuming that all CO_2 is absorbed and the CO_2 flow rate is 4.13 g/s according to the proposed fuel cell operation, then a reboiler of 5 kW might be enough to regenerate CO_2 from the physical solvent instead of a refrigeration system of 7.5 kW and hence further increasing roundtrip efficiency. In order to select the appropriate solvent, one has to take into account many different criteria such as 1) Equilibrium CO_2 retention, 2) Rate of reaction, 3) Heat of regeneration, 4) Thermochemical Stability, 5) Cost, 6) Volatility.
- In addition, it has been detected that the higher the difference between cell voltage and thermoneutral voltage, the more the heat requirement for electrolysis. For example, during fuel cell mode, the outlet stack temperature for the oxidant stream was picked to be 1023.15 K instead of 1073.15 K because in the latter case, an insufficient amount of heat can be stored in the latent heat storage system. However, if this heat was enough to feed the electrolysis stack, then roundtrip efficiency would be further increased because of possible operation of electrolysis at 1023.15 K which would result in lower overpotential losses and reduced cell voltage. In co-electrolysis, the thermoneutral voltage can be appropriately reduced if an additional heat source exists. The regulation of thermoneutral voltage can give an extra tool for the regulation of stack heating requirements. Therefore one could easier combine easier the low current density, low overpotential losses and also low heat requirement in the stack. In the existing case, operation at 1023.15 K was leading to excessive heating requirements because thermoneutral voltage remains almost constant during steam electrolysis. In addition, oxidant

expanders during fuel cell operation would produce a slightly higher amount of electricity, improving overall roundtrip efficiency. Therefore, it is believed that co-electrolysis could potentially induce bigger benefits in roundtrip efficiency. Finally, a huge benefit that might be unveiled is the fact that during co-electrolysis no separation of CO/CO_2 from H_2 is needed. The gas product can be directly stored and a refrigeration or CO_2 capture system might be omitted. Despite all the possible advantages, co-electrolysis at such high temperature, would not be beneficial for the exothermic methane production and therefore the electrolysis temperature will be reduced and higher overpotential losses will be induced due to decreased electrical resistance. In total, the advantages of the proposed system are expected to overshadow the potential disadvantages.

- Another minor improvement of the system can be the removal of the distillation column and storage of a pressurized methanol/water mixture. In the perfect heat integration system, hot and cold utility remain almost the same because reboiler and condenser duty were completely covered by the system. In a real system, where a perfect heat integration system does not exist, this change will induce benefits by reducing the total amount of necessary equipment and hence, less CAPEX will be required, but also hot and cold utility will be reduced. In addition, the pressurized storage will be able to lessen the feed (i.e. water and methanol) pump load in fuel cell operation. Those changes may potentially increase roundtrip efficiency especially by alleviating pump load during fuel cell operation. Also, the minor exergy losses associated with the throttling valve prior to distillation column as well as the steam/methanol mixer will be discarded.

Apart from RT optimization, other important aspects of the project can also be studied, so that the system can be realized.

- Long-term operation of rSOC. Research on materials for rSOC stacks must further be performed in order to ensure the uninterrupted operation of a reversible fuel cell stack without excessive corrosion and degradation. For example, the oxidant inlet at a temperature 200^{o}C below the stack temperature might increase exergy, energy and roundtrip efficiency, but on the other hand, it might induce excessive temperature gradients inside the stack, sacrificing its mechanical integrity for the sake of efficiency. Research on materials is also crucial since new materials will further reduce overpotential losses and hence enable enhanced system roundtrip efficiency
- Long-term operation of latent heat energy storage. Despite the fact that latent heat storage is accompanied with high volumetric energy density compared to sensible heat storage, there is limited data on the cyclic performance of such materials [82]–[84]. Thermal cycling diminishes system performance after a certain amount of cycles. Another difficulty is the heat storage at such high temperature, as well as the availability of heat when needed. Latent heat storage is accompanied with low thermal conductivity and generally, it is a slow process and may induce difficulties when switching between the modes where fast responses are required
- Establishing a more reliable steam electrolysis and fuel cell operation in Aspen Plus. For example, CO electrochemical conversion has been completely ignored as stated in Chapter 3. An in-house model of the I-V curve should be made after conducting a set of experiments and fitting all the necessary parameters as seen in Appendix A
- Identification of the heat exchanger network which minimizes hot and cold utility accompanied by process economics. The author reckons that a major cost of the whole system is the heat exchanger network. Therefore a study including the correlation between roundtrip efficiency, the extent of the heat exchanger network and its capital cost could be useful for system development. For example, achieving minimal heat and cold utility might be not cost-effective, while on the other hand a lesser amount of heat exchangers can make the system economically feasible without sacrificing too much of efficiency. In addition, the lowest storage pressure induces the highest roundtrip efficiency, but a correlation between

roundtrip efficiency, storage pressure and cost of storage tanks must be made. It is plausible that the lower the storage pressure, the lower the thickness of the storage tanks, however, the larger their respective volume in order to store the same amount of substance under lower pressure. Higher pressure necessitates lower volume storage tanks but thicker walls. Finally, the dimensions of the storage tank will determine the specific area of the tank. The highest the specific area, the more the heat losses of the system. With proper insulation and storing materials in their heated state, a minor increase in exergy efficiency will occur, but of course, the additional cost of the insulating materials has to be taken into account for a complete analysis

- After optimizing the whole system, dimensioning of each component such as heat exchangers must be done. Some heat exchangers include heat exchange between air or flue gas streams. The low conductivity of the air side might require a larger surface area for successful heat exchange, which will result in heightened cost
- Process economics for the whole system and comparison with other energy storage systems such as CAES or PHS storage which are mostly specialized for long-term energy storage
- Lastly, a pilot plant must be manufactured in order to validate model performance but also understand the system dynamics in practice. Apart from rSOC operation for hydrogen production, a pilot plant for rSOC operation coupled with fuel synthesis has not been built so far

Appendix A: Thermochemistry properties of H_2O, H_2, O_2

Enthalpy and entropy for each component with respect to temperature can be calculated by the following expressions:

$$H^0 - H^0_{298.15} = At + B\frac{t^2}{2} + C\frac{t^3}{3} + D\frac{t^4}{4} - \frac{E}{t} + F - H$$

$$S^0 = Aln(t) + Bt + C\frac{t^2}{2} + D\frac{t^3}{3} - \frac{E}{2t^2} + G$$

where $t = T/1000$, T is temperature in K, H^0 is the standard enthalpy in kJ/mol and S^0 is the standard entropy in J/molK. Below, the constants from A-H will be given tabulated for each component as well as formation enthalpy at reference temperature ($H^0_{298.15}$).

Table A- 1: Constants from A to H and reference enthalpy for estimation of enthalpy and entropy for H_2O, H_2, and O_2

Component	H_2O	H_2	O_2
Temperature Range (K)	500-1700	298-1000	700 - 2000
A	30.09200	33.066178	30.03235
B	6.832514	11.363417	8.772972
C	6.793635	11.432816	-3.988133
D	-2.534480	-2.772874	0.788313
E	0.082139	-0.158558	-0.741599
F	-250.8810	-9.980797	-11.32468
G	223.3967	172.707974	236.1663
H	-241.8264	0	0
$H^0_{298.15}$	-241.826	0	0

According to the reaction:

$$H_2O \xrightarrow[+heat]{+electricity} 0.5O_2 + H_2 \qquad \Delta h = 248\ KJmol^{-1}[9]$$

$$\Delta H_R(T) = \sum H_{Prod} - \sum H_{React} = H^0_{H_2} + 0.5H^0_{O_2} - H^0_{H_2O}$$

$$\Delta G_R(T) = \sum G_{Prod} - \sum G_{React} = G^0_{H_2} + 0.5G^0_{O_2} - G^0_{H_2O}$$

where:

$$G^0_i = H^0_i + TS^0_i$$

In Figure A- 1 the results are being shown for a temperature range between 400-1200 K.

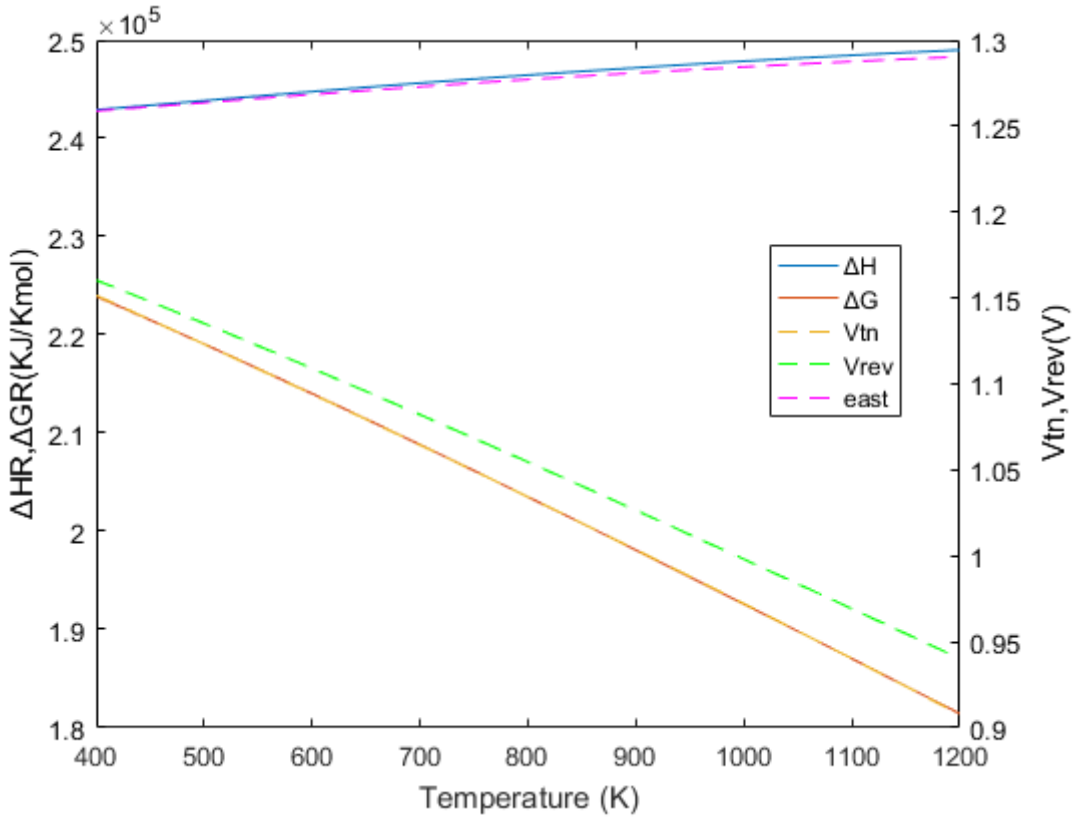

Figure A- 1: ΔH, ΔG, Reversible and thermoneutral voltage according to thermodynamics

The corresponding 2nd order polynomial curves obtained from curve fitting are:

$$\Delta H_R(T) = -0.00311454T^2 + 12.66447909T + 2.38298927 * 10^5$$

$$\Delta G_R(T) = -0.00513012T^2 - 45.1316855T + 2.42889441 * 10^5$$

Appendix B: Activation, ohmic and concentration losses modeling

Hauck et al. [13] provide a detailed model for the modeling of each type of losses:

Activation Losses

$$V_{act,i} = \frac{RT}{Fza}\text{asinh}(\frac{j}{2j_{0,i}})$$

where F is the Faraday constant (96485C/mol), R is the universal gas constant (8.314 J/molK), z is the number of electrons transferred during the reaction. For the fuel electrode and steam electrolysis $z = 2$, while for the oxidant/oxygen electrode $z = 4$, j is the current density and $j_{0,i}$ is the exchange current density and α is the reduction or oxidation transfer coefficient [85].

The current density is estimated as:

$$j = z\dot{n}_{H_2O}FU_f$$

where $\dot{n}_{H_2O}$ is equal to the molar flow of water and U_f corresponds to the fuel utilization which is defined by the user in the stoichiometric reactor.

The exchange current density obeys an Arrhenius type of law according to the equation:

$$j_{0,i} = \gamma_i e^{(-\frac{E_{act,i}}{RT})}$$

where $\gamma_i$is the preexponential factor and $E_{act,i}$ is the activation energy

According to Noren et al. [85], this factor α is equal to 1-β where β is called the symmetry factor and for modeling most of the times a value of 0.5 is used. In general, a range of 0.3-0.6 has been used for experimental data fitting. In this model, a value of 0.5 has been assumed.

Ohmic Losses

Ohmic losses are given from the following equation:

$$n_{ohmic} = j\left(\frac{\delta_{el}}{\sigma_{el}} + r_{ohmic,const}\right) = j\left(r_{ohmic,el} + r_{ohmic,const}\right)$$

where δ_{el} is the electrolyte thickness, σ_{el} is the electrolyte conductivity, $r_{ohmic,el}$ is the specific ohmic resistance of the electrolyte and $r_{ohmic,const}$ is the specific resistance from interconnects and wires of the stack. In this model, the ohmic losses induced by the interconnects and wiring will be considered constant even though they are dependent on temperature. This is due to the fact that the final result minorly affected by this quantity (i.e. interconnect and wiring losses are much less compared to electrolyte losses) [13].

Electrolyte conductivity also obeys an Arrhenius type law and is calculated as follows:

$$\sigma_{el} = \sigma_{0,el}e^{(-\frac{E_{act,el}}{RT})}$$

where $\sigma_{0,el}$ is the preexponential factor and $E_{act,el}$ is the activation energy for the conductivity of the electrolyte

Concentration Losses

Concentration losses have to be included from both electrodes. Those losses are calculated respectively as:

$$V_{conc,fuel} = \frac{RT}{2F}\ln\left(\frac{p_{H_2O,tpb}p_{H_2,bulk}}{p_{H_2O,bulk}p_{H_2,TPB}}\right)$$

$$V_{conc,oxygen} = \frac{RT}{2F}\ln\left(\sqrt{\frac{p_{O_2,bulk}}{p_{O_2,TPB}}}\right)$$

where all the terms are referring to partial pressure of the mentioned species at the bulk and at the triple phase boundary as described by the respective subscripts.

According to [23] the triple phase boundaries partial pressures for each component can be found as follows:

$$P_{H_2,TPB} = P_{H_2,bulk} - \frac{RT\delta_{fel}j}{2FD_{eff,H_2}}$$

$$P_{H_2O,TPB} = P_{H_2O,bulk} + \frac{RT\delta_{fel}j}{2FD_{eff,H_2O}}$$

$$P_{O_2,TPB} = P - (P - p_{O_2,air})e^{\frac{RT\delta_{oxel}j}{4FPD_{eff,O_2}}}$$

where δ_{fel} and δ_{oxel} are the thickness of the fuel and oxidant/oxygen electrode respectively and $D_{eff,i}$ is the effective diffusion coefficient of species i.

The effective diffusion coefficient is calculated with the following equation as given by Hauck [13].

$$D_{eff,i} = \frac{\varepsilon}{\tau}\frac{D_{kn,i}D_{i-j}}{D_{i-j} + D_{kn,i}}$$

where ε and τ are the electrode porosity and tortuosity respectively, $D_{kn,i}$ describes the Knusden diffusion coefficient for species i, while D_{i-j} represents the binary diffusion coefficient between 2 species (i.e. H_2O/H_2 and N_2/O_2).

The Knudsen regime diffusion coefficient is calculated as:

$$D_{kn,i} = \frac{d_p}{3}\sqrt{\frac{8RT}{\pi M_i}}$$

where M_i is the molecular weight of the concerning species

The binary diffusion coefficient is given as follows according to VDI Heat Atlas [86]:

$$\frac{D_{i-j}}{cm^2/s} = \frac{0.00143\left(\frac{T}{K}\right)^{1.75}\left[\frac{M_i}{\frac{g}{mol}}^{-1} + \frac{M_j}{\frac{g}{mol}}^{-1}\right]}{\frac{p}{[bar]}\sqrt{2}\left(V_{d,i}^{\frac{1}{3}} + V_{d,j}^{\frac{1}{3}}\right)}$$

where $V_{d,i}$ is the dimensionless diffusion volume of species i

Table B- 1 illustrates the diffusion volumes of the involved species:

Table B- 1: Diffusion Volume for selected molecules

Molecule	*Diffusion Volume(-)*
H_2	6.12
N_2	18.5
O_2	16.3
H_2O	13.1

Table B- 2 summarizes all the model parameters used for validation.

Table B- 2: Model Parameters provided by Hauck et al. [13]

Parameter	*Value*	*Unit*
$r_{Ohmic,Const}$	0.057	Ωcm^2
$\sigma_{0,el}$	333.3	$\Omega^{-1}cm^{-1}$
$E_{act,el}$	85.634	J/mol
δ_{el}	$1.25 \cdot 10^{-5}$	m
δ_{fel}	$3.2 \cdot 10^{-5}$	m
δ_{oxel}	$1.75 \cdot 10^{-5}$	m
A_{tot}	16	cm^2
r_P	$1 \cdot 10^{-6}$	m
ε	0.3	-
τ	5	-
γ_{fuel}	$1.344 \cdot 10^6$	Acm^{-2}
γ_{oxygen}	$2.051 \cdot 10^5$	Acm^{-2}
$E_{act,fuel}$	$1 \cdot 10^5$	J/mol
$E_{act,oxygen}$	$1.2 \cdot 10^5$	J/mol

All the aforementioned parameters were also used in this study apart from the total active electrode area.

Appendix C: I-V and Power Curves for steam electrolysis (Electrolysis Mode)

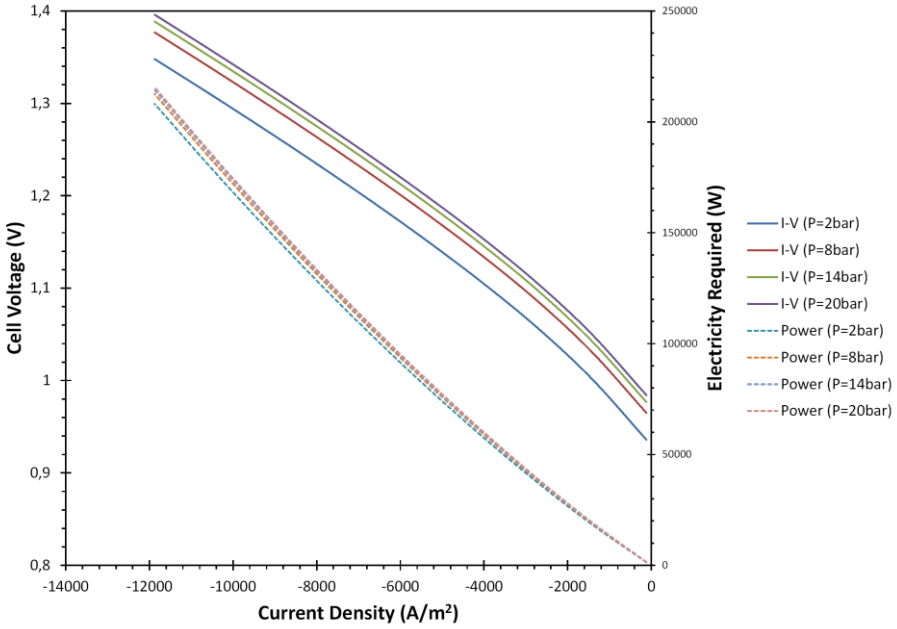

Figure C- 1: I-V and Power Curves for varying stack pressure

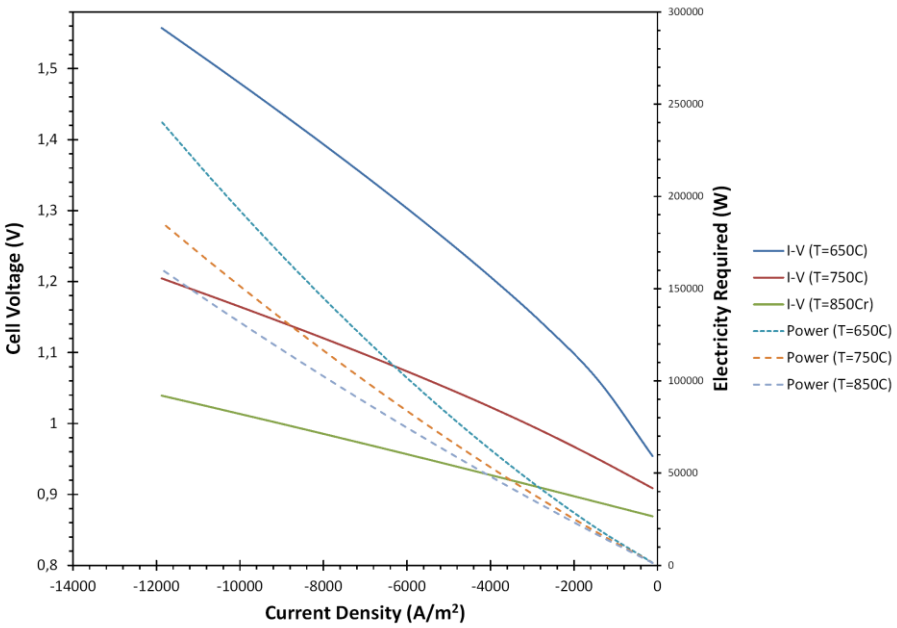

Figure C- 2: I-V and Power Curves for varying stack temperature

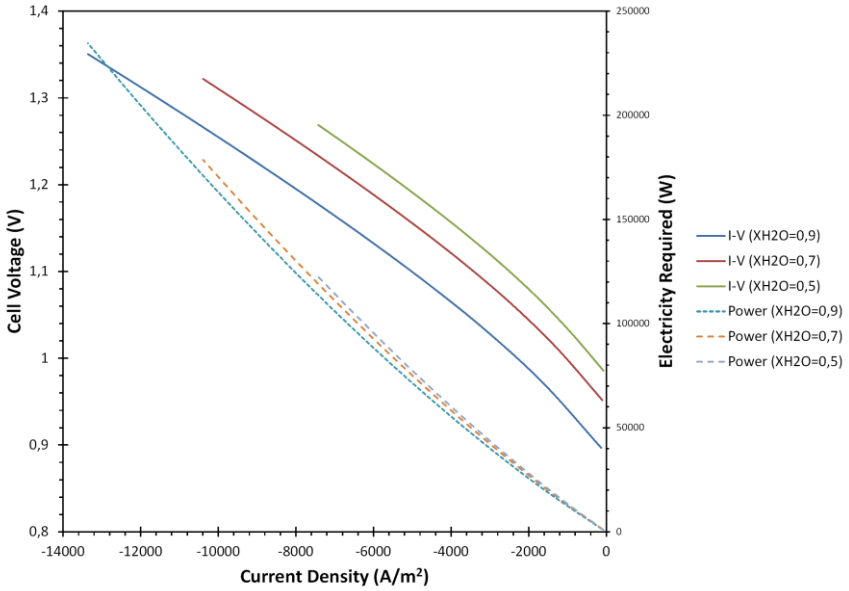

Figure C- 3: I-V and Power Curves for varying steam mole fraction

Appendix D: Validation of Methanol Synthesis Model from Scientific Literature

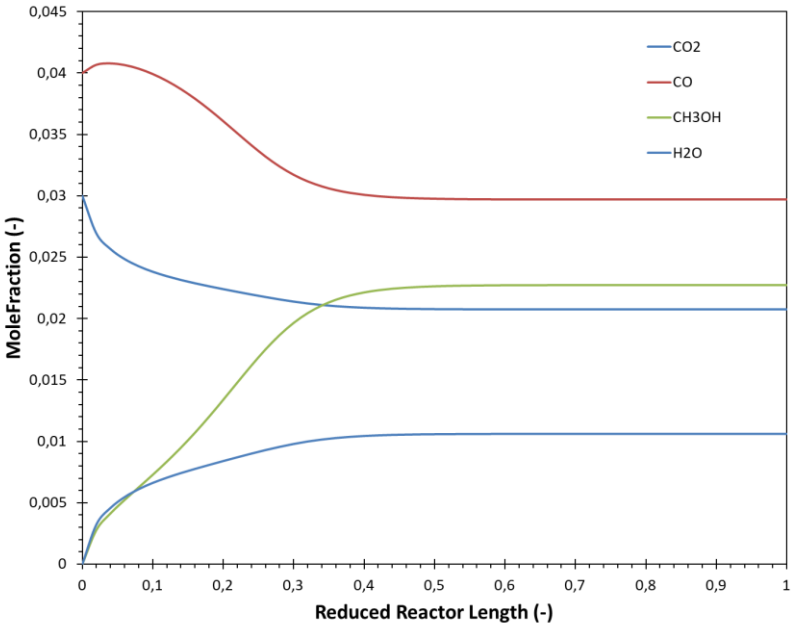

Figure D- 1: Methanol Synthesis Results from Aspen Plus Model by using proposed process conditions

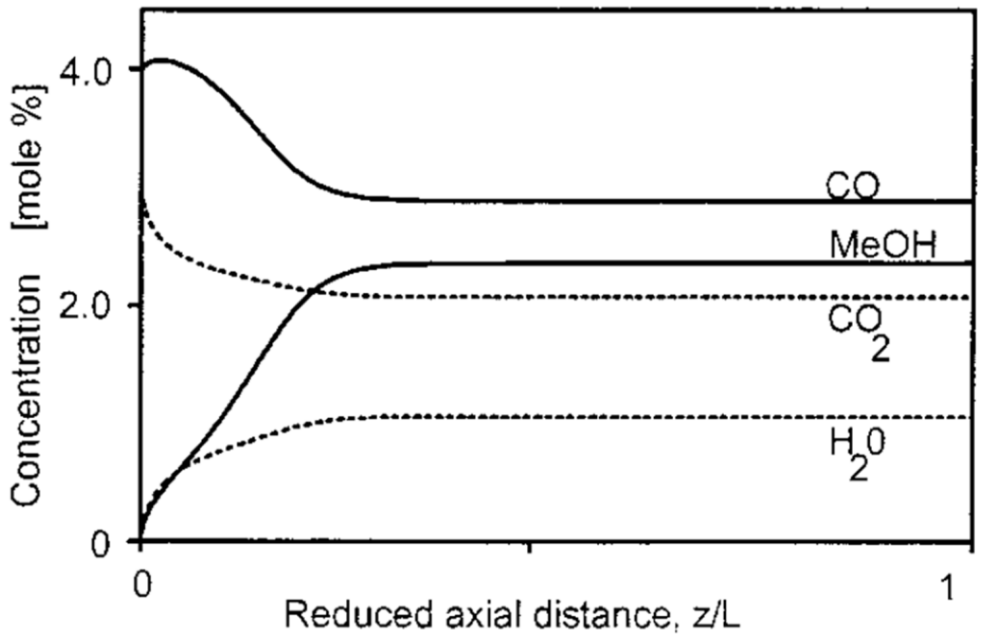

Figure D- 2: Methanol Synthesis Results from Van de Bussche and Froment [67] by using proposed process conditions

Appendix E: Exergy flow Diagrams for Electrolysis Mode

Appendix F: Exergy flow Diagrams for Fuel Cell Mode

Appendix G: About Multistage Compression & Expansion

According to Black & Hartley [87], the Carnot cycle is a reversible cycle but it is not the only one. Stirling and Ericsson cycle are reversible cycles as well and their efficiency is equal to that of Carnot cycle. Ericsson cycle consists of 1 isothermal compression, 1 isobaric heating, 1 isothermal compression, and 1 isobaric cooling. On the other hand, the ideal Brayton cycle consists of adiabatic processes instead of isothermal ones. If someone could transform those adiabatic processes into isothermal ones, then maximum efficiencies could be obtained. Therefore compression in its ideal case (i.e. minimization of work spent) should be isothermal. On the other hand, an ideal expansion (i.e. maximization of work output) is done when the expansion is isothermal. Irreversibilities of both processes do not allow for isothermal expansion and compression.

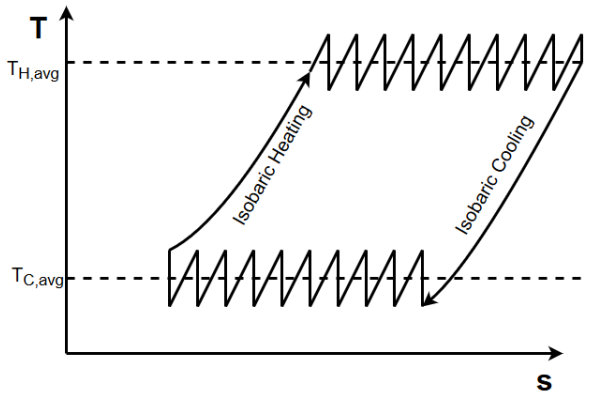

Figure G- 1: Real life approach to Ericsson cycle – A series of infinite expansion/reheating and compression/intercooling sections

According to Figure G- 1 one way to simulate an isothermal process is by employing multistage compressors with intermediate coolers and multistage expanders with intermediate reheaters. In order to theoretically simulate an exact isothermal process, numerous stages should be incorporated and capital expenditure would be excessive. In addition, according to thermodynamics lecture slides of Mohsin Mohd Sies [88], in an ideal Brayton cycle work maximization for turbine or work minimization for compressors is achieved when pressure ratios are the same.

$$PR = \sqrt[n]{p_{init} p_{final}}$$

In addition, the end temperature for all reheaters and for all intercoolers is the same, and those elements have been incorporated in the model. In reality, the process is not ideal and entropy is increasing either with compression or expansion, but the teachings from ideal thermodynamic cycle theory will be used as a decent approximation the optimum situation.

Process engineering heuristics have defined the number of stages with the respect of the final pressure ratio of the system. According to Seader [89], the following rules (see Table G- 1) can be used to determine the number of stages in each compression or expansion process. This rule has also been embodied in the model design.

Table G- 1: Rule of thumb for picking the number of compression/expansion stages based on overall pressure ratio [89]

Pressure Ratio	Number of Stages
<4	1
4-16	2
16-64	3
64-256	4

Appendix H: Different "types" of exergy

H-1 Chemical Exergy

Chemical exergy – Reference Substances

In this case, the chemical exergy refers to the obtainable work when expanding a reference substance from the environmental state (p_0, T_0) to the corresponding dead state (p_{p0}, T_0). The environmental, as well as the dead state, have the same temperature, therefore, the work of the isothermal expansion can be evaluated through the equation:

$$\varepsilon_i = RT_0 \ln\left(\frac{p_0}{p_{p0}}\right) \qquad \text{Eq. (H- 1)}$$

This quantity is equivalent to the molar chemical exergy of a reference substance. Through a semipermeable membrane, the expanded component can be transferred to the environment without the addition of additional work. The units are in [J/mol].

Chemical exergy – Gaseous & Liquid fuel

The gaseous fuel is not an environmental substance. The process of determining the exergy of a gaseous fuel has to include a reversible reaction where the substance reacts with oxygen brought from the environment (i.e. compression) while the products are expanded to the dead state. During the reaction, there is also a change in Gibbs free energy of the chemical compound during the conversion and this has to be taken into account as well. In the current project, 3 gaseous fuels are included: H_2, CH_3OH, and CO. Their corresponding chemical exergy can be calculated as:

$$\varepsilon_{H_2} = -(\Delta G)_{H_2} + \varepsilon_{H_2O} - \frac{1}{2}\varepsilon_{O_2}$$

$$\varepsilon_{CO} = -(\Delta G)_{CO} + \varepsilon_{CO_2} - \frac{1}{2}\varepsilon_{O_2}$$

$$\varepsilon_{CH_3OH} = -2(\Delta G)_{CH_3OH} + 2\varepsilon_{CO_2} + 4\varepsilon_{H_2O} - 3\varepsilon_{O_2}$$

where the corresponding reversible reactions are:

$$H_2 + \frac{1}{2}O_2 \rightarrow H_2O$$

$$CO + \frac{1}{2}O_2 \rightarrow CO_2$$

$$2CH_3OH + 3O_2 \rightarrow 2CO_2 + 4H_2O$$

The units are in [J/mol]. The molar chemical exergy of substances such as H_2O, O_2, and CO_2 can be calculated according to Eq. (H- 1) to since they constitute reference substances. To sum up, a reversible reaction is added. This reaction demands the compression of oxygen, expansion of products and the corresponding

change of Gibbs free energy during the conversion. After the expansion, the products will be transferred to the environment through a semipermeable membrane without the addition or extraction of mechanical work.

Empirical relations have also been derived for the determination of exergy of liquid fuels, according to the mass composition ratios H/C, O/C, N/C, and S/C. In general, the chemical exergy is determined by the following equation

$$\varepsilon_{fuel} = (LHV)_{fuel}\varphi \qquad \text{Eq. (H- 2)}$$

where φ is estimated as:

$$\varphi = 1.0401 + 0.1728\frac{H}{C} + 0.0432\frac{O}{C} + 0.2169\frac{S}{C}\left(1 - 2.0628\frac{H}{C}\right) \qquad \text{Eq. (H- 3)}$$

Finally, chemical exergy of fuels can also be obtained from tables. An important note is that Gibbs energy of formation is changing when referring to different phases, and this has to be taken into account in the calculations. LHV values for hydrogen and methanol have been obtained by [90].

Chemical exergy – Mixture

In the case of a mixture, each substance is found at its partial pressure (p_{pi}). After separation of the substances through semipermeable membranes, each substance has to be compressed to environmental pressure (p_0). Even after the compression, each substance will still contain its chemical exergy as well. Therefore the total chemical exergy of the mixture, will be equal the summation of the molar chemical exergy of its consistuents minus the compression work. This can be expressed as:

$$\varepsilon_{Mix} = \sum_i x_i\varepsilon_i + RT_0\sum_i x_i ln x_i \qquad \text{Eq. (H- 4)}$$

The second term of the right-hand side is always negative which means that the chemical exergy of the mixture is always less than the summation of molar chemical exergy of its constituents. The aforementioned formulas can also be used for idea liquid phases but in case of real liquid phase it is advisable to include the activity coefficient (γ_i).

$$\varepsilon_{Mix} = \sum_i x_i\varepsilon_i + RT_0\sum_i x_i\gamma_i ln x_i \qquad \text{Eq. (H- 5)}$$

Summary of chemical Exergy

Schematically, the summary of chemical exergy is included in Figure H- 1. The mixture is separated into its components through semipermeable membranes. Each component is then compressed to the environmental state through a reversible isothermal process. The non-reference components are converted to reference components through oxidation and due to their elimination, they release useful work equal to the Gibbs energy of formation at environmental state. The products of the reaction are still in environmental state and each component will be expanded to its partial pressure through an isothermal expansion process and will be transferred to the environment through a semipermeable membrane.

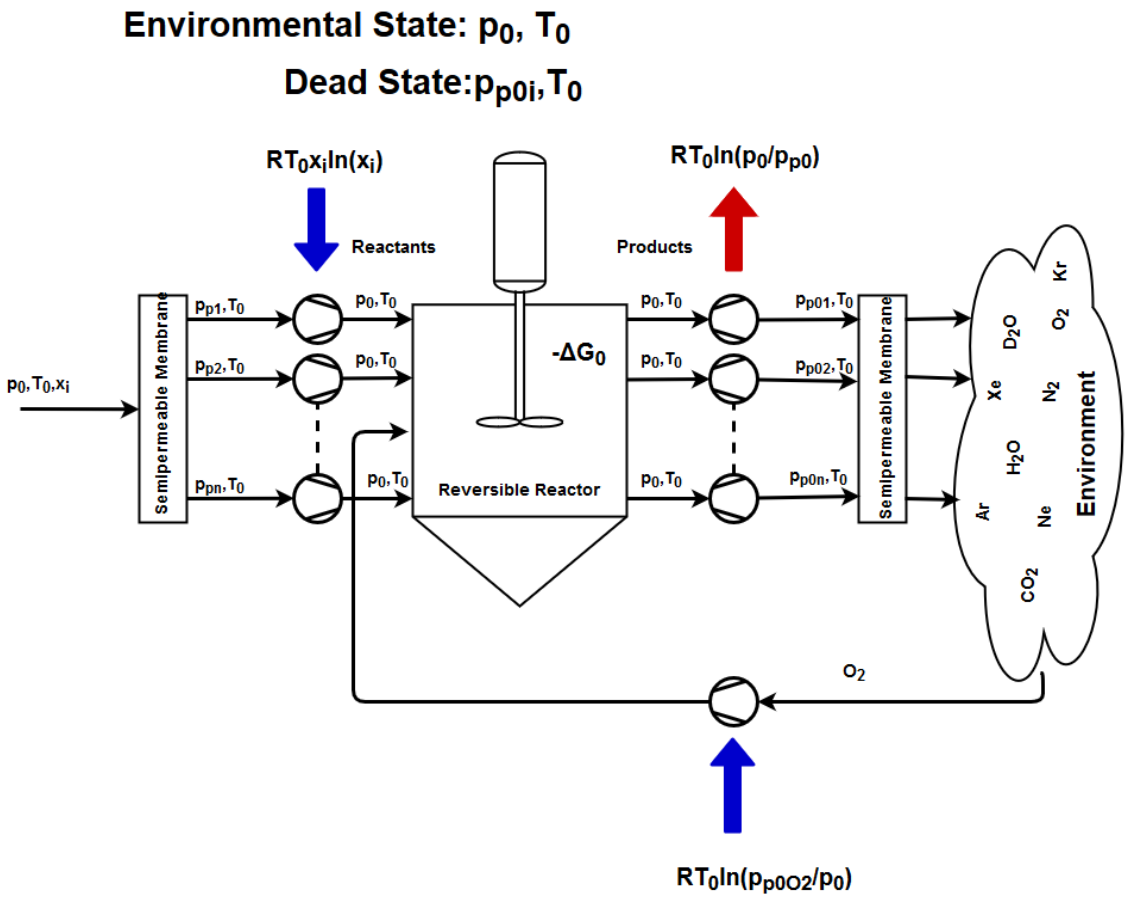

Figure H- 1: Schematic definition of Chemical Exergy of a mixture

The state where each component is found at its environmental partial pressure and reference temperature is the dead state. The compression work of oxygen utilized in the conversion of reactants to products should also be included in the calculations.

H-2 Physical Exergy

As it is understood in the previous section, chemical exergy is the exergy contained in substances and mixtures when transferred from environmental state to dead state reference components. However, in calculations, the initial mixture is not at environmental conditions but in random conditions. According to the formal definition:

"Physical exergy is equal to the maximum amount of work obtainable when the stream of substance is brought from its initial state to the environmental state defined by p_0 and T_0 by physical processes involving only thermal interaction with the environment"

If the initial condition is denoted with 1 and the environmental state is denoted with 0, then physical exergy is given by the following formula:

$$\varepsilon_{physical} = (h_1 - h_0) - T_0(s_1 - s_0) \qquad \text{Eq. (H- 6)}$$

In component analysis, in order to determine losses, usually difference in exergy from an initial state (1) to a final state (2) is used such that:

$$\varepsilon_{physical,loss} = (h_1 - h_2) - T_0(s_1 - s_2) \qquad \text{Eq. (H- 7)}$$

H-3 Exergy of Work and Heat

Till now, exergy content due to flow and streams has been discussed but exergy appears also in forms of heat and work. As already illustrated in the statement of the introduction of this chapter, if someone needs 1MJ of energy to compress a certain amount of gas, it is different if this amount is derived directly from electricity, high-temperature heat or lower temperature heat.

Electricity is a highly ordered form of energy. This means, that it is possible to extract all the energy content if the procedure is performed reversibly. Therefore by definition work is equivalent to exergy since processes can add or remove work without mechanical losses (i.e. friction) if the process is performed in a well-developed manner. For example, the work of one shaft can be transferred to another shaft reversibly (i.e. the kinetic energy will be maintained).

On the other hand, heat is a disordered form of energy and the maximum obtainable work obtained from heat transfer is restricted by Carnot efficiency. Therefore, if an amount of heat Q is delivered at temperature T, the maximum obtainable work is:

$$E_{heat} = Q(1 - \frac{T_0}{T}) \qquad \text{Eq. (H- 8)}$$

Exergy of heat will be useful in cases where hot and cold utility will be added during heat integration. If temperature T is not a constant value, the exergy of this heat stream is estimated by integration as:

$$E_{heat} = \int_1^2 (1 - \frac{T_0}{T})dQ = (1 - \frac{T_0}{\bar{T}})dQ \qquad \text{Eq. (H- 9)}$$

where $\bar{T} = \frac{\Delta h}{\Delta s}$ is the thermodynamically equivalent temperature of heat transfer

Appendix I: Open System Exergy Efficiency & Exergy efficiency for each component

As it has already been stated in the introduction of this chapter, exergy analysis quantifies the losses in the maximum obtainable work due to irreversibility. In other words, it quantifies the degradation of energy. In Figure I- 1, if (1) denotes the inlet stream condition and (2) denotes the outlet stream condition, while the system produces irreversible work W and accepts heat at a nonconstant temperature T (ranging from T_1 to T_2).

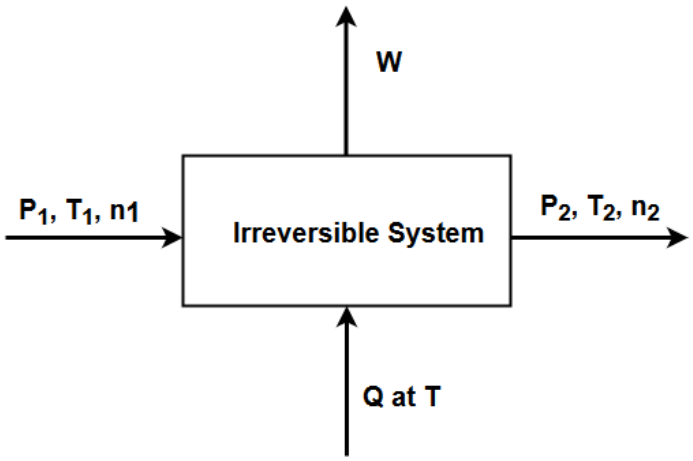

Figure I- 1: A thermodynamically irreversible system

The exergy loss of the system is given as:

$$Ex_{loss} = Ex_{in} - Ex_{out} \qquad \text{Eq. (J- 1)}$$

As can be seen from Eq. (J- 1):

$$Ex_{in} = Ex_1 + Ex_Q = Ex_1 + \int_1^2 (1 - \frac{T_0}{T}) dQ$$

$$Ex_{out} = Ex_2 + W$$

Therefore:

$$Ex_{loss} = (Ex_1 - Ex_2) + \int_1^2 \left(1 - \frac{T_0}{T}\right) dQ - W$$

where

$$Ex_1 - Ex_2 = n_1\big((h_1 - h_0) - T_0 \cdot (s_1 - s_0)\big) - n_2\big((h_2 - h_0) - T_0 \cdot (s_2 - s_0)\big)$$

The explanation above can be used to characterize single components or even whole systems.

Heater

$$Ex_{in} = Ex_1 + Ex_Q = n_1\big((h_1 - h_0) - T_0 \cdot (s_1 - s_0)\big) + \int_1^2 \left(1 - \frac{T_0}{T}\right) dQ$$

$$Ex_{out} = Ex_2 = n_2\big((h_2 - h_0) - T_0 \cdot (s_2 - s_0)\big)$$

$$n_1 = n_2$$

Cooler

$$Ex_{in} = Ex_1 = n_1\big((h_1 - h_0) - T_0 \cdot (s_1 - s_0)\big)$$

$$Ex_{out} = Ex_2 + Ex_Q = n_2\big((h_2 - h_0) - T_0 \cdot (s_2 - s_0)\big) + \int_1^2 \left(1 - \frac{T_0}{T}\right) dQ$$

$$n_1 = n_2$$

It must be noted that a simple heater or cooler does not have any exergy loss. Exergy losses occur to heat exchangers where the quality of heat is decreased since heat is transferred from high to low temperatures.

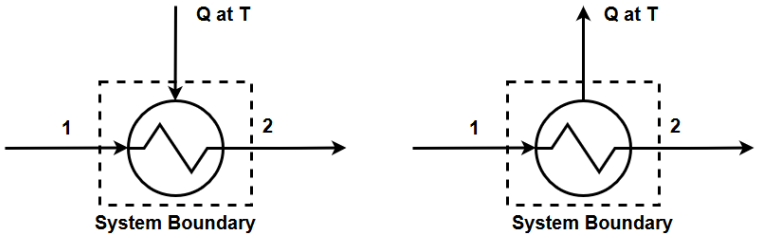

Figure I- 2: Thermodynamic representation of Heater/Cooler

Heat exchanger

$$Ex_{in} = Ex_1 + Ex_3 = n_1\big((h_1 - h_0) - T_0 \cdot (s_1 - s_0)\big) + n_3\big((h_3 - h_0) - T_0 \cdot (s_3 - s_0)\big)$$

$$Ex_{out} = Ex_2 + Ex_4 = n_2\big((h_2 - h_0) - T_0 \cdot (s_2 - s_0)\big) + n_4\big((h_4 - h_0) - T_0 \cdot (s_4 - s_0)\big)$$

$$n_1 = n_2, n_3 = n_4$$

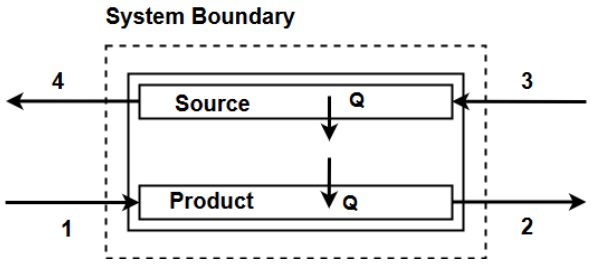

Figure I- 3: Thermodynamic representation of Heat Exchanger

Expander

$$Ex_{in} = Ex_1 = n_1\big((h_1 - h_0) - T_0 \cdot (s_1 - s_0)\big)$$

$$Ex_{out} = Ex_2 + Ex_W = n_2\big((h_2 - h_0) - T_0 \cdot (s_2 - s_0)\big) + W$$

$$n_1 = n_2$$

Compressor

$$Ex_{in} = Ex_1 + Ex_W = n_1\big((h_1 - h_0) - T_0 \cdot (s_1 - s_0)\big) + W$$

$$Ex_{out} = Ex_2 = n_2\big((h_2 - h_0) - T_0 \cdot (s_2 - s_0)\big)$$

$$n_1 = n_2$$

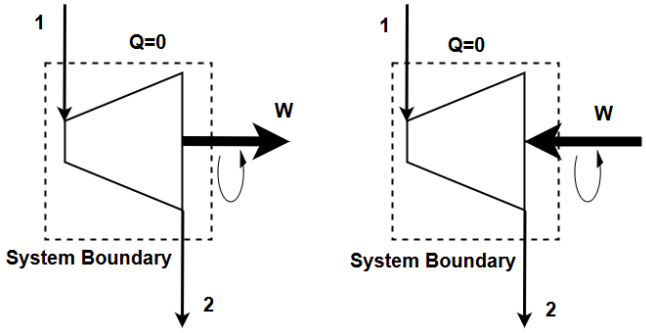

Figure I- 4: Thermodynamic representation of Expander/Compressor

Exothermic Reactor

$$Ex_{in} = Ex_1 = n_1\big((h_1 - h_0) - T_0 \cdot (s_1 - s_0)\big)$$

$$Ex_{out} = Ex_2 + Ex_Q = n_2\big((h_2 - h_0) - T_0 \cdot (s_2 - s_0)\big) + \int_1^2 \left(1 - \frac{T_0}{T}\right) dQ$$

$$n_1 \neq n_2$$

Endothermic Reactor

$$Ex_{in} = Ex_1 + Ex_Q = n_1\big((h_1 - h_0) - T_0 \cdot (s_1 - s_0)\big) + \int_1^2 \left(1 - \frac{T_0}{T}\right) dQ$$

$$Ex_{out} = Ex_2 = n_2\big((h_2 - h_0) - T_0 \cdot (s_2 - s_0)\big)$$

$$n_1 \neq n_2$$

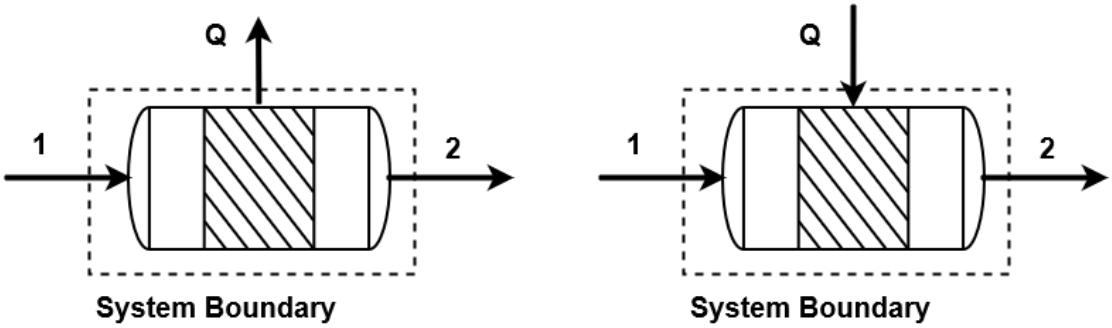

Figure I- 5: Thermodynamic representation of an exothermic/endothermic reactor

Electrolysis Stack (i.e. Exothermic Mode)

$$Ex_{in} = Ex_{F1} + Ex_{SG1} + Ex_W == n_{F1}\big((h_{F1} - h_0) - T_0 \cdot (s_{F1} - s_0)\big) + n_{SG1}\big((h_{SG1} - h_0) - T_0 \cdot (s_{SG1} - s_0)\big) + W$$

$$Ex_{out} = Ex_{F2} + Ex_{SG2} + Ex_Q = n_{F1}\big((h_{F2} - h_0) - T_0 \cdot (s_{F2} - s_0)\big) + n_{SG2}\big((h_{SG2} - h_0) - T_0 \cdot (s_{SG2} - s_0)\big) + \int_1^2 \left(1 - \frac{T_0}{T}\right) dQ$$

$$n_{F1} \neq n_{F2}, n_{SG1} \neq n_{SG2}$$

Fuel Cell Stack

$$Ex_{in} = Ex_{F1} + Ex_{SG1} = n_{F1}\big((h_{F1} - h_0) - T_0 \cdot (s_{F1} - s_0)\big) + n_{SG1}\big((h_{SG1} - h_0) - T_0 \cdot (s_{SG1} - s_0)\big)$$

$$Ex_{out} = Ex_{F2} + Ex_{SG2} + Ex_Q + Ex_W = n_{F1}\big((h_{F2} - h_0) - T_0 \cdot (s_{F2} - s_0)\big) + n_{SG2}\big((h_{SG2} - h_0) - T_0 \cdot (s_{SG2} - s_0)\big) + \int_1^2 \left(1 - \frac{T_0}{T}\right) dQ + W$$

$$n_{F1} \neq n_{F2}, n_{SG1} \neq n_{SG2}$$

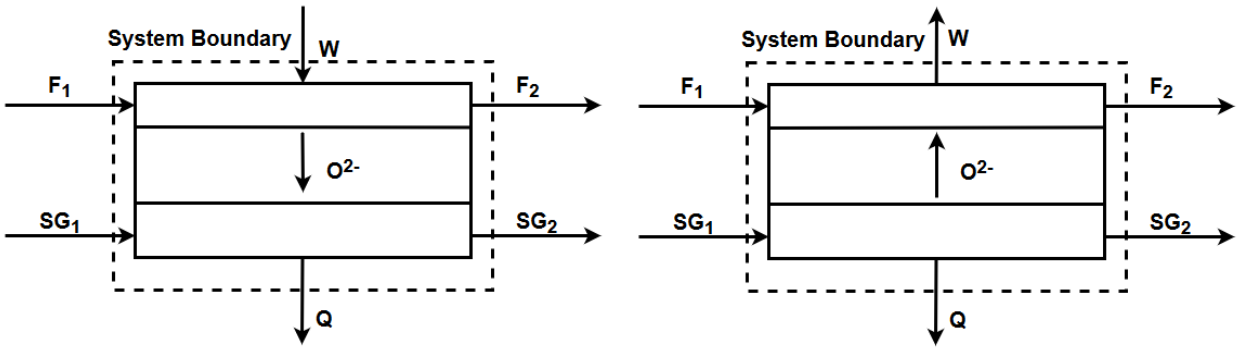

Figure I- 6: Thermodynamic representation of electrolysis/fuel cell stack

Appendix J: About Thermodynamic Models

In order to do a process simulation, a very important part is the selection of appropriate thermodynamic models for different parts of the simulation. A simulation still remains something idealistic and even though thermodynamic models have been developed for various components and process conditions, a simulation cannot represent reality with perfect accuracy but of course, there is high precision in the calculations.

Choosing the most appropriate thermodynamic models for each case is a tedious task, but Aspen Plus offers online help and practical guidelines on thermodynamic model selection. In reality, even in a single unit operation, more than one thermodynamic models can be applied since process conditions are different in each part of the unit. These guidelines can also be found in the thermodynamic wizard incorporated in Aspen Plus. The main criteria for choosing thermodynamic models are the pressure if the mixture is an electrolyte or a non-electrolyte and if the mixture is polar or non-polar, if the components are real or pseudo-real and in the cases of liquid-liquid equilibrium, if the interaction parameters are known. Choice of wrong thermodynamic models can lead to erroneous results and sometimes to non-convergence of the process simulator.

Figure J- 1 & Figure J- 2 give an overview of the selection guide that has been used in this project [91]. The thermodynamic models for each model and section will be mentioned for completeness (see Table J- 1).

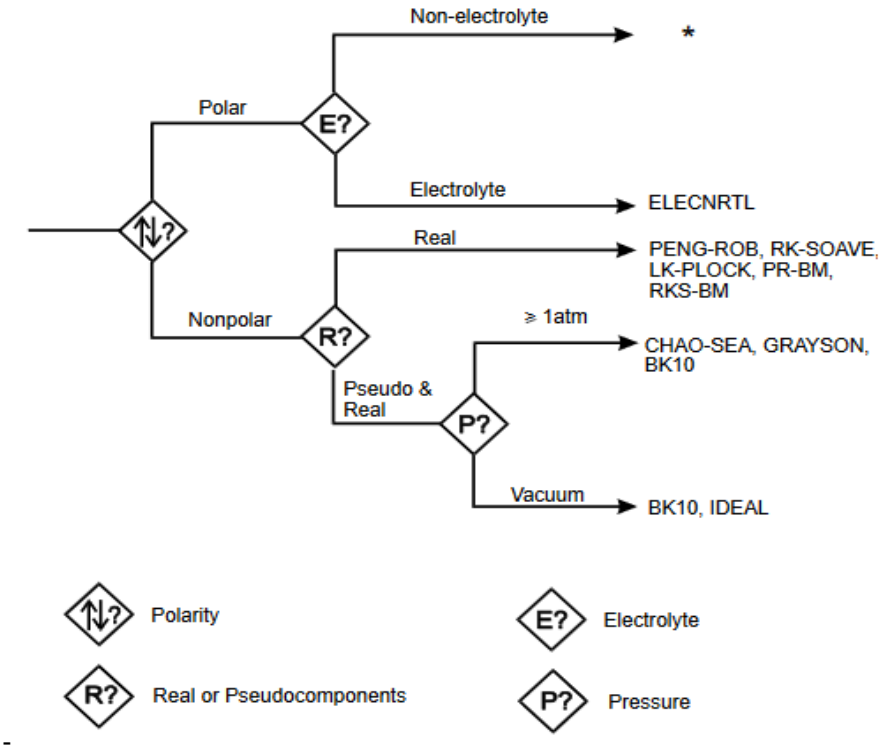

Figure J- 1: Thermodynamic model selection (1), [91]

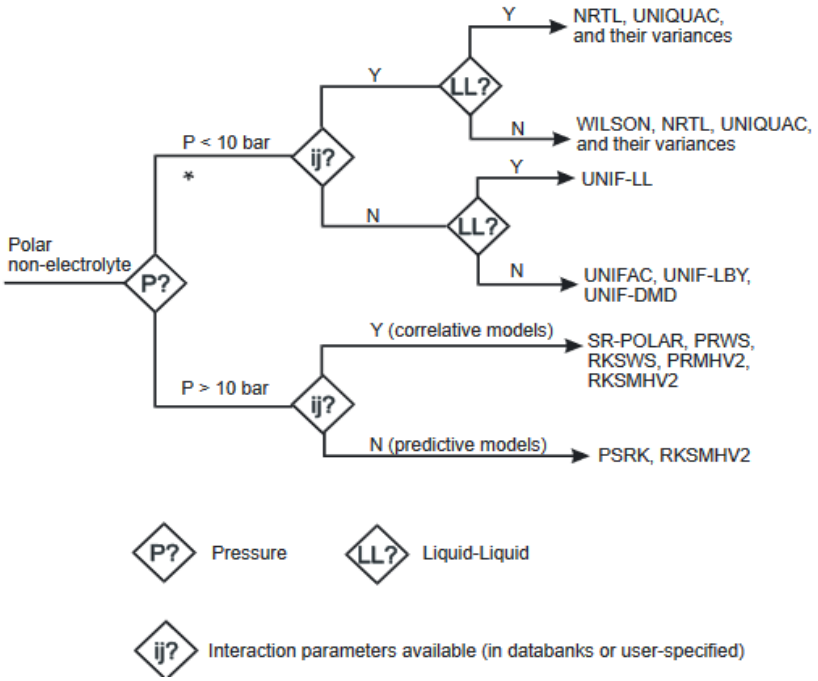

Figure J- 2: Thermodynamic model selection (1), [91][91]

Table J- 1: A summary of the thermodynamic models employed for each section of electrolysis and fuel cell mode

Electrolysis Model	
H_2 multistage expansion section	Peng-Robinson
H_2O pumping and evaporation	Wilson
Anode modeling	PSRK
H_2O condensation	PSRK
H_2 compression and intercooling section	Peng-Robinson
CO_2 heating and expansion	Peng-Robinson
Methanol synthesis reactor and subsequent condensation	PSRK
Recycle Loop	Peng-Robinson
Light separation, Distillation column, and methanol cooling	NRTL
Afterburner section	PSRK
Sweep Gas train	IDEAL
Fuel Cell Model	
Initial pumping and heating section for methanol and water	PSRK
Methanol Steam reforming and subsequent heating	PSRK
Fuel Cell Anode	PSRK
Water Gas Shift Reactor	PSRK
Subsequent condensation and water removal	NRTL
Storage compressor section	Peng-Robinson
Oxidant gas train	IDEAL
Refrigeration Cycle	Peng-Robinson

References

[1] D. Ferrero, A. Lanzini, P. Leone, and M. Santarelli, "Reversible operation of solid oxide cells under electrolysis and fuel cell modes : Experimental study and model validation," *Chem. Eng. J.*, vol. 274, pp. 143–155, 2015.

[2] G. Léonard, D. Giulini, and D. Villarreal-singer, "Design and Evaluation of a High-Density Energy Storage Route with CO2 Re-Use , Water Electrolysis and Methanol Synthesis," in *ESCAPE 26*, 2016, vol. 2, pp. 0–5.

[3] R. Rivera-tinoco, M. Farran, C. Bouallou, and F. Aupr, "Investigation of power-to-methanol processes coupling electrolytic hydrogen production and catalytic CO2 reduction," *Int. J. Hydrogen Energy*, vol. 1, 2016.

[4] A. Perna, M. Minutillo, S. P. Cicconardi, E. Jannelli, and S. Scarfogliero, "Performance Assessment of Electric Energy Storage (EES) systems based on reversible solid oxide cell," *Energy Procedia*, vol. 101, no. September, pp. 1087–1094, 2016.

[5] S. H. Jensen *et al.*, "Large-scale electricity storage utilizing reversible solid oxide cells combined with underground storage of CO2 and CH4," *Energy Environ. Sci.*, vol. 8, pp. 2471–2479, 2015.

[6] P. Kazempoor and R. J. Braun, "Model validation and performance analysis of regenerative solid oxide cells for energy storage applications : Reversible operation," *Int. J. Hydrogen Energy*, vol. 39, no. 11, pp. 5955–5971, 2014.

[7] M. De Saint, P. Baurens, and C. Bouallou, "Parametric study of an efficient renewable power-to-substitute-natural-gas process including high-temperature steam electrolysis," *Int. J. Hydrogen Energy*, vol. 39, no. 30, pp. 17024–17039, 2014.

[8] V. N. Nguyen and L. Blum, "5 - Reversible fuel cells," in *Woodhead Publishing Series in Energy*, F. Barbir, A. Basile, and T. N. B. T.-C. of H. E. Veziroğlu, Eds. Oxford: Woodhead Publishing, 2016, pp. 115–145.

[9] C. H. Wendel, P. Kazempoor, and R. J. Braun, "Novel electrical energy storage system based on reversible solid oxide cells : System design and operating conditions," *J. Power Sources*, vol. 276, pp. 133–144, 2015.

[10] D. M. Bierschenk, J. R. Wilson, and S. A. Barnett, "High efficiency electrical energy storage using a methane–oxygen solid oxide cell," *Energy Environ. Sci.*, vol. 4, no. 3, pp. 944–951, 2011.

[11] E. I. Al-musleh, D. S. Mallapragada, and R. Agrawal, "Continuous power supply from a baseload renewable power plant," *Appl. Energy*, vol. 122, pp. 83–93, 2014.

[12] M. Ni, M. K. H. Leung, and D. Y. C. Leung, "Energy and exergy analysis of hydrogen production by solid oxide steam electrolyzer plant," *Int. J. Hydrogen Energy*, vol. 32, pp. 4648–4660, 2007.

[13] M. Hauck, S. Herrmann, and H. Spliethoff, "Simulation of a reversible SOFC with Aspen Plus," *Int. J. Hydrogen Energy*, vol. 42, no. 15, pp. 10329–10340, 2017.

[14] IEA, "Technology Roadmap - Energy storage," 2014.

[15] EASE/EERA, "European Energy Storage Technology Development Roadmap towards 2030."

[16] A. Dicks and J. Larminie, *Fuel Cell Systems Explained*, 2nd ed. England: John Wiley & Sons Ltd, 2003.

[17] N. Mahato, A. Banerjee, A. Gupta, S. Omar, and K. Balani, "Progress in Materials Science Progress in material selection for solid oxide fuel cell technology : A review," *Prog. Mater. Sci.*, vol. 72, pp. 141–337, 2015.

[18] C. H. Wendel, Z. Gao, S. A. Barnett, and R. J. Braun, "Modeling and experimental performance of an intermediate temperature reversible solid oxide cell for high-ef fi ciency , distributed-scale electrical energy storage," *J. Power Sources*, vol. 283, pp. 329–342, 2015.

[19] C. H. Wendel, "Design and Analysis of Reversible Solid Oxide Cell Systems for Electrical Energy Storage," Colorado School of Mines, 2015.

[20] M. Wang, A. Lawal, P. Stephenson, J. Sidders, and C. Ramshaw, "Post-combustion CO2 capture with chemical absorption: A state-of-the-art review," *Chem. Eng. Res. Des.*, vol. 89, no. 9, pp. 1609–1624, 2011.

[21] S. F. Au, "Innovative High Temperature Fuel Cell systems," Delft University of Technology, 2003.

[22] S. Srinivasan, *Fuel cells, From Fundamentals to Applications*. Springer US, 2006.

[23] N. James, *Fuel cell technology reaching towards commercizlization*. Springer Berlin Heidelberg, 2006.

[24] E. Giglio, A. Lanzini, M. Santarelli, and P. Leone, "Synthetic natural gas via integrated high-temperature electrolysis and methanation : Part I — Energy performance," *J. Energy Storage*, vol. 1, pp. 22–37, 2015.

[25] J. B. Hansen, N. Christiansen, and J. U. Nielsen, "Production of Sustainable Fuels by Means of Solid Oxide Electrolysis J. B. Hansen," *ECS Trans.*, vol. 35, no. 1, pp. 2941–2948, 2011.

[26] V. N. Nguyen and L. Blum, *Chapter 5 - Reversible fuel cells*. Elsevier Ltd., 2016.

[27] C. H. Wendel, P. Kazempoor, and R. J. Braun, "A thermodynamic approach for selecting operating conditions in the design of reversible solid oxide cell energy systems," *J. Power Sources*, vol. 301, pp. 93–104, 2016.

[28] W. Doenitz, R. Schmidberger, E. Steinheil, and R. Streicher, "Hydrogen production by high temperature electrolysis of water vapour," *Int. J. Hydrogen Energy*, vol. 5, no. 1, pp. 55–63, 1980.

[29] J. F. Mcelroy and D. B. Hickey, "Optimization & Demonstration of a Solid Oxide Regenerative Fuel Cell System," 2004.

[30] E. Giglio, A. Lanzini, M. Santarelli, and P. Leone, "Synthetic natural gas via integrated high-temperature electrolysis and methanation : Part II — Economic analysis," *J. Energy Storage*, vol. 2, pp. 64–79, 2015.

[31] F. Alenazey *et al.*, "Production of synthesis gas (H2 and CO) by high-temperature Co-electrolysis of H2O and CO2," *Int. J. Hydrogen Energy*, vol. 40, no. 32, pp. 10274–10280, 2015.

[32] Y. Wang, T. Liu, S. Fang, G. Xiao, H. Wang, and F. Chen, "A novel clean and effective syngas production system based on partial oxidation of methane assisted solid oxide co-electrolysis process," *J. Power Sources*, vol. 277, pp. 261–267, 2015.

[33] F. Bidrawn, G. Kim, G. Corre, J. T. S. Irvine, J. M. Vohs, and R. J. Gorte, "Efficient Reduction of CO2 in a Solid Oxide Electrolyzer," *Electrochem. Solid-State Lett.*, vol. 11, no. 9, pp. 167–170, 2008.

[34] X. Sun, M. Chen, S. H. Jensen, S. D. Ebbesen, C. Graves, and M. Mogensen, "Thermodynamic analysis of synthetic hydrocarbon fuel production in pressurized solid oxide electrolysis cells," *Int. J. Hydrogen Energy*, vol. 37, no. 22, pp. 17101–17110, 2012.

[35] M. J. Bos and D. W. F. Brilman, "A novel condensation reactor for efficient CO2 to methanol conversion for storage of renewable electric energy," *Chem. Eng. J.*, vol. 278, pp. 527–532, 2015.

[36] L. Barelli, G. Bidini, and A. Ottaviano, "Hydromethane generation through SOE (solid oxide electrolyser): Advantages of H2O - CO2 co-electrolysis," *Energy*, vol. 90, pp. 1180–1191, 2015.

[37] Q. Fu, C. Mabilat, M. Zahid, A. Brisse, and L. Gautier, "Syngas production via high-temperature steam/CO2 co-electrolysis: an economic assessment," *Energy Environ. Sci.*, vol. 3, no. 10, pp. 1382–1397, 2010.

[38] J. Guan *et al.*, "High Performance Flexible Reversible Solid Oxide Fuel Cell," Torrance, 2006.

[39] S. D. Ebbesen, C. Graves, and M. Mogensen, "Production of Synthetic Fuels by Co-Electrolysis of Steam and Carbon Dioxide," *Int. J. Green Energy*, vol. 6, no. 6, pp. 646–660, Dec. 2009.

[40] P. Kazempoor and R. J. Braun, "Hydrogen and synthetic fuel production using high temperature solid oxide electrolysis cells (SOECs)," *Int. J. Hydrogen Energy*, vol. 40, no. 9, pp. 3599–3612, 2015.

[41] S. L. Ebbehøj, "Integration of CO2 air capture and solid oxide electrolysis for methane production," Technical University of Denmark, 2015.

[42] M. Reytier *et al.*, "Stack performances in high temperature steam electrolysis and co-electrolysis," *Int. J. Hydrogen Energy*, vol. 40, no. 35, pp. 11370–11377, 2015.

[43] J. Laurencin, D. Kane, G. Delette, J. Deseure, and F. Lefebvre-joud, "Modelling of solid oxide steam electrolyser: Impact of the operating conditions on hydrogen production," *J. Power Sources*, vol. 196, no. 4, pp. 2080–2093, 2011.

[44] J. Ren, S. R. Gamble, A. J. Roscoe, J. T. S. Irvine, and G. Burt, "Modeling a Reversible Solid Oxide Fuel Cell as a Storage Device Within AC Power Networks," no. 5, pp. 773–786, 2012.

[45] Q. Cai, C. S. Adjiman, and N. P. Brandon, "Optimal control strategies for hydrogen production when coupling solid oxide electrolysers with intermittent renewable energies," *J. Power Sources*, vol. 268, pp. 212–224, 2014.

[46] G. Botta, M. Solimeo, P. Leone, and P. V Aravind, "Thermodynamic Analysis of Coupling a SOEC in Co-Electrolysis Mode with the Dimethyl Ether Synthesis," *Fuel Cells*, vol. 15, no. 5, pp. 669–681, Jul. 2015.

[47] C. H. Wendel and R. J. Braun, "Design and techno-economic analysis of high efficiency reversible solid oxide cell systems for distributed energy storage," *Appl. Energy*, vol. 172, pp. 118–131, 2016.

[48] W. L. Becker, R. J. Braun, M. Penev, and M. Melaina, "Production of Fischer - Tropsch liquid fuels from high temperature solid oxide co-electrolysis units," *Energy*, vol. 47, no. 1, pp. 99–115, 2012.

[49] P. Kazempoor and R. J. Braun, "Model validation and performance analysis of regenerative solid oxide cells: Electrolytic operation," *Int. J. Hydrogen Energy*, vol. 39, no. 6, pp. 2669–2684, 2014.

[50] D. M. Bierschenk, J. R. Wilson, E. Miller, E. Dutton, and S. A. Barnett, "A Proposed Method for High Efficiency Electrical Energy Storage Using Solid Oxide Cells," vol. 35, no. 1, pp. 2969–2978, 2011.

[51] T. Wang, "Fuel Synthesis with CO2 captured from Atmosphere: Thermodynamic Analysis," vol. 41, no. 33, pp. 13–24, 2012.

[52] S. Diego Villareal., "Reversible solid oxide cells for bidirectional energy conversion in spot electricity and fuel markets," Columbia University, 2017.

[53] R. K. Akikur, R. Saidur, H. W. Ping, and K. R. Ullah, "Performance analysis of a co-generation system using solar energy and SOFC technology," *Energy Convers. Manag.*, vol. 79, pp. 415–430, 2014.

[54] B. M. Ni, M. K. H. Leung, and D. Y. C. Leung, "An Electrochemical Model of a Solid Oxide Steam Electrolyzer for Hydrogen Production," no. 5, pp. 636–642, 2006.

[55] M. Ni, M. K. H. Leung, and D. Y. C. Leung, "Parametric study of solid oxide steam electrolyzer for hydrogen production," *Int. J. Hydrogen Energy*, vol. 32, no. 13, pp. 2305–2313, 2007.

[56] X. Chen, C. Guan, G. Xiao, X. Du, and J. Wang, "Syngas production by high temperature steam/CO2 coelectrolysis using solid oxide electrolysis cells," *Faraday Discuss.*, vol. 182, pp. 341–351, 2015.

[57] E. C. S. Transactions and T. E. Society, "Efficiency Calculations for SOFC/SOEC Reversible System and Evaluations of Performances of Button-size Anode-supported Cell M. Shiraki," vol. 57, no. 1, pp. 3261–3267, 2013.

[58] K. Atsonios, K. D. Panopoulos, and E. Kakaras, "Thermocatalytic CO2 hydrogenation for methanol and ethanol production : Process improvements," *Int. J. Hydrogen Energy*, vol. 41, no. 2, pp. 792–806, 2015.

[59] M. Bertau, H. Offermanns, L. Plass, F. Schmidt, and H.-J. Wernicke, *Methanol: The Basic Chemical and Energy Feedstock of the Future*. Springer-Verlag Berlin Heidelberg, 2014.

[60] A. Goeppert, G. K. S. Prakash, and G. A. Olah, "Recycling of carbon dioxide to methanol and derived products - closing the loop," *Chem. Soc. Rev.*, vol. 43, no. 23, pp. 7995–8048, 2014.

[61] J. R. van Ommen and J. Grievink, "Synthesis Gas Utilization for Transportation Fuel Production," *Biomass as a Sustainable Energy Source for the Future*. 03-Oct-2014.

[62] O. Mäyrä and K. Leiviskä, "Chapter 17 - Modeling in Methanol Synthesis," A. Basile and F. B. T.-M. Dalena, Eds. Elsevier, 2018, pp. 475–492.

[63] E. Fiedler, G. Grossmann, D. B. Kersebohm, G. Weiss, and C. Witte, "Methanol," *Ullmann's Encyclopedia of Industrial Chemistry*. 15-Jun-2000.

[64] G. Bozzano and F. Manenti, "Efficient methanol synthesis : Perspectives , technologies and optimization strategies," vol. 56, pp. 71–105, 2016.

[65] G. A. Olah, A. Goeppert, and G. K. S. Prakash, *Beyond Oil and Gas: The Methanol Economy*. Wiley-VCH Verlag GmbH & Co. KGaA, 2009.

[66] G. H. Graaf, E. J. Stamhuis, and A. A. C. M. Beenackers, "Kinetics of low-pressure methanol synthesis," *Chem. Eng. Sci.*, vol. 43, no. 12, pp. 3185–3195, 1988.

[67] K. M. Vanden Bussche and G. F. Froment, "A Steady-State Kinetic Model for Methanol Synthesis and the Water Gas Shift Reaction on a Commercial Cu/ZnO/Al2O3 Catalyst," *J. Catal.*, vol. 10, no. 156, pp. 1–10, 1996.

[68] M. Šetinc and J. Levec, "Dynamics of a mixed slurry reactor for the three-phase methanol synthesis," *Chem. Eng. Sci.*, vol. 56, no. 21, pp. 6081–6087, 2001.

[69] A. Y. Rozovskii and G. I. Lin, "Fundamentals of Methanol Synthesis and Decomposition," *Top. Catal.*, vol. 22, no. 3, pp. 137–150, 2003.

[70] G. H. Graaf, H. Scholtens, E. J. Stamhuis, and A. A. C. M. Beenackers, "Intra-particle diffusion limitations in low-pressure methanol synthesis," *Chem. Eng. Sci.*, vol. 45, no. 4, pp. 773–783, 1990.

[71] N. Park, M. Park, Y. Lee, K. Ha, and K. Jun, "Kinetic modeling of methanol synthesis over commercial catalysts based on three-site adsorption," *Fuel Process. Technol.*, vol. 125, pp. 139–147, 2014.

[72] T. Kubota *et al.*, "Kinetic study of methanol synthesis from carbon dioxide and hydrogen," *Appl. Organomet. Chem.*, vol. 15, no. 2, pp. 121–126, Jan. 2001.

[73] H. Lim, M. Park, S. Kang, H. Chae, J. W. Bae, and K. Jun, "Modeling of the Kinetics for Methanol Synthesis using Cu/ZnO/Al2O3/ZrO2 Catalyst : Influence of Carbon Dioxide during Hydrogenation," *Ind. Eng. Chem. Res.*, pp. 10448–10455, 2009.

[74] D. Broom, *Hydrogen Storage Materials: The Characterisation of their storage properties*. Springer-Verlag London, 2011.

[75] R. B. Gupta, *Hydrogen Fuel: Production, Transport and Storage*. CRC Press, 2009.

[76] S. Niaz, T. Manzoor, and A. Hussain, "Hydrogen storage : Materials , methods and perspectives," *Renew. Sustain. Energy Rev.*, vol. 50, pp. 457–469, 2015.

[77] Z. Zhang and D. Huisingh, "Carbon dioxide storage schemes: Technology, assessment and deployment," *J. Clean. Prod.*, vol. 142, pp. 1055–1064, 2017.

[78] "Carbon dioxide." [Online]. Available: https://pubchem.ncbi.nlm.nih.gov/. [Accessed: 01-Mar-2018].

[79] R. Thattarathody and M. Sheintuch, "Kinetics and dynamics of methanol steam reforming on CuO/ZnO/alumina catalyst," *Appl. Catal. A Gen.*, vol. 540, pp. 47–56, 2017.

[80] T. J. Kotas, *The Exergy Method of Thermal Plant Analysis*. Butterworth-Heinemann, 1985.

[81] S. A. Rackley, *Carbon Capture and Storage*. Butterworth-Heinemann, 2017.

[82] A. Dinker, M. Agarwal, and G. D. Agarwal, "Heat storage materials, geometry and applications: A review," *J. Energy Inst.*, vol. 90, no. 1, pp. 1–11, 2017.

[83] K. Nithyanandam, J. Stekli, and R. Pitchumani, "10 - High-temperature latent heat storage for concentrating solar thermal (CST) systems," in *Woodhead Publishing Series in Energy*, M. J. Blanco and L. R. B. T.-A. in C. S. T. R. and T. Santigosa, Eds. Woodhead Publishing, 2017, pp. 213–246.

[84] Y. Tian and C. Y. Zhao, "A review of solar collectors and thermal energy storage in solar thermal applications," *Appl. Energy*, vol. 104, pp. 538–553, 2013.

[85] D. A. Noren and M. A. Hoffman, "Clarifying the Butler – Volmer equation and related approximations for calculating activation losses in solid oxide fuel cell models," vol. 152, pp. 175–181, 2005.

[86] *VDI Heat Atlas*, 2nd ed. Springer-Verlag Berlin Heidelberg, 2010.

[87] W. Black and J. Hartley, *Thermodynamics*, 3rd ed. Pearson, 1996.

[88] M. M. Sies, "Thermodynamics II, Chapter - 3 Compressors, Lecture Slides."

[89] J. . Seader, J. E. Henley, and D. K. Roper, *Separation Process Principles*, 3rd ed. John Wiley & Sons, Inc., 2011.

[90] "Calorific Values of Various Fuels." [Online]. Available: https://www.engineeringtoolbox.com/fuels-higher-calorific-values-d_169.html.

[91] "Thermodynamic Model Selection in Process Simulation." [Online]. Available: http://people.clarkson.edu/~wwilcox/Design/TherModl.pdf. [Accessed: 10-Feb-2018].